

**Supramolecular hydrogels
based on 1,3,5-benzene tricarboxamides**

Dissertation

zur Erlangung des akademischen Grades
eines Doktors der Naturwissenschaften (Dr. rer. nat.)
im Promotionsprogramm „Polymer Science“
der Bayreuther Graduiertenschule für Mathematik und Naturwissenschaften

vorgelegt von

Marina Cornelia Behr

geboren in Würzburg, Deutschland

Bayreuth, 2014

Die vorliegende Arbeit wurde in der Zeit von Februar 2010 bis November 2014 am Lehrstuhl Makromolekulare Chemie I der Universität Bayreuth unter der Betreuung von Prof. Dr. Hans-Werner Schmidt angefertigt.

Vollständiger Abdruck der von der Bayreuther Graduiertenschule für Mathematik und Naturwissenschaften (BayNAT) der Universität Bayreuth genehmigten Dissertation zur Erlangung des akademischen Grades eines Doktors der Naturwissenschaften (Dr. rer. nat.).

Tag der Einreichung: 20. November 2014

Zulassung durch das Leitungsgremium: 26. November 2014

Wissenschaftliches Kolloquium: 27. April 2015

Amtierender Direktor der Bayreuther Graduiertenschule für Mathematik und Naturwissenschaften (BayNaT): Prof. Dr. Franz Xaver Schmid

Prüfungsausschuss:

Prof. Dr. Hans-Werner Schmidt (Erstgutachter)

JProf. Dr. Matthias Karg (Zweitgutachter)

Prof. Dr. Thomas Scheibel (Vorsitz)

Prof. Dr. Georg Papastavrou

Meiner Familie

Ein guter Anfang braucht Begeisterung,
ein gutes Ende Disziplin.

Motto der Deutschen Fußballnationalmannschaft bei der WM 2014
von Prof. Dr. Hans-Jürgen Quadbeck-Seeger (Chemiker)

Table of contents

| | | |
|----------|--|-----------|
| 1 | Introduction | 1 |
| 1.1 | Hydrogels..... | 1 |
| 1.1.1 | Definition and classification of gels..... | 1 |
| 1.1.2 | Important intermolecular interactions | 5 |
| 1.1.3 | Gelation mechanisms and hierarchical structures of lmw hydrogels | 6 |
| 1.1.4 | Considerations regarding the design of lmw hydrogelators | 7 |
| 1.1.5 | Typical molecular structures of lmw hydrogelators..... | 11 |
| 1.2 | 1,3,5-Benzene tricarboxamides..... | 14 |
| 1.2.1 | A versatile structural motif..... | 14 |
| 1.2.2 | BTAs as trivalent building block in synthesis and metal ion coordination | 17 |
| 1.2.3 | Self-assembly of BTA derivatives in various environments..... | 18 |
| 1.3 | Possible applications of lmw hydrogelators..... | 25 |
| 1.3.1 | Application as adsorption material | 26 |
| 1.3.2 | Application of lmw hydrogelators in the field of controlled drug delivery | 27 |
| 1.4 | Surface coatings <i>via</i> electrogelation | 33 |
| 2 | Objective | 37 |
| 3 | Self-Assembly behavior of pH-sensitive 1,3,5-benzene tricarboxamides in aqueous systems | 41 |
| 3.1 | Structural concept | 41 |
| 3.2 | Synthesis and characterization..... | 44 |
| 3.2.1 | Synthesis of the 1,3,5-benzene tricarboxamides 1 - 5 | 44 |
| 3.2.2 | Characterization | 46 |
| 3.2.3 | Solubility tests | 58 |
| 3.3 | pH-Sensitive aggregation and gel formation..... | 62 |
| 3.3.4 | Investigation of pH-sensitive aggregation..... | 62 |
| 3.3.5 | Gel preparation methods for compound 4 | 73 |
| 3.3.6 | Characterization of gel properties of compound 4 | 83 |
| 3.4 | Proposed structural model..... | 89 |
| 4 | “Formation of a supramolecular chromophore: a spectroscopic and theoretical study” | 93 |
| 4.1 | Spectroscopic studies of compounds 4 and 4Na | 93 |
| 4.1.1 | Absorption studies in solution, film, and during pH-sensitive aggregation | 93 |
| 4.1.2 | Photoluminescence studies in solution, bulk and hydrogel state..... | 97 |
| 4.1.3 | Photoluminescence studies upon gel formation | 101 |
| 4.2 | Theoretical calculations..... | 102 |
| 4.3 | Considerations regarding the proposed structural model..... | 108 |

| | | |
|----------|---|------------|
| 5 | Dye adsorption and release studies: towards a pH-sensitive supramolecular drug delivery system | 111 |
| 5.1 | Requirements for controlled drug delivery systems | 111 |
| 5.1.1 | Biocompatibility and nontoxicity..... | 111 |
| 5.1.2 | Responsiveness of hydrogels of 4 | 112 |
| 5.1.3 | Mechanical stability of hydrogels of 4 | 113 |
| 5.1.4 | Specific surface area | 113 |
| 5.2 | Adsorption of rhodamine B using pre-formed hydrogels..... | 115 |
| 5.2.1 | Sample preparation and experimental set up..... | 116 |
| 5.2.2 | Time-dependent adsorption studies with different initial dye concentrations..... | 124 |
| 5.2.3 | Thermal stability of adsorbed dye-gel systems | 139 |
| 5.3 | Hydrogel formation in the presence of rhodamine B with <i>in situ</i> adsorption | 142 |
| 5.3.1 | Sample preparation and experimental set up..... | 143 |
| 5.3.2 | Release of rhodamine B in water at r. t. | 149 |
| 5.4 | Comparison of the different loading techniques..... | 158 |
| 5.5 | Release of <i>in situ</i> adsorbed rhodamine B in biologically relevant media...160 | |
| 5.5.1 | Release of rhodamine B upon dissolution in PBS (pH = 7.4) at r. t. | 160 |
| 5.5.2 | Release of rhodamine B upon dissolution in SBF (pH = 7.4) at 37 °C..... | 166 |
| 5.5.3 | Release of rhodamine B in simulated gastric fluid containing pepsin (pH = 1.6) at 37 °C | 169 |
| 5.5.4 | Release of rhodamine B in simulated intestinal fluid (pH = 6.5) at 37 °C..... | 174 |
| 5.6 | Achievements and further investigations towards a pH-sensitive drug delivery system | 179 |
| 6 | “Electrogelation” – controlled formation of hydrogel films on conductive substrates | 183 |
| 6.1 | Concept and set up | 184 |
| 6.2 | Hydrogel film formation and characterization of the dried films..... | 186 |
| 6.2.1 | Influence of the distance between working and counter electrode | 187 |
| 6.2.2 | Influence of the applied potential | 188 |
| 6.2.3 | Influence of the gelator concentration..... | 193 |
| 6.2.4 | Influence of the concentration of the background electrolyte | 198 |
| 6.2.5 | Influence of the gelation time | 201 |
| 6.3 | Tunable gel film properties <i>via</i> electrogelation and possible fields of application | 205 |
| 7 | Summary..... | 209 |
| 8 | Zusammenfassung..... | 215 |

| | | |
|-----------|--|------------|
| 9 | Experimental part | 223 |
| 9.1 | Materials..... | 223 |
| 9.2 | Standard characterization methods..... | 223 |
| 9.3 | Synthesis..... | 224 |
| 9.3.1 | <i>N,N',N''</i> -Tris(4-aminophenyl)-1,3,5-benzene tricarboxamide 1 | 224 |
| 9.3.2 | <i>N,N',N''</i> -Tris[4-(<i>N,N</i> -dimethyl)-aminophenyl]-1,3,5-benzene tricarboxamide 2 | 225 |
| 9.3.3 | <i>N,N',N''</i> -Tris(4-hydroxyphenyl)-1,3,5-benzene tricarboxamide 3 | 226 |
| 9.3.4 | <i>N,N',N''</i> -Tris(4-carboxyphenyl)-1,3,5-benzene tricarboxamide 4 | 227 |
| 9.3.5 | Sodium salt of <i>N,N',N''</i> -tris(4-carboxyphenyl)-1,3,5-benzene tricarboxamide 4Na | 228 |
| 9.3.6 | <i>N,N',N''</i> -Tris(4-carboxyphenyl)-1,3,5-benzene tricarboxamide trimethyl ester 5 | 229 |
| 9.4 | Advanced methods and preparation techniques..... | 230 |
| 9.4.1 | Morphological studies and X-ray diffraction investigations..... | 231 |
| 9.4.2 | Investigations regarding the pH-sensitive aggregation and gel formation..... | 233 |
| 9.4.3 | Gel preparation methods..... | 235 |
| 9.4.4 | Characterization of gel properties..... | 237 |
| 9.4.5 | Spectroscopic investigations..... | 238 |
| 9.4.6 | Theoretical calculations..... | 240 |
| 9.4.7 | Biocompatibility tests..... | 240 |
| 9.4.8 | Investigations regarding the adsorption properties of gels of 4 | 242 |
| 9.4.9 | Hydrogel formation in presence of rhodamine B and release in water..... | 246 |
| 9.4.10 | Release studies in biologically relevant media..... | 247 |
| 9.4.11 | Hydrogel film formation <i>via</i> electrogelation..... | 251 |
| 10 | References | 253 |
| | List of Publications | 279 |
| | Danksagung | 281 |
| | (Eidesstattliche) Versicherungen und Erklärungen | 285 |

1 Introduction

1.1 Hydrogels

1.1.1 Definition and classification of gels

1.1.1.1 Definition

Gels are important materials that are omnipresent in our daily life, although we are often not aware of it. Depending on their constitution and properties, they can be found in very different applications and industries, such as food industry, cosmetics and medical applications.^{1,2} Amongst others natural hydrogel components can be found in jelly fish, connective tissue joints, in the cornea of the eye, and inside cells.³ Very prominent naturally derived gels are pectin, alginate, agars, collagen and of course gelatin. Although they have been used as thickeners in jellies, hair styling products or for the growth of bacteria cultures for a long time, up to now a clear definition of a gel is still missing. This is due to the fact that despite its characteristic form, the term “gel” describes several different states of matter and material classes.⁴ And so the famous quote of Jordan D. Lloyd from 1926 is still valid today: “The colloidal condition, the gel, is one which is easier to recognize than to define”.^{5,6}

Despite these difficulties, P. H. Hermans gave the first definition for gels in 1949 connecting the macroscopic appearance with the proposed microscopic structure.⁷ He stated the following three propositions: i) a gel consists of a coherent colloidal system with at least two components; ii) the mechanical properties are that of a solid (solid-like behavior); and iii) both, the dispersed component (the gelator) and the dispersion medium (the gelation medium) extend themselves continuously throughout the whole system. If taken literally, for example vulcanized rubber, dry gelatin and polymeric xerogels are excluded by this definition.⁸ Therefore, Flory proposed in 1974 that the imminent property for a gel is the solid-like behavior on the time scale of the experiment and that every other proposition, such as the continuity of the structure on a macroscopic scale as well as the coherent distribution of the gelator in the medium, can be derived from that property.⁸ This definition still leaves room for interpretations, as the “time scale of the experiment” is not defined in detail to avoid the exclusion of a material that is widely accepted as a “gel”. As a phenomenological definition, Almdal *et al.* proposed the following: “i) a gel is a soft, solid or solid-like material of two or more components one of which is a liquid, present in substantial quantity; and ii) solid-like gels are characterized by the absence of an equilibrium modulus, by a storage modulus, $G'(\omega)$, which exhibits a pronounced plateau extending to times at least of the order of seconds, and

by a loss modulus, $G''(\omega)$, which is considerably smaller than the storage modulus in the plateau region.”⁶ Thus, gels usually show viscoelastic properties with a flow behavior between that of an ideal fluid and an ideal solid.^{9,10} Depending on the difference between the storage and the loss modulus, gels are classified as “strong” and “weak” gels. All gels independent on their mechanical strength are assigned to the class of “soft materials”. These soft materials comprise emulsions, foams, colloids, polymers, and gels and have gained more and more importance in the recent decade.¹¹⁻¹⁴

1.1.1.2 Classification

Due to the complexity of a definition of a gel it is more reasonable to characterize this class of material by assigning the gels to different categories dependent on their gelation medium, their origin, or their constitution.

In respect to the gelation medium, gels are classified in *organogels* that immobilize organic solvents and *hydrogels* that trap high amounts of water or aqueous solvents. A special type of gels are *xerogels* or *aerogels*, as in these gels the solvent is absent. According to the IUPAC definition Freundlich described xerogel system as follows: “When the gel is completely freed of the liquid, a coherent framework with a certain, though sometimes very low, porosity may still exist.”¹⁵ So usually these terms are used for dried hydro- or organogels.

Natural derived gels are mainly hydrogels with water as gelation medium. They are used for drug delivery, tissue engineering, cell culturing and even the new trend “molecular cooking”.^{2,16-20} Natural derived gels are often promoted and favored as they are thought to be more biocompatible. However, hydrogels derived from animals, bacteria or carcinoma have serious disadvantages, as they show batch-to-batch differences and their use as biomaterials for pharmaceutical therapies in humans is limited.^{11,21} Therefore, the interest in synthetic or man-made gels increased since the middle of the last century and many different gelators have been discovered.

Gels can also be distinguished according to the constitution of the gel network. A gradient from fully covalent bound gel networks to gels that are solely held together by non-covalent interactions can be observed. According to this, gels can be classified into four different categories: i) polymeric hydrogels, that are chemically cross-linked, result in a fully covalent bound network,^{6,22-31} ii) physically cross-linked polymeric gels form cross-links between polymer chains *via* non-covalent interactions or simply by entanglements,^{16,32-35} iii) recently low molecular weight polymers or oligomers with molecular weights of 2000 – 12000 g mol⁻¹ were introduced, that can be cross-linked by small organic molecules *via* non-covalent interactions.³⁶⁻³⁸ This class forms a bridge between the polymeric gelators and the fourth class: iv) low molecular weight (lmw) gelators are small organic molecules with molecular weights

below 2000 g mol⁻¹ that self-assemble into hierarchical three-dimensional structures solely by non-covalent interactions.

Chemically cross-linked polymeric gels usually show a high mechanical stability due to the covalent nature of the cross-links and bonds. Addition or removal of the solvent causes swelling or shrinkage of the network. Thus, gelation is mainly a swelling process and the expansion of the network is limited by the non-reversible bonds.¹²

Physically cross-linked gels are often reversible and by changing the temperature, the polymers can be dissolved. Analogously to the chemically networks they often have a high gelator content from 5 to 15 % w/v (weight per volume) of polymer, but generally a lower mechanical stability.³⁰ Most natural gels, such as gelatin, collagen, and starch belong to this class of polymeric gels.³⁹ Since the 1950s, there is a great interest in applying chemically and physically cross-linked polymeric hydrogels as biomaterials in medicine and pharmacy. The most prominent example is probably polyhydroxyethylmethacrylate (polyHEMA), widely used for contact lenses. Polymeric hydrogels are also used as artificial extracellular matrices, as wound-healing materials, as drug and gene delivery systems, and as scaffolds for cell therapy, tissue engineering, and regeneration.^{2,20,33,35,40,41}

The third class of gels, *oligomers* that are *cross-linked by small organic molecules via* non-covalent interactions, have gained interest in the scientific community in the last decade. The separate solutions usually have a low viscosity, while after mixing gels are formed with a sufficient high mechanical stability. Therefore, they are investigated regarding their ability to serve as scaffolds for tissue engineering, and as injectable and degradable drug delivery systems.^{16,17,42}

The class of *low molecular weight (lmw) gelators* will be discussed in more detail in the following as the studies presented in this thesis deals with this class and the resulting supramolecular hydrogels.

Lmw gels are supramolecular gels in the strictest sense, as the interactions between the small molecules as well as the interactions between the resulting superstructures are non-covalent.³⁹ A typical gel is prepared by heating a mixture of gelator and solvent above the critical gelation temperature. During the subsequent cooling the gelator forms a three-dimensional network that can immobilize large amounts of liquid *via* capillary forces and due to the surface tension of the fluid phase. Often this network is referred to as “self-assembled fibrillar network” (SAFIN).^{4,39,43–46} Lmw gelators have been investigated for decades, but only in the last ten years the systematic studies resulted in some achievements regarding the design of the gelators. In the middle of the last century gelling agents were only found by serendipity, *e. g.* when purification treatments, such as crystallization and precipitation failed and

produced a solid-like material. At the beginning of the research effort regarding low molecular weight (lmw) gelators mainly gels, that were able to immobilize great amount of organic solvents, were investigated, as they were thought to be useful in many different areas of application.^{44,47-49} Truly, nowadays, these so-called organogels are used in hydrometallurgy, for the recovery of crude oil, in food processing, in cosmetics as thickener in ointments, shampoos, and creams, as aviation fuel, and in lubricants. With increasing research interest in the properties and applications of molecular gels, the wish to design gelators that were also able to gel aqueous systems (lmw hydrogelators) with distinct characteristics became more and more imminent.^{9,50-55}

Low molecular weight (lmw) gelators show various *interesting properties* that makes them competitive to polymeric systems: i) the spontaneous self-assembly leads to hierarchical supramolecular structures with well ordered domains within the fibers; ii) the molecular arrangement within the gel network is based on molecular recognition. Thus, the overall structure and the resulting properties of the gel can be changed by varying the structure of the gelator molecule. iii) The gels are responsive to external triggers due to the presence of solely non-covalent interactions; and iv) due to the high gelation efficiencies of the low molecular weight (lmw) gelators only low amounts of gelator are needed compared to polymeric systems.⁹ This raises the hopes of scientists that low molecular weight (lmw) gelators cannot only find applications in low cost, mass products such as shampoos and lubricants, but also in high tech applications, such as biomaterials for controlled drug release, as scaffolds for biomineralization and tissue engineering or in electronic devices for sensors, actuators, or as molecular wires.⁵⁶

In the progress of *finding new low molecular weight (lmw) gelators* important structure-property relations could be determined that clearly state, that the molecular structure of the gelator, but also the solvent plays an important role on the involved interactions and, therefore, on the self-assembly of the molecules.⁹ Two different approaches are used for the systematic identification of new gelators, the molecular engineering and the crystal engineering approach. The molecular engineering approach tries to modify known gelators to identify new gelators. With this approach only gelators similar to the parent gelators can be prepared and often large libraries of molecules must be investigated to achieve results. The crystal engineering approach tries to identify important intermolecular interactions and effective functional moieties or groups of functional moieties (building blocks) that enable or promote gelation.⁵⁰ To be able to understand the principles of gel formation, it is inevitable to understand the interactions between the gelator molecules and between the gelator molecules and the solvent.

1.1.2 Important intermolecular interactions

Already in 1987 the Nobel Prize in chemistry was awarded to Donald J. Cram, Jean-Marie Lehn, and Charles J. Pederson “for their development and use of molecules with structure specific interactions”. These important findings in *supramolecular chemistry*, as Lehn called it, enable us now to understand the non-covalent interactions between molecules.^{57,58}

While covalent bonds have binding strengths in the range of 50 kJ mol⁻¹ to 1000 kJ mol⁻¹, the physical or non-covalent binding strengths are mostly lower and therefore are often referred to as “weak” interactions. In Table 1.1 the binding strengths of non-covalent interactions are summarized.¹²

Table 1.1: Bindings strength of typical non-covalent interactions.¹²

| type of bond | binding strength [kJ mol ⁻¹] |
|---------------------------|---|
| ion bond | 100 - 350 |
| ion-dipole bond | 50 - 200 |
| hydrogen bond | 5 - 120 |
| cation- π interaction | 8 - 80 |
| dipole-dipole interaction | 5 - 50 |
| π - π interaction | 0 - 50 |
| van-der-Waals interaction | < 5 |
| hydrophobic interaction | - |

Despite the low binding strength of these interactions, self-supporting gel networks that are able to immobilize high amounts of solvents can be formed by lmw gelators. Often gelator concentrations of only 1 % w/v or lower are reported, which means that a gel network develops its solid-like behavior while consisting of 99 % or more of solvent. Such macroscopic stable gels obtained at so low gelator concentrations are only feasible by using gelator molecules consisting of several functional moieties or building blocks and by the combination and cooperation of different physical bonds. These building blocks are based on the principles of molecular recognition that are also found in biological systems and enable directed aggregation into very specific superstructures.^{33,38,59-62}

Although most lmw gels do not display the same mechanical strength as polymeric gels, due to the “weakness” of their bonds they have several advantages over covalently bound gels, such as the spontaneous association of small molecules into hierarchical structured aggregates, the reversibility of the gel formation, and the possibility to tailor the properties of the gel by designing the molecular structure of the gelator.

1.1.3 Gelation mechanisms and hierarchical structures of lmw hydrogels

Although the intermolecular non-covalent interactions and the respective functional moieties are known, up to now it is still challenging to design lmw gelators. This is mainly because the underlying gelation mechanism is not completely understood.

As the interaction with the solvent plays an important role in the self-assembly of the gelator molecules, when discussing possible aggregation routes and gelation mechanisms it is reasonable to distinguish between the formation of organo- and hydrogels. Although some main principles of the processes explained below may also be true for lmw organogels, the main focus of this work lies on the better understanding of lmw hydrogelators.

Similar to the *hierarchical structure* of protein aggregation the self-assembly process of lmw gelators can be distinguished into different hierarchical levels that are all influenced by non-covalent interactions.⁹ The molecular structure of the gelator molecule is the *primary structure* and dependent on the present functional moieties anisotropic aggregation is induced *via* directed non-covalent interactions, such as hydrogen bonds, and π - π -stacking.⁵⁵ The molecular structure lies within the range of Ångström and nanometers and can be easily investigated by techniques, such as nuclear magnetic resonance spectroscopy (NMR), mass spectrometry (MS), and elemental analysis.

The resulting mostly one-dimensional aggregates are the *secondary structure*, which are usually in the range of nano- to micrometers. Depending on the molecular structure of the gelator their form can vary from (worm-like) micelles, vesicles, to threads, fibers and tapes. While it is known that micelles and vesicles are mainly formed by classical surfactants with gelation abilities, recently the interest increased in understanding the mechanisms that drive the formation of one-dimensional aggregates with a high aspect ratio, so called “supramolecular polymers”.⁶³ Supramolecular polymers are solely formed by non-covalent interactions between the single molecules that act as molecular repeating units, but exhibit polymeric properties in bulk or diluted solutions. The different identified supramolecular polymerization mechanisms are limited to linear aggregates and do not describe the formation of supramolecular networks. Nevertheless, the insights into one-dimensional aggregation mechanisms might also help to understand processes that enable gel formation.

The aggregation of secondary structures *via* non-covalent interactions, such as van-der-Waals interactions, dipole-dipole interactions and electrostatic forces, gives in turn superstructures, such as rod-like micelles, lamella, fiber bundles, and ribbons in the range of micro- to millimeters. This *tertiary structure* forms the continuous and stable network that shows solid-like behavior. The macroscopic properties of the gel can be investigated by various techniques,

such as scanning electron microscopy (SEM), transmission electron microscopy (TEM), rheology, spectroscopy, diffraction, and modeling.^{10,45,64}

Usually it is most challenging to analyze the meta-state or the secondary structure, as the dynamic processes during the gelation are disturbed by most characterization methods and *in situ* techniques are rare. Thus, it is still challenging to get reliable data and to interpret them correctly. Therefore, the exact gelation mechanism and all the essential parameters are not yet fully understood.

In 2009 Rhagvan proposed the existence of two different *gelation mechanisms*, one with “crystalline assemblies” and one with “amorphous assemblies”.⁴³ The first one is based on a nucleation and growth mechanism. At high temperatures the gelator molecules are molecularly dissolved, and upon cooling a saturation effect of the solution leads to the formation of crystalline nuclei. From these nuclei, fibers start to grow which might interconnect resulting in a three-dimensional network. As the gelation is kinetically controlled, the gels formed *via* this mechanism are usually turbid, rigid and have a defined melting temperature.⁴³

It is important to note that this mechanism might lead to kinetically trapped gels that are meta-stable and might alter their properties upon aging. Furthermore, the exact preparation protocol is needed to reproduce gel samples with the same properties.⁶⁵

The mechanism with amorphous assemblies is thermodynamically controlled and based on the self-assembly of amphiphiles or tensides. Above the critical micellar concentration the gelator molecules form small micelles. By decreasing the temperature, adding more gelator or a second component, worm-like micelles with a high aspect ratio are formed. These elongated assemblies can interconnect to form transparent gels. Often these gels show softening before melting and are rather highly viscous solutions with “self-healing” properties.

Although Raghaven only proposed these two mechanisms, there might be also gels that are formed by a combination of both approaches.⁶⁶ Information about the gelation mechanism is very important when trying to predict the properties of the resulting gels. Therefore, the molecular structure of the gelator has to be designed carefully to yield effective hydrogelators with very distinct properties.

1.1.4 Considerations regarding the design of lmw hydrogelators

1.1.4.1 Hydrophilic-lipophilic balance (HLB)

Despite the structural diversity of identified supramolecular hydrogelators and the variety of successfully used building blocks, all lmw hydrogelators have one thing in common: a sensitive balance between hydrophilic and hydrophobic interactions.^{9,66–68}

This hydrophilic-lipophilic balance (HLB) is not only determined by the interactions between the gelator molecules, but also by the contribution of the solvent. It provides a sufficient solubility and avoids neat crystallization or the formation of an amorphous precipitate with subsequent phase separation. If this balance is disturbed, *e. g.* by slightly changing the molecular structure, the molecule is either perfectly soluble or precipitates. This is impressively demonstrated by a series of maleamic acid based amphiphilic hydrogelators, which were recently published by our group (Figure 1.1).⁶⁶

maleamic headgroup amide unit phenyl ring alkyl chain

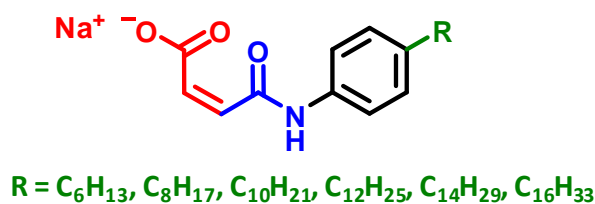


Figure 1.1: A series of maleamic acid based amphiphilic hydrogelators with different alkyl chain lengths.⁶⁶

Dependent on the length of the alkyl chain the molecules assemble in a different manner, which can be illustrated by the calculated aggregation modes of the dimer. Compounds with a short alkyl chain (C_6 and C_8) show a yellow color. It is proposed that in the dimer the molecules stack on top of each other with one molecule being rotated by 180° . This arrangement is favored due to π - π interactions between the double bond of the maleamic acid headgroups of one molecule and the phenyl ring of the second molecule. Aggregation is furthermore promoted by hydrogen bonding between the amide moieties. Above an alkyl chain length of C_{10} the hydrophobic interactions of the alkyl chain become more pronounced. This leads to a dimerization with both molecules being aligned above each other resulting in a white color of the compounds. Besides the hydrophobic interactions of the alkyl chains there are also π - π interactions between the two phenyl rings and a hydrogen bond between the two amide moieties. Such an arrangement of the molecules with an alkyl chain length of C_{14} leads further to the formation of anisotropic aggregates that are able to immobilize high amounts of aqueous sodium hydroxide solutions. Thus, with the increase of the alkyl chain length the solubility of the compounds in aqueous media decreases resulting either in hydrogel formation (C_{14}) or no solubility at all (C_{16}).

This clearly demonstrates the importance of the HLB and the influence of small changes in molecular structure on the gelation ability. The aim in designing low molecular weight hydrogelators is to encode the macroscopic properties in the molecular structure, similar to the genetic

information that is stored in the structure of the DNA. Thus, upon self-assembly very distinct superstructures with specific properties can be achieved.

1.1.4.2 Influence of the environmental conditions and responsiveness to external stimuli

Not only the molecular structure of the gelator molecule is crucial when trying to design low molecular weight gelators with specific properties, but also the environmental conditions, such as the ionic strength, the pH value, and the temperature of the solvent, must be considered.

In organic solvents mainly hydrogen bonds promote the directed one-dimensional aggregation. As hydrogen bonds lose their efficiency in water, if they are not shielded from the water, hydrophobic interactions become more important in aqueous environments. Different building blocks have been identified to be important for the design of low molecular weight organo- and hydrogelators. Therefore, there are only a limited number of ambidextrous gelators reported in the literature that are able to gel organic and aqueous solvents.^{69–72}

In the literature examples of low molecular weight “hydrogels” are known that only form, or show improved mechanical stability, in the presence of an organic co-solvent, such as DMSO, methanol or ethanol.^{12,73–75} These gels are not hydrogels in the strictest sense, as they consist of 1 % to 10 % of an organic solvent. Therefore, they are not further considered in this work.

In aqueous media the aggregation of the hydrophobic gelator molecules *via* non-covalent interactions leads in general to a decrease of the interface between hydrophobic aggregates and water. Due to this decrease of the surface energy the high order of the gelator molecules is possible in the gel state.¹² This fact furthermore enables the system to restore the gel state after destruction. As low molecular weight hydrogelators are usually thermo-reversible, this can be achieved by simply applying a heating and cooling cycle. However, also other external stimuli might be used to influence the gelation process.

When dealing with low molecular weight hydrogel systems, one must distinguish between parameters that are changed to optimize the gel properties and external stimuli that lead to a transition from the gel to the sol state and *vice versa*. There have been many attempts to alter gel properties, *e. g.* the gel-sol-transition temperature^{76,77} or the viscoelastic properties⁷⁸ by a change of the pH value or the addition of salt. The drug release rate of a hydrogel was successfully adjusted by the temperature, the enzyme concentration or the pH value,^{79,80} and the morphology and the photoluminescence properties of a two-component gelator could be changed by varying the composition of the respective components.⁸¹

All of the gels described above show some kind of responsiveness to the change of environmental conditions. However, usually in the literature the responsiveness of a gel

system to an external trigger describes the reversible transition between the gel and the molecularly dissolved sol state.

Dependent on the molecular structure of the gelator molecules many different external stimuli can be realized for the sol-gel transition. The thermal responsiveness is the most common trigger for gel formation or dissolution.^{9,39} But there are also examples of gels that are additionally responsive to another stimuli, such as change of pH,^{46,65,78,82-89} change of ionic strength,⁸² metal ion coordination,⁹⁰ light,⁹¹⁻⁹³ oxidation or reduction.⁹⁴ Discussions about multi-stimuli responsive gelators mostly refer to gelators that are sensitive to more than one stimulus additionally to the thermal-responsiveness. Recently, a ferrocenyl-phenylalanine-based hydrogelator was presented.⁵⁴ Its phase transition was induced by changing the pH value, the redox potential, the temperature, or by agitation. Every stimulus worked independently from the other. In other hydrogel systems, however, several external triggers have to be altered consecutively to change the gel to the sol state.⁹⁵ It is often reported that hydrogels only show stable gel formation within a distinct range of *e. g.* the pH value or the concentration of a specific salt. Outside of this range, either gel dissolution or precipitation eventually occurs.⁹⁶

To achieve sensitivity towards other stimuli than temperature, usually a receptor or molecular recognition unit must be integrated in the molecular structure of the hydrogelator. As this receptor unit can alter the properties of the whole gel or even affect the gelation ability, it must be chosen carefully to fit into the self-assembly concept of the gelator.³⁹ Usually an acidic or basic group is used to induce pH-sensitivity. Very prominent is the class of Fmoc-peptides that contain a carboxylic acid group which can induce solubility or molecular self-assembly depending on the pK_A value of the respective acidic moiety.^{17,51,82,88,97} Many of these gelators form gels between a pH value of 3 to 5. Their gel formation *via* the addition of a mineral acid solution, such as aqueous HCl solution, often results in the formation of inhomogeneous gels, as gel formation takes place faster than the homogeneous distribution of the added acid. Consequently, this leads to an inhomogeneous pH value in the solution. By adding glucono-delta-lactone (GdL, Figure 1.2) instead of aqueous HCl solution to the gelator solution, pH-sensitive gels can be prepared homogeneously.^{54,88,98-102} The GdL molecules are dissolved and distributed in the solution faster than their hydrolysis and proton formation occurs.¹⁰³ This can lead to hydrogels with improved mechanical properties showing that despite forming the gel *via* the same external stimuli, such as decreasing the pH value, the exact gelation method is crucial for the resulting properties of the gel.⁷³ Recently, independent studies in the groups of Wang and Adams confirmed the importance of the gelation method on the gel properties, especially regarding the mechanical stability.^{65,93}

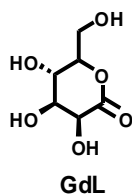


Figure 1.2: Structure of glucono-delta-lactone (GdL).

Concluding, the molecular structure of new lmw hydrogelators must be design considering the hydrophilic-lipophilic balance, the environmental conditions, such as the solvent system, and the gelation method. As these factors influence the self-assembly of molecules dependently on each other, the design of new lmw hydrogelators or the *a priori* determination of the respective gel properties under specific conditions is still a major challenge for scientists. There might be even more relevant effects present in such complex aggregation processes, that - up to now - we are not aware of. However, the development of some successful concepts for the adjustment of gel properties and the systematical approach to find new gelators raise the hope that one day self-assembly processes will be fully understood.

1.1.5 Typical molecular structures of lmw hydrogelators

In the following, some typical classes of lmw hydrogelators and their molecular structures are presented exemplarily to give a small insight in the high structural diversity of this field, but also to derive some similarities that might help to design new lmw hydrogelators.

Due to the increased interest in lmw hydrogelators in the recent decades, obviously, not every class of lmw hydrogelators can be discussed in this work. However, there are several review articles summarizing the late achievements very well.^{9,10,12,82,104}

The first reported lmw hydrogelator was published in 1892. It was found incidentally during the synthesis of benzoylcystine as the precipitation of the product from aqueous NaOH solution with aqueous HCl solution resulted unexpectedly in a “thick jelly”.¹⁰⁵ The molecular structure is depicted in Figure 1.3 and shows that this first lmw hydrogelator comprises several functional moieties, such as an amide group, a primary amine, and two carboxylic acids. These moieties stand out due to the ability to form directed or complementary hydrogen bonds. Furthermore, the amine and carboxylic acid groups provide the necessary solubility and the reported pH-sensitivity. The second important building block in the molecular structure is the presence of the benzene ring that enables π - π -stacking as well as hydrophobic interactions. Even though, at that time, the importance of the right combination of different intermolecular

interactions to provide gel formation was still unknown, this first lmw hydrogelator clearly shows a hydrophilic-lipophilic balance (HLB).

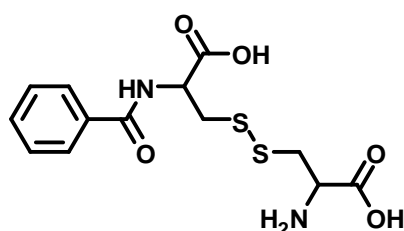


Figure 1.3: Molecular structure of benzoylcystine, the first reported lmw hydrogelator in 1892.¹⁰⁵

This HLB is mandatory for all lmw hydrogelators despite their structural diversity. As such a balance is also present in surfactants, tensides, and lipids, especially the investigation of this class resulted in the serendipitous discovery of new lmw hydrogelators. These are categorized in conventional amphiphiles,^{10,106,107} bolaamphiphiles^{83,108,109} that have a hydrophobic unit between two headgroups, and gemini-surfactants^{110,111} that consist of a headgroup between two hydrophobic units (Figure 1.4). Due to high number of amphiphilic lmw hydrogelators with a polar or ionic water-soluble headgroup, their sub-classification is based on the type of the headgroup.⁹ Very common headgroups are for example saccharides or sugars,^{91,112,113} bile acids,⁴⁵ urea moieties, cholesterol,^{94,114} quaternized amines, amino acids⁶¹ and especially peptides.^{65,67,82,88,93,97,115–117}

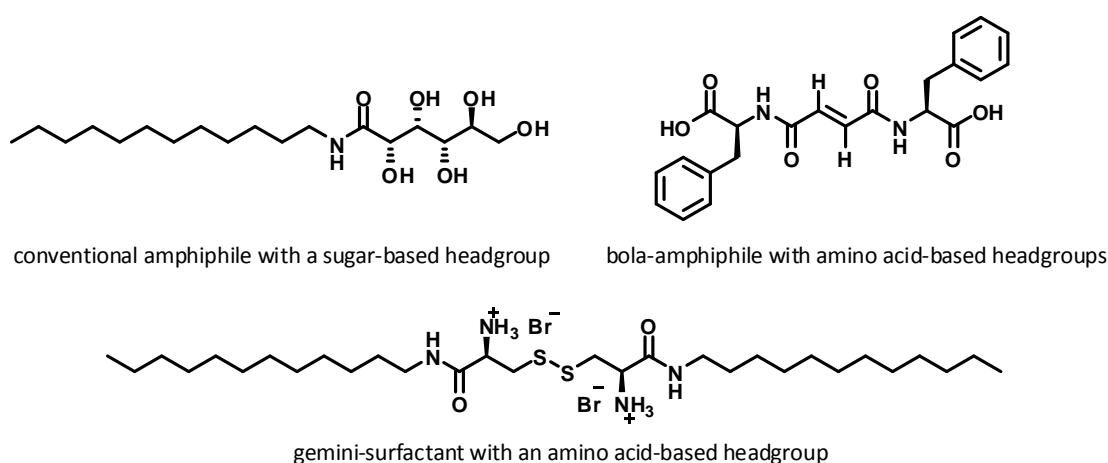


Figure 1.4: Typical molecular structures of amphiphilic lmw hydrogelators.^{106,109–111}

As essential structural motifs for amphiphilic lmw hydrogelators four different segments were identified: a hydrophilic headgroup, a rigid unit, a flexible linker, and a hydrophobic tail.¹⁰ Keeping this molecular concept in mind, different amphiphilic lmw hydrogelators were

prepared successfully in our group.^{66,76,77} Dependent on the kind and the arrangement of those different units, hydrogels with different properties were obtained.

Beside amphiphilic low molecular weight hydrogelators, there are also many examples with a rather different molecular structure, such as dendrimers, C₃-symmetric cyclohexane derivatives,¹¹⁸ resorcin-based gelators,⁸⁹ metallopolymers,^{83,119–122} two-component hydrogelators,^{85,123–125} or azobenzenes,^{126–128} which are usually known as coloring agents or dyes. In Figure 1.5, exemplarily one of the first azobenzene-based hydrogelators benzopurpurin,¹²⁶ a metallopolymers based on a trinuclear Cu(II) complex of inositol,⁸³ and a two-component hydrogelator based on two guanosine derivatives¹²⁹ are shown.

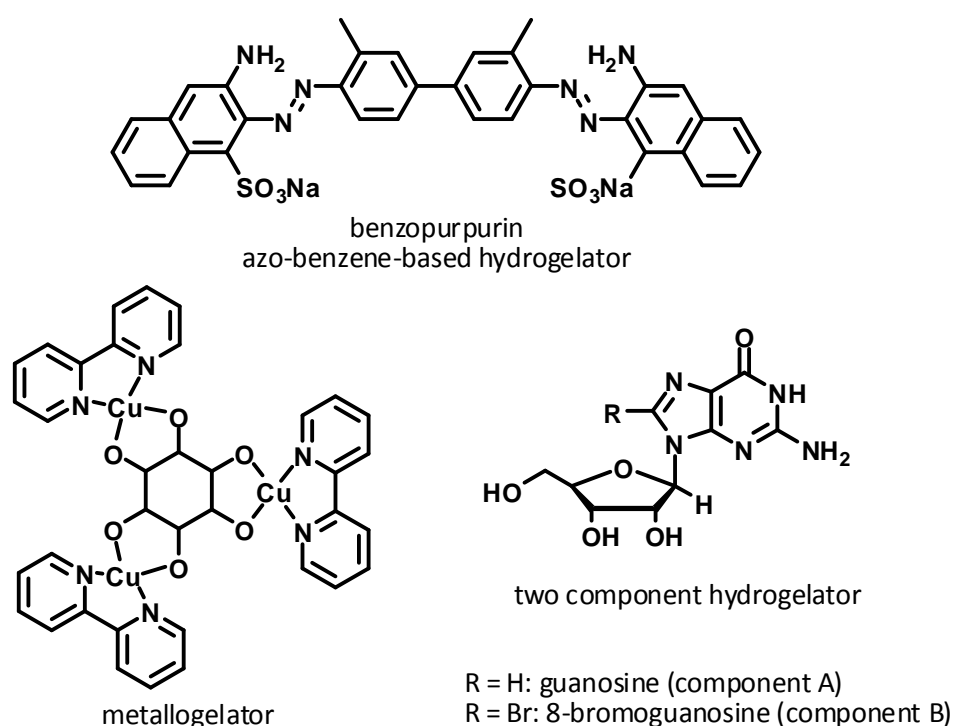


Figure 1.5: Examples of low molecular weight hydrogelators showing the large variety of molecular structures.^{83,126,129}

Interestingly, some of the found low molecular weight hydrogelators are based on organogelators. By systematic changing the molecular structure of known low molecular weight organogelators, hydrogelators could be obtained.^{70,130} However, when transferring the structure of an organogelator to that of a hydrogelator, one has to keep in mind that hydrophobic interactions are usually more pronounced in water than in organic solvents, while hydrogen bonds often lose their directionality, if they are not shielded.^{131,132} Furthermore, interactions such as metal ion coordination and salt bridges become more important in aqueous systems.¹⁰

Summarizing, up to now many different low molecular weight hydrogelators with a large range of molecular structures have been identified. The large variety of concepts that could be successfully

applied nourishes the idea that any molecular structure might be transferred into a potent lmw hydrogelator, if it is combined with the right building blocks and tested under adequate environmental conditions.

In the following (chapter 1.2), a well-known self-assembly motif is illuminated in detail. Interestingly, although numerous studies regarding the self-assembly of 1,3,5-benzene tricarboxamide (BTA) derivatives have been performed, only few BTA-based, lmw hydrogelators are known up to now. The detailed insights into the performed self-assembly studies of various BTA derivatives in different environments might help to understand the complex task to design a new lmw hydrogelator system for a specific application, even when it is based on a well-known self-assembly motif. Subsequently, possible applications of lmw hydrogelators (chapter 1.3) and the advantages of the “electrogelation” technique (chapter 1.4) are discussed in more detail.

1.2 1,3,5-Benzene tricarboxamides

1.2.1 A versatile structural motif

Nearly a century ago the first 1,3,5-benzene tricarboxamide (BTA) was synthesized and its molecular structure published (Figure 1.6a).¹³³ Since then, many groups have been interested in the structural modification and application of this, originally C_3 -symmetric, building block. The review of Palmans *at al.* from 2012 nicely summarizes the recent achievements in synthesizing BTAs and investigating their self-assembly properties in bulk and different dilute solutions.¹³⁴ The common structural motif of all BTA derivatives consists of three structural specifications: i) a planar benzene core; ii) three C-centered amide groups in the positions 1, 3, and 5 leading to a C_3 -symmetry of the molecule; and iii) lateral functional moieties or substituents R that are attached to the amide units. The lateral substituents R can be varied in multifold ways, thus eventually breaking the C_3 -symmetry (Figure 1.6b).

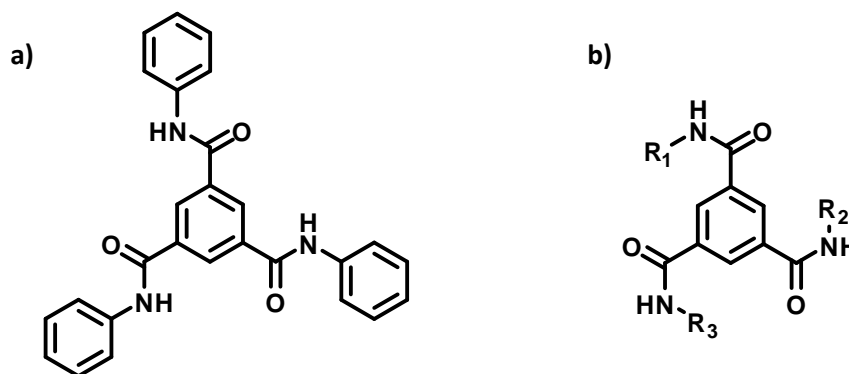


Figure 1.6: a) The first published BTA derivative¹³³ and b) the basic molecular structure of BTAs with three C-centered amide moieties.

Usually, this basic molecular structure leads to supramolecular columnar aggregates, where the benzene cores are stacked on top of each other with π - π -distances mostly in the range of 0.33 nm to 0.38 nm. Thereby, adjacent molecules in the stack are rotated by 60° so that the amide moieties and the respective substituents R are staggered. Triple hydrogen bond formation between amide moieties of adjacent molecules is enabled by a slight twist of the amide units out of the plane of the benzene core.^{134,135} In columnar aggregates the triple hydrogen bond formation, usually leads to a helicity in the columns that can be enhanced or driven to a preferred direction by using chiral substituents.¹³⁶ The deviation angles of the three amide units are important tools to determine, if the molecular packing results in rather askew or straight columnar aggregates.¹³⁷ These angles can range from about 10° to about 45° and might deviate for the three amide units in one molecule, thus resulting in different core-core-distances and different length of the hydrogen bonds.

The exact molecular arrangement is strongly determined by the type of substituents and the environmental conditions, such as the solvent system and the temperature. Many different studies have been performed that have systematically varied the three specifications of BTAs. All together, they give a wide overview of the found structure-property relations and emphasize the unique combination of interactions present in such a small supramolecular motif.

To obtain insights into the role that the benzene core plays in self-assembling processes, often C_3 -symmetric cyclohexane-based 1,3,5-tricarboxamides were used for comparative reasons.^{135,138,139} Cyclohexane-based tricarboxamides feature the same molecule symmetry than BTA derivatives, but can interact very differently.^{46,84,86,118,140–142} While the benzene core is planar due to the conjugation of the π -electrons, the cyclohexane core is more flexible and can adopt the chair or boat configuration. Furthermore, the sp^3 -hybridization of the C-atoms in cyclohexane leads to different possibilities, how the amide moieties can be attached to the

core. Usually, cyclohexane-based 1,3,5-tricarboxamides with an *all syn* or *cis, cis* configuration are used, where all amide moieties are attached at the same side of the ring. De Loos *et al.* described the systematic change of the BTA-core to cyclohexane, thus giving interesting insight in the structure-property relation of BTA-based organogelators.⁴⁹

BTA derivatives that are additionally functionalized in the 2, 4, and 6 position are called “crowded aromatic” BTAs. Due to the enhanced steric interactions at the core, they exhibit quite different properties and are therefore not included in this work.^{55,143}

As the amide moieties act as hydrogen bonding units, they have a great influence on the aggregation behavior. First of all, the constitution of the amide moieties must be considered, *i. e.* whether they are *N*-centered, *C*-centered, or a combination of both resulting in an asymmetric substitution of the core.^{144,145} While the term *1,3,5-benzene trisamide* comprises both *N*- and *C*-centered derivatives, the term *1,3,5-benzene tricarboxamide* (BTA) used in this study solely refers to the *C*-centered derivatives. By inverting the amide moieties, so that the nitrogen atom is bound to the benzene core, also columnar aggregates are obtained, however, with slightly different molecular packing modes. Usually, lower torsion angles of the amide moieties out of the molecular plane are observed, that results in lower core-core-distances of adjacent molecules. Further information of the aggregation characteristics of *N*-centered or inverted BTAs can be found in the literature and will be not part of this work.^{139,145–147}

Often columnar assemblies of BTAs are displayed in such a manner that all amide moieties point in the same direction.^{147,148} However, recently it was shown by detailed molecular dynamic simulations that an antiparallel alignment of the hydrogen bonds, with only two moieties pointing in the same direction, is more likely.¹⁴⁹ It might also be possible that the two aggregation modes occur for different BTA derivatives.¹³⁹ Nevertheless, in all columnar aggregates of BTAs a macrodipole alongside the molecular stack is present. Solely its strength is depending on the alignment of the amide units and their respective torsion angles.^{139,150,151}

The influence of the trivalent hydrogen bonding unit on the aggregation behavior was investigated in different studies using urea groups or thioamides instead of the *C*-centered amide group. These studies showed that for BTAs with urea groups stronger hydrogen bonding interactions can be achieved leading to higher thermal stabilities and pronounced kinetic effects.^{49,152} In contrast, for thioamide derivatives weaker hydrogen bonding interactions can be expected compared to the respective amide derivative, resulting in dynamic supramolecular aggregates.¹⁵³ In some studies additionally the respective triester was synthesized as reference substance. As in these molecules no hydrogen bonds between the cores of adjacent molecules are possible, usually the directed one-dimensional aggregation of the compounds is lost.¹²⁸

Although this study is restricted to C-centered BTAs, the numerous possible substituents for the three side arms and the possibility for an asymmetric substitution of the core lead to an almost endless number of derivatives with multifold properties. Many different studies have been performed to investigate the influence of the lateral substituents regarding its size, its polarity, the presence of specific functional moieties and the introduction of a chiral center.¹³⁶ However, these substituents are mainly responsible for the interactions of the molecule with the surrounding media and thus determine possible fields of applications. Therefore, when discussing studies regarding the variation of the substituents, a classification of the BTAs regarding their application or their self-assembly environment is reasonable.

Summarizing, all these studies give a good idea about the unique combination of interactions that are present in BTA derivatives, which renders this a potent and widely used self-assembly motif. Dependent on the characteristics of the substituents and their interactions with the surrounding media, BTA-based compounds might be interesting for many different fields of application.

1.2.2 BTAs as trivalent building block in synthesis and metal ion coordination

In the 70s of the last century the interest in BTA compounds was mainly motivated by the need of new multivalent crosslinking agents for branched and hyper-branched polyamide and polyester networks.^{154–163} Since then, it has been used as trivalent building block for the synthesis of various organic molecules that have been investigated in very different fields of applications, *e. g.* in energy transfer processes, for studying glass transition temperatures of molecular glasses, for mimicking biological structures and processes, and many more.^{164–180}

Furthermore, BTA compounds are interesting trivalent ligands for the coordination and complexation of metal ions. Examples of BTA-based structures, that stabilize ruthenium nanoparticles have been published, as well as new complexes for the catalysis of different reactions or the study of stable binuclear structures and their crystal structures.^{120,181,182,182–188} The preparation of new metal complexes for the catalysis of complex reactions is important, as suitable ligands can improve *e. g.* the reaction rate, the yield or stereoselectivity of a reaction and the reaction conditions.¹⁸⁹ These improvements might one day lead to the preparation of artificial enzymes that perform specific cascade reactions under mild and environmental friendly conditions.

Especially in the last five years the interest in highly ordered and porous materials increased. These so called organic coordination polymers^{190–196} or metal organic frameworks (MOFs)^{197–210} are formed by the spontaneous association of organic molecules and, in case of

MOFs, also metal ions. Due to their high porosity, they are interesting for adsorption and storage of gases, such as hydrogen, nitrogen, and carbon dioxide. The use of various different substituents for the preparation of these porous materials leads to a high number of published crystal structures. However, in most of these porous structures the BTA molecules assemble into sheet-like aggregates with structures similar to that of honeycombs. The stacking and intertwining of such two-dimensional structures usually results in complex three-dimensional networks with defined channels and pores in the range of several nanometers.^{198,205,209,211}

Thus, these structures differ very much from the one-dimensional, columnar or fiber-like structures usually gained by self-assembly studies of BTAs in bulk or organic liquids. The choice or the absence of a solvent as well as the preparation technique are therefore very important factors, when discussing the self-assembly behavior of BTA derivatives.

1.2.3 Self-assembly of BTA derivatives in various environments

1.2.3.1 In bulk

Many studies describe the self-assembly behavior of BTA compounds with various alkyl chain rests in bulk depending on the temperature.²¹² Often a liquid crystalline (LC) behavior with various mesophases can be found. Due to the unique combination of π - π -interactions of the benzene cores and the hydrogen bonds between the amide moieties, the disc-like molecules stack into more or less ordered columnar structures. Very typical is the columnar hexagonal phase in which the columns are arranged in a hexagonal ordered state. But also rectangular, plastic crystalline, and ordered LC phases could be identified for various BTA compounds.^{135,136,138,139,145,150,212–219}

Interestingly, the non-covalent interactions present between BTA molecules even at elevated temperatures allow the electrospinning of these molecules from the melt into nano- and microfibers.²²⁰ As no other material, such as a polymer, is present as a matrix material, the melt electrospinning process can only be realized for few small organic molecules with sufficient strong intermolecular interactions.²²¹ The BTA molecules that self-assemble upon cooling form stable electrospun fibers with Young's moduli comparable to self-assembled fibers from solution in the range of 3 to 5 GPa.²²⁰

1.2.3.2 In polymer melts

The application of BTAs as polymer additives is most advanced in terms of commercial use in industry. Many successful derivatives have linear, branched or cyclic alkyl rests. Besides the use as nucleating agent and clarifier for isotactic polypropylene (*i*-PP),^{144,222–224} BTAs can also be used to improve the electret properties of *i*-PP.²²⁵ The modifications of the polymer properties can be explained by the formation of small aggregates of the respective BTA

compound in the polymer melt upon cooling. These can act as nuclei for a more homogeneous crystallization of the polymer. Furthermore, recently the favored crystallization of *i*-PP into the mechanical more stable β -modification in presence of a BTA compound as additive was reported.²²⁶

1.2.3.3 In organic solvents

The aggregation of BTAs in various polar, apolar, protic and aprotic organic liquids was intensely studied and many different aggregation modes were found.

The self-assembly in organic solvents upon thermal treatment mainly results in one-dimensional columnar aggregates.^{132,214,227–234} The benzene cores of the disc-like molecules thereby stack above each other *via* π - π -interactions and triple hydrogen bonding. The induced helicity in the molecular stacks can be tuned by using BTA compounds with chiral side arms. Due to the “sergeant and soldier” principle even low concentrations of chiral substituted BTAs can force achiral BTA molecules into a preferred helicity.^{136,231}

Dependent on the substituents, supramolecular polymers, lyotropic liquid crystalline phases^{235–237} or superstructures, such as fibrils, fibers and needles can be obtained. While the formed superstructures are often kinetically trapped upon cooling, columnar mesophases and supramolecular polymers are usually thermodynamically stable and dynamic.²³⁸ Thus, the length of supramolecular polymers can be controlled by adding BTAs with tertiary amides.²³⁰ These are not able to form hydrogen bonds and therefore act as some kind of end-capper or terminating agent for the supramolecular assembly.

Some long, intertwining superstructures, mainly fibers, have the ability to immobilize the solvent molecules and form so-called organogels.^{49,239} The formation and the resulting properties of the organogels do not only depend on the BTA derivative, but are also influenced by the used solvent. It should be noted that not every organic solvent can be immobilized by the same BTA.²⁴⁰ Besides fibrillar structures of organogels, also nanorods can lead to a gelation effect.²⁴¹

As BTA compounds usually have a tendency to form anisotropic aggregates, there is only a limited number of BTAs that form two-dimensional aggregates, such as chiral sheets, in organic solvents.¹⁴⁶ Jana *et al.* investigated the influence of the side chain onto the aggregation behavior of BTAs to promote the formation of assemblies without a preferred one-dimensional direction. Finally, a porous material with an underlying three-dimensional network and high gas adsorption properties was obtained by introducing bulky side chains.²⁴²

Furthermore, for some derivatives single crystals could be obtained by using the right solvent system.^{128,146,194,210} However, one should keep in mind that the structure in the single crystal does not necessarily agree with the molecular arrangement obtained *via* a self-assembly

process.²⁴³ Due to the different preparation processes usually different structures are obtained. This is further supported by the observed polymorphism of some BTA derivatives.¹⁷⁵

Summarizing, although it is still not possible to predict which BTA derivative will form a distinct structure in a given organic solvent, there are many different self-assembly systems that have been intensely studied and are rather well-understood.

Recently, such BTA systems were used as side-arm functionalizations of a linear random copolymer. By changing the temperature or the solvent composition it was possible to introduce the self-assembly of the BTA motifs in the polymer chain. The folding of the polymers is similar to protein folding in nature and results in single chain nanoparticles (SCNPs).^{244–250} The folding of such SCNPs is not limited to organic solvents, but could also be realized for water-based solvent systems.²⁵¹

1.2.3.4 In mixtures of water and organic solvent

Based on the knowledge gained from the self-assembly studies in organic solvents, more complex solvent systems, such as mixtures of water and organic solvents, gained the interest of scientists. By changing the solvent composition, a wide range of polarities can be realized.

In mixtures of water and organic solvents, such as DMSO, DMF or THF, an azobenzene-substituted BTA compound self-assembled into fibers, gels and hollow spheres dependent on the solvent composition.¹²⁸ While the formation of single helices of stacked molecules in DMSO-water mixtures was expected due to the directionality of the threefold hydrogen bonding, in pure DMSO and aqueous THF solutions sphere formation could be observed, which is rather unusual for supramolecular BTA assemblies. Interestingly, the addition of water to DMF solutions led to gel formation *via* an entangled network of fibers.

Investigations regarding the self-assembly behavior of a 3,3'-bis(acylamino)-2,2'-bipyridine substituted BTA in water/alcohol mixtures showed that the composition of solvent as well as the solution temperature influences the aggregation of molecules.²⁵² At high *iso*-propanol concentrations and elevated temperatures single helical stacks of molecules are formed. Below a critical alcohol content short helical fibers consisting of three intertwined helical stacks are formed. In pure water these triple helices are elongated. This is attributed to the change of hydrophobicity at different solvent compositions and the different enthalpies of mixing.

These examples in aqueous organic solvents clearly show that the transformation of a well-known BTA derivative to aqueous systems can lead to completely new structures.

1.2.3.5 In water

As discussed above, the interactions for the self-assembly in water differ quite from those in organic solvents.

Studies of Stals *et al.* describe the self-assembly behavior in organic and aqueous solvents of BTA derivatives with different numbers of hydrophilic oligo(ethylene glycol) and hydrophobic alkyl side chains.^{131,132} They proposed that due to their flexibility, the ethylene glycol rests might fold back to the core to form intramolecular hydrogen bonds with the amide moiety of the BTA motif. This weakens the aggregation into single helical stacks in alkane solutions. In water for BTAs with two or three hydrophilic side arms no aggregation could be observed, as the amide moieties of the BTA core were not sufficiently shielded from the water molecules by a hydrophobic spacer.

The attempt of Leenders *et al.* to transfer the BTA self-assembly motif to aqueous solvents showed that even by slight changes in the constitution of the hydrophobic spacer different molecular packing modes can be obtained.²⁵³ The importance of the hydrophobic shielding of the core was systematically investigated by Besenius *et al.*. He and his co-workers used BTAs consisting either of a small, medium, or large hydrophobic spacer between the amide units of the core and the hydrophilic headgroups, that consisted of chelated metal ions.²⁵⁴ From this study it became obvious that the larger the hydrophobic spacer, the stronger the formed BTA aggregates in water. This was explained by the fact that hydrogen bonds between adjacent molecules can only form when they are shielded from the water molecules. Thus, the threefold hydrogen bonding was claimed to be the main driving force for the self-assembly of hydrophobic shielded BTA derivatives. Due to the electrostatic repulsion of the metal ion charges at the lateral headgroups, only globular aggregates were obtained.²⁵⁴

Self-assembly studies with related BTA derivatives, *i. e.* consisting of various large hydrophobic spacers and differently charged hydrophilic headgroups at the lateral substituents, were performed.^{255,256} These studies showed that at low salt concentrations well-defined spherical particles were formed *via* a frustrated growth mechanism. With increasing ionic strength in the solution, the screening of the charges led to a cooperative supramolecular polymerization mechanism with elongated helical aggregates. These elongated structures could even exist in a partially charged state, which led to the formation of nanorods with distinct degrees of surface charges.²⁵⁷

Frustrated growth due to repulsive Coulomb interactions was also reported by von Gröning *et al.* using nonaphenylalanines as hydrophobic shielding.²⁵⁸ These were linked to flexible spacers with three carboxylic acid headgroups per substituent for solubility. Besides the increase of the ionic strength of the solution, also the decrease of the pH value led to one-

dimensional aggregation due to electrostatic shielding or protonation of the ionic headgroups. At high salt contents and low pH values, the molecules were completely uncharged which resulted in unlimited fiber growth and even hydrogelation.

The formation of superstructures dependent on the BTA concentration in water was observed for an aramid-containing BTA derivative with sulfonic acid headgroups.²³⁶ With increasing concentration, the molecular dissolved molecules assembled first into stable clusters of seven molecules then into robust columns and further into nanofibers. High concentrations of the BTA compound in water even led to microfibers and fiber bundles that could be aligned by shearing. As the powder contained 83 % of relative humidity even in solid state, it might be assumed that the water molecules are trapped within or between the columns and fibers acting as some kind of hydrogen bonding bridge. It was proposed that the aggregation into superstructures was driven by the interactions of the sulfonic acid headgroups with water. However, this assumption could not be proven within the scope of the publication, although single crystals could be obtained for the compound. Two polymorphic structures with different orthorhombic cells could be identified. Due to steric reasons both structures consisted of laterally intercalating molecules. Thus, the molecular arrangements in the single crystals were very different from the columnar aggregates obtained during the self-assembly studies.

Junjun Li *et al.* described the self-assembly of sodium carboxylate decorated oligoamide-based BTAs that formed nanofibrils in a staggered fashion.²⁵⁹ Thereby, one sodium ion was bridged between the carboxylate groups of two adjacent molecules in the columnar stack. The alignment of these nanofibers to microfibers with several millimeters in length was directed by the alternating charges present at the surface of the single helical stacks.

These examples as well as the studies of Frisch *et al.*²⁶⁰ impressively demonstrate that Coulomb interactions are an effective tool to control the aggregation of BTA molecules in water.

The dynamic nature of such supramolecular BTA aggregates in water was shown by the co-assembly of BTAs with either neutral or different cationic headgroups. While upon mixing the charged BTAs were evenly distributed in the columnar stacks, a clustering of the charged BTAs could be achieved by using a polyanion as template.^{60,261}

BTA derivatives with crown ethers as hydrophilic headgroups at the side arms show a rather atypically self-assembly behavior as aggregation is induced by increasing the temperature.²⁶² A similar behavior is known for polymers with a lower critical solution temperature (LCST). Analogously to these polymers, the aggregation at elevated temperatures is ascribed to the loss of the hydration shell of the crown ethers.

Summarizing, the aggregation of BTAs in water can be achieved by introducing a large hydrophobic spacer that shields the amide unit of the core from the water and also prevents intramolecular hydrogen bonding. Charged hydrophilic headgroups at the lateral substituents allow for the control of solubility and aggregation *via* change of ionic strength and pH value. Although these generalized guidelines are valid for many different BTA derivatives, they cannot be applied for bipyridyl substituted BTAs. As the amide units of the core form intramolecular hydrogen bonds with the amine of the second pyridyl ring, the molecules can be described as rigid discs with an “extended core”. The one-dimensional aggregation of these derivatives in water is caused by π - π -interactions of the core and hydrogen bonds between functional moieties in the side arms.^{59,263}

Besides the experimental investigations on the self-assembly behavior of BTAs, computational studies and simulations become more and more important. Some of the studies presented above combine experimental and theoretical approaches. However, up to now mostly density functional theory (DFT) calculations were carried out in the gas state at zero Kelvin and did not consider supramolecular interactions with the solvent. Only recently, an atomistic molecular dynamics simulation study of BTAs in a realistic solvent was presented.¹⁴⁹ It indicated that the technical progress will lead to improved simulations that might one day render experimental self-assembly studies unnecessary.

1.2.3.6 BTA-based hydrogelators

Despite the various self-assembly studies of BTAs in water, only few BTA-based hydrogelators are known. Hydrogels can only be obtained when the aggregation is not limited by repulsive forces.²⁵⁸ Then, the formation of superstructures might lead to three-dimensional, self-supporting networks.

In 1983 the surfactant properties of crown ether-substituted benzenes at high concentration were investigated.²⁶⁴ One of the derivatives was based on the BTA motif. It was reported that the solutions became highly viscous and eventually immobilized the whole solvent volume. However, it was not clear from the description if this behavior was also observed for the BTA compound.

Finally in 2004, the first “real” BTA-based hydrogelators were reported by Kumar *et al.* (Figure 1.7a).²⁶⁵ The 3-pyridyl and 4-pyridyl substituted derivatives showed pH-sensitive gelation abilities with structures containing hydrophobic cavities on the nanometer scale, but fibrous structures on the macroscopic scale.^{78,265} Especially the 3-pyridyl derivative is interesting, as it can be used as scaffold for biomineralization.²⁶⁶ Furthermore, crystal structure analyses were performed for this compound by different groups.^{175,194} Polymorphic structures were reported dependent on the concentration of the compound in methanol, the presence of

water and the crystallization technique. However, it is important to keep in mind that these crystal structures might differ from the molecular arrangements in the hydrogel state.

Recently Leenders *et al.* published a BTA derivative with the gelation ability being dependent on the ratio of hydrophilic and hydrophobic side arms (Figure 1.7b).¹³¹ The fragile balance between aggregation and solubility was provided by the asymmetric substitution of the BTA core with either branched alkyl chains or *n*-decane side arms with tetraglycol headgroups.

The pH-sensitive aggregation behavior and the luminescence properties of a 4-benzoic acid derivative were reported by our group (Figure 1.7c).¹⁰² This BTA compound will be discussed in detail in this work.

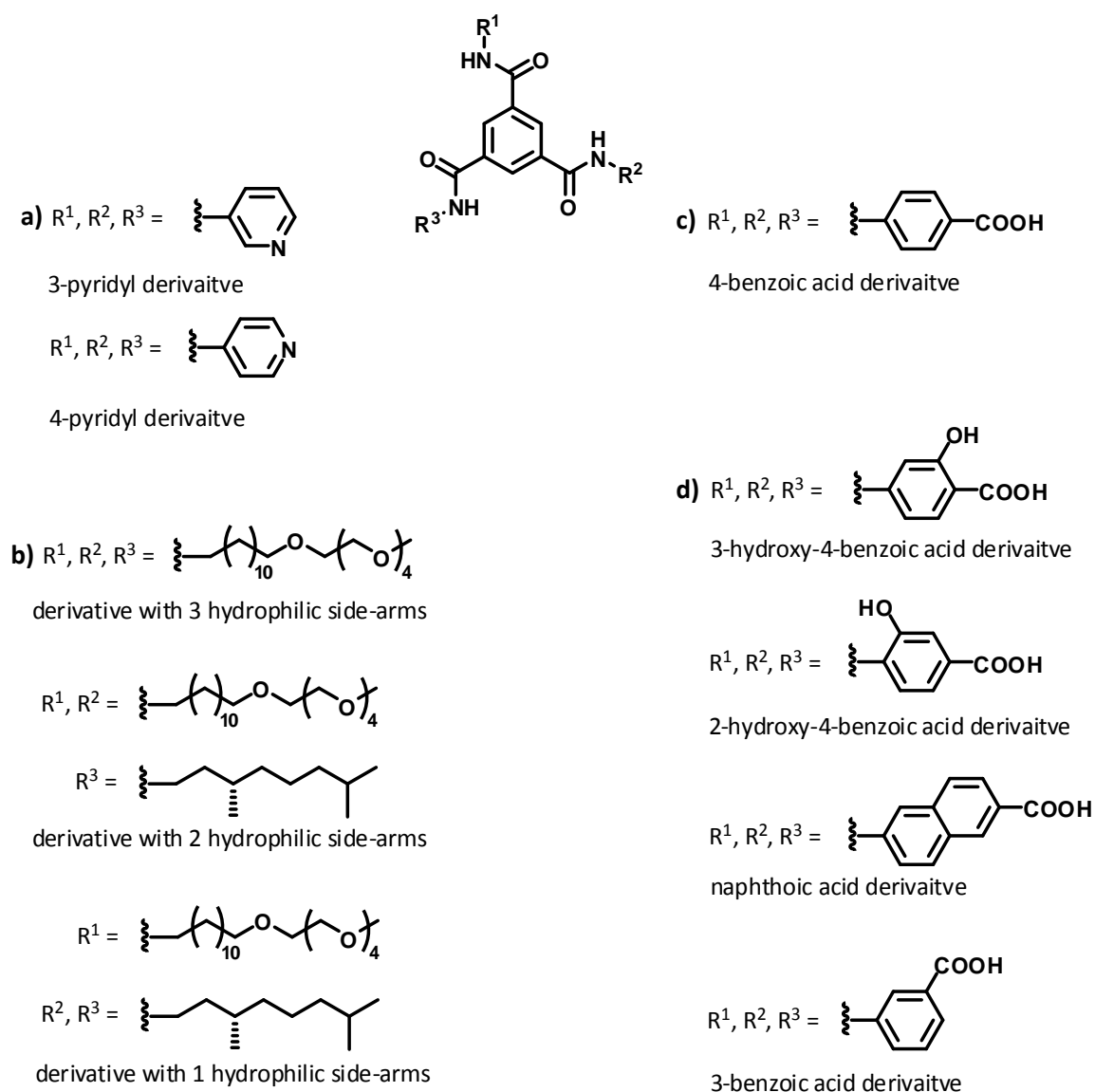


Figure 1.7: Molecular structures of BTA-based low molecular weight hydrogelators reported in literature by a) Kumar *et al.*²⁶⁵, b) Leenders *et al.*¹³¹, c) Bernet *et al.*¹⁰², and d) Howe *et al.*²⁶⁷

Howe *et al.* also investigated the gel properties of the 4-benzoic acid derivative and complemented the findings of our work.²⁶⁷ Further, the gelation abilities of related compounds were presented (Figure 1.7d). However, the 4-benzoic acid derivative is most interesting, as it can also be used as ligand for the coordination of different metals and the preparation of MOFs.^{190,198–203,268} Single crystals of this compound were obtained serendipitously during hydrothermal treatment in the presence on tin ions.²¹⁰ The structure obtained by single crystal analysis was described as a two-dimensional layer similar to that of a honeycomb grid. The stacked layers are shifted to each other and have an inter-sheet distance of 3.4 nm. At a close look, this structure seems to be similar to the reported columnar helical stacks of other derivatives with additional strong lateral hydrogen bonding interactions.

Summarizing, many different BTA derivatives have been reported in literature and various different applications have been explored. Besides the use of BTAs as trivalent building block in the synthesis of complex organic or polymeric compounds or as ligands for the coordination of metals and the formation of porous organic or metal organic frameworks, the self-assembly of this interesting supramolecular motif was extensively studied in polymer melts and organic solvents. Only recently, the substituents of BTAs were varied to achieve supramolecular assemblies in water. Up to now, only few BTA-based hydrogelators are known. All reported examples exhibit a quite unique balance between the hydrophobic shielding of the core and the hydrophilicity of the lateral headgroups.

Despite the large basic knowledge about the self-assembly of BTAs in various environments, there are still many things to learn, making BTA-based systems not only ideal candidates for basic research projects, but also for the realization of various applications. As the BTA-based hydrogelator identified in this work, will be investigated regarding its potential as an adsorption material and as a biomaterial for the controlled delivery of drugs, the ongoing efforts to use lmw hydrogelators in these fields are displayed in the following.

1.3 Possible applications of lmw hydrogelators

Lmw hydrogels have great potential for various fields of application, *e. g.* in the food industry, in cosmetics, as sensors, actuators or molecular wires in electronic devices, as templates for the preparation of metal nanoparticles, as scaffolds for tissue engineering, and in many more.^{39,56} However, the BTA-based hydrogelator presented in this work was investigated regarding its performance as adsorption material for toxic dyes and as matrix material for the controlled release of drugs. Therefore, in the following an overview of the material requirements and achievements for these two fields of application is given.

1.3.1 Application as adsorption material

The process of selective adsorption is of great importance in many different fields, such as the heterogenic catalysis and separation processes. Dealing with separation processes, the purification of waste-water from toxic dyes has become a major objective in many industries. In textile, paper, printing, plastic, cosmetic and pharmaceutical industries colors are essential to increase the value of the final product. Solely in the textile industry 10 000 different dyes and pigments with a worldwide production output of over 7×10^5 tons per year are used. It is assumed that *ca.* 10 - 25 % of these dyes are released in water during the coloring processes.²⁶⁹ Colors are either derived from toxic heavy metal ions, such as iron (Fe^{+2}), manganese (Mn^{+2}) and chromium (Cr^{+3}), or solely consist of organic materials.²⁷⁰ While heavy metals and some of the organic dyes have *per se* a toxic effect on the microorganisms and animals in water, all dyes additionally block the penetration of the sunlight into the water. Therefore dyes – even in very low concentrations – can inhibit the growth of aquatic bacteria and plants, which are very important for the self-regulating ability of the ecological system “water”.⁸⁷ Thus, it is essential that such dye residues are completely removed from industrial waste-water.

Rhodamine B, also known as Basic violet 10, is an important red coloring agent in textile industries (Figure 1.8). As after-treatment with antimony results in colored complexes and therefore permanent dyeing, it is used as staining agent and sensor for antimony in biological fluids.²⁷¹ Rhodamine B is a cationic dye that is classified as a xanthenic dye.²⁶⁹ As it causes serious irritation of the skin and the eyes and is harmful to aquatic organisms, efficient adsorption strategies are of importance.²⁷² It has unique spectroscopic properties,²⁷³ such as a high light absorbance even at low concentrations, a high emission extinction coefficient and no bleaching upon irradiation. Furthermore, rhodamine B is very well soluble in water. These properties qualify rhodamine B as a fluorescence lifetime standard²⁷⁴ and as an ideal model compound for adsorption and desorption studies in water.^{for examples see: 87,271,275–277}

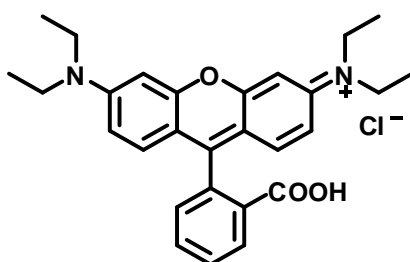


Figure 1.8: Chemical structure of rhodamine B.

A very effective and simple method to remove rhodamine B from water is the adsorption onto activated carbon.^{278,279} Due to the high surface area of activated carbon it exhibits a high adsorption capacity and its porous structure results in high adsorption rates. Besides these two essential properties, an efficient adsorbent should be cheap, easy to regenerate and the produced toxic waste or slurry should be easy to dispose. As synthesis and preparation of activated carbon is very costly in terms of resources, time and energy consumption, new low-cost materials with high efficiencies have to be realized.²⁸⁰ Hybrid materials that are based on polymer or surfactant coated porous ceramics often require multiple complex preparation steps.^{281,282} Metal oxide nanoparticles, on the other hand, exhibit toxicological effects due to their small sizes.²⁸³ Waste-products or easily accessible natural products, such as banana pith,²⁷⁶ wood,²⁸⁴ peat,²⁸⁵ brown seaweed,²⁸⁶ and bagasse fly ash,²⁷¹ are very cheap and non-toxic. Unfortunately, these adsorbents often show a low adsorption capacity. Thus, large quantities of toxic solid waste occur, which are not easily regenerated or disposed.

Responsive hydrogels, that can be triggered to adsorb and release the toxic dyes *via* an externally applied stimuli, might solve this problem. While polymeric hydrogels²⁴ and organic-inorganic hybrid hydrogels have been widely studied to efficiently remove various toxic dyes from waste-water,^{25,83,124,275,287} investigations regarding lmw hydrogels are rare^{87,288–292} and deal often only with the xerogels.^{70,123,129} However, especially this material class is worth exploring. By finding the right molecular structure, responsive gels with a high surface area, a high porosity and a specially functionalized surface for the selective and efficient adsorption of toxic dyes or heavy metal ions might be obtained by simply using the self-assembly process.^{60,80,87,288}

Furthermore, there is always an interest in using enzymes²⁸⁰ and biomass of bacteria and fungi^{293,294} for the precipitation, transformation or degradation of organic dyes. If these enzymes are immobilized within the hydrogel scaffold, two mechanisms to treat waste-water can be combined.

1.3.2 Application of lmw hydrogelators in the field of controlled drug delivery

1.3.2.1 Advantages of the controlled release of drugs

In the field of drug delivery^{295,296} the controlled release of bioactive guest molecules, such as drugs, vitamins or growth factors, from a hydrogel network at a specific target site in the body is of high interest.

When administering drugs in conventional delivery systems, such as injections, solutions, and pills, often higher doses than actual necessary have to be used due to the following reasons: i) some of the drug molecules are degraded before they can reach the infected site; ii)

the drugs are spread and thus diluted in the whole body, so that the concentration at the desired site is low; and iii) hydrophobic drugs are only poorly water soluble and thus, only small amounts can be absorbed by the body.^{12,296–298} The administration of high drug doses has, of course, many disadvantages, such as the higher costs, the increased risk of side-effects, and the weakening of the immune system, because some drugs display toxicity in high concentrations and harm healthy cells.

Scientists hope to overcome the drawbacks of conventional administration methods by using responsive drug-delivery systems. The aim is to design hydrogels that can be formed and dissolved in a very specific biological environment. Thus, they can act as a long-term depot for drugs in the body and target *e. g.* infection sites or tumor cells in the body. Such a specific administration technique has several advantages. By embedding the drugs in a hydrogel matrix, the drugs could be protected from degradation by enzymes or hostile milieus, such as the acidic conditions in the stomach.⁸⁵ The local drug concentration can be increased by specifically targeting the infected site. Thus, the drug concentration at the target site exceeds the minimum inhibitory concentration, while it falls below the toxic concentration in the rest of the organism. This should clearly reduce the risk of side effects and enhance the efficiency of the drug.^{74,95} The concept of targeted drug delivery is already used, *e. g.* when administering eye drops, ointments or using an inhaler for asthmatics.¹² Finally, a hydrogel-drug system that acts as a drug-depot, releases the respective drug over a long period of time. Thus, the time between treatments can be increased and this improves the quality of life of the patients.

1.3.2.2 Advantages of lmw hydrogels in the field of drug delivery

While polymeric hydrogels have been studied for a few decades regarding their application as drug delivery system,^{23,28,31,33,35,38,299} lmw hydrogelators have gained interest in this field just recently.^{for example see: 51,67,74,88,115–118,300} This might be due to the fact, that the first lmw hydrogels were often formed in the presence of an organic co-solvent such as DMSO or methanol.^{12,73–75} Naturally, such gels are not suitable for applications in biological environments.⁷⁴ Nevertheless, “real” lmw hydrogels show promising properties and furthermore some advantages over polymeric hydrogels as they consist of small molecules instead of covalently bound polymer chains.⁵⁶

As hydrogels in general obtain a high water content in the “solid-like” gel state, their composition is similar to that of organic tissue. This enlarges the possibility of good biocompatibility. The critical gelation concentration (cgc) of lmw gelators is mostly far beyond the gelator concentration used for polymeric gels.³⁰ Thus, they contain an even higher water content than polymeric gels and should therefore be better biocompatible.

The small hydrogelator molecules can usually be synthesized in few easy steps with good yields, showing a worthwhile cost-value ratio and no need for potential toxic polymer crosslinking agents.³⁸ As starting materials often natural derived building blocks, such as amino acids⁶¹ or peptides,^{67,82,88,115–117} sugars,^{10,34,75,122} and lipids,⁹¹ are used to diminish the risk of toxic metabolites and ensure a better biodegradability. Due to the non-covalent character of the supramolecular hydrogels, their response to external stimuli is fast and the complete dissolution of the gel simply results in small molecules. These can be easily degraded by enzymes and excreted by the body.⁸⁸ However, polymeric hydrogels consist of physically or chemically cross-linked networks that can only swell and shrink. This results in a much slower response to external stimuli. Furthermore, bulky polymer chains and chemical cross-links limit the accessibility for solvents, enzymes, and bacteria that ought to cleave bonds.²³ Thus, the degradation rate is lower and bioaccumulation might stress the organism.

Summarizing, due to the concept of low molecular weight (lmw) hydrogels, most of these gels fulfill at least some of the basic requirements for a successful controlled drug delivery system,³¹ such as: i) good biocompatibility and nontoxicity; ii) sufficient stability against mechanical and thermal stress, to allow easy handling and processing in the physiological relevant region; iii) high surface area and porosity to increase the number of adsorption sites and allow easy diffusion of the drugs out of the gel; iv) a high loading capacity due to adsorption or encapsulation of the drug molecules; and v) responsiveness of the hydrogel to an external stimuli, such as temperature, pH, ionic strength or enzymes to enable targeted and controlled release of the drug.^{33,36}

1.3.2.3 Drug delivery concepts for low molecular weight hydrogels

In literature two different kinds of controlled drug delivery concepts based on low molecular weight compounds have been reported: i) The drug molecules exhibit gelling properties under certain conditions or are structurally modified so that they can act as low molecular weight hydrogelators; and ii) the hydrogel is solely acting as a matrix for the drug.

Using the first concept, either the hydrogelator already possesses a bioactive effect after the gel is dissolved at the active site or the hydrogelator molecules must be partially decomposed to regain the drug.^{3,51,74,76,118,301–303} A very prominent example for a chemically modified antibiotic drug that shows the ability to gelate water is pyrene-functionalized vancomycin. Bing Xu *et al.* showed that due to this modification the hydrogelator showed high activity against vancomycin resistant *enterococci*.³⁰⁴

In the second concept the drug molecules are attached to the hydrogel matrix *via* physisorption, chemisorptions or due to steric reasons. Loading of a supramolecular hydrogel can be either accomplished by the adsorption of the drug on the surface or by forming the hydrogel in the presence of a drug. While in the first case the drug is merely bound at the

surface of the hydrogel, in the latter case the drug can be encapsulated in the fibers or pores of the gel.^{21,36,67,83,88,115–117,300,305,306} Using the encapsulation method, often higher loading capacities can be achieved compared to the adsorption technique.¹¹⁵ Further, also the loading of gels with hydrophobic and only poorly water-soluble drug molecules might be realized *via* encapsulation. As most of the lmw hydrogels are thermo-responsive,^{67,115–117,306} the drug or model compound is encapsulated in the gel *via* a heating and cooling cycle. However, high temperatures can destroy thermo-labile drugs, vitamins or other bioactive molecules. Thus, lmw gelators responding to other external stimuli, such as change of pH, change of salt concentration and enzymatic bond formation or cleavage, are of interest.^{21,36,83,88,150,305}

For advanced drug delivery systems both concepts can be combined by using a modified drug as hydrogelator that encapsulates a second drug. A prominent example is the modification of acetaminophen, a drug used as pain reliever and fever reducer.⁷⁹ By attaching fatty acids to the drug molecules, they are able to gelate water. The hydrophobic drug curcumin, that has anti-cancerogenic and anti-inflammatory properties, can be encapsulated without showing any signs of outburst release. Upon addition of an enzyme both drugs can be released without the production of toxic metabolites.

To ensure that a drug is really only released at the targeted site, two stimuli-responsive motifs can be implemented in the delivery system that have to be triggered consecutively. Van Bommel *et al.* showed that the model drug 6-aminoquinoline is only released, after the disassembly of the hydrogel at elevated temperature and an subsequent enzymatic bond cleavage.⁹⁵ There also have been attempts to tune the release rate by post-production treatments, such as covalent cross-linking *via* “click” chemistry³⁰⁷ or by incorporating liposomes in the gel, that release the drug dependent on the duration of a heating step just before the administration.¹¹⁸ Besides such multi-step triggers for the drug delivery, also hydrogels that respond to the presence of very specific enzymes were developed.^{51,112,308,309}

Although such complex or specific triggers are promising tools for the targeting of active sites, most drug delivery studies do not address the challenge of administering the drug loaded hydrogel. However, when designing “smart” drug delivery systems, the administration route plays a crucial role, as it determines the way the drug-hydrogelator system comes into the body and how it is distributed.^{31,295}

1.3.2.4 Administration routes for drugs

Mainly two different administration routes have been investigated *in vitro* or *in vivo* for the application of hydrogels: i) the parenteral; and ii) the oral route.

Parental administration includes the injection of the drug intramuscularly, intravenously, and subcutaneously. This technique is mainly used in the field of tissue engineering, wound

treatment and sustained release of specific drugs from a hydrogel depot under the skin or in the abdomen.^{21,300} An interesting example is the treatment of uranium contaminated wounds of mice with a hydrogel. The gel not only reduced the scar tissue formation, but more importantly adsorbed uranyl oxide from the wound site. Thus, the toxic effect of the heavy metal ion was reduced and the survival rate of the mice was drastically increased.^{33,51,303} Even more sophisticated is the treatment of the heart after an infarct. Here, the growth factors to reduce scar formation must be injected into the heart *via* a catheter. Unfortunately, solutions containing drugs or growth factors are pumped out of the heart very fast, thus reducing their effect. Bastings *et al.* found a hydrogel system that could be injected into the model heart of a pig in the sol state. Due to the slight change of pH at the infected site, the hydrogel was immediately formed after contact with the infarcted tissue, accelerating the healing process and reducing the scar formation.²¹

The oral route, *i.e.* the ingestion of a dosage form such as a pill or a capsule, is the most common and convenient method of drug administration, due to its low costs, its high acceptability by patients, and the ease of administration.²⁹⁷ Nevertheless, it also bears some challenges that have to be overcome for a successful drug delivery system.

The gastrointestinal tract is one of the largest organs in human bodies and is very complex. It consists of different sections, such as the stomach, the small intestine, the large intestine and the rectum. These all have very versatile biological functions and thus conditions, such as a specific pH value.³¹ All biological systems display certain diversity due to genetic differences. The conditions in the gastrointestinal tract are furthermore influenced by the age, the activity level, the stress level, possible diseases and of course the diet of the patient.²⁹⁸ Usually, the pH value in the stomach is below 2 in the fasted state and ranges between 4 and 7 after food intake. As the composition of the gastric acid consists of the ingested food and beverages, and the fluids that are secreted by the tract itself, it can change very rapidly within minutes. In the upper small intestine the pH value is approximately 6.5 in the fasted state. Due to the intake of gastric acid from the stomach, it varies between 4 and 7 in the fed state. In the distal small intestine the pH value increases to about 7.5 and in the large intestine it usually ranges between 5.7 and 8.4. In the rectum a final pH of about 7 is reached.

Summarizing, while the stomach and the upper small intestine are influenced heavily by the composition of the ingested food, conditions in the distal small intestine and the large intestine are very stable due to proceeding digestion. Therefore, when dealing with oral administration of drugs, scientists differentiate between the fasted and the fed state of the stomach and the small intestine. As in the fasted state the food intake and changes in the food composition due to digestion are not relevant, this state is easier to simulate.

The composition of the stomach and the upper small intestine are very well simulated by the simulated gastric fluid (SGF) and simulated intestinal fluid (SIF) developed by Dressman *et al.*³¹⁰ These fluids mimic physical properties such as pH, buffer capacity, osmotic pressure, and surface tension. However, not only the composition of the secretion changes along the gastrointestinal tract, but also the hydrodynamics, the bacterial flora, the presence of enzymes and the residence times. Hence, simulations of the gastro-intestinal tract, to investigate the dissolution and release behavior of a drug delivery system, are challenging.

It is known, that bioabsorption of nutrients or drug molecules mainly takes place in the small intestine and in the proximal large intestine due to the permeable membrane of the intestine. Unfortunately, many drug molecules are decomposed as a result of the harsh conditions in the stomach, such as the low pH value and the high amounts of pepsin, an enzyme for the hydrolysis of amid-bonds. Thus, there is a great need for colon-specific targeting, that prevents the degradation of the drug in the upper gastro-intestinal tract.^{23,297} The drug molecules might be protected by an acid-stable carrier matrix that releases the drug only after reaching the intestinal tract. Furthermore, by using such a carrier system the bioavailability of hydrophobic and hardly water-soluble drugs might be enhanced.³¹¹

As the development of new responsive biomaterials in the field of controlled drug delivery gained more and more interest in recent years, different low molecular weight hydrogelators were tested regarding their ability to encapsulate and slowly release bioactive molecules. Often the release of a model compound was shown in a proof-of-principle experiment. However, some studies further investigated the tuning of the release rates by varying different parameters, such as the gelator concentration, the drug concentration, the accepting media, or the temperature.^{36,79,95,116–118,307} Unfortunately, most of these hydrogel systems either do not fulfill basic requirements, such as non-toxicity, or simply neglect the challenges of the administration route.

Ray *et al.* showed that approximately 17 mg of vitamin B₁₂ can be encapsulated in 1 g of a metallo-hydrogel.⁸³ The vitamin was slowly released upon lowering the pH value to about 2. Thus, this hydrogel system is not suitable for oral administration, as the vitamin would already be released in the stomach. Furthermore, the hydrogel was formed by a mixture of phenylalanine-based bolaamphiphile and CuCl, which makes an application as biomaterial impossible. In the study of de Loos *et al.* the release behavior of salicylic acid from a phenylalanine-based hydrogel was influenced by the pH of the accepting media, and the temperature.¹¹⁶ As a result, for oral drug delivery applications the testing conditions should be chosen similar to that *in vivo*, as increasing temperature, as well as a change of the pH value can drastically enhance the release rate.

A very promising example of a low molecular weight hydrogel as drug delivery system is the biocompatible dipeptide-based hydrogelator published by Panda *et al.*¹¹⁷ Structurally very versatile bioactive molecules, such as vitamins, antibiotics, antimalarial drugs, anticancer drugs, antituberculosis drugs, and polypeptide insulin, were encapsulated in the gel. All of the – probably physically entrapped – guest molecules showed a sustained release behavior with faster release rates for drugs with a lower molecular weight. The release rate of the vitamin riboflavin could be adjusted by applying an external stimulus. Extreme acidic or alkaline pH values of the accepting media destabilized the gel network and thus enhanced the release rates of the vitamin.

Although these investigations give a good overview of the parameters that can influence the release behavior of an encapsulated guest molecule, neither of these studies were performed using physiological conditions similar to that in the gastrointestinal tract. However, good *in vitro* testing conditions at an early stage of the study are important to achieve reliable predictions for the behavior *in vivo*. Furthermore, it is important to note that so far most pH-sensitive hydrogels tested for a drug release application exhibit gel rupture and a pronounced release rate at highly acidic pH values.^{for example see: 83,85,116,117} Thus, the number of low molecular weight hydrogel systems that are suitable for the oral administration route with colon-specific targeting is, up to now, rather low.

1.4 Surface coatings via electrogelation

Surface coatings are important in very different fields of application. They are used for protection and decoration, *e. g.* in form of finishes and paints. But they can also be used to alter the roughness and hydrophobicity of a surface.³¹²

Hydrogel coatings are mainly used in the biomedical sector, *e. g.* to ensure the better acceptance of an implant by mimicking surface properties similar to that of natural tissue. Additional incorporation of drugs into the gel layer on the implant can further help to increase the local drug concentration and to reduce side-effects.⁷⁴ Moreover, gel coatings can be used to avoid the formation of biofilms on implants, in water pipes, and air-conditioning systems. By using gel films loaded with antibacterial and antifouling agents the accumulation of bacteria on surfaces is hindered, thus limiting the formation of biofilms. As biofilm formation increases the risk of infections or disease transmission, it is a major issue in sanitation and medicine.¹²

Usually, films are prepared by processes such as drop-casting, spin-coating, or dip-coating of the respective solution with a subsequent drying step. Although these techniques can be used to obtain films of self-assembled low molecular weight compounds, the morphologies might differ from

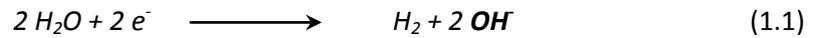
the porous three-dimensional network structures of wet hydrogels. Furthermore, when applying conventional techniques, it is difficult to obtain thin films, as always the whole volume of the gelator solution is solidified. Thus, the gel size and form are dependent on the surrounding vial or mold. The thickness of supramolecular gel films is also highly dependent on the surface tension of the gelator solution and the hydrophilicity of the substrate. A basic rule is the lower the contact angle of the solution on the substrate, the thinner the hydrogel films that can be obtained.

To overcome these coating problems electrochemical processes can be used.³¹³ Although, electrochemistry is a very versatile field, mainly three approaches are used to obtain surface coatings: i) electrophoresis; ii) oxidation and reduction reactions; and iii) the electrolysis of water.

Electrophoresis is the separation or alignment of objects in an electrical field due to their different charges.¹⁴² It can be used for the adhesion and delamination of polyelectrolyte films and polyelectrolyte multilayers due to Coulomb interactions between the electrode surface and the charged polymers.^{314–319} In biochemistry gel electrophoresis is a standard technique for the analysis and preparation of peptides, proteins, and amino acids.³²⁰ Therefore, a polymer gel such as alginate is prepared as matrix material between two glass plates. Subsequently, the peptide solution is applied and the electrical field is switched on. So far only one supramolecular gel, based on a C_3 -symmetric tris-pentaacetyl alpha-D-glucoside derivative, was used as matrix in this process.³²¹ However, it should be noted that the gelation process itself was not triggered by the electrical field.

The oxidation or reduction of dissolved molecules at the surface of the electrodes into a less soluble state can also lead to the coating of surfaces. This technique is often used for the preparation of metal coatings and metal oxide films. Therefore, it is usually associated with the terms electroplating and the galvanic process. However, it can also be used to change the oxidation state of organic compounds and thus induce electropolymerization.³²² Especially the preparation of defined polyaniline hydrogel films using electropolymerization was investigated, as these polymers tend to have a high electronic conductivity, a porous structure on the nanometer scale, and a high surface area. These properties qualify this material as high-performance supercapacitor electrode and as glucose oxidase sensor.²⁹ Recently, the electropolymerization of a C_3 -symmetric BTA derivative with triphenylamine moieties was reported.³²³ The formation of a thin organic layer on the electrode acted as a primer for the adhesion of self-assembled BTA-based organic nanoparticles. After the assembly on the electrode the nanoparticles could be electrochemically crosslinked to obtain a stable film within seconds.

Surface coatings can also be obtained by the electrochemical change of the pH value near the electrodes. Due to the electrolysis of water the following chemical reaction occurs at the cathode:



This leads to an increase of the pH value, as hydroxide ions are formed.

At the anode, on the other hand, the pH is decreased due to the formation of protons, as described in the following reaction equation:



To obtain hydrogen and oxygen from the electrolysis of water usually a potential of at least 1.9 V is used in technical processes.

Gabi *et al.* investigated the gradual decrease of the pH value in the solution near the anode by monitoring the diffusion of protons.³²⁴ They described a steep pH gradient in the solution already 1.5 s after the application of a current density of about 4 A m⁻². Directly at the anode a pH value of 4.5 could be found, while at a lateral distance of 50 μm from the anode the pH value was 6.5. After 6 s an equilibrium gradient was reached, as the hydroxide ions diffused from the cathode into the solution. In equilibrium a proton concentration gradient could be found between the anode (pH = 4.5) and at a lateral distance of 170 μm from the anode (pH = 6.5).

The low efficiency of the electrochemical reaction was ascribed to the side reaction of the sodium chloride that was used as background electrolyte. Chloride can be electrochemically oxidized to chlorine. Although chlorine disassociates to hydrochloric acid and hypochloric acid in water, it is only moderately soluble. Thus, it might mainly volatilize as gas without decreasing the pH value.

To avoid the evolution of gases during the electrochemical change of the pH value, polyaniline films and polystyrene sulphonates or polyperfluorosulphuric acids can be used on the electrodes to mediate the change of pH.³²⁵ Also the oxidation of hydroquinone to 1,4-benzoquinone can be used to induce a pH change. This demonstrates that the different electrochemical coating methods discussed here may occur parallel in a system.

While electrochemistry is widely used for the preparation of metal coatings,³²⁶ polymer films or self-assembled monolayers,³²⁷ the interest in lmw coatings with hydrogelation abilities has only emerged recently. Since then, the term “electrogelation” was used for two different processes.

It was first mentioned in a patent published in 2010 that describes the conversion of a silk fibroin solution into a silk gel by the direct application of a potential.³²⁸ The adhesion of silk

proteins from the silkworm onto different substrates was reversible. By applying shear stress to the obtained gels, a β -sheet-like structure typically for protein assemblies was obtained. This method proved to be an effective method to prepare gel films. Additionally, also bulk gel samples as well as extruded gel streams could be prepared.³²⁹

Furthermore, the term “electrogelation” was used to describe the film formation of pH-sensitive low molecular weight (lmw) peptides.³³⁰ These peptides form supramolecular hydrogels in bulk upon decrease of the pH value. For the film formation the pH value at the anode was decreased by the electrochemical oxidation of hydroquinone. Dependent on the applied potential, this resulted in gel films with thicknesses between tens of nanometer and a millimeter. Furthermore, for the first time dense hydrogel membranes with diameters of about 95 μm to 230 μm could be obtained from lmw compounds.

Summarizing, these first steps to combine electrochemical coating methods with lmw hydrogelators are very promising. They raise the hope that this technique might also be used for other pH-sensitive lmw hydrogelators to obtain thin hydrogel films. The basic research studies presented in this thesis will hopefully contribute to reveal the full potential of this method.

Please note that in the following work the term “electrogelation” is solely used for the preparation of supramolecular hydrogel films by the decrease of the pH value due to the electrolysis of water.

2 Objective

This thesis focuses on the investigation of pH-sensitive, low molecular weight (lmw) compounds based on the 1,3,5-benzene tricarboxamide (BTA) motif and their ability to form nanofiber networks in aqueous systems and supramolecular hydrogels.

The design of lmw hydrogelators forming gels with distinct properties, such as the responsiveness to specific external stimuli, is an ongoing challenge in supramolecular chemistry and material science. Up to now, there is only a limited understanding of possible gelation mechanisms and the interactions and conditions that enable the formation of supramolecular hydrogels with responsiveness to external stimuli.

To meet these challenges, this thesis covers the following *four subjects*: i) the self-assembly behavior of pH-sensitive BTAs in aqueous systems is investigated with regard to their ability to form nano-fiber networks and supramolecular hydrogels; ii) the formation of supramolecular chromophores during gelation is studied using spectroscopic methods; iii) the possible application of the supramolecular, pH-sensitive hydrogel as an adsorption material for small molecules and for the controlled delivery is elucidated; and iv) the formation of controlled hydrogel films on conductive substrates *via* electrogelation is investigated.

i) Self-assembly behavior of pH-sensitive 1,3,5-benzene tricarboxamides in aqueous systems

Supramolecular hydrogels have great potential in various applications, *e. g.* in technical devices as sensors, actuators, or molecular wires and in biomedicine as scaffolds for tissue engineering or as drug delivery systems. However, to find suitable lmw hydrogelators for these different fields of application, structure-property relations as well as the gelation processes need to be further explored. Although the BTA self-assembly motif has been widely investigated in apolar organic environments, controlling the intermolecular interactions in aqueous systems is still a challenge.

The main objectives of this chapter are:

- synthesis and characterization of BTA derivatives with different lateral functional groups to allow pH-sensitive aggregation in aqueous media,
- investigation of structure-property relations regarding the pH-sensitive aggregation behavior of the compounds and to reveal conditions that lead to supramolecular hydrogel formation,
- in case of hydrogel formation, comparison of different gelation methods and the investigation of the hydrogel properties,

- investigation of the gelation mechanism to propose a structural model for the formation of a supramolecular, pH-sensitive hydrogel based on the BTA motif.

ii) Formation of a supramolecular chromophore

For the identified hydrogel a blue photoluminescence was observed upon aggregation. The formation of a supramolecular chromophore is highly interesting for basic research on aggregation induced emission enhancement (AIEE).

The main objectives of this chapter are:

- investigation of the influence of the state of aggregation on the absorption properties using UV-Vis spectroscopy in bulk and solution,
- investigation of the photoluminescence (PL) properties in bulk and solution to clarify if AIEE occurs for this BTA derivative and during gel formation to monitor the formation of the supramolecular chromophore,
- discussion of the experimental findings in respect to theoretical calculations performed by Rodrigo Q. Albuquerque to elucidate the probable molecular arrangements at an early stage of aggregation.

iii) Dye adsorption and release studies: towards a pH-sensitive, supramolecular drug delivery system

Supramolecular hydrogels have advantages over covalently crosslinked polymer hydrogels, such as a fast response to external trigger. They can find applications as adsorption materials or in controlled drug delivery. To realize such an application many different requirements must be fulfilled. For the application as adsorption material in waste water treatment the time-dependent adsorption of dyes from water is important. In controlled drug delivery applications the adsorption or encapsulation of a model drug as well as the controlled release in different environments must be considered. To be able to cover both areas, detailed adsorption and release studies are performed with the model compound rhodamine B. In this chapter the BTA-based hydrogelator system will be investigated to elucidate its potential as adsorption material and for controlled delivery of small molecules.

Here, the main objectives are:

- investigation of the hydrogelator system regarding the basic requirements for drug release systems
- investigation of concentration- and time-dependent adsorption of rhodamine B on preformed hydrogels,
- analysis of the adsorption process regarding the valid isothermal models and the adsorption kinetics to better understand the underlying processes,

- investigation of the thermal stability of the adsorbed dye-gel systems in water by monitoring the release of the dye at different temperatures,
- preparation of hydrogels in presence of different amounts of the dye rhodamine B to realize *in situ* adsorption and encapsulation and to investigate the influence of the dye on the gelation ability of the low molecular weight hydrogelator,
- investigation of the release of rhodamine B in water from hydrogels prepared in the presence of dye and comparison of the results with the findings obtained from the adsorption studies,
- investigation of the dissolution and release profiles of hydrogels prepared in the presence of rhodamine B in biologically relevant media with different pH values.

iv) Electrogelation – controlled formation of hydrogel films on conductive substrates

The previous chapters focus on the formation of supramolecular gels *via* conventional gel preparation routes. However, the gelation method plays a major role regarding the hydrogel properties. New gelation techniques are therefore an interesting way to adjust the gel properties. There are only a limited number of methods to obtain thin hydrogel films from low molecular weight compounds. Electrogelation as a rather new method was explored. Here, the coating of a conductive substrate with defined hydrogel films is realized. This technique might be a useful tool for coating biomedical tools or sensor devices. To be fully able to evaluate the potential of this electrogelation method, the parameters that might influence the hydrogel film formation must be investigated.

The main objectives of this chapter are:

- development of an experimental concept and set up to be able to obtain reproducible hydrogel films on conductive substrates,
- investigation of different parameters of the electrogelation process, such as electrode distance, applied potential, gelator concentration, concentration of the background electrolyte, and gelation time, and their influence on the dried film thickness, the morphology and the spectroscopic properties,
- outlook on the *in situ* investigation of the mechanical properties of defined hydrogel films using atomic force microscopy techniques that are performed in cooperation with the group of Prof. Georg Papastavrou (Physical Chemistry II, University of Bayreuth).

3 Self-Assembly behavior of pH-sensitive 1,3,5-benzene tricarboxamides in aqueous systems

3.1 Structural concept

The aim of this work was to develop a structural concept for the synthesis of pH-sensitive low molecular weight (lmw) compounds on the basis of 1,3,5-benzene tricarboxamides (BTAs) for detailed self-assembly studies in water and the identification of new lmw hydrogelators. At the beginning of this research project only pyridyl-substituted BTA-based hydrogelators were known which had been found serendipitously.^{78,265,266}

In the introduction of this work it is discussed in detail that despite the growing interest in recent decades for new classes of supramolecular hydrogels with specific properties, it is still not possible to design new lmw hydrogelators and predict the properties of the resulting gels (chapter 1.1.4). However, it could be shown that for the directed self-assembly in water mainly hydrophobic interactions are the driving force, as hydrogen bonds lose their directionality, if they are not shielded from the water molecules (chapter 1.1.4).^{9,10,131,132} Additionally, electrostatic interactions have been identified to be a useful tool to tune the solubility of lmw compounds.^{10,84,258} The numerous examples of hydrogelators with very different molecular structures and functional moieties showed that the presence of a distinct balance between hydrophilic and lipophilic interactions (*hydrophilic-lipophilic balance*, HLB) is common for all successful lmw hydrogelators (chapter 1.1.4.1).⁹

Due to the necessity of this HLB, many lmw hydrogelators are classical amphiphiles and can act as surfactants (chapter 1.1.5). For amphiphilic lmw hydrogelators four different segments were identified as essential structural motifs: a hydrophilic headgroup, a rigid unit, a flexible linker, and a hydrophobic tail.¹⁰ In our group it could be shown that by the systematic variation of these structural motifs, different classes of new amphiphilic lmw hydrogelators could be easily synthesized.^{66,76,77} For this modular system the following building blocks were used: different carboxylic acids acted as polar headgroups, a phenylene spacer in combination with an amide group acted as a rigid hydrophobic unit with the ability to form hydrogen bonds in aqueous systems, and alkyl chains with different lengths were used to tune the necessary balance between solubility and aggregation due to hydrophobic interactions. The identified classes of amphiphilic hydrogelators showed hydrogel formation in the presence of alkaline salts depending on the pH value and the ionic strength of the solution.^{66,76,77} This special feature enables the use of new and rather unique tools for the monitoring of phase transitions, such as sodium nuclear magnetic resonance (NMR) relaxometry.³³¹

This work aims to further develop the investigations on amphiphilic low molecular weight hydrogelators and to transfer the concept to the C_3 -symmetric BTA self-assembly motif. By van Bommel *et al.* a similar modular concept for C_3 -symmetric hydrogelators has been published using amino acids with phenyl moieties as spacers and cyclohexane-based tricarboxamides as cores.⁸⁴

As discussed in chapter 1.2.3, the self-assembly of BTA derivatives has mainly been studied in bulk, organic solvents, and polymer melts. In water it is rather difficult to find the right balance between attractive and repulsive interactions. Thus, BTAs are often either completely soluble or simply precipitate. Due to these difficulties, reports about the self-assembly of BTAs in aqueous systems are rather new and were mostly published during the work on this thesis. A detailed overview of self-assembly studies of BTAs in mixtures of organic solvents and water (chapter 1.2.3.4), in water (chapter 1.2.3.5), and of BTA-based hydrogelators (chapter 1.2.3.6) can be found in the introduction.

The developed structural concept for the synthesis of BTA compounds that show responsive self-assembly behavior in water is presented in Figure 3.1.

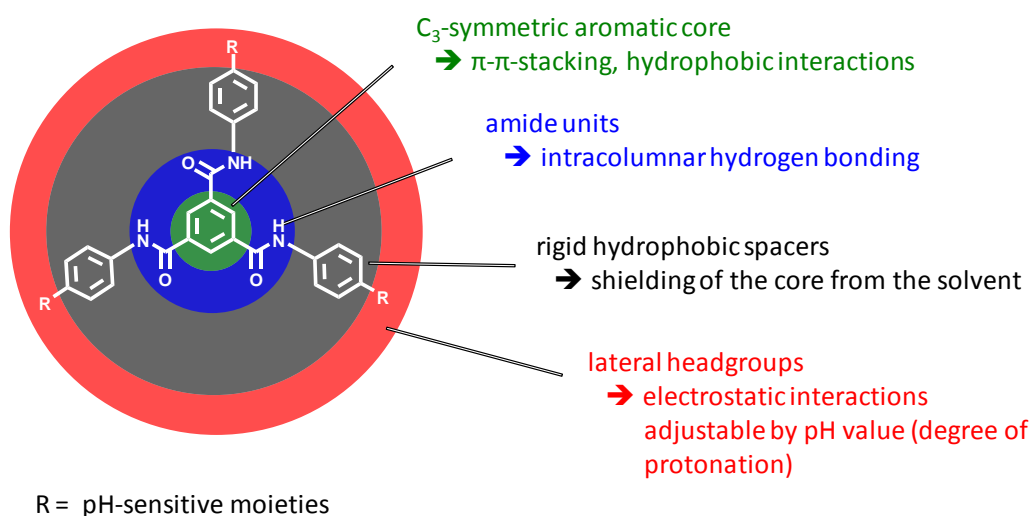


Figure 3.1: Structural concept for pH-sensitive BTA-based hydrogelators.

The BTA core with the benzene ring and the amide units provide attractive intermolecular interactions by π - π -stacking, hydrophobic interactions, and hydrogen bonding that should lead to the formation of molecular stacks. The rigid aromatic spacer should provide the necessary shielding of the core from water molecules and might furthermore enable π - π -interactions between the side arms of the molecules. It is known in the literature that the BTA compound bearing phenylene spacers without a lateral functional moiety (R = H) is insoluble in aqueous system due to its high aggregation tendency.^{137,218} Hence, to provide the solubility of the BTAs in water, electrostatic interactions are utilized by introducing pH-sensitive lateral headgroups.

These functional groups were chosen according to three different aspects: i) all groups ought to be able to respond to a change of pH to use it as a pH-sensitive switch; ii) they should differ in their acidity or basicity and thus respond in a different pH region; and iii) their ability to form lateral hydrogen bonds should differ in terms of their tendency to act as a donor, an acceptor, none, or both (Figure 3.2).

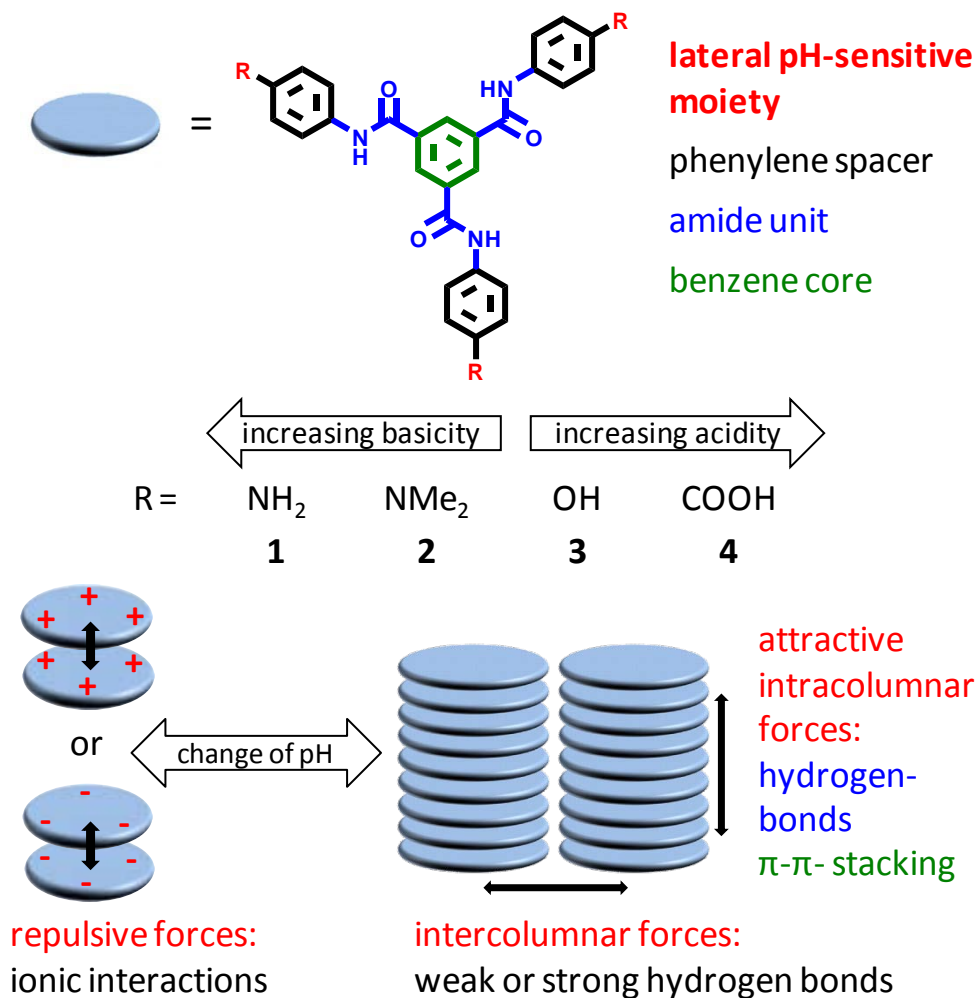


Figure 3.2: The self-assembly concept of 1,3,5-benzene tricarboxamides with pH-sensitive lateral groups.

The following functional moieties fulfill these requirements and might enhance the solubility by repulsive electrostatic interactions in their ionic form: R = -NH₂ (**1**), -NMe₂ (**2**), -OH (**3**), and -COOH (**4**). Furthermore, for comparison purposes the trimethylester of compound **4** (R = -COOMe, **5**) was included in this study, as its molecular structure is very similar to compound **4**, but lacks the ability to respond to different pH values and to form self-complementary hydrogen bonds.

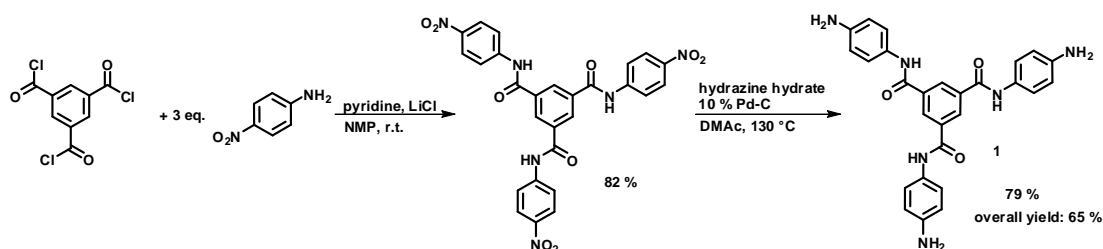
While compound **1** and **2** are protonated in acidic aqueous solution and thus positively charged, **3** and **4** are deprotonated in basic media and negatively charged. Due to these charges and the resulting repulsive intermolecular interactions, it is proposed that the compounds are molecularly dissolved. Upon change of the pH value the molecules should become uncharged by subsequent protonation or deprotonation of the three headgroups. This should result in the increase of the attractive interactions of the core and thus pronounced one-dimensional aggregation. The superstructures of those aggregates are supposed to be mainly governed by the lateral groups and their ability to form hydrogen bonds between molecular stacks.

3.2 Synthesis and characterization

3.2.1 Synthesis of the 1,3,5-benzene tricarboxamides 1- 5

The synthesis of various BTA compounds was published by E.W. Meijer *et al.* and the synthesis presented here are modifications of this procedure.¹⁵² As compounds **1** - **5** have already been mentioned in the literature as cross-linking agents in polyamide or polyamide-ester networks,^{for example see: 156,332–336} as precursors in the synthesis of liquid crystal materials and organogelators,²¹³ or as ligands in metal complexes and metal organic frameworks (MOFs)^{for example see: 200,203,210,337} different synthetic routes to obtain these compounds have been published. The successful optimization of the synthesis of compounds **2** and **4** was conducted during my diploma thesis with the aim to achieve a simple synthesis under mild conditions with commercially available educts resulting in high yields without laborious purification steps.³³⁸

Synthesis of **1** was carried out by a two step reaction (Scheme 3.1).

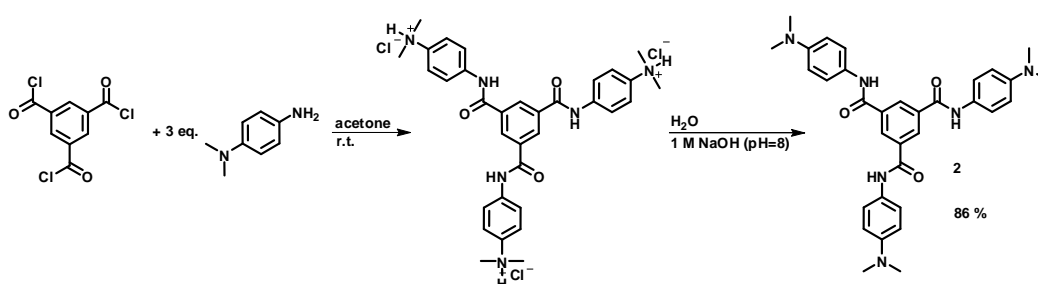


Scheme 3.1: Synthesis of the BTA derivative **1**.

At first the trinitro-substituted intermediate was synthesized by reaction of 1,3,5-benzene tricarboxylic acid trichloride and 4-nitroaniline at room temperature (r. t.). To ensure a good

solubility of all reactants, *N*-methyl-2-pyrrolidone (NMP) was used as solvent. Pyridine was used as base to remove the hydrochloric acid formed during the reaction of the carboxylic acid chlorides with the amine moieties. To increase the reactivity of the reaction, catalytic amounts of lithium chloride were added. Afterwards the nitro groups were hydrated by hydrazine hydrate in the presence of palladium on charcoal. Due to the presence of the palladium catalyst, the second reaction step was carried out in inert gas atmosphere. The compound was filtrated over Alox and precipitated in water for purification.

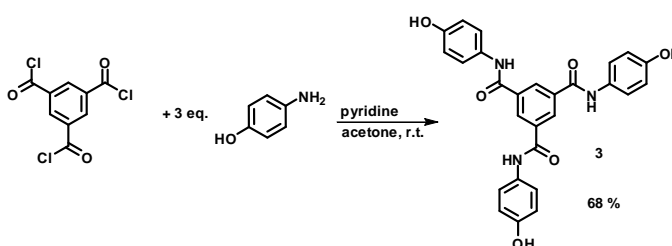
Compounds **2** – **5** were prepared under ambient conditions without inert gas atmosphere. The synthesis of compound **2** is displayed in Scheme 3.2.



Scheme 3.2: Synthesis of the BTA derivative **2**.

For this reaction the addition of pyridine was not necessary as *N,N*-dimethyl-1,4-phenylenediamine acted as internal base to remove the formed HCl during synthesis. The resulting hydrochloride salt of compound **2** could not be characterized properly. This might be explained by the presence of a mixture of the single (**2** · 1 HCl), double (**2** · 2 HCl), and triple (**2** · 3 HCl) hydrochloride salt of **2**. The isolated intermediate was dissolved in water and precipitated by the addition of aqueous sodium hydroxide solution, which yielded the pure product.

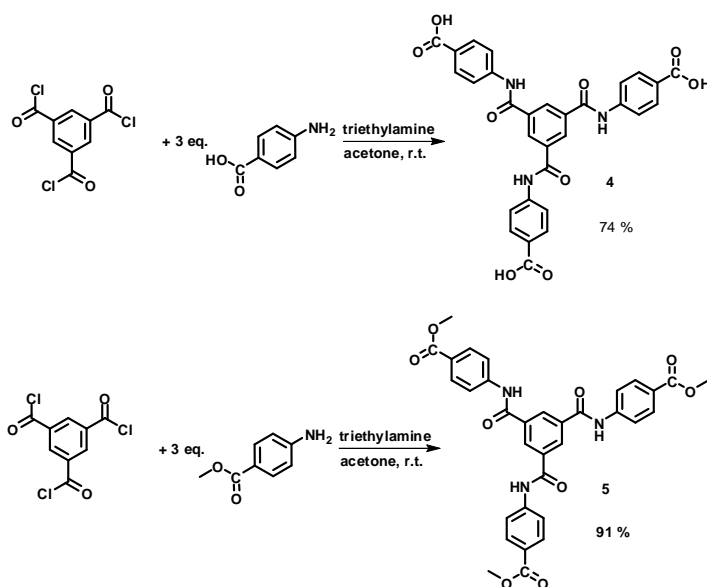
Compound **3** was synthesized by reaction of 1,3,5-benzene tricarboxylic acid trichloride and 4-hydroxyaniline at r. t. in the presence of pyridine (Scheme 3.3).



Scheme 3.3: Synthesis of the BTA derivative **3**.

Subsequently, the compound was precipitated in ice water, filtrated, and thoroughly washed with water to remove traces of NMP and the pyridinium salt.

For the synthesis of compounds **4** and **5** 4-aminobenzoic acid and the respective methyl ester were reacted with 1,3,5-benzene tricarboxylic acid trichloride, respectively (Scheme 3.4). Triethylamine was used as base for both reactions, as the removal of pyridine residues from compound **4** would have afforded an additional purification step.³³⁸



Scheme 3.4: Synthesis of BTA derivatives **4** and **5**.

Both compounds were isolated by precipitation in ice water. While compound **4** was crystallized from a DMSO/water-mixture to remove traces of mono- and disubstituted BTA derivatives, compound **5** could be used without further purification steps. For compound **4** also the sodium salt of the respective compound (**4Na**) could be isolated by precipitation with *iso*-propanol from an alkaline sodium hydroxide solution.

Summarizing, all compounds could be synthesized with large-scale approaches in high yields (65 % - 92 %) resulting in several grams of the respective product.

3.2.2 Characterization

Characterization of the products **1 - 5** via ¹H- and ¹³C-nuclear magnetic resonance (NMR) spectroscopy, mass spectrometry and elemental analysis confirmed that the compounds were synthesized with high purity.¹ Elemental analysis of the sodium salt **4Na** could not be performed due to the lack of a sodium ion detector. Despite intensive drying steps prior to the elemental analysis, for compounds **1**, **3**, **4** and **5** the presence of 3, 0.5, 1.5, and 2 water

¹ For more details see chapter 9.3.

molecules was found per molecule of the compound, respectively. This indicates a high affinity of the compounds to form hydrogen bonds with water, which was further confirmed by the thermal analysis.

3.2.2.1 Thermal characterization and determination of the water uptake

Thermal analysis was performed by a combined DSC/TGA measurement. The obtained results are summarized in Table 3.1. The decomposition temperature was given by the analysis software as the onset of the final mass loss, while the melting temperature is the maximum of the exothermic peak.

Table 3.1: Results of the thermal analysis of compounds **1** – **5** and **4Na**.

| | R | loss of water ^a [%] | decomposition temperature ^b [°C] | weight loss ^c [%] | endothermic peak [°C] | exothermic peak [°C] |
|-------------------------------|-------------------|--------------------------------|---|------------------------------|-----------------------|----------------------|
| 1 | -NH ₂ | 7.3 | 325.3 | 20.4; 25.9 | 85.3; 314.2 | |
| 2 | -NMe ₂ | 0.0 | 301.7 | 59.8 | 374.0 | 348.0 |
| 3 | -OH | 0.9 | 386.6 | 45.8 | 63.4; 396.1 | |
| 4 | -COOH | 5.7 | 294.6 | 47.7 | 76.2; 329.6 | 528.6 |
| 4 (50 °C) ^d | -COOH | 3.3 | 307.5 | 45.5 | 82.7; 328.3 | 526.2 |
| 4 (90 °C) ^d | -COOH | 1.9 | 309.2 | 45.1 | 80.4; 328.3 | 501.9 |
| 4Na | -COONa | 15.4 | 330.0 | 30.9 | 108.7; 394.3 | |
| 5 | -COOMe | 2.8 | 362.8 | 43.1; 22.5 | 327.6 | 207.7; 558.9 |

^a summarized weight loss up to 110 °C (loss of water); ^b the decomposition temperature is the onset of the final mass loss; ^c summarized weight losses above 110 °C per step (without loss of water); ^d temperature of the oil bath in parentheses at which the compound was dried under vacuum (0.1 mbar) overnight prior to the thermal analysis.

The obtained data show that compounds **1** – **4** and **4Na** are stable up to about 300 °C before they decompose without melting, while compound **5** melts at 208 °C and decomposes at 363 °C.

For compounds **1**, **3**, **4**, **4Na** and **5** the first step of weight loss can be observed between about 63 °C to 109 °C (first endothermic peak). As the endothermic peaks at low temperatures are very broad, for compound **5** the indication of the maximum was not possible. The elemental analysis showed the presence of water in the compounds **1**, **3**, **4**, and **5**. Therefore, the summarized weight loss up to 110 °C was assigned to the loss of water. This hypothesis is further supported by the fact that the first step of weight loss of compound **4** decreased upon increasing the oil bath temperature during drying under vacuum prior to the measurements.

The amount of water present during elemental analysis is compared with the amount of lost water during thermal analysis by giving the respective molar ratio of the compound and water (Table 3.2). Interestingly, the values calculated from the lost water in the thermal analysis are generally lower than the amounts of lost water obtained from the elemental

analysis. This underestimation might be explained by the lower accuracy of the determination by thermal analysis. However, it might also be possible that some of the water molecules are strongly bound to the respective solid and are not removed by heating to 110 °C.

Table 3.2: Comparison of the lost water during thermal analysis and of the amount of water present during elemental analysis.

| | R | determined molar ratio of compound to water | |
|------------------------------|-------------------|--|-----------------------|
| | | thermal analysis | elemental analysis |
| 1 | -NH ₂ | 1 : 2 | 1 : 3 |
| 2 | -NMe ₂ | no water | no water |
| 3 | -OH | 1 : 0.25 | 1 : 0.5 |
| 4 (90°C) ^a | -COOH | 1 : 0.6 | 1 : 1.5 |
| 4Na | -COONa | 1 : 6.4 | - ^b |
| 5 | -COOMe | 1 : 1 | 1 : 2 |

^a temperature of the oil bath in parentheses at which the compound was dried under vacuum (0.1 mbar) over night prior to the measurements; ^b no elemental analysis possible.

As for compound **4** the water could not be removed completely despite intensive drying, the water uptake behavior of compounds **4** and **4Na** were further investigated in dependence of the relative (rel.) humidity. Using a moisture analyzer the samples were heated up to 140 °C *via* infrared irradiation. The weight loss was determined in % and mg until the weight loss rate was below 1 mg min⁻¹. Prior to the experiments, compound **4** was stored at different rel. humidity, respectively. With increasing water content in the surrounding atmosphere, the weight loss in the subsequent measurement increased (Table 3.3).

Table 3.3: Average loss of water in dependence of the rel. humidity.

| compound | R | rel. humidity [%] | temperature [°C] | loss of water [%] |
|------------|--------|----------------------|---------------------|------------------------|
| 4 | -COOH | 33 – 36 | 24 | 4.2 ± 0.4 ^a |
| | | 55 ^b | 22 | 7.3 ^b |
| | | 78 ^c | 23 | 8.7 ^c |
| 4Na | -COONa | 37 – 38 | 23 | 9.3 ± 0.5 ^a |

^a average of 3 measurements; ^b one measurement after storage for 16 h;

^c one measurement after storage for 96 h.

Under similar conditions the water uptake of the sodium salt **4Na** is nearly twice as much as the water uptake of **4**, which is an expected behavior for salts. It could be shown that the water uptake is a fully reversible process and already takes place during the cooling phase between two measurements. The water uptake is mainly dependent on the rel. humidity and

reaches a maximum value independent on the time of storage in the respective atmosphere. As no climate chamber was available, the exact adjustment of the rel. humidity was rather challenging and for the tests at an enhanced rel. humidity only one measurement could be performed. Interestingly, even at a high rel. humidity no liquefaction of the solids could be observed. The high association of compound **4** to water was also reported in the literature, when elemental analysis was performed on crystals of **4**.²⁰⁰

3.2.2.2 Investigation of hydrogen bond formation via infra-red spectroscopy

Fourier transform infrared (FT-IR) spectroscopy is a convenient method to analyze the presence and strength of hydrogen bonds. As discussed in the introduction (chapter 1.2.1), the amide units of BTAs play an important role in supramolecular self-assembly as triple intermolecular hydrogen bond formation usually leads to one-dimensional aggregation.^{134,135}

In general, amides show three distinct bands in IR spectra:³³⁹ i) The C=O stretch vibration or amide I band is usually a pronounced band that can be found between 1700 - 1670 cm⁻¹ in dissolved state and between 1680 - 1630 cm⁻¹ for solids, when hydrogen bonds are present. ii) The amide II band describes the N-H bending vibration. It is weak for most amides and might therefore be easily missed in the spectrum. The band can be found between 1550 - 1510 cm⁻¹ in solutions and 1570 - 1515 cm⁻¹ in solids. iii) The N-H valence vibration band occurs between 3460 - 3400 cm⁻¹ in solutions, but is shifted by about 150 cm⁻¹ to lower wavelength if hydrogen bonds are present. This band is often overlapped by bands from hydroxyl or amino moieties. For columnar stacked BTAs with alkyl side chains the C=O stretch vibration of the amide units at about 1640 cm⁻¹ is an important indication for intermolecular hydrogen bonds.^{132,214} Furthermore, the N-H stretch vibrations and the amide II band are expected at ~3240 cm⁻¹ and ~1560 cm⁻¹, respectively. These vibrational bands can shift to lower energy values when alkyl side chains are replaced by aromatic rings. It was recently shown by Nagarajan *et al.* that in columnar stacks of BTA derivatives the amide units of one molecule can adapt different deviation angles.¹³⁷ Such differences lead to different types of hydrogen bonds in the stacks, which might result in several bands for the amide vibration.

The relevant regions for the amide bands in the FT-IR spectra of compounds **1 - 5** and **4Na** are displayed in Figure 3.3. The typical ranges for the three amide bands in the presence of hydrogen bonds as reported in the literature³³⁹ are highlighted in blue (N-H valence vibration), orange (amide I, C=O vibration), and green (amide II, N-H bending vibration).

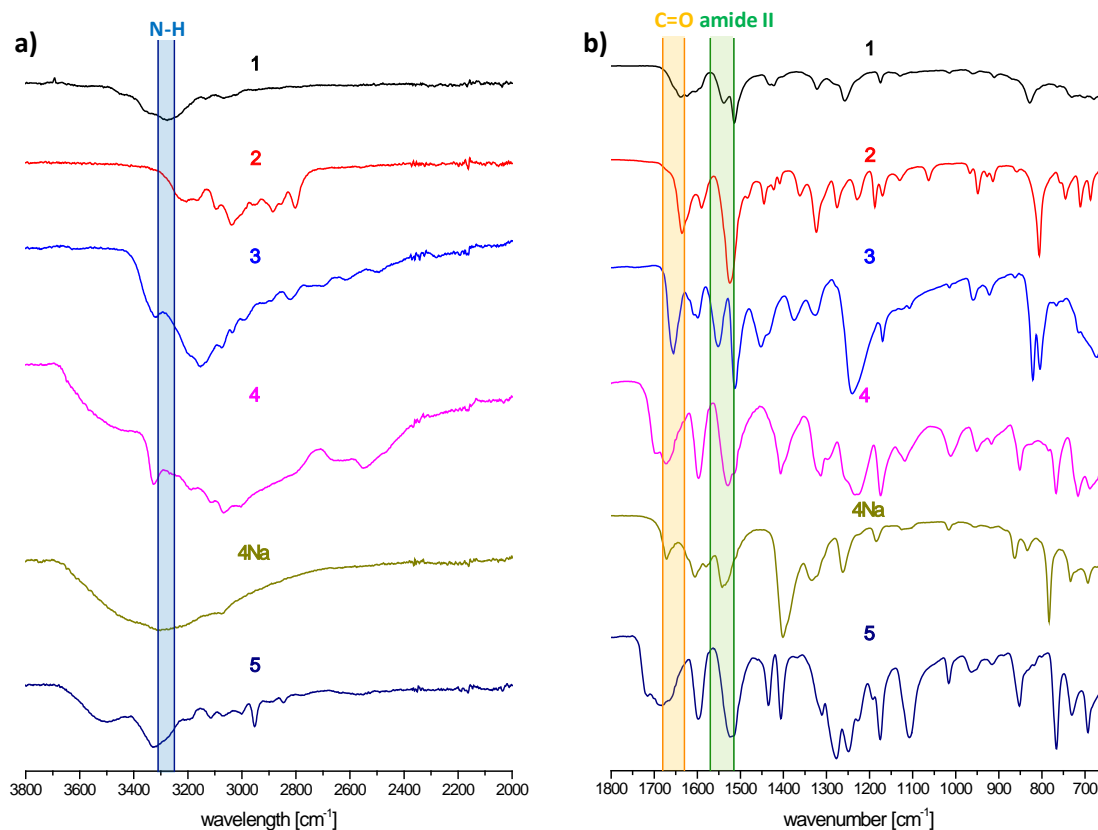


Figure 3.3: FT-IR spectra of compounds **1** – **5** and **4Na** as obtained from synthesis.¹ The highlighted regions refer to typical amide band regions in the presence of hydrogen bonds.³³⁹ Note: Plots have been offset in the y-axis in order to ease visualization.

The wavenumbers of the amide vibrations of the BTA core of compounds **1** - **5** and **4Na** are summarized in Table 3.4.

Table 3.4: Vibrations of the amide unit at the BTA core in bulk samples of compounds **1** – **5** and **4Na**.

| vibrations of amide unit at the BTA core | | | | |
|--|-------------------|---------------------|------|----------|
| | | [cm ⁻¹] | | |
| | R | N-H | C=O | amide II |
| 1 | -NH ₂ | 3276 | 1638 | 1514 |
| 2 | -NMe ₂ | 3220 | 1636 | 1525 |
| 3 | -OH | 3205 | 1655 | 1513 |
| 4 ¹ | -COOH | 3327 | 1672 | 1529 |
| 4Na | -COONa | 3322 | 1671 | 1542 |
| 5 | -COOMe | 3329 | 1683 | 1524 |

¹ For FT-IR spectroscopic investigations the recrystallized compound **4** from DMSO-water was used.

Especially the carbonyl stretch vibrations of all compounds between 1636 and 1683 cm^{-1} are in good accordance with findings from the literature and clearly indicate the presence of intermolecular hydrogen bonds in the bulk samples after synthesis.^{132,214} The assignment of the N-H vibration band was rather difficult, as the band is overlapped by O-H vibrational bands due to the presence of water as shown by elemental and thermal analysis.

For compound **1** an additionally N-H deformation vibration should be present between 1650 cm^{-1} and 1560 cm^{-1} due to the lateral amino moieties.³³⁹ In the relevant region two bands can be found in the IR spectrum of **1**. The band at 1605 cm^{-1} as well as at 1624 cm^{-1} might be assigned to the N-H deformation vibration. The lateral dimethylamino moieties in compound **2** should give a band between 2820 - 2720 cm^{-1} due to N-CH₃ valence vibrations.³³⁹ The respective band can be found at 2802 cm^{-1} . The absence of a band around 2500 cm^{-1} indicates that the tertiary amine is not protonated.³³⁹ The vibrational bands of O-H moieties in solids can be found between 3200 - 2500 cm^{-1} . However, in the spectrum of compound **3** too many bands can be found in the respective region for a distinct assignment. For compounds **4** and **5** a second vibration for the C=O stretch can be found at 1697 cm^{-1} and 1714 cm^{-1} , respectively. These can be attributed to the lateral carboxylic acid moieties. The difference between the two vibrational bands can be explained by intermolecular interactions in case of compound **4**, as its C=O vibration lies in the range of carboxylic acid dimers (1725 - 1700 cm^{-1}) and indicates the formation of lateral hydrogen bonds. The lateral C=O stretch vibration of the sodium salt derivative **4Na** is shifted to lower wavenumbers. Due to the anionic character of the carboxylates and the mesomeric distribution of the electrons, two valence bands can be found between 1610 - 1550 cm^{-1} and 1420 - 1300 cm^{-1} , respectively.³³⁹ In the spectrum of compound **4Na** the vibrational bands at 1579 cm^{-1} and 1334 cm^{-1} are assigned to the sodium carboxylate moieties.

3.2.2.3 Morphological studies and x-ray diffraction investigations

The compounds **1** - **5** as well as the sodium carboxylate derivative **4Na** were investigated regarding their bulk morphology as obtained from synthesis by scanning electron microscopy (SEM) and X-ray diffraction (XRD) experiments.

The SEM image of compound **1** shows structures that resemble broad and short ribbons with widths of about 0.5 μm and several micrometer in length (Figure 3.4a). The XRD pattern of the obtained precipitate from synthesis displays a crystalline structure (Figure 3.4b).

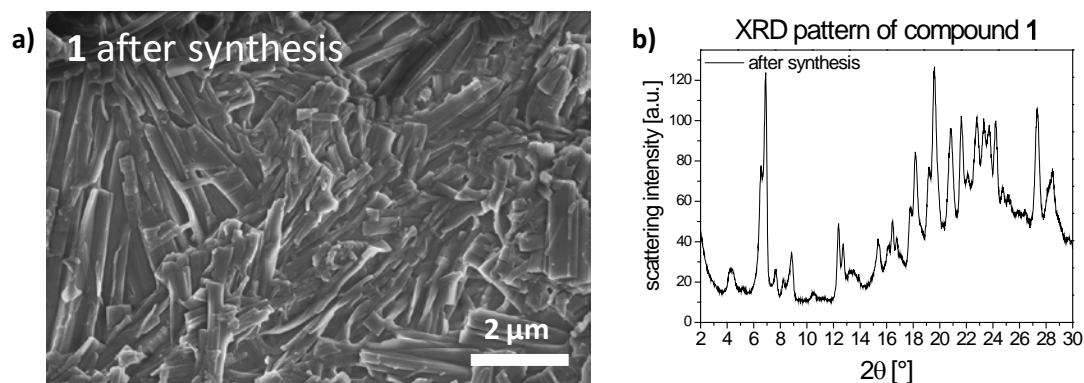


Figure 3.4: a) Morphological characterization of compound **1** ($R = \text{NH}_2$) as obtained from synthesis by a typical SEM image and b) the XRD pattern.

Usually XRD patterns of BTA assemblies with an underlying columnar structure show a broad peak between 25.1° and 25.8° (2θ) that corresponds to the π - π -distance of *approx.* 0.35 nm of the BTA cores.^{132,138,139,214} As the FT-IR spectrum of compound **1** shows the participation of the BTA core amides in hydrogen bonds, it seems obvious to expect an underlying columnar structure with the respective π - π -distance. However, no peak can be found in the respective 2θ -range in the XRD pattern of **1**.

Recently, the aggregation behavior of a BTA with three unsubstituted phenyl side arms ($R = \text{H}$) was investigated.¹³⁷ The XRD pattern of the single crystal obtained from DMSO and of xerogels from DMSO/water mixtures are very similar and do not show a typical peak for the distance of the BTA cores. The detailed structure analysis showed an inclined columnar stacking with $\text{O-H}\cdots\text{N}$ hydrogen bonds utilizing two of the amide units. The third amide moiety was involved in hydrogen bonds with DMSO that acted as bridge between two adjacent molecular stacks. Besides the lack of typical indications for π - π -interactions of the BTA cores, also no rotation of adjacent molecules in the stack by 60° could be observed. This example demonstrates that anisotropic aggregates of BTAs can be crystalline and, despite the presence of an underlying columnar structure, strongly differ from the aggregation modes typically reported for BTAs.^{134,135} A similar inclined columnar structure might be present in bulk samples of compound **1** as obtained from synthesis. Due to the ability of the lateral amino moiety to form hydrogen bonds it might also be possible that intercalating structures are present that are formed by hydrogen bonds between the lateral amino moiety of one molecule with the core-amide moiety of a second molecule. For the structurally similar 3- and 4-pyridyl-substituted BTA derivatives such rosette-like structures have been reported in the literature.²⁶⁵ To identify the underlying structures and the molecular packing of the BTA molecules, a detailed structure analysis has to be carried out for compound **1**.

Compound **2** differs from compound **1** due to the dimethyl substitution of the lateral amine. Thus, compound **2** is sterically more demanding and can only act as a weak hydrogen bond acceptor in the periphery of the molecule. The SEM image of **2** shows thin fibrils with a diameter in the range of 40 nm to 80 nm and a length of several hundred nanometers (Figure 3.5a). The fibers are mainly isolated and do not entangle with each other to form bundles of fibers.

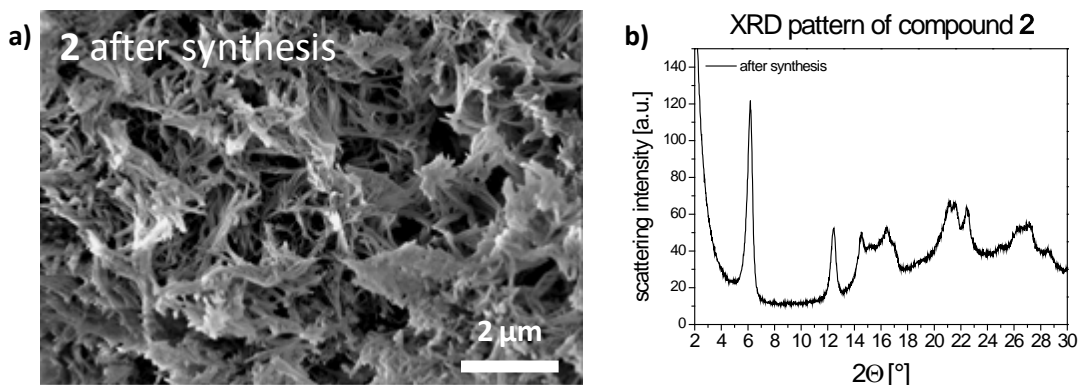


Figure 3.5: a) Morphological characterization of compound **2** ($R = \text{NMe}_2$) as obtained from synthesis by a typical SEM image and b) the corresponding XRD pattern.

The XRD pattern shows a less ordered morphology compared to the crystalline structure of compound **1** (Figure 3.5b). This might be due to the presence of aggregates with sizes in the nanometer range thus leading to less order on a long range scale. The 2θ values of the peaks show a 1 : 2 : $\sqrt{5}$: $\sqrt{6}$: $\sqrt{7}$ ratio that could not be assigned to a typical mesophase. The broad peak at 26.96° (2θ) corresponds to a π - π -distance of the BTA cores of 0.33 nm. In combination with the anisotropic aggregates found in the SEM images, the presence of an underlying columnar structure might be assumed, although a detailed structure analysis is necessary to elucidate the molecular packing of compound **2**.

The SEM image of compound **3** as obtained from synthesis shows agglomerated spheres with varying diameters from the submicron range to several microns (Figure 3.6a).

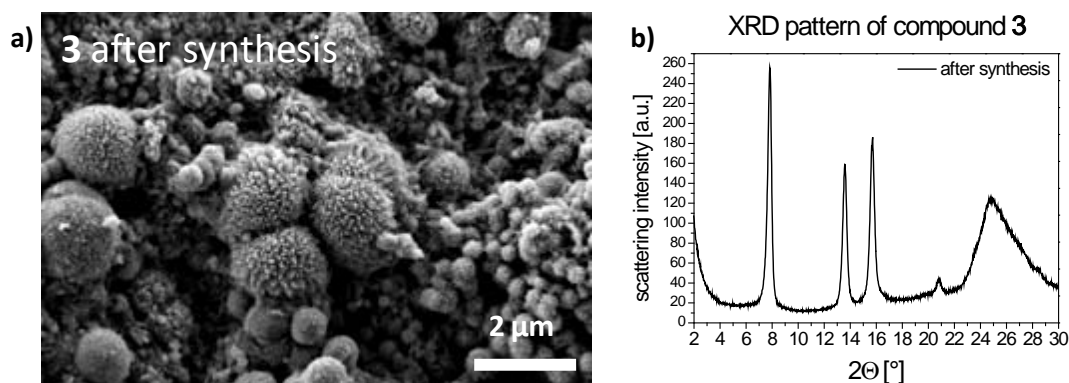


Figure 3.6: a) Morphological characterization of compound **3** (R = OH) as obtained from synthesis by a typical SEM image and b) the corresponding XRD pattern.

Those spheres consist of smaller underlying rod- or needle-like aggregates. In the literature the formation of organic nanoparticles from a triphenylamine-substituted BTA compound was described.³²³ Upon drop wise addition of a THF solution of the BTA derivative into water nanoparticles with diameters of 80 ± 20 nm were obtained. It therefore can be assumed that the formation of spherical aggregates might be due to the precipitation of compound **3** from *N*-methyl-2-pyrrolidone (NMP) solution by water during synthesis.

The XRD analysis reveals that the molecules are arranged in a columnar hexagonal crystalline mesophases (Figure 3.6b). The 2θ values of the Bragg peaks at 7.82° , 13.58° , 15.72° , and 20.80° show a $1:\sqrt{3}:2:\sqrt{7}$ ratio that is typical for columnar hexagonal arrangements. The π - π -distance of the BTA cores can be deduced from the peak at 24.86° (2θ) that corresponds to a real space distance of 0.36 nm which is within the typical range for amide hydrogen bonding lengths of stacked BTA molecules.²⁶⁷ The lattice distance a of the hexagonal columnar unit cell can be calculated using the following equation:²¹²

$$a = d_{hk0} \cdot \sqrt{\frac{4}{3}(h^2 + k^2 + hk)} \quad (3.1)$$

with d_{hk0} being the distance of the lattice planes with the Miller indices h , k , and $l = 0$.

The calculated lattice distance is 1.3 nm and gives the core-core distance of adjacent columns of stacked BTA molecules. Taken into account the estimated diameter of 1.7 nm of molecules of **3**, it is assumed that the side arms of molecules in adjacent columns interdigitate. Thus, the hydroxyl moiety in the periphery of the molecule might form weak hydrogen bonds with the amide moiety of the core. This could weaken the columnar stacking. The work of Jana *et al.* showed that strong core-side chain interactions of BTAs can have a drastic effect on the structure of the assemblies and might even lead to porous structures with a loss of the C_3 -symmetry and the triple amide-amide hydrogen bonds.²⁴² However, this is not the case for

aggregates of compound **3** as a hexagonal columnar mesophase could clearly be assigned to the measured XRD pattern of **3**.

After synthesis of **4** a porous, sponge-like structure is obtained, while after recrystallization from DMSO-water mixtures fiber fragments with a diameter around 80 nm and a length of about 1 μm can be observed in SEM images (Figure 3.7a and b).

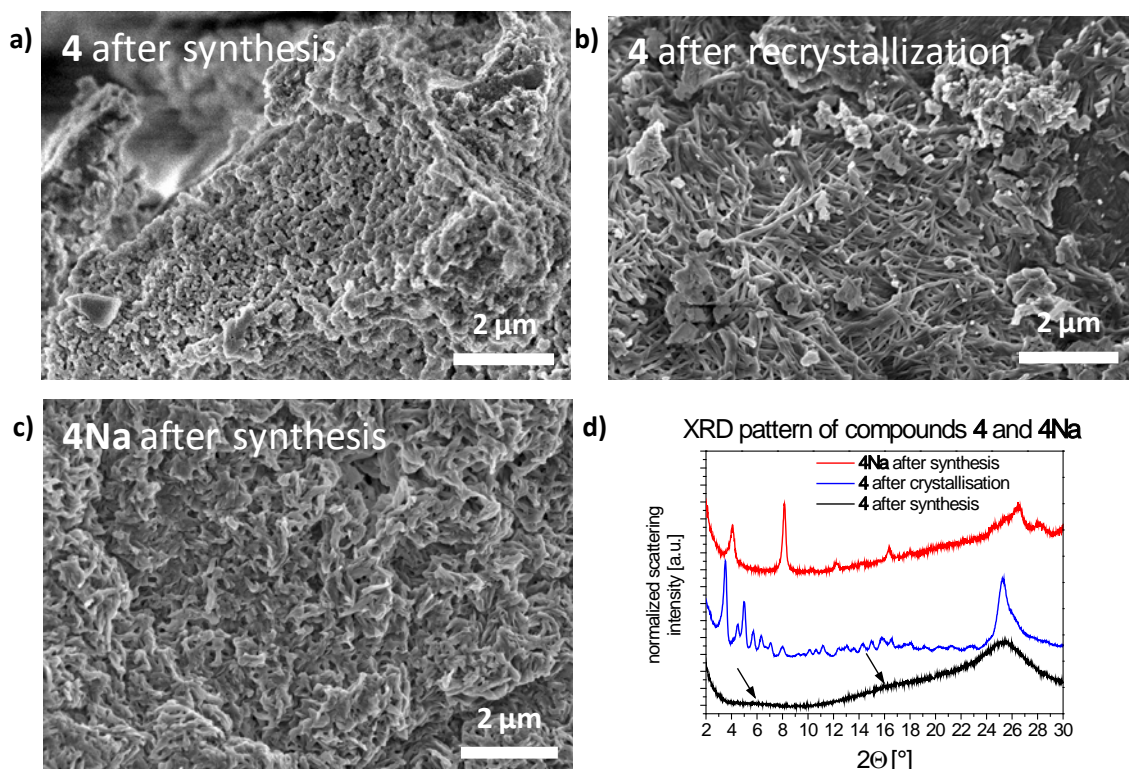


Figure 3.7: Morphological characterization by typical SEM images of a) compound **4** ($R = \text{COOH}$) as obtained from synthesis, b) of **4** after recrystallization from DMSO-water, and c) of compound **4Na** ($R = \text{COONa}$) as obtained from synthesis. d) Plots of the corresponding X-ray diffraction patterns of compound **4** after synthesis (black line), after crystallization (blue line) and of **4Na** after synthesis (red line). Note: Plots have been offset in the y-axis in order to ease visualization.

During synthesis compound **4** precipitates which is attributed to the substitution of the BTA core with three arms. Therefore, the system does not have the time to arrange in a one-dimensional manner. The cooling process after recrystallization, however, is slow so that the molecules can self-assemble into the fibrous structure. This is an indication that molecules of **4** have a tendency to aggregate in one-dimensional aggregates with high aspect ratios, if the system is given enough time for the self-assembly. The SEM image of the sodium salt derivative **4Na** shows a porous surface structure on the mesoscale with short rod-like substructures.

The XRD analysis shows that directly after synthesis compound **4** is amorphous (Figure 3.7d). Besides two very weak and broad peaks at 2θ values of approx. 6° and 17° (indicated

by black arrows), one broad peak with a maximum at 25.46° (2θ) can be found. This angle corresponds to a π - π -distance of 0.35 nm. After recrystallization compound **4** is crystalline and gives a completely different XRD pattern. However, the peak maximum found at 25.30° (2θ) also corresponds to a π - π -stacking distance of 0.35 nm (Figure 3.7d). The fact that the peak is more distinct and slightly shifted to lower 2θ values compared to the peak found in the XRD pattern of **4** directly after synthesis indicates that a higher ordered state is obtained in molecular stacks of **4** by crystallization.

The exact evaluation of the structure of **4** after recrystallization is rather difficult although single crystals of **4** were obtained serendipitously by hydrothermal synthesis in the presence of zinc and analyzed in detail by Y. Zhang *et al.*²¹⁰ Analysis of these single crystals gave a planar rosette-like or honeycomb-like arrangement of molecules of **4**. Thereby, adjacent layers are stacked on top each other and rotated by 180° . This leads to stacks of the BTA cores with the side arms of adjacent molecules being rotated by 60° . The layer-to-layer-distance of the two-dimensional honeycomb-like structure obtained from single crystals of **4** was reported to be 0.29 nm, however, in the respective CIF-file the structure gives a distance of about 0.32 nm. It was stated that hydrogen bond formation mainly occurs in plane between amide moieties of the core and lateral carboxylic acid moieties rather than intracolumnar amide hydrogen bonds. This is supported by the core-core distance of 0.32 nm which is significantly smaller than the average amide-amide hydrogen bond length of $0.36 \text{ nm} \pm 0.01 \text{ nm}$ between stacked BTA molecules.²⁶⁷ Thus, in the crystal structure of **4** adjacent sheets only interact *via* π - π -interactions. The influence of core-side chain interactions on the molecular assembly was shown for a tyrosine-substituted BTA derivative.²⁴² Thereby, the presence of core-side chain interactions instead of core-core interactions led to a loss of the C_3 -symmetry in the assembly and the formation of a porous structure.

Taking these considerations into account, it can be assumed that the molecular packing of **4** after recrystallization is different from the structure in the single crystal. In contrast to the layered structure in the single crystal, for compound **4** after recrystallization a columnar arrangement with hydrogen bonds between the amide moieties of the BTA cores is proposed. It is also possible that only two amides of the BTA core form hydrogen bonds with adjacent molecules in the stack, while the third one interacts with solvent molecules thus forming a bridge to adjacent columnar assemblies.¹³⁷ A similar arrangement might also be present for molecules of **4** as core-core as well as core-side chain interactions have been reported.^{210,267}

When comparing the data obtained in this thesis with the findings reported in the literature, it is important to note that polymorphism might occur for compound **4**. For the structurally similar pyridyl-substituted BTA-based hydrogelator that also can interact via core-

core, core-side chain and side chain-side chain interactions polymorphism was found.^{78,175,194,265} Four different crystal structures were obtained out of only two different solvent systems depending on the preparation method. These findings demonstrate that the arrangement of the molecules is greatly influenced by the sample preparation method and that the structure in the single crystal is not necessarily equal to the structure obtained after recrystallization or in reported xerogels of **4**.^{210,267}

Compound **4Na** is obtained from synthesis in a lamellar arrangement. The 2θ values of the peaks at 4.08° , 8.16° , 12.20° , and 16.38° feature a ratio of 1 : 2 : 3 : 4, which is typically for lamellar structures. The lattice parameter c of a lamellar structure can be calculated using the following equation:²¹²

$$c = h \cdot d_{h00} \quad (3.2)$$

with d_{h00} being the distance of the lattice planes with the Miller indices h and $k=l=0$.

The calculated lattice parameter c is 2.2 nm and corresponds well to the estimated diameter of 2.1 nm of molecules of **4Na**. This means that the molecule is only slightly smaller than the width of a lamella. Usually the intensity of the peaks decreases with increasing values for 2θ . This is not the case for the pattern obtained here which might be due to structure factor fluctuations. The peak at 26.50° (2θ) can be assigned to the π - π -distance between the benzene cores which is about 0.34 nm.

The SEM image of compound **5** reveals that also this compound has the tendency to form anisotropic structures. The obtained aggregates have diameters of about 140 nm and length of about several microns (Figure 3.8a).

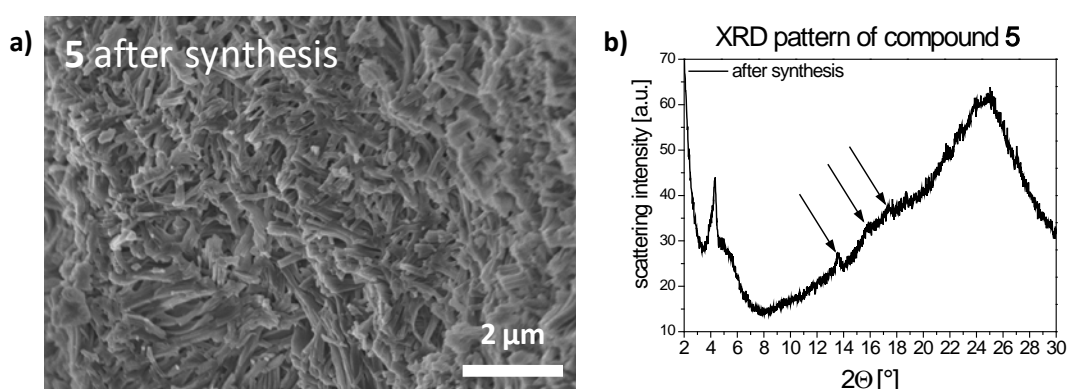


Figure 3.8: a) Morphological characterization of compound **5** ($R = \text{COOMe}$) as obtained from synthesis by a typical SEM image and b) the corresponding XRD pattern (small peaks are indicated by an arrow for better visualization).

The rod-like structures seem to be rather short and straight with few tendencies to intertwine and form bundles. The broad halo for high 2θ values in the XRD pattern of compound **5**

indicates large amorphous domains (Figure 3.8b). It seems that the halo overlaps the peaks in that region, such as at 15.82° and 17.36° (2θ) corresponding to a real space distance of 0.51 nm and 0.56 nm, respectively (indicated by an arrow). Only two further distinct peaks can be found at $2\theta = 4.34^\circ$ (2.03 nm) and 13.64° (0.65 nm), while the peak at 24.68° (2θ) is rather broad and corresponds to a real space distance of 0.36 nm, which is assigned to the π - π -distance.

Summarizing, the morphological characterization of the synthesized compounds is rather difficult, as small changes in the molecular structure, *i. d.* the type of the lateral headgroups, result in very different structures. However, for nearly all compounds a tendency to form anisotropic aggregates can be found. Furthermore, from the XRD peaks one can conclude π - π -interactions with distances in the range of 0.33 nm to 0.36 nm.

3.2.3 Solubility tests

The synthesized compounds **1** - **5** were all investigated regarding their solubility in common organic solvents and in aqueous solutions with different pH values at a fixed concentration of 10 g L^{-1} .

3.2.3.1 Solubility in organic solvents

As can be seen in Table 3.5, compounds **1** - **5** are insoluble in the apolar solvent n-hexane, while they show good solubility only in *N,N*-dimethyl formamide (DMF) and dimethyl sulfoxide (DMSO), which are very polar solvents that are known to break up even strong hydrogen bonds. This is an indication that hydrogen bonding is a major driving force regarding the aggregation of these compounds. The compounds also show high stability against other tested organic solvents and are often not or only partially soluble.

Compound **1** is only partially soluble in methanol and tetrahydrofuran (THF) at r. t. and shows a slightly increased solubility in ethanol upon heating, while compound **2** is partially dissolved in nearly all tested solvents except n-hexane. Thus, the possibility of compound **1** to form hydrogen bonds with the lateral amino moieties might be important for the stability of the solid in organic solvents. While compounds **3** and **5** are not dissolved in any other tested solvent, compound **4** is partially dissolved in tetrahydrofuran (THF). Compound **4Na** is not listed in the table below as it is insoluble in the tested organic solvents.

Interestingly, increasing the temperature to the boiling point of the respective solvent does not significantly increase the solubility of the compounds. Therefore, a heating and cooling cycle in organic solvents does not lead to the self-assembly of the molecules. The aim to design BTA derivatives for aqueous system thus led to molecules that do not show self-assembly

behavior in a broad variety of organic solvents. This confirms that self-assembly motifs designed for aqueous systems usually do not apply for organic solvents and *vice versa*.

Table 3.5: Overview of the solubility of compounds **1-5** in common organic solvents at a fixed concentration of 10 g L⁻¹.

| solvent | mixing at r. t. | | | | | mixing at b. p. | | | | | after heating to b. p. and cooling to r. t. | | | | |
|--------------------|-----------------|-----|---|-----|---|-----------------|-----|---|-----|---|---|-----|---|-----|---|
| | 1 | 2 | 3 | 4 | 5 | 1 | 2 | 3 | 4 | 5 | 1 | 2 | 3 | 4 | 5 |
| n-hexane | - | - | - | - | - | - | - | - | - | - | - | - | - | - | - |
| ethyl acetate | - | (+) | - | - | - | - | (+) | - | - | - | - | (+) | - | - | - |
| methanol | (+) | (+) | - | - | - | (+) | (+) | - | - | - | (+) | (+) | - | - | - |
| ethanol | - | (+) | - | - | - | (+) | (+) | - | - | - | - | (+) | - | - | - |
| isopropanol | - | (+) | - | - | - | - | (+) | - | - | - | - | (+) | - | - | - |
| dichloromethane | - | (+) | - | - | - | - | (+) | - | - | - | - | (+) | - | - | - |
| acetone | - | (+) | - | - | - | - | (+) | - | - | - | - | (+) | - | - | - |
| chloroform | - | (+) | - | - | - | - | (+) | - | - | - | - | (+) | - | - | - |
| tetrahydrofuran | (+) | (+) | - | (+) | - | (+) | (+) | - | (+) | - | (+) | (+) | - | (+) | - |
| acetonitrile | - | (+) | - | - | - | - | (+) | - | - | - | - | (+) | - | - | - |
| dioxane | - | (+) | - | - | - | (+) | (+) | - | - | - | (+) | (+) | - | - | - |
| dimethyl formamide | + | + | + | + | + | + | + | + | + | + | + | + | + | + | + |
| dimethyl sulfoxide | + | + | + | + | + | + | + | + | + | + | + | + | + | + | + |

r. t.: room temperature; b. p.: boiling point of the respective solvent;
+: soluble; (+): partially soluble, -: not soluble.

3.2.3.2 Solubility in aqueous solvents

To verify that the designed and synthesized BTAs **1-5** are soluble in aqueous media dependent on the pH value, solubility tests in aqueous solutions with different pH values were performed (Table 3.6).

It was expected that compound **1** should be soluble in an acidic milieu due to the protonation of the lateral amino moieties resulting in electrostatic repulsion between single molecules. However, it was found that it is insoluble in all tested media at r. t.. This indicates that despite the possibility to protonate the lateral amino moieties, the attractive interactions predominate. Interestingly, heating in 1 M phosphoric acid leads to the formation of yellow gels. This process is, however, not thermo-reversible, as the amine groups are oxidized upon heating in phosphoric acid and this oxidation step is strongly dependent on the time the enhanced temperature is applied. Due to more detailed studies performed in a practical course carried out by Alessia Weiß at the University of Bayreuth, it is suspected that partial oxidation is needed to ensure solubility upon heating, while too much oxidation hinders the

formation of a gel upon cooling. As compound **1** cannot be used as a pH-sensitive hydrogelator in aqueous hydrochloric acid and gel formation in phosphoric acid was not reproducible, detailed gelation studies of compound **1** are not included in this work.

Table 3.6: Overview of the solubility of compounds **1** - **5** in aqueous solution at different pH values at a fixed concentration of 10 g L⁻¹.

| aqueous solvent | mixing at r. t. | | | | | mixing at b. p. | | | | | after heating to b. p. and cooling to r. t. | | | | |
|-----------------------------------|-----------------|----------|----------|----------|----------|-----------------|----------|----------|----------|----------|---|----------|----------|----------|----------|
| | 1 | 2 | 3 | 4 | 5 | 1 | 2 | 3 | 4 | 5 | 1 | 2 | 3 | 4 | 5 |
| NaOH (pH = 14) | - | - | + | + | - | - | - | + | + | - | - | - | + | + | - |
| NaOH (pH = 13) | - | - | (+) | + | - | - | - | (+) | + | - | - | - | (+) | + | - |
| NaOH (pH = 12) | - | - | - | - | - | - | - | (+) | - | - | - | - | (+) | - | - |
| NaOH (pH = 11) | - | - | - | - | - | - | - | - | - | - | - | - | - | - | - |
| NaHCO ₃ sat. (pH = 10) | - | - | - | + | - | - | - | - | + | - | - | - | - | + | - |
| H ₂ O (pH = 7) | - | - | - | - | - | - | - | - | - | - | - | - | - | - | - |
| NaCl sat. (pH = 7) | - | - | - | - | - | - | - | - | - | - | - | - | - | - | - |
| HCl (pH = 2) | - | - | - | - | - | - | - | - | - | - | - | - | - | - | - |
| HCl (pH = 1) | - | + | - | - | - | - | + | - | - | - | - | + | - | - | - |
| HCl (pH = 0) | - | + | - | - | - | - | + | - | - | - | - | + | - | - | - |
| 5 M HCl (pH < 0) | - | + | - | - | - | - | + | - | - | - | - | + | - | - | - |
| 1 M acetic acid | - | (+) | - | - | - | - | (+) | - | - | - | - | (+) | - | - | - |
| conc. acetic acid | - | + | - | - | - | (+) | + | - | - | - | - | + | - | - | - |

r. t.: room temperature; b. p.: boiling point of the respective solvent; sat.: saturated
+: soluble; (+): partially soluble; -: not soluble.

The dimethyl amino functionalized BTA derivative **2** is soluble in aqueous hydrochloric acid with a pH value of or below 1, as well as in concentrated acetic acid. The different solubility of compound **2** compared to **1** can be explained by their different basicity. In aqueous media tertiary amines are more basic than primary ones, which is mirrored by the pK_a values of the conjugate acid of aniline (pK_a = 4.6) and *N,N*-dimethylaniline (pK_a = 5.8), respectively.³⁴⁰ Therefore, compound **2** is much easier protonated compared to **1** and thus better soluble in acidic milieu. In aqueous sodium hydroxide solutions with alkaline pH values, as well as in plain water and saturated sodium chloride solution with neutral pH value, compound **2** does not dissolve even upon heating. This pH-dependent solubility behavior is promising for further studies regarding the pH-sensitive self-assembling behavior.

As compound **3** and **4** have acidic lateral functional moieties, the lateral groups should be deprotonated in alkaline media. Consequently, the molecules should be soluble due to the electrostatic repulsive forces of the formed anions. As expected both BTA derivatives dissolve in aqueous sodium hydroxide solution with a pH value higher than 13, while they are insoluble

in aqueous HCl solution, plain water and saturated sodium chloride solutions. Thus, both compounds show pH-sensitive solubility. Their pH-sensitive solubility and aggregation behavior was investigated in more detail which is presented in the following chapter.

The sodium salt derivative of compound **4** (**4Na**) is soluble in plain water resulting in a slight alkaline solution, depending on the concentration of **4Na**, while it is not soluble in acidic milieu.

For BTAs containing chelated gadolinium(III) ions as headgroups it was reported that screening of the charges by addition of salt resulted in the formation of elongated nanorods and cooperative supramolecular polymerization.^{255,257} To prove if this technique also works for the compound **4Na**, to a **4Na** solution in water NaCl was added in small portions. While no aggregates could be observed in sat. NaCl solution, the further increase of the NaCl concentration led to the formation of a white precipitate. However, this is probably due to oversaturation and the increased hydrophobicity of the water upon addition of the salt, which is usually known as “salting out”-effect.

As compound **5** does not feature pH-sensitive moieties, no pH-sensitive solubility behavior is expected. Its solubility was tested in plain water, as well as in highly alkaline and highly acidic milieus. However, it did not dissolve in any of the tested solvents, even upon heating. As compound **5** shows good to moderate solubility in DMSO, but poor solubility in water, temperature-dependent dissolution experiments in DMSO/water mixtures were performed in a practical course by Manuel Suchy at the University of Bayreuth. Depending on the concentration of **5** and the solvent composition, gels could be produced in two ways. While adding the non-solvent water to a solution of **5** in DMSO often led to the formation of inhomogeneous gels, heating and cooling of a solution of **5** in DMSO/water mixtures resulted in homogeneous gels. At a final concentration of 10 g L⁻¹ of **5** in DMSO/water with a volume ratio of 1 : 1 thermo-stable, but inhomogeneous gels were obtained. Increasing the DMSO content to a ratio of 4 : 1 (DMSO/water), homogeneous gels could be obtained by a heating and cooling cycle. Thus, gels of **5** are formed at water contents of 20 % to 50 %. As the gel formation in mixtures of organic solvents and water is not the objective of this work, the detailed studies are not discussed here.

Due to the promising results of compounds **2**, **3**, and **4** gained by the solubility tests in aqueous solvents with different pH values, their pH-sensitive aggregation behavior was investigated further and the results are presented in the following.

3.3 pH-Sensitive aggregation and gel formation

In this chapter the aggregation behavior of compounds **2** - **4** in dependence of the pH value is investigated in view of their potential to form supramolecular hydrogels. The sensitivity towards the pH value is demonstrated on macroscopic scale by optical images and on micrometer scale during titration experiments combined with optical transmittance measurements. The resulting aggregates after change of pH are examined regarding their morphology in comparison to the structure obtained after synthesis. As compound **4** showed a high potential for the formation of stable supramolecular hydrogels upon change of pH, the aggregation behavior as well as the resulting gels of **4** were further studied using different gelation techniques.

3.3.4 Investigation of pH-sensitive aggregation

For the gelation tests of compound **2** an aqueous solution with a concentration of 10 g L^{-1} of **2** was prepared in diluted hydrochloric acid to yield a final pH value of 1. At this pH value the lateral dimethyl moieties of the BTA derivative should be fully protonated. By drop wise addition of a 1 M solution of sodium hydroxide the pH value was increased until an alkaline milieu was reached and the lateral functional moieties should be uncharged.

Compounds **3** and **4** were dissolved in aqueous (aq.) sodium hydroxide solution to yield a final pH value of 14 at a concentration of 10 g L^{-1} , respectively. Subsequently, both solutions were acidified by drop wise addition of a 1 M solution of hydrochloric acid. This change of the pH value should transfer the molecules of both compounds from the anionic to the neutral state. For the three tested compounds upon change of pH the transfer from the dissolved to the solid state could be observed, proofing that the pH-sensitive switches incorporated in the molecular structure work as expected. As three pH-sensitive moieties are present in each molecule of compounds **2**, **3**, and **4**, not only the uncharged or fully charged state is possible. It must be assumed that protonation or deprotonation occurs stepwise resulting in intermediate forms bearing one or two charges per molecule.

For identifying the gel state the inversion test tube method has been established in the literature.^{10,64} If the resulting solid can immobilize the water to resist gravitational flow in an inverted test tube, it is considered as a gel. Compound **2** and **3** precipitated as green and white solid, respectively, without formation of a stable gel (Figure 3.9). Compound **4**, however, formed a white hydrogel as confirmed by inverting the test tube.

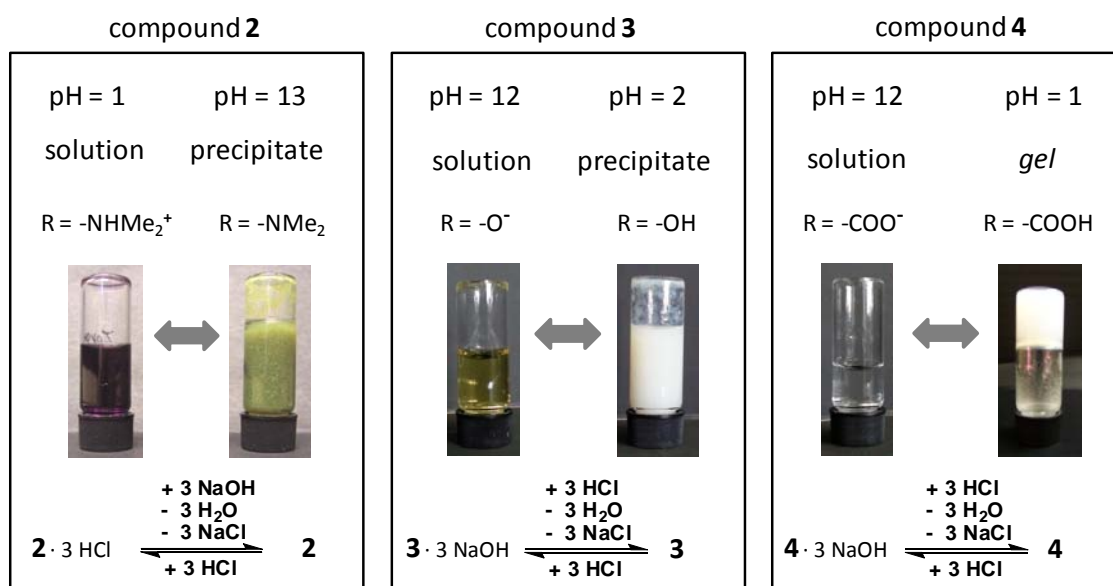


Figure 3.9: Transition from sol to solid by change of pH of compounds 2 - 4.

3.3.4.1 pH-Titration experiments

For all three pH-sensitive compounds titration experiments were performed combined with detection of the optical transmittance of the solution at a wavelength of 523 nm. Solutions of **2**, **3** and **4** were prepared with a final concentration of 1 g L⁻¹ each. The measurements were performed under stirring to achieve homogeneous distribution of the respective precipitate and to prevent the formation of a stable gel for compound **4**.

For compound **2** the starting pH value of the solution was adjusted by addition of aq. HCl to a final pH value of 2.25. A 0.1 M solution of NaOH was used as titer solution. The pH value and the relative (rel.) transmittance of the solution were measured and plotted against the amount of added titer volume (Figure 3.10).

The rel. transmittance is normalized in relation to pure water, which consequently has a rel. transmittance of 1. As compound **2** gives a purple color in solution, it absorbs light in the range of the used laser (523 nm). Therefore, the rel. transmittance of the solution of **2** is about 0.2. Upon addition of HCl, the solution of **2** slightly clears off before aggregation begins and the transmittance decreases again. The correlation between the rel. transmittance and the pH value shows that measurable aggregation for compound **2** starts at a pH value above 3.68.

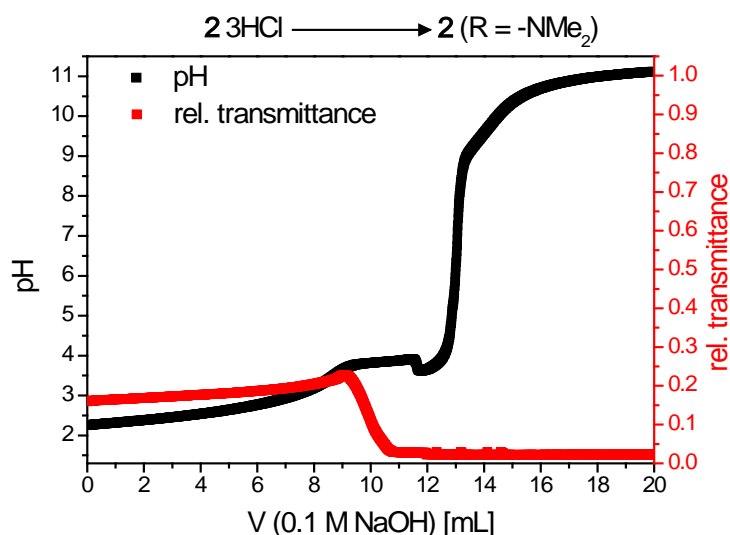


Figure 3.10: Titration curve of compound **2** with the pH value and rel. transmittance plotted versus the titer volume of 0.1 M NaOH solution.

The starting pH value of the aqueous solution of **3** was adjusted by addition of aq. NaOH solution until complete dissolution at a final pH value of 11.76 was achieved (Figure 3.11).

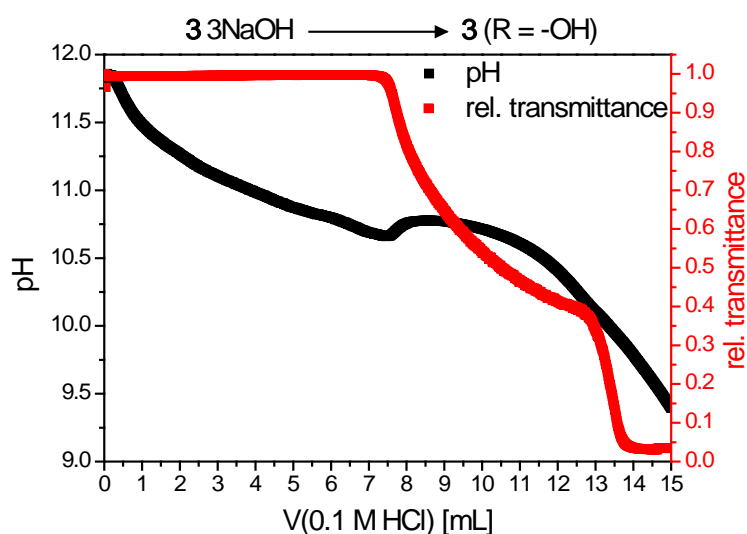


Figure 3.11: Titration curve of compound **3** with the pH value and rel. transmittance plotted versus the titer volume of 0.1 M HCl solution.

The titration was performed with a 0.1 M HCl titer solution and the rel. transmittance of the solution decreased in two steps. Below a pH value of 10.66 the rel. transmittance of the solution decreased indicating the formation of pre-aggregates. The subsequent rise of the pH value from 10.68 to 10.78 upon further addition of the titer solution might be explained by the buffer effect of **3** or a non-equilibrium state due to the experimental conditions. At a pH value

of 10.20 the rel. transmittance further decreases which is associated with the assembly of the pre-aggregates into bigger structures.

Such a two-step aggregation behavior in dependence of a pH change is known from peptide-based low molecular weight hydrogelators that have a terminal carboxylic acid group.³⁴¹ For these molecules two apparent pK_a values are observed. The first one is associated with the self-assembly of charged and uncharged molecules into paired fibrils. At a sufficiently high concentration these paired fibrils or fibers can entangle and immobilize the solvent to form a stable hydrogel. Due to the arrangement of the molecules in the paired fibrils, the charges of the carboxylate moieties are located at the aggregate surface preventing aggregation into superstructures. Further decrease of the pH value leads to a decrease of the surface charges enabling the fibers to assemble into large rigid ribbons due to lateral hydrophobic interactions. Below the second apparent pK_a value the ribbons further aggregate and precipitate. Such a shift of the apparent pK_a value was also reported for other compounds in the literature.^{60,89,93,267,342}

Similar to compound **3** the BTA-derivative **4** was dissolved in diluted aq. NaOH solution. The solution with a final pH value of 10.70 showed a decrease of the rel. transmittance in two steps upon titration with 0.1 M HCl solution (Figure 3.13).

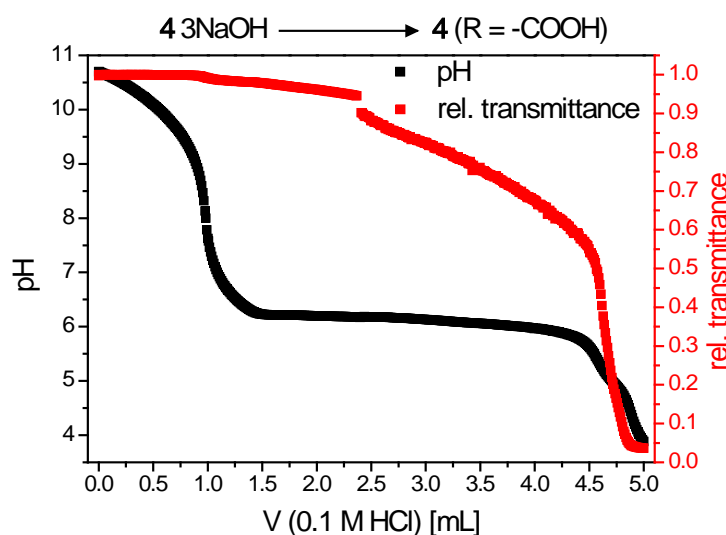


Figure 3.12: Titration curve of compound **4** from alkaline to acidic pH values with the pH value and rel. transmittance plotted versus the titer volume of 0.1 M HCl solution.

At the beginning of the titration experiment molecules of **4** should be present in their completely deprotonated state. By dynamic light scattering (DLS) experiments, the absence of any larger aggregates of compound **4** at such high pH values was proven. A slight decrease of the rel. transmittance was already observed at pH values around 10, indicating the presence of

first aggregates. However, it should be noted that due to the drop wise addition of the acid, the pH value is locally strongly decreased. This inhomogeneous decrease of the pH value in the solution might lead to the formation of kinetically trapped aggregates.

In analogy to the literature it is assumed that the first aggregates are formed by a combination of charged and uncharged molecules.³⁴¹ As compound **4** contains three carboxylic acid groups, also partially charged molecules can participate in the aggregate formation. During titration the pH value reaches a pronounced plateau at 6.25, while simultaneously the rel. transmittance continuously decreases. This phenomenon is probably caused by the buffer effect of compound **4** and the subsequent protonation of the three carboxylic acid groups, which results in a decreased surface charge of the formed aggregates and thus further self-assembly. The drop of the pH value after the plateau is accompanied by a sudden decrease of the transmittance at and below a pH value of 5.42. This is probably caused by the formation of bigger aggregates or superstructures.

The dissolution of assemblies of **4** was investigated by titrating back the acidic suspension to an alkaline pH value using 0.1 M NaOH solution (Figure 3.13).

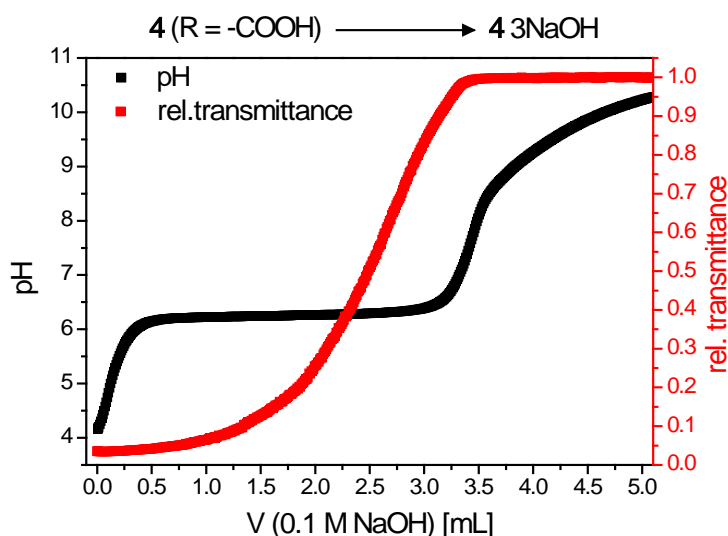


Figure 3.13: Titration curve of compound **4** from acidic to alkaline pH values with the pH value and rel. transmittance plotted versus the titer volume of 0.1 M NaOH solution.

The increase of the rel. transmittance and thus disassembly of the aggregates occurs in one step at a pH value of 6.17, indicating that the formation of the first aggregates at a pH value of about 10 is caused by the inhomogeneous decrease of the pH value and kinetic effects.

In the literature the calculated and measured pK_a values of different BTA-based hydrogelators with carboxylic acid moieties and compound **4** have been compared.²⁶⁷ The predicted pK_a value of **4** was about 2.2 units higher than the apparent pK_a value. This

observation can be supported by the measurements presented here. The apparent pK_a value of compound **4** was determined to be 6.25. This significantly differs from the apparent pK_a s of similar structural motifs with only one carboxylic acid moiety, such as benzoic acid and 4-benzamidobenzoic acid, which have a pK_a value of 4.19 and 4.06, respectively. The discrepancy between the expected and measured pK_a value can be explained by an apparent pK_a -shift upon aggregation. This phenomenon is well documented for amino-acids and peptides.^{60,89,93,267,341,342} While α -carboxylic acid groups of amino acids and N-protected nonpolar peptides have a pK_a value of about 3.5, most peptide-based hydrogelators aggregate at a pH value of about 5.^{32,98} The shift is associated with the aggregation of the molecules and the resulting change of hydrophobic interactions.

To visualize the early stages of the pH-dependent aggregation of compound **4**, titration experiments combined with DLS and cryo-transmission electronic microscopy (cryo-TEM) imaging were performed. During titration experiments first aggregates can be detected at a pH value of 9.2 using DLS, while in cryo-TEM images anisotropic rod-like aggregates can be observed at pH values of 7.5 and 5.9 (Figure 3.14).

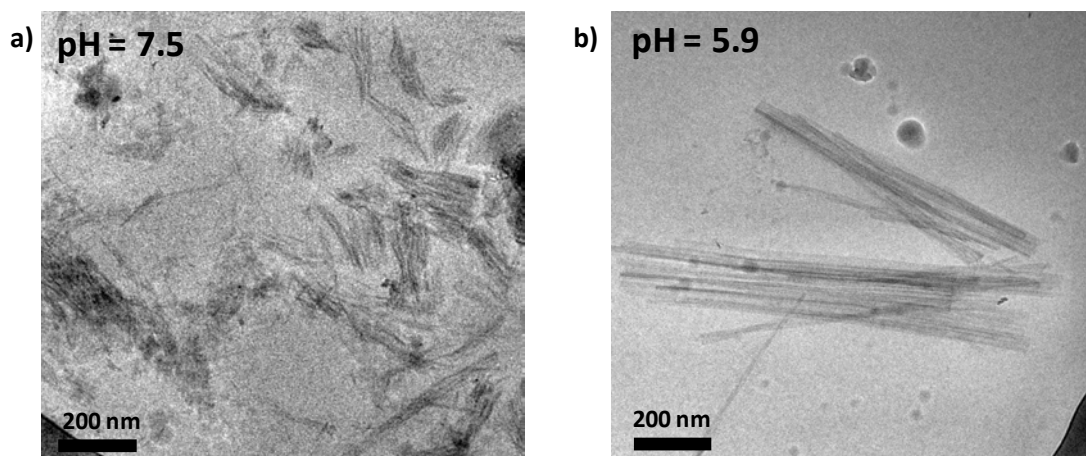


Figure 3.14: cryo-TEM images of **4** dissolved in diluted NaOH solution and titrated with 0.1 M HCl solution to a pH value of a) 7.5 and b) 5.9.

Usually with DLS autocorrelation curves the hydrodynamic radius of formed aggregates can be calculated. For this calculation it is assumed that hard, solid, and isolated spheres are present in the solution. As from cryo-TEM images it can be clearly seen that anisotropic aggregates are formed, the evaluation of a hydrodynamic radius is not reliable for this system. Nevertheless, it can be stated that at a pH of 9.2 aggregates in the range of 10 nm to 100 nm are present. However, as discussed above the presence of aggregates at such a high pH value might be due to the local change of the pH value by the drop wise addition of the aq. HCl solution which can result in kinetically trapped aggregates. The evaluation of the cryo-TEM images reveals that

underlying anisotropic aggregates are parallel aligned to form loose bundles with a length of around 500 nm. The smallest measured distance between electron-rich areas are about 2.2 nm. This is slightly greater than the estimated diameter of a single molecule of **4** (1.9 nm), but in good accordance with the lattice parameter $c = 2.2$ nm of the lamellar arrangement of **4Na** after synthesis. The underlying structures align to form ribbon-like structures with diameters between 10 nm and several tens of nanometer. Most probably molecules of **4** are not completely protonated at a pH value of 7.5 and 5.9. Thus, partially protonated forms are present that bear one or two charged carboxylate moieties per molecule. Consequently, the formed aggregates should also bear surface charges that prevent further aggregation.

In the literature the thermo-sensitive aggregation of crown-ether substituted BTAs led to the formation of aggregates at elevated temperature.²⁶² SEM images showed parallel aligned strands of fibers with diameters in the range of 20 nm which is larger than the diameter of a single molecule thus implying the formation of a more complex structure than a columnar stack of BTA molecules. For BTAs with pH-sensitive headgroups the self-assembly in aqueous systems showed single or triple helical aggregates depending on the applied conditions.²⁵² Obviously, the formation of helical stacks with three BTA molecules in the cross-section leads to diameters of the underlying aggregates that exceed the diameter of a molecule. In case of azobenzene substituted BTAs with sulphonic acid headgroups even the formation of helical tubes with water channels displaying diameters of about 3 nm could be observed.²³⁷ And studies on halogen-phenyl-substituted BTAs showed that side arm-side arm interactions, such as halogen-halogen interactions are one of the driving forces for the assembly into triple helices.^{193,196}

Considering these findings from the literature, it might be possible that the underlying aggregates observed in the TEM images with dimensions of 2.2 nm consist of single or triple helical stacks. Due to the presence of partially charged molecules of **4** and the resulting surfactant activity of these molecules, it is reasonable to assume that upon formation of such helical arrangements protonated and thus uncharged side arms are enclosed inside the helix, while charged side arms are located at the surface of the assembly.

The investigation of partially fluorinated BTA derivatives showed that the self-assembly occurred in two steps.²³⁴ First, thermodynamic controlled aggregation into one-dimensional helical assemblies was observed that was mainly driven by hydrogen bonding interactions. Second, the kinetically controlled nucleation led to the formation of hierarchical bundles. Prior to the bundling the one-dimensional aggregates showed some kind of microphase separation that led to fluorine enriched patches or ribbons. Such a step-wise aggregation is proposed for the pH-sensitive self-assembly of **4**. The formation of the underlying anisotropic aggregates is

proposed to be mainly driven by hydrogen bonding interactions between amides of adjacent BTA cores and between amides and protonated side arms. Dependent on the pH value and the present surface charges, these probably triple helical structures align to form ribbon-like assemblies as observed in the cryo-TEM images.

3.3.4.2 Investigation of compounds 2 - 4 after change of pH

The resulting aggregates of compounds **2**, **3**, and **4** after change of pH from a solution with a respective compound concentration of 10 g L^{-1} were investigated using FT-IR spectroscopy, SEM imaging and XRD measurements.

The FT-IR spectra of all three compounds after change of pH are equal to the spectra from the bulk materials as obtained from synthesis (chapter 3.2.2.2). This proves that hydrogen bonds are also present after solidification of the compounds by change of pH value.

Compound **2** was isolated after synthesis by change of pH from acidic solution to pH 8. For the gelation tests the pH value was switched from pH 0 to 13 by addition of aq. NaOH solution. Due to the similarity of the sample preparation method, it is expected that the resulting aggregates have a similar morphology. Therefore, it was not surprising that the SEM images obtained from the washed and dried precipitate after change of pH strongly resembled the image of the bulk material after synthesis as displayed in Figure 3.7 in chapter 3.2.2.3. As both samples show thin fibrillar structures with diameters of 40 nm to 80 nm, no additional image is presented here. The comparison of the XRD patterns of both preparation methods for compound **2** shows that indeed the same underlying molecular arrangement is present in both cases (Figure 3.15).

The sharp peak at 27.24° (2θ) that corresponds to a real space distance of 0.33 nm is attributed to small crystals of sodium chloride that might have formed during the drying process.

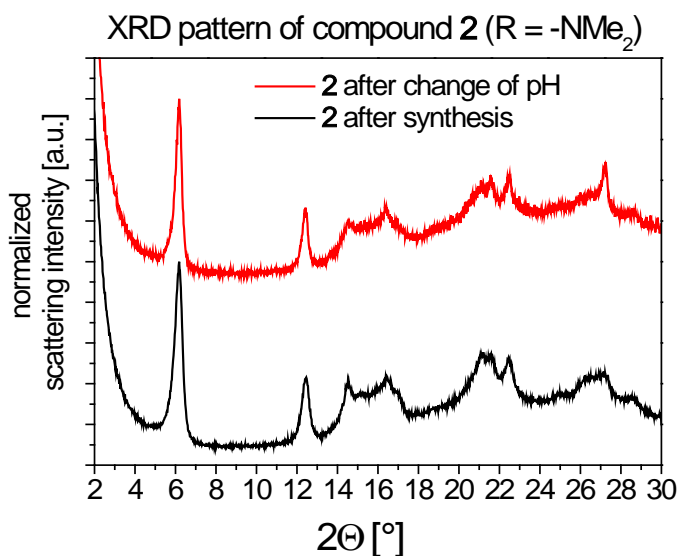


Figure 3.15: X-Ray diffraction patterns of the washed and dried compound **2** ($R = \text{NMe}_2$) as obtained from synthesis (black line) and after change of pH from acidic solution ($\text{pH} = 0$) to alkaline solution ($\text{pH} = 13$) with aq. NaOH solution (red line). Note: Plots have been offset in the y-axis in order to ease visualization.

Compound **3** was isolated after synthesis by precipitation in neutral water from *N*-methyl-2-pyrrolidone (NMP) solution. For the experiments regarding the change of pH, the compound was dissolved at a pH value around 12. Subsequently, aq. HCl solution was added drop wise until a final pH value of about 1 was reached. The obtained precipitate was washed and dried prior to the investigations.

The SEM images of compound **3** after change of pH show a different superstructure than images obtained from samples directly after synthesis. While from synthesis spherical objects with underlying fibrous structures were observed (Figure 3.6, chapter 3.2.2.3), after the change of pH solely one-dimensional aggregates and bundles thereof can be detected in the SEM images (Figure 3.16a). The rod-like structures have diameters of about 30 nm and are 0.5 μm to 1 μm in length. Although different superstructures can be observed in SEM investigations due to the different preparation methods, the XRD pattern show that in both cases the molecules are arranged in a columnar hexagonal crystalline phase (Figure 3.16b). For both samples the π - π -distance of the BTA cores in the columns is 0.36 nm and the lattice distance a of the unit cell is $a = 1.3$ nm (equation 3.1, chapter 3.2.2.3). The peak found at 27.20° (2θ) indicates the presence of sodium chloride crystals analogous to the peak observed in the XRD pattern of compound **2** after change of the pH value.

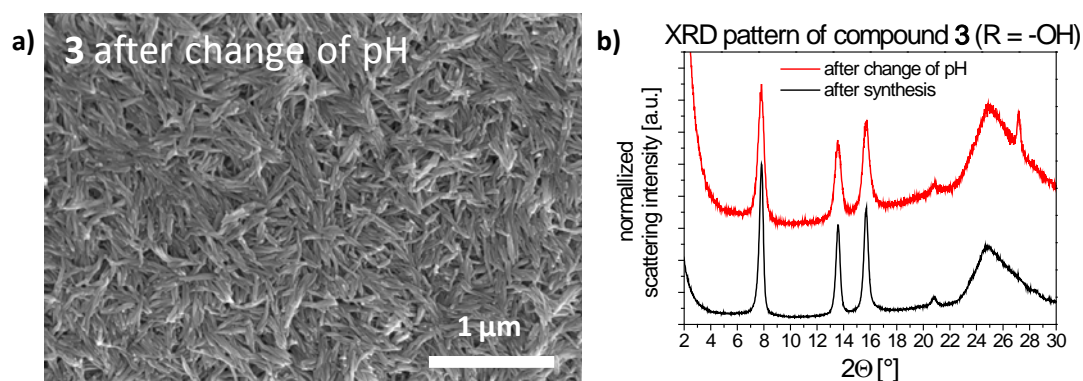


Figure 3.16: a) Morphological characterization of the washed and dried compound **3** ($R = \text{OH}$) after change of pH from alkaline solution ($\text{pH} = 12$) to acidic solution ($\text{pH} = 1$) with aq. HCl solution by a typical SEM image and b) the corresponding X-ray diffraction pattern (red line). For comparison reasons the XRD pattern of compound **3** as obtained from synthesis is also shown (black line). Note: Plots have been offset in the y-axis in order to ease visualization.

After synthesis, compound **4** was recrystallized from a DMSO/water mixture yielding a crystalline precipitate. For the hydrogel formation the compound was dissolved in aq. NaOH solution with a final pH value of about 12. By drop wise addition of aq. HCl solution the pH value was decreased to about 1. The obtained gel sample was washed and dried prior to the investigations.

Gelation of compound **4** with aq. HCl solution gives rod-like structures with diameters in the range of 20 nm as can be seen in the SEM image displayed in Figure 3.17a. When discussing the morphology displayed in the SEM image and the pattern obtained from the XRD measurements, it should be noted that the drying of the gel sample might lead to a closer molecular packing than in the native (wet) state.

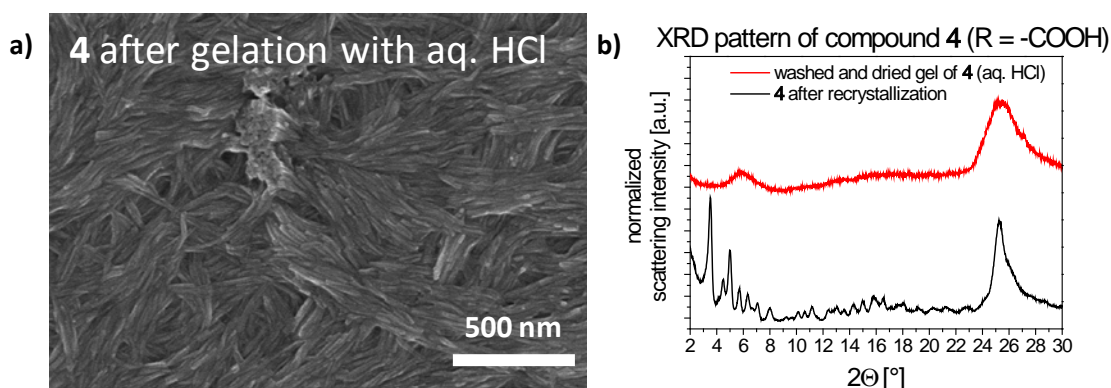


Figure 3.17: a) Morphological characterization of the washed and dried compound **4** after hydrogel formation by change of pH from alkaline solution ($\text{pH} = 12$) to acidic solution ($\text{pH} = 1$) with aq. HCl solution by a typical SEM image and b) the corresponding X-ray diffraction pattern (red line). For comparison reasons the XRD pattern of compound **4** as obtained after recrystallization is also shown (black line). Note: Plots have been offset in the y-axis in order to ease visualization.

The obtained diameters of underlying fibrillar aggregates determined in SEM images of about 20 nm are significantly larger than the distances of 2.2 nm obtained from the cryo-TEM images during titration (Figure 3.14). Thus, it must be assumed that the fibrillar aggregates observed in the SEM image consist of several underlying, probably triple helical, aggregates. As molecules of **4** should be fully protonated and uncharged in the washed and dried gel, the formation of superstructures is possible. Thus, in contrast to the fibrous structures obtained from recrystallization, the fibers present in the dried hydrogel align and bundle to form superstructures with diameters of about 200 nm. Due to this entanglement and bundling the length of a single fiber is difficult to evaluate.

The XRD pattern of the dried hydrogel sample shows only a weak diffraction pattern (Figure 3.17b) which is consistent with reports from the literature.²⁶⁷ One broad peak in the range of 25.56° (2 θ) can be assigned to the π - π -distance of the BTA cores of 0.35 nm. This peak was also observed in the bulk material of **4** after recrystallization from DMSO-water. The smaller bandwidth of the peak in the XRD pattern of **4** after recrystallization indicates a larger size of the respective crystalline domains and thus a higher order compared to the dried gel sample. As discussed above, in the literature the distance of the benzene cores of about 0.35 nm was taken as indication that amide hydrogen bonds between stacked molecules are present.²⁶⁷

The second peak in the XRD pattern of dried hydrogels of **4** prepared with aq. HCl solution is very broad and can be found at about 16° (2 θ). The low long-range order in the hydrogel results in a low resolution of single peaks. Thus, the broad peak at about 16° (2 θ) might consist of several underlying peaks. Due to the higher order in the sample of **4** after recrystallization, in the respective XRD pattern single peaks can be found in this region.

The peak at 5.86° (2 θ) in the XRD pattern of the hydrogel corresponds to a real space distance of 1.51 nm. This is slightly smaller than the diameter of molecules of **4** (1.9 nm) and the distance of 2.2 nm obtained from the cryo-TEM images during titration with aq. HCl solution.

Due to the removal of water molecules, drying can lead to a closer molecular packing of the underlying structures, thus resulting in smaller real space distances. Interestingly, the structure analysis of the single crystal of **4** in the literature gave a hexagonal unit cell with unit cell dimensions of $a = b = 1.51$ nm and $c = 1.89$ nm.²¹⁰ However, as discussed above in the layered structure of the single crystal hydrogen bonding interactions are only present between the amide moiety of the core and the lateral carboxylic acid group of the adjacent stack. This leads to a molecular packing with interdigitating side arms of adjacent molecules in one layer.

The differences between the XRD pattern of the dried hydrogel sample and the recrystallized sample of **4** show that for compound **4** the molecular arrangement is influenced by the preparation method. On the other hand, for compounds **2** and **3** the XRD patterns of

the materials as obtained from synthesis and after change of pH were equal and no stable hydrogels could be obtained. These different properties regarding the pH-sensitive self-assembly of the compounds indicate that the lateral headgroups of the BTA derivatives not only induce the pH-sensitivity but also strongly influence the formation of superstructures. One should always keep in mind that for the self-assembly of BTAs besides core-core interactions, also core-side chain and side chain-side chain interactions determine the resulting structure of the aggregate. Compound **4** seems to fulfill the delicate balance of these interactions so that the formation of stable hydrogels is possible. It is proposed that the ability of the lateral headgroups of **4** to participate in hydrogen bonds as donor and acceptor is a major criterion for the success of the structural concept.

As of the tested derivatives only compound **4** with its carboxylic acid functionalization is able to form hydrogels, different gel formation methods as well as gel properties of **4** are presented in the following.

3.3.5 Gel preparation methods for compound **4**

Only in the last few years the influence of different gelation methods on the properties of supramolecular hydrogels has gained interest in the scientific community. Studies on the gel properties of pH-sensitive peptide-based hydrogelators as well as gel formation by catalytic *in situ* preparation of the gelator showed the high impact of the gelation method on the resulting gel structures and therefore mechanical properties.^{65,73,93,343}

In the following, different methods for the gelation of hydrogels of **4** are presented and discussed. Interestingly, the blue photoluminescence of hydrogels of **4** upon irradiation with UV light at 366 nm proved to be an effective tool to visualize inhomogeneities in the gels by the naked eye.¹ To ease the preparation of the hydrogels and guarantee analogous testing conditions for all methods, the water soluble sodium salt derivative **4Na** was used in desalted water at a concentration of 10 g L⁻¹ for all gelation tests. DLS (dynamic light scattering) experiments showed the absence of any large aggregates in solutions of **4Na** in desalted water at that concentration. The investigations regarding the gel properties in dependence of the gelation method are a continuation of preliminary studies during my diploma thesis.³³⁸

3.3.5.1 Gelation by addition of aqueous acid solutions

The simplest way to decrease the pH value of a solution and thus induce pH-sensitive gel formation is to add aqueous acid solutions. It was already shown above that gels of **4** can be prepared by addition of aq. HCl solution to an alkaline gelator solution and that the resulting

¹ Detailed spectroscopic investigations of the photoluminescence of compound **4** in bulk and as hydrogel are discussed in chapter 4 and in the literature.¹⁰²

fibrils observed in SEM images were very short and bundled to fibers (Figure 3.17, chapter 3.3.1.2). However, gelation can also be induced by the addition of other aqueous acid solutions, *e. g.* sulfuric acid, acetic acid, phosphoric acid, nitric acid, as well as acidic salts, such as sodium hydrogen sulfate and sodium dihydrogen phosphate (Figure 3.18).

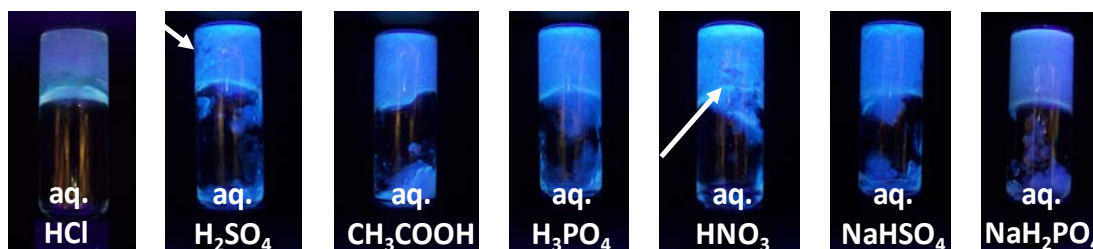


Figure 3.18: Images of gels prepared by addition of a few drops of different aqueous acids to a solution of **4Na** with a concentration of 10 g L^{-1} ; from left to right: 1 M HCl, 1 M H_2SO_4 , 1 M CH_3COOH , 1 M H_3PO_4 , 1 M HNO_3 , sat. NaHSO_4 solution and sat. NaH_2PO_4 solution. Note: Images were taken under UV irradiation at $\lambda_{\text{exc}} = 366 \text{ nm}$ in order to visualize inhomogeneities in the gels (indicated by the arrows).

The final pH value in the gel is dependent on the amount and concentration of added acid, but was determined to be 1 or below for all samples in this study. A great advantage of this preparation method is the ease of the procedure and the rapid change of the pH value in the solution. Thus, gel formation takes place within seconds. However, this often leads to inhomogeneous gels, as the sample partially solidifies before a homogeneous pH value can be obtained in the gelator solution. The gel properties are very dependent on the addition rate of the acid solution and the mixing of the sample. Due to the fast gelation rate inhomogeneities in these gel samples can often be observed on a macroscopic scale (see arrows in Figure 3.18). In the literature the formation of inhomogeneous gels from pH-sensitive supramolecular hydrogelators by addition of aqueous acid solutions is a known problem.^{65,93,98}

Summarizing, as this gelation method is not suitable to get reproducible and reliable data, no further characterization of the resulting hydrogels was performed.

3.3.5.2 Gelation *via* acidic gas

To overcome the problem of inhomogeneities in the gel samples due to the rapid change of the pH value and gel formation already during the mixing process, alternative methods to change the pH value were needed. It was shown in the literature that acetic acid vapor is adequate for inducing gelation of dicarboxylic L-valyl-L-valine bolaamphiphile hydrogelators.¹⁰⁸ Using this technique on aqueous **4Na** solutions for the preparation of gels of **4**, only samples with enlarged inhomogeneities could be prepared, thus making further analysis of the gel properties unreasonable (Figure 3.19a). However, hydrochloric acid vapor or gas can easily be used to prepare macroscopic homogeneous gel samples (Figure 3.19b). Gelation begins at the

surface of the solution and as diffusion of the gas continues, the whole sample is solidified. Gelation time is dependent on the volume of the solution and the surface area exposed to the acidic atmosphere. It can vary between *approx.* 3 h for a sample volume of 2 mL with an exposed surface area of about 177 mm² to up to 24 h for a sample volume of 35 mL and an exposed surface area of about 707 mm². The pH value after complete gelation is about 1 in the whole sample.

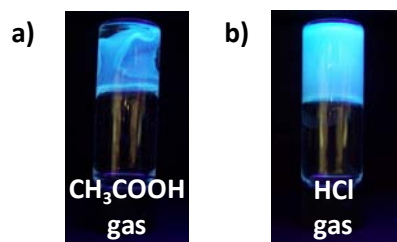


Figure 3.19: Images of gels prepared by diffusion of a) acetic acid vapor and b) gaseous hydrochloric acid into a solution of **4Na** with a concentration of 10 g L⁻¹ (gelation time: 3 h). Note: Images were taken under UV irradiation at $\lambda_{\text{exc}} = 366$ nm in order to visualize inhomogeneities in the gels.

Fibers visible in SEM images of dried samples prepared with gaseous HCl are very similar to fibers prepared by addition of acidic solution (Figure 3.20).

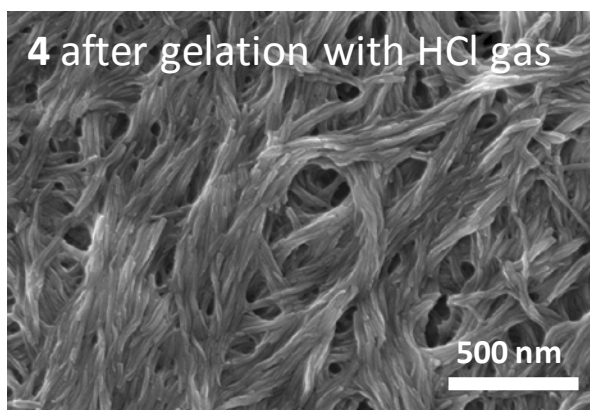


Figure 3.20: A typical SEM image of a washed and dried gel of **4** prepared by diffusion of gaseous HCl into an aqueous solution of **4Na** with a concentration of 10 g L⁻¹.

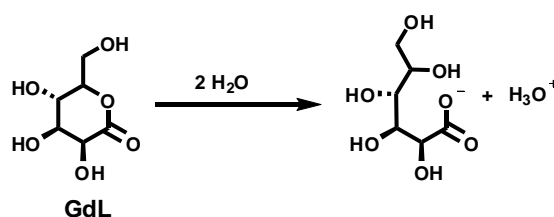
While the underlying structures have diameters of about 20 nm, the formation of superstructures leads to fiber bundles with diameters in the range of several hundreds of nanometer. Due to the bundling, the evaluation of the fiber length is rather difficult. However, the fiber lengths seem to be greater after gelation with HCl gas compared to gel samples prepared by addition of aq. HCl solution. This might be explained by the different gelation times and thus different kinetic conditions. Nevertheless, the underlying anisotropic

aggregates seem to be very similar for both preparation methods indicating that the intermolecular interactions that act as driving forces for the self-assembly are the same.

Further analysis of properties of gels prepared by diffusion of gaseous HCl is presented in chapter 3.3.3.

3.3.5.3 Gelation *via* hydrolysis of glucono-delta-lactone (GdL)

A very successful method to prepare homogeneous pH-sensitive hydrogels is the decrease of the pH value using the hydrolysis of glucono-delta-lactone (GdL) in water (Scheme 3.5).^{16,73,88,98,100,101}



Scheme 3.5: Hydrolysis of glucono-delta-lactone (GdL) in water.

As hydrolysis of the lactone is slower than its homogeneous distribution and dissolution, the pH value in the whole solution can be decreased simultaneously. Using this method very slow and homogeneous gelation can be induced. The hydrolysis reaction follows that of an exponential decay. This can be monitored by the time-dependent decrease of the pH value in combination with the rel. transmittance of the solution similar to the titration experiments performed for compounds **2** – **4** (chapter 3.3.1.1). To protonate the three carboxylate moieties of each **4Na** molecule three molecules of GdL are needed. Due to the method used for the isolation of **4Na**, it might be possible that excessive sodium hydroxide is present in solutions of **4Na**. To make sure that the pH value decreases below the critical gelation pH value, four times the molar amount of GdL (4 equivalents; eq.) compared to the molar amount of **4Na** were used, if not stated otherwise. This relation can be expressed by the following equation:

$$n(\text{GdL}) = x \cdot n(\mathbf{4Na}) \quad (3.3)$$

with $n(\text{GdL})$ being the molar amount of GdL, $n(\mathbf{4Na})$ the molar amount of **4Na**, and x the chosen equivalents, in this case 4 eq.. Assuming that 3 eq. GdL are needed for the protonation of the carboxylate moieties of **4Na**, 1 eq. GdL causes the decrease of the pH value.

The decrease of the pH value over a time period of 8 h due to the hydrolysis of GdL in plain water is shown in Figure 3.21. The GdL amount was chosen to be 1 eq. for a **4Na** solution with a concentration of 1 g L^{-1} ($c(\mathbf{4Na}) = 1.58 \text{ mmol L}^{-1}$).

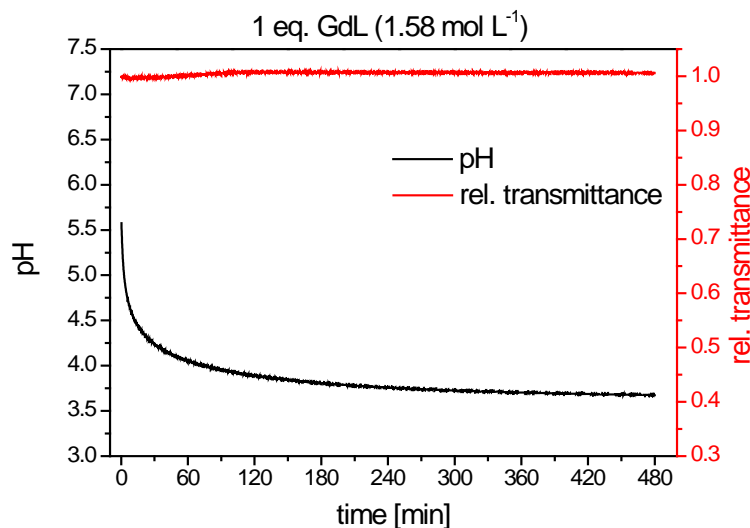


Figure 3.21: Change of the pH value and rel. transmittance over time by hydrolysis of GdL in water. The GdL amount was chosen to be equimolar to a solution of **4Na** with a concentration of 1 g L^{-1} .

While the rel. transmittance of the solution is constant over the whole period of the experiment, the pH value exponentially decreases from about 5.5 to 4.7. This experiment shows that the pH value mainly decreases within the first 60 min after the addition of the GdL and hydrolysis is completed within 8 h.

Time-dependent pH value and optical transmittance measurements of **4Na** solutions with different equivalents of GdL were performed similar to the titration experiments discussed in chapter 3.3.1.1. These investigations show the dependence of the optical transmittance and the pH value on time of a solution of 1 g L^{-1} of **4Na** after the addition of 4 eq., 5 eq. or 6 eq. of GdL (Figure 3.22a - c). Before the addition of GdL the pH value of the solutions was about 7. DLS experiments confirmed the absence of any large aggregates in these solutions.

After addition of the respective GdL amount, a small decrease of the rel. transmittance can be observed, independent on the amount of added GdL until a pH of around 6.2 is reached. This is probably due to the formation of pre-aggregates. At a pH value of 5.5 a second decrease of the rel. transmittance indicates the formation of bigger aggregates. This is in good accordance with the results obtained from titration experiments with aq. HCl solution (Figure 3.13, chapter 3.3.1.1). Depending on the amount of added GdL, the significant decrease of the rel. transmittance of the solution is reached after 200 min, 140 min or 100 min for 4 eq., 5 eq. or 6 eq. of GdL, respectively (Figure 3.22a - c).

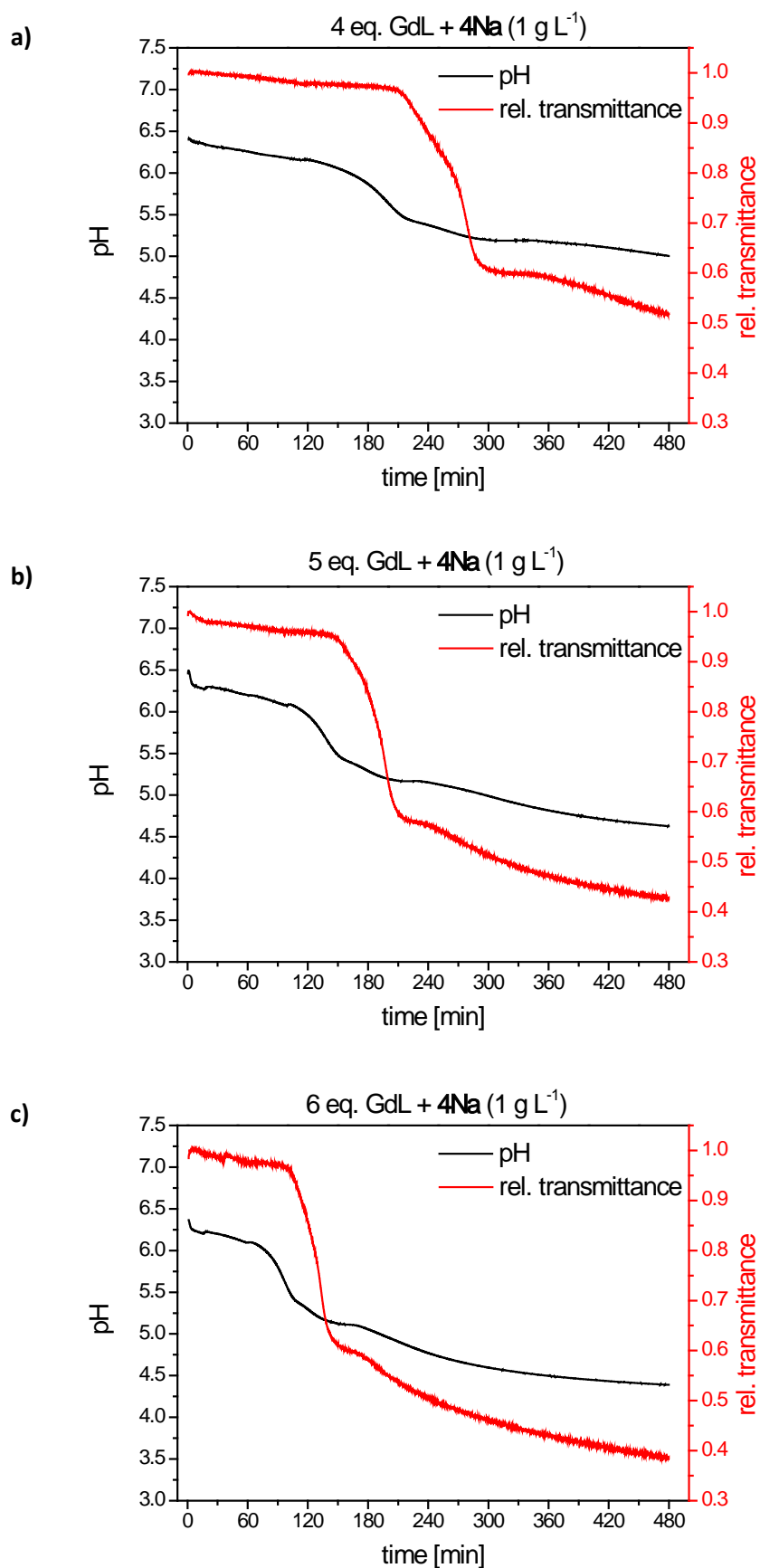


Figure 3.22: Results of time-dependent pH value and rel. transmittance measurements of 4Na solutions ($c = 1 \text{ g L}^{-1}$) with a) 4 eq., b) 5 eq., and c) 6 eq. of GdL.

The pH value at the end of hydrolysis and therefore gelation is dependent on the amount of added GdL. The excess of 1 eq. of GdL in solution leads to a decrease of the pH value of about 2 units (Figure 3.21). This results in a final pH value of 5.0, 4.6 and 4.4 8 h after the addition of 4 eq., 5 eq., and 6 eq. of GdL, respectively, to a solution of **4Na** with a concentration of 1 g L^{-1} . Thus, it is obvious that for all three GdL amounts the pH value falls below the critical gelation pH value and only the onset of gelation differs. This phenomenon was also observed for other pH-sensitive low molecular weight hydrogelators that were prepared *via* the hydrolysis of GdL.⁸⁸ Thereby, the different amounts of GdL led to different final pH values and different degrees of protonation of the hydrogelator.

Analogous time-dependent pH value measurements combined with DLS were performed to detect aggregates in a solution of **4Na** with a concentration of 1 g L^{-1} after the addition of 4 eq. of GdL. These experiments showed that already after about 2 min first aggregates can be detected. As mentioned above, the evaluation of the hydrodynamic radius of these aggregates is not reasonable.

To observe the assembled structures shortly after the addition of GdL, TEM images were taken. Therefore, the TEM grid was dipped into a solution of **4Na** with a concentration of 10 g L^{-1} 2 min after the addition of 4 eq. of GdL. According to the time-dependent pH value and rel. transmittance measurements a pH value of about 5.1 is expected at that time. The concentration of **4Na** was increased compared to the time-dependent pH value and rel. transmittance measurements, as imaging of any aggregates in TEM images is unlikely in highly diluted solutions. By blotting the grid with paper bulk, dipping it into desalted water, and anew blotting, the remaining GdL and hydrolysis products should have been removed to avoid further decrease of the pH value, although there was no possibility to prove this hypothesis. Only few aggregates could be observed in the resulting TEM images, indicating that only few structures had already assembled 2 min after the addition of GdL.

As shown in Figure 3.23, the detected aggregates are anisotropic with high aspect ratios and the tendency to branch and form network-like structures.

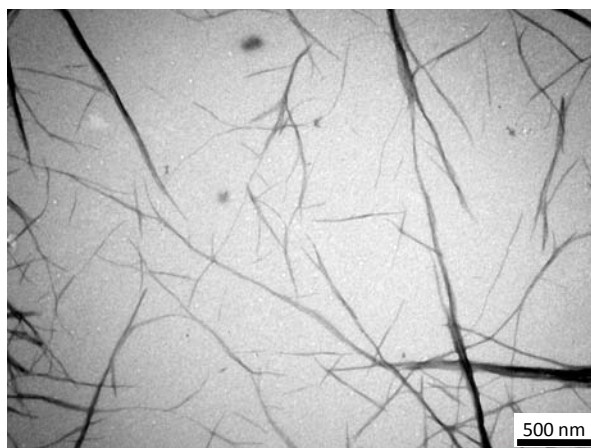


Figure 3.23: TEM image of a solution of **4Na** (10 g L^{-1}) 2 min after the addition of 4 eq. of GdL.

The smallest observed diameters of these fibrous structures are about 10 nm to 20 nm, which is in good accordance to the diameters of the substructures obtained from the SEM image of the xerogel prepared with aqueous and gaseous HCl (Figure 3.17 and Figure 3.20). Due to the formation of superstructures, diameters of up to 150 nm can be observed. Additionally to bundling of fibers also intertwining and twisting of the structures occurs indicating the presence of an underlying helical structure. Although the molecule of **4** itself is achiral, the formation of helical structures is possible as shown for other achiral BTAs in the literature.^{193,196,205,234,237} This further supports the hypothesis that the underlying structures consist of triple helical arrangements similar to those reported in the literature.^{193,196,237,252}

The lengths of the assemblies obtained by acidification with GdL are difficult to evaluate due to the branching, but lie within the range of 500 nm to several micrometers. Thus, they are significantly longer than the structures from titration experiments with aq. HCl solution.

Altogether, the findings from the cryo-TEM, TEM, and SEM studies indicate that the underlying thin anisotropic aggregates are the same for both preparation methods, but the further aggregation and the resulting superstructures slightly differ. This can be explained by the different experimental parameters that had to be applied for the different measurements and the different kinetics that occur during both preparation techniques.

The XRD pattern of a washed and dried hydrogel prepared *via* hydrolysis of GdL using a **4Na** solution with a concentration of 10 g L^{-1} (Figure 3.24, red line) was similar to the XRD pattern obtained from a washed and dried hydrogel prepared with aq. HCl solution.¹

¹ As large amounts of GdL were used to prepare the hydrogel samples, prior to the drying the GdL and hydrolysis products thereof were removed by several washing steps. Thereby, it could be shown that GdL molecules are not incorporated into the fibers of the hydrogel. For further details see chapter 9.4.3.

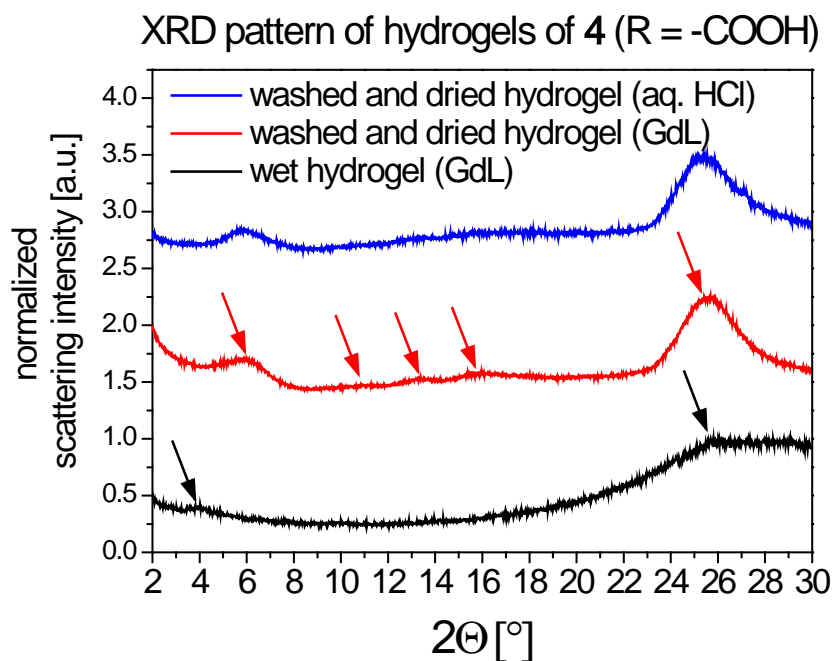


Figure 3.24: XRD pattern of a washed and dried hydrogel of **4** prepared with 10 g L^{-1} of **4Na** and 4 eq. of GdL (red line) and the XRD pattern of a native (wet) hydrogel of **4** prepared with 50 g L^{-1} of **4Na** and 4 eq. of GdL (black line). For comparison purposes the XRD pattern of the washed and dried hydrogel prepared with 10 g L^{-1} of **4Na** and aq. HCl solution is also shown (blue line). Note: Plots have been offset in the y-axis in order to ease visualization. Small peaks are indicated by an arrow.

This indicates that the underlying molecular arrangement is the same for both preparation methods. Solely, the peak in the XRD pattern of the xerogel prepared with aq. HCl solution at about 16° is resolved into three weak peaks in the XRD pattern of the xerogel prepared with GdL. An explanation for this might be the different kinetics of both preparation methods. As gelation times for hydrogels prepared with GdL are much longer compared to the addition of aq. HCl solution, this might lead to assemblies with a higher order.

Native (wet) hydrogels of **4** prepared from **4Na** solutions with GdL showed no peaks at a **4Na** concentration of 10 g L^{-1} due to the low signal to noise ratio. The pattern obtained with a concentration of 50 g L^{-1} of **4Na** is displayed in Figure 3.24 (black line). The peak at $2\theta = 4.02^\circ$ corresponds to a real space distance of about 2.2 nm. This distance is equal to the dimensions obtained from the cryo-TEM images taken during the titration of an alkaline gelator solution with aq. HCl solution (Figure 3.14, chapter 3.3.1.1). In the XRD pattern of the dried hydrogels this peak shifts to 5.92° (2θ) and a real space distance of 1.5 nm. As discussed above, this distance is consistent with the lattice parameters a and b of the hexagonal unit cell of the single crystal of **4**.²¹⁰ This might indicate that upon drying the underlying helical stacks merge closer together to form a molecular packing with interdigitating side arms similar to the molecular arrangement in a layer of the single crystal structure of **4**.

The second indicated peak of the XRD pattern of the wet hydrogel (Figure 3.24, black line) corresponds to a BTA core distance of 0.35 nm ($2\theta = 25.80^\circ$), which is in the same range as the BTA core distance in the dried hydrogel (0.35 nm, $2\theta = 25.56^\circ$). Thus, it can be assumed that in hydrogels of **4**, in the wet as well as in the dried state, the molecules are stacked above each other with intracolumnar hydrogen bonds between the amide units of the core. In the literature it was shown that core-core interactions and core-solvent respectively core-side arm interactions can be present at the same time.²⁴² Thereby, two amide moieties formed intracolumnar hydrogen bonds, while the third interacted with the solvent DMSO that formed a bridge to the side chain of the next molecule. As water molecules can also participate in hydrogen bonds, an analogous assembly might be present in wet hydrogels of **4**. Consequently, drying could then lead to a removal of such bridging water molecules resulting in smaller *d*-spacings.

Summarizing, analysis of the XRD pattern shows that the underlying assemblies in the hydrogel converge upon drying indicating a change of the lateral intermolecular interaction, while on the other hand the arrangement of the molecules in the columnar stacks remains qualitatively the same.

The slow and homogeneous decrease of the pH value due to the hydrolysis of GdL influences the morphology of the resulting supramolecular assemblies as shown by SEM imaging of the washed and dried hydrogels prepared with a gelator sodium salt (**4Na**) concentration of 10 g L^{-1} and 4 eq. of GdL (Figure 3.25). Long entangled fiber bundles with diameters in the range of 80 nm to 120 nm and lengths of several micrometers can be observed. These fibers are superstructures of smaller fibrils in the range of 10 - 20 nm. Due to the slower gelation *via* GdL hydrolysis compared to gelation with gaseous HCl longer fibers are formed.

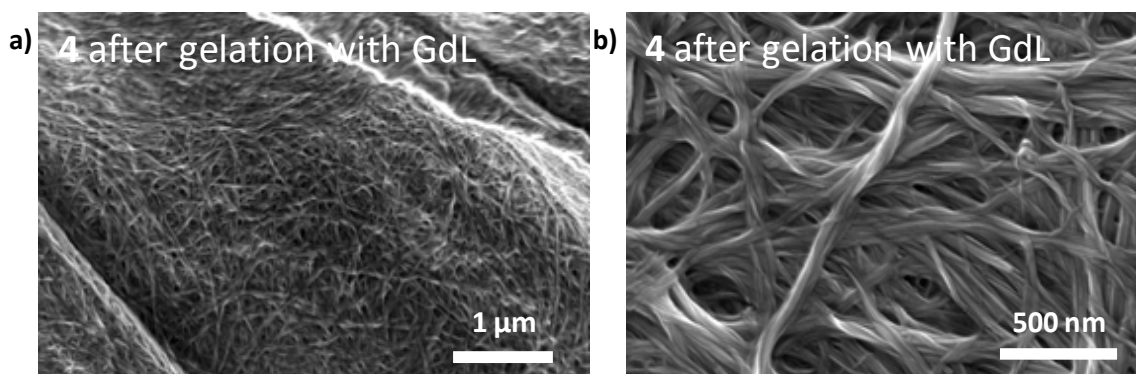


Figure 3.25: Typical SEM images of washed and dried hydrogels of **4** prepared by gelation of a solution of **4Na** (10 g L^{-1}) with 4 eq. of GdL at different magnifications. b) Reproduced from reference 102 with permission from *The Royal Society of Chemistry*.

As the gel preparation method influences the superstructure of gels of **4**, it is reasonable to assume that also the macroscopic gel properties differ. Therefore, properties of gels prepared *via* hydrolysis of GdL are investigated in detail in the next chapter and compared to properties of gels prepared by diffusion of HCl gas.

3.3.5.4 Gelation *via* electrolysis of water

A change of the pH value can also be realized by electrolysis of water due to the decomposition of water and the formation of protons at the anode of an electrochemical cell. Thus, comparably thin films and membranes on conductive substrates can be prepared rather than bulk samples of the gel. This method has recently been applied for a dipeptide-based amphiphilic hydrogelator,³³⁰ but is also feasible for solutions of **4Na** and the formation of surface coatings of **4**. The results of this preparation method are separately discussed in chapter 6.

3.3.6 Characterization of gel properties of compound **4**

It is known from the literature that different gel preparation methods can lead to different macroscopic properties.^{14,65,73,93} In the previous chapter it was shown that macroscopically homogeneous hydrogels of **4** can be prepared by acidification of a solution of **4Na** either *via* diffusion of HCl gas into the solution or by hydrolysis of glucono-delta-lactone (GdL). While the first method results in a final pH value of the gel of about 1, the final pH value using the hydrolysis of GdL can be adjusted by the amount of added GdL. If not stated otherwise, in the following the gels were prepared from aqueous solutions of **4Na** and 4 eq. (equivalents) of GdL regarding the molar amount of the gelator sodium salt **4Na**. It is important to note that although solutions of **4Na** were used for the gel formation, in the resulting hydrogel compound **4** should be present due to the change of the pH value. Dependent on the final pH value the carboxylic acid moieties might be either fully or partially protonated. As the superstructure of the resulting gels for the two preparation methods differ, it is very likely that also the gel properties are influenced by the gel preparation method. In the following the gels are characterized regarding their critical gelation concentration (cgc), their mechanical and thermal stability, and their stability against various solvents. These investigations are a continuation of preliminary studies performed during my diploma thesis.³³⁸

3.3.6.1 Critical gelation concentration (cgc)

The critical gelation concentration (cgc) is the lowest gelator concentration at which a stable gel can be produced. The stability of the gel was determined by i) the inverse tube test; and ii) by the falling steel ball method. Gel state was determined when i) upon inversion of the test

tube no gravitational flow was observed; or ii) the gel could bear the weight of a small steel ball (~ 33 mg). The results of the assay regarding the cgc are summarized in Table 3.7.

Table 3.7: Critical gelation concentration (cgc) of gels prepared from solutions of **4Na** with GdL or gaseous HCl determined by the inverse tube test and the falling steel ball method.

| preparation method | test method | c (4Na) [g L ⁻¹] | | | | | | |
|--------------------|---------------------------|------------------------------|-----|-----|-----|-----|-----|-----|
| | | 10.0 | 8.0 | 6.0 | 4.0 | 2.0 | 1.0 | 0.5 |
| 6 eq. GdL | "inverse-tube"-test | + | + | + | + | + | - | - |
| | falling steel ball method | + | + | + | + | + | (+) | - |
| 5 eq. GdL | "inverse-tube"-test | + | + | + | + | + | - | - |
| | falling steel ball method | + | + | + | + | + | - | - |
| 4 eq. GdL | "inverse-tube"-test | + | + | + | + | + | - | - |
| | falling steel ball method | + | + | + | + | + | - | - |
| HCl gas | "inverse-tube"-test | + | + | + | + | + | + | + |
| | falling steel ball method | + | + | + | + | + | - | - |

+: gel; (+): weak gel that collapses on application of slight mechanical stress; -: no gel.

Gels prepared with GdL are stable down to a **4Na** concentration of 2.0 g L⁻¹ independent on the exact amount of added GdL. Below this concentration a partially gelated sample with a non-gelated supernatant solution is obtained. Obviously, these samples cannot pass the inversion tube test due to the supernatant solution. Nevertheless, for the samples prepared with 1.0 g L⁻¹ of **4Na** and different amounts of GdL it was observed that the gelated part can bear the weight of the used steel ball if no additional mechanical stress, *e.g.* by slightly shaking the vial, is applied. The gelation ability of a lmw hydrogelator can also be given by the gelation number. This number gives the ratio of the molar amount of the gelation medium (n(H₂O)) in respect to the molar amount of the gelator (n(**4Na**)) at the cgc. At a cgc of 2.0 g L⁻¹ of **4Na** for the gelation *via* hydrolysis of GdL the gelation number is about 17581, *i. e.* that about $1.76 \cdot 10^4$ molecules of water can be immobilized by just one gelator molecule.

Mukhopadhyay et al. investigated the gelation ability of a tripodal cholamide in different acetic acid/water mixtures.⁴⁵ At an acetic acid content of 0.01 % in water this "supergelator"¹ was able to form stable hydrogels at a concentration as low as 0.15 mM. This corresponds to a gelation number of $3 \cdot 10^5$, which is only one order of magnitude higher than the hydrogelator presented here.

The cgc of gels prepared with gaseous HCl is 0.5 g L⁻¹ upon inversion of the test tube, as by using this gelation method the whole volume of the gelation medium is immobilized. However, due to the low concentration of the gelator, the hydrogel network is too weak to bear the weight of the small steel ball. This difference in gel stability upon different testing methods can

¹ The term "supergelator" is used for lmw hydrogelators with a cgc of 1 g L⁻¹ or less.

be explained by the lower pH value at the end of gelation of gels prepared with gaseous HCl and the different kinetic processes that occur during gelation. Nevertheless, both gelation methods are suitable to prepare stable hydrogels at very low gelator concentrations.

3.3.6.2 Thermal stability

Usually the falling steel ball method is used to determine the thermal stability of the gel. For thermal reversible gels upon heating a softening and subsequent dissolution of the gel can be observed. The temperature at which the steel ball reaches the bottom of the vial is termed *gelation temperature* T_{gel} .

Gel samples prepared with 10 g L^{-1} and 2 g L^{-1} of **4Na** and 4 eq. of GdL, respectively, were equipped with the small steel ball on top of the gel sample. The experiment was terminated at a sample temperature of $100 \text{ }^\circ\text{C}$ (boiling point of water). During the whole experiment the gel samples kept their integrity and no changes of the gel appearance, such as softening, dissolution, shrinkage or swelling could be observed. Thus, this gel system is thermally stable.

3.3.6.3 Mechanical stability

The mechanical stability of gels is usually determined by rheological measurements. For hydrogels of **4** prepared with GdL rheological measurements were recently published by Howe *et al.* showing that for low pH values the gel acts like a solid.²⁶⁷ The storage modulus G' was determined to be 4000 Pa , while the loss modulus G'' was only about 230 Pa . As typical for gels the storage modulus showed a plateau over a wide range of frequencies at a gelator concentration of 10 g L^{-1} . The gel started to flow at a yield stress of about 1.1 mN .

An easier method to get a qualitative insight into the mechanical strength of the gel for comparison purposes is the indentation of a stainless steel cylinder into the gel sample. The resulting indentation stress-indentation depth curves give information about the stiffness of the sample and about the maximum indentation stress at break or flow (Figure 3.26).

The stiffness of the gels can be calculated as the initial slope of the indentation stress-indentation depth curves. In this study it is calculated for the first indentation region, where linear proportionality occurs. The indentation stress at break is the maximum indentation stress after which the stress abruptly decreases. Flow behavior occurs if no abrupt decrease of the stress, but a non-linear behavior above the indentation stress at flow can be observed.

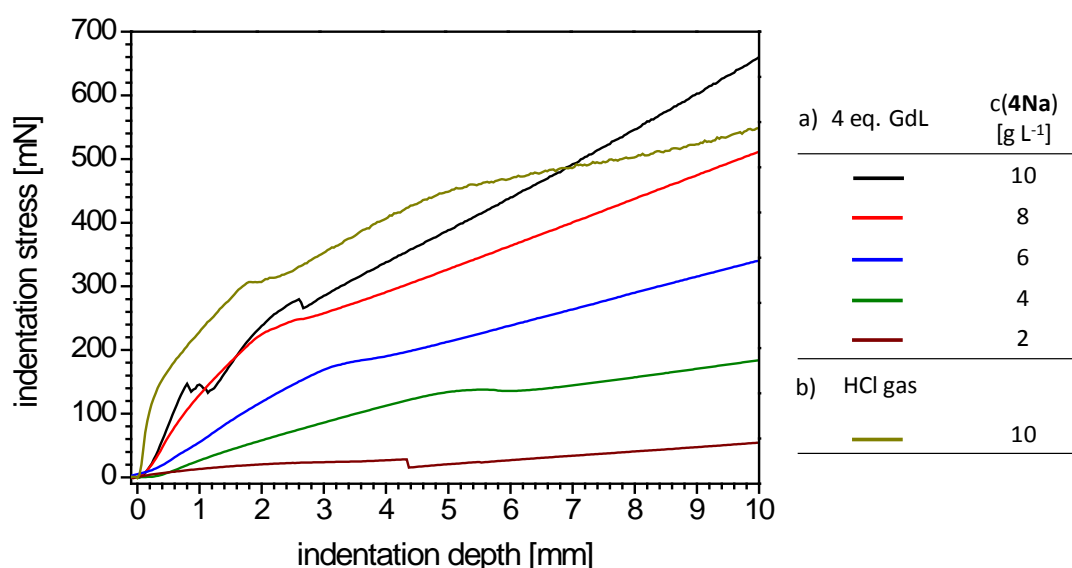


Figure 3.26: Indentation stress plotted versus indentation depth for indentation experiments performed on gels prepared at different **4Na** concentrations by a) addition of 4 eq. of GdL, respectively and b) by diffusion of gaseous HCl.

The stiffness and the indentation stress at break or flow for the tested gels are summarized in Table 3.8.

Table 3.8: Stiffness and indentation stress at break or flow of gels prepared with different **4Na** concentration and 4 eq. of GdL or gaseous HCl, respectively.

| preparation method | c (4Na) [g L ⁻¹] | stiffness ^a [N m ⁻¹] | indentation stress at break ^b or flow ^c [mN] |
|--------------------|------------------------------|---|--|
| 4 eq. GdL | 2 | 12.6 ± 0.2 | 28.2 ^b |
| | 4 | 28.2 ± 0.1 | 137.8 ^c |
| | 6 | 58.0 ± 0.2 | 177.0 ^c |
| | 8 | 121.1 ± 0.8 | 245.8 ^c |
| | 10 | 168.6 ± 5.3 | 146.8 ^b |
| HCl gas | 10 | 520 ± 31 | 307.0 ^c |

^a The stiffness of the gels is calculated as the slope of the indentation stress-indentation depth curves in the first region, where linear proportionality occurs, ^b indentation stress at break; ^c indentation stress at flow.

As expected, the stiffness of gels prepared with 4 eq. of GdL increases with increasing **4Na** concentration, ranging from approx. 12 N m⁻¹ for gels with 2 g L⁻¹ of **4Na** to approx. 170 N m⁻¹ for gels with 10 g L⁻¹ of **4Na**. The maximum stress at break or flow increases from 28 mN to 245 mN for gels prepared with 4 eq. of GdL and 2 g L⁻¹ to 8 g L⁻¹ of **4Na**. While the gel with the

lowest **4Na** concentration breaks, gels with higher concentrations of **4Na** show rather a flow behavior. A different behavior can be observed for the gel prepared with 10 g L^{-1} of **4Na** and 4 eq. of GdL. This gel breaks at a stress of about 150 mN, but shows subsequent flow behavior. The graphical representation of the data in Figure 3.27 shows that for gels prepared with 4 eq. of GdL there is a linear dependence between the stiffness as well as the indentation stress at break or flow and the **4Na** concentration. Solely, the values for gels prepared with 10 g L^{-1} of **4Na** are an exception indicating that the linear dependence is only valid for low gelator concentrations.

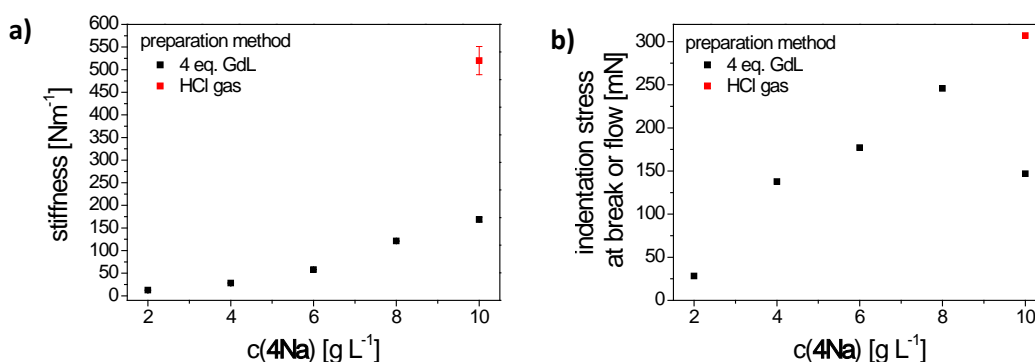


Figure 3.27: a) Stiffness and b) indentation stress at break or flow versus the **4Na** concentration of gels prepared with 4 eq. of GdL or gaseous HCl.

The gel prepared with gaseous HCl using 10 g L^{-1} of gelator **4Na** had a stiffness of about 500 N m^{-1} , which is around 3 times higher than for gels prepared with 4 eq. of GdL. This distinct increase in mechanical stiffness might be explained by the much shorter but bundled rod-like structures found in SEM images of gels prepared with gaseous HCl (Figure 3.20, chapter 3.3.2.2). It is furthermore possible that the lower final pH value after gelation with gaseous HCl leads to more stabilized structures and thus a higher mechanical stability. Interestingly, above an indentation depth of about 7 mm the curve of the indentation stress for gels prepared with gaseous HCl flattens and falls below the curve for gels prepared with 4 eq. of GdL. As the same gelator sodium salt concentration was used for the preparation of both samples, these deviations in the mechanical behavior can be assigned to the different preparation methods. While the pH value is decreased simultaneously in the whole sample volume using the gelation method *via* hydrolysis of GdL, the pH value in samples prepared with gaseous HCl decreases subsequently from the surface of the sample that is exposed to the gas to the bottom of the sample vial. Therefore, the gelation method with gaseous HCl leads to a gradual decrease of the pH value, which results in the gradually decrease of the mechanical strength of the gel

from the surface to the bottom of the sample. Hence, this gelation method might be a way to prepare supramolecular gradient materials.

Due to the observed gradient regarding the mechanical stability of hydrogels prepared by diffusion of HCl gas further characterization and application investigations are solely performed with gels prepared *via* the hydrolysis of GdL. With this method the mechanical stiffness of the gel can be adjusted by changing the gelator concentration.

3.3.6.4 Stability of gels against various solvents

As compound **4** in bulk as obtained after crystallization from a DMSO-water mixture showed already good stability against various aqueous and organic solvents, the hydrogels of **4** obtained from solutions of **4Na** by hydrolysis of GdL were also investigated regarding their stability against solvolysis in aqueous and organic solvents. Small gel samples prepared from 0.3 mL of a 10 g L⁻¹ **4Na** solution and 4 eq. of GdL were put in 3 mL of the respective solvent. The stability against various aqueous and organic solvents shortly after the addition of the solvent (10 min), after complete exchange of the gelation medium (3 d) and after two weeks is displayed in Table 3.9.

Table 3.9: Stability of gels prepared from solutions of **4Na** with a concentration of 10 g L⁻¹ and 4 eq. of GdL against various aqueous and organic solvents.

| solvent | immersion time | | |
|-----------------------------|----------------|-----|------|
| | 10 min | 3 d | 14 d |
| NaOH (pH = 14) | - | - | - |
| PBS ^a (pH = 7.4) | + | - | - |
| NaCl sat. (pH = 7) | + | + | + |
| H ₂ O (pH = 7) | + | + | + |
| HCl (pH = 5) | + | + | + |
| HCl (pH = 4) | + | + | + |
| HCl (pH = 3) | + | + | + |
| HCl (pH = 2) | + | + | + |
| HCl (pH = 1) | + | + | + |
| HCl (pH = 0) | + | + | + |
| 1 M acetic acid | + | + | + |
| n-hexane | + | + | (+) |
| ethyl acetate | + | + | + |
| methanol | + | + | + |
| ethanol | + | + | + |
| dichloromethane | + | + | + |
| acetone | + | + | (+) |
| chloroform | + | + | + |
| tetrahydrofuran | - | - | - |
| dimethyl formamide | - | - | - |
| dimethyl sulfoxide | - | - | - |

+: stable; (+): loss of shape and integrity, but no complete dissolution; -: not stable.

^a phosphate buffered saline.

As expected, gels are stable in aqueous acidic solutions, but dissolve in aqueous alkaline solutions due to the formation of lateral carboxylate anions and the resulting electrostatic repulsion of the molecules. It could be shown that the gels are also stable in solutions with high ionic strength, *e.g.* in saturated sodium chloride solution. Interestingly, they slowly dissolve over a time period of 3 days in phosphate buffered saline (PBS), which is often used in biochemistry for the purification of cells or proteins. Such a slow dissolution could be interesting for applications in the field of controlled drug release or even tissue engineering, where cells need a scaffold to grow on, but that is subsequently degraded.¹

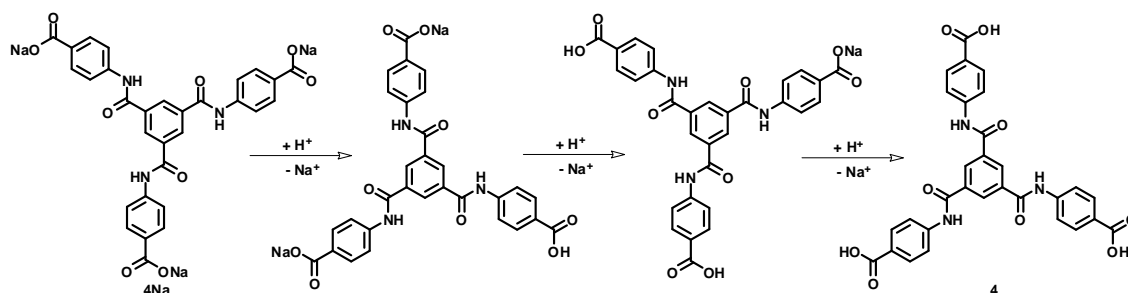
Stability tests against organic solvents showed that hydrogels can be transferred into stable organogels by a simple solvent exchange. Only very polar solvents that can participate in hydrogen bonds, such as DMSO and DMF dissolve the gel samples. To be able to test also water-immiscible organic solvents, gels were first transferred into organogels with ethanol as the liquid component and then the ethanol was exchanged by unpolar solvents, such as dichloromethane and chloroform. This transfer from hydrogels into organogels under preservation of shape opens up many new applications, such as templating of inorganic materials, catalysis, and scaffolding.

3.4 Proposed structural model

Combining the findings reported in the literature and the results obtained in this study the following structural model can be proposed for the pH-sensitive aggregation of the BTA-based hydrogelator **4**.

In alkaline media or as sodium salt **4Na** the gelator is molecularly dissolved due to repulsive electrostatic interactions of the lateral carboxylate groups. This could be proven by the absence of any larger aggregates in DLS measurements. A decrease of the pH value leads to a step-wise aggregation as can be seen by the step-wise decrease of the rel. transmittance of a **4Na** solution during titration experiments with aq. HCl solution. Upon decrease of the pH value, at first the lateral carboxylate moieties of the gelator are partially protonated leading to molecules with either one or two uncharged carboxylic acid headgroups (Scheme 3.6). Such partially protonated molecules exhibit a surfactant activity, as protonated carboxylic acid side arms are more hydrophobic than the charged carboxylate side arms.

¹ Further investigations regarding the application of this hydrogelator system in biomedical applications and especially as controlled drug release matrix are presented in chapter 5.



Scheme 3.6: Step-wise protonation of compound **4Na** to compound **4**.

It is proposed that this leads to the formation of helical aggregates with three strands of molecular stacks. Thereby, protonated side arms should be enclosed within the aggregates, while charged side arms point to the surrounding water. The formation of triple helical aggregates is supported by the results from XRD measurements of the wet (native) hydrogel of **4** and from cryo-TEM images upon titration of a **4Na** solution with aq. HCl solution. While cryo-TEM images show the formation of anisotropic aggregates with width of about 2.2 nm that align parallelly to form ribbon-like superstructures, the XRD measurements of wet hydrogels give distances of 2.2 nm and 0.35 nm. The distance of 0.35 nm can be assigned to core-core distances of BTAs that are stacked above each other with hydrogen bonds between the amide units. In accordance with examples found in the literature adjacent BTA molecules should be rotated by 60° so that the respective side arms are staggered and the formation of amide-amide hydrogen bonds is possible.^{59,131,255} As the estimated diameter of a molecule of **4** is only 1.9 nm, the found distance of about 2.2 nm cannot be assigned to the diameter of a single column, but indicates the presence of a more complicated underlying assembly. Recently, in the literature the self-assembly of structural similar BTA derivatives into single and triple helical aggregates has been reported (Figure 3.28).^{128,193,200,205,237,252} It is assumed that a similar triple helical arrangement might be the underlying substructure for the pH-sensitive aggregation of molecules of **4**.

Dependent on the degree of protonation, these anisotropic pre-aggregates can bear surface charges. The presence of these surface charges determines the further self-assembly. It is proposed that the ribbon-like aggregates found in the cryo-TEM images upon titration with aq. HCl solution form due to some kind of microphase separation as shown for partially fluorinated BTAs.²³⁴ Thereby, the formation of fluorine-enriched patches or ribbons was observed prior to the bundling of the underlying anisotropic aggregates.

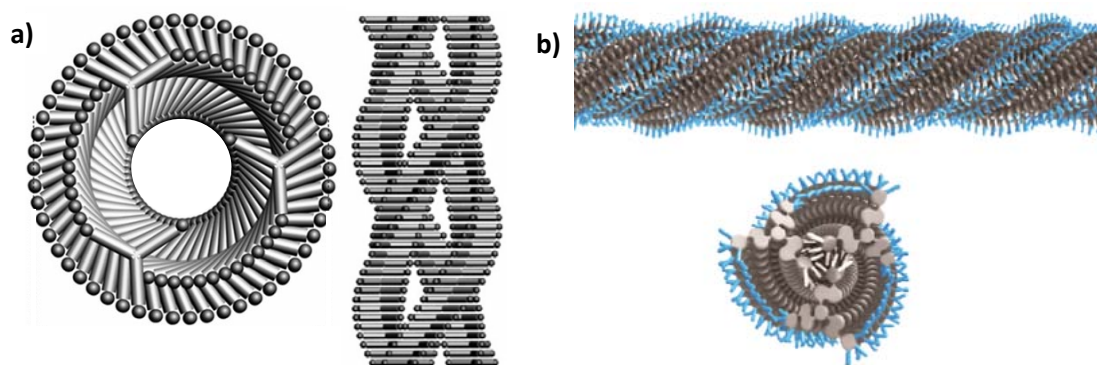


Figure 3.28: Schematic representation of triple helical aggregates of BTAs from the literature: Reproduced a) from reference 237 with permission from *Wiley* and b) from reference 252 with permission from *The American Chemical Society*.

Upon further decrease of the pH value, the surface charges of the aligned triple helices decrease which results in the self-assembly of bigger aggregates. In the SEM images of washed and dried hydrogels of **4** underlying fibrillar assemblies with diameters in the range of about 20 nm can be observed independent of the gelation method. These fibrillar assemblies further intertwine to form fibers and fiber bundles. As in the final hydrogels, molecules of **4** should be fully protonated, the lateral carboxylic acid groups can participate in hydrogen bonds and thus might lead to the stabilization of intertwined fibrils or fiber.

Interestingly, the resulting superstructures differ for hydrogels prepared by different gelation methods. While gels prepared with aqueous or gaseous HCl have rather short fibers and fiber bundles, the preparation with GdL leads to elongated fibers that are intertwined and thus form a more homogeneous network. The different morphologies of the hydrogels might be explained by the different kinetics during gelation. The presence of twisted and intertwined assemblies in the SEM images, when the gelator molecules are fully protonated, supports the hypothesis that the underlying molecular packing exhibits a helicity although molecules of **4** are achiral. The formation of helical assemblies by achiral BTA molecules was also reported by other groups in the literature.^{193,196,205,234,237}

Analysis of XRD pattern of dried hydrogels of **4** showed that upon drying the distance of about 2.2 nm decreases to 1.5 nm, while the intracolumnar core-core distance remains to be 0.35 nm. This indicates that also in the dried state molecules are stacked above each other with intracolumnar amide hydrogen bonds between adjacent molecules. However, as the distance of 2.2 nm which is associated with the width of the triple helical assembly decreases, it must be assumed that the underlying anisotropic aggregates converge laterally, which also might lead to a change of the lateral intermolecular interactions. The structure elucidation of the single crystal of **4** gave a hexagonal unit cell with the cell parameters $a = b = 1.5$ nm.²¹⁰ Interestingly, this is equal to the found d -spacing in dried hydrogels of **4**. The molecular

packing in the single crystal differs from the hydrogel structure, as no hydrogen bonds between adjacent cores, but only core-side chain interactions are present in the single crystal. Nevertheless, this might be an indication that also in the dried hydrogels of **4** side arms of laterally adjacent molecules interdigitate. Recently, a BTA derivative was reported in the literature that formed columnar assemblies, in which core-core as well as core-side chain interactions were present.²⁴²

To evaluate the exact molecular packing in hydrogels of **4** and to get further insight into the gel formation mechanism, structure analysis is currently performed in cooperation with Sebastian With from the group of Prof. Stephan Förster (Physical Chemistry I) at the University of Bayreuth. In chapter 4 theoretical calculations and spectroscopic investigations are presented. Especially the optimized geometries of tetramers of **4** support the model of underlying helical aggregates.

Summarizing, the pH-sensitive aggregation of **4** into a supramolecular hydrogel is a combination of multifold interactions. It is proposed that triple helical assemblies are formed that align to form ribbon-like structures prior to the assembly into fibrillar aggregates with diameters in the range of about 20 nm. These twist to form helical fibers that intertwine and bundle to result in a three-dimensional network. As the underlying fibrils have the lateral carboxylic acid headgroups of **4** directed to the surrounding, the resulting superstructures have a surface that consists of multiple carboxylic acid moieties. This functional surface that is obtained by spontaneous self-assembly upon change of the pH value might be interesting for further application, such as the adsorption of dyes or the complexation of metal ions.

4 “Formation of a supramolecular chromophore: a spectroscopic and theoretical study”¹

Upon investigation of the hydrogel properties of **4**, a blue luminescence of the gels was observed upon irradiation of the samples with UV light (chapter 3.3.2). Due to these interesting optical properties in the gel state, detailed spectroscopic studies were performed for compounds **4** and **4Na**. In cooperation with Prof. Anna Köhler and Dr. Sebastian T. Hoffmann from the department of “Experimental Physics II” of the University of Bayreuth and Prof. Rodrigo Q. Albuquerque from the University of São Paulo the photoluminescence (PL) behavior was elucidated in detail by means of spectroscopic investigations and theoretical calculations.

4.1 Spectroscopic studies of compounds **4** and **4Na**

Compounds **4** and **4Na** were investigated regarding their optical properties in solution, as bulk material in film, and additionally for compound **4** also in the hydrogel state. Therefore, UV-Vis absorbance spectra and PL spectra of the respective compounds were recorded in continuous wave mode, respectively.

4.1.1 Absorption studies in solution, film, and during pH-sensitive aggregation

The solubility tests performed in chapter 3.2.3 revealed that compound **4** shows good solubility in dimethyl sulfoxide (DMSO) and dimethyl formamide (DMF). Concentration-dependent absorbance measurements showed that the spectra for compound **4** in the two respective solvents are analogous to each other. The spectra of **4** in DMSO are displayed exemplarily in Figure 4.1.

For concentrations below 10^{-6} mol L⁻¹ no absorption could be detected with the used set up. At concentrations higher than 10^{-6} mol L⁻¹ the respective maximum of the optical density (O.D.) can be found at a wavelength $\lambda_{\text{max}} = 292$ nm. Additionally, a broad shoulder at *approx.* 260 nm is present in the recorded spectra of **4**. The optical density of solutions of **4** with a concentration higher than 10^{-4} mol L⁻¹ exceeds the limit of the set up leading to erratic spectra. Within the range of the detector limit the respective absorbance maxima show no shift. Therefore, it can be assumed that compound **4** is molecularly dissolved at concentrations

¹ The main results of this chapter were published in *Soft Matter* by Andreas Bernet, Rodrigo Q. Albuquerque, Marina Behr, Sebastian T. Hoffmann and Hans-Werner Schmidt.¹⁰²

below $10^{-4} \text{ mol L}^{-1}$. The shift of the tail at higher wavelength of the absorbance spectrum at a concentration of $10^{-3} \text{ mol L}^{-1}$ in respect to the spectra at lower concentrations indicates that aggregates might be present at that concentration.

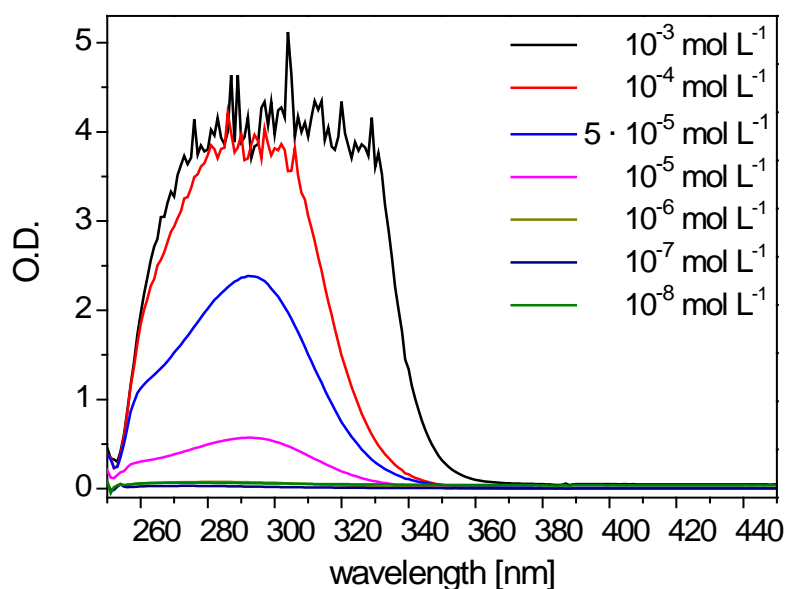


Figure 4.1: UV-Vis spectra of compound **4** in DMSO at different concentrations (O.D.: optical density).

The respective optical densities at 292 nm of the spectra with concentrations between $10^{-5} \text{ mol L}^{-1}$ and $10^{-4} \text{ mol L}^{-1}$ show a linear correlation between the optical density at 292 nm and the concentration of the solution, which is in accordance with the Beer-Lambert law.³⁴⁴

Analogous absorbance measurements were performed for compound **4Na** in desalted water. While below concentrations of $10^{-6} \text{ mol L}^{-1}$ of **4Na** no absorbance could be observed, the limit of the set up was reached for solutions with concentrations higher than $10^{-4} \text{ mol L}^{-1}$. In Figure 4.2 the UV-Vis absorbance spectra of **4Na** in desalted water are displayed.

The respective maximum optical density of the spectra can be found at $\lambda_{\text{max}} = 280 \text{ nm}$. As already observed for solutions of **4** in DMSO and DMF the respective maximum optical densities do not shift with increasing concentration proving that no aggregation occurs at the measured concentrations. This is in accordance with the DLS experiments of solutions of **4Na** in desalted water that were discussed in chapter 3.3.2.3 and showed that even at a **4Na** concentration of 10 g L^{-1} (15.8 mol L^{-1}) no larger aggregates could be observed.

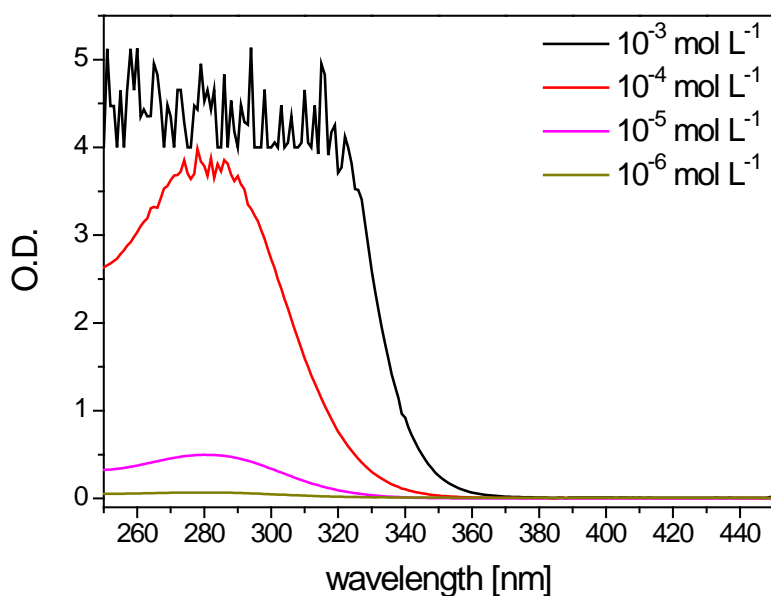


Figure 4.2: UV-Vis spectrum of compound **4Na** in desalted water.

To measure the optical density of compound **4** in solid state, films were prepared from solutions of **4** in DMSO with a concentration of 20 g L^{-1} by drop casting and subsequent drying at 80°C . The morphological characterization of these films was performed by scanning electron microscopy (SEM) imaging and X-ray diffraction (XRD) measurements. The typical SEM image shows short anisotropic aggregates with diameters in the range of 100 nm to 200 nm (Figure 4.3a). These aggregates are formed by substructures with diameters in the range of 10 nm to 20 nm. The ostensible orientation of these aggregates is probably caused by drying effects.

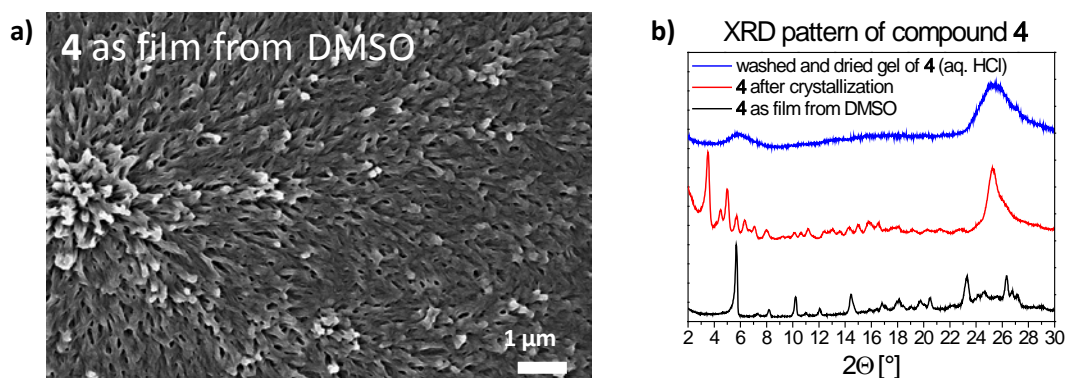


Figure 4.3: a) A typical SEM image and b) the XRD pattern of the carboxylic acid derivative **4** after drop casting and drying a solution of **4** in DMSO (20 g L^{-1} ; black line). For comparison also the XRD pattern of compound **4** after recrystallization (red line) and of the washed and dried hydrogel prepared by addition of aqueous HCl solution (blue line) are displayed.

The XRD pattern shows a mesocrystalline morphology (Figure 4.3b) that is different from the XRD pattern of the hydrogel and of compound **4** after recrystallization. While films of **4** exhibit less long range order compared to the recrystallized compound, in the film a higher long range order is present compared to hydrogels of **4**. The peak at $2\Theta = 5.68^\circ$, which corresponds to a real space distance of 1.5 nm, is also retrievable in the XRD pattern of the washed and dried hydrogel of **4**.

The absorbance spectrum of the film was repeatedly measured to improve the signal to noise ratio and the average spectrum of 10 runs is displayed in Figure 4.4. The artifact at a wavelength of 360 nm is caused by the internal lamp change of the spectrometer. Additionally, scattering effects due to the use of a glass slide as substrate for the film can interfere with the spectra at low optical densities. The respective maximum of the optical density is at $\lambda_{\text{max}} = 306$ nm. In comparison to solutions of **4** in DMSO the respective maximum of the optical density shifts from 292 nm to 306 nm. Thus, the change from the molecularly dissolved state in solutions of DMSO to aggregates in the film results in a red shift of the respective maximum optical densities of 14 nm. Furthermore, upon aggregation the shoulder at *approx.* 260 nm observed in the spectra of solutions of **4** vanishes.

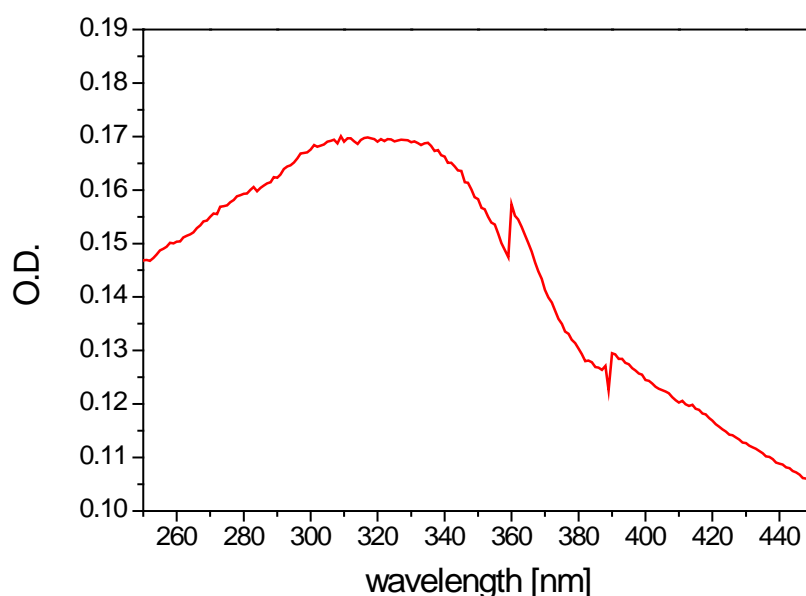


Figure 4.4: Optical density (O.D.) of compound **4** in film prepared from a solution in DMSO (20 g L^{-1}). The displayed spectrum is the average of ten individual UV-Vis absorbance measurements of the film.

The absorbance spectra of the hydrogel of **4** cannot be measured due to the high scattering of the hydrogel sample. Nevertheless, the spectra of a diluted aqueous solution of **4Na** ($c = 10^{-5} \text{ mol L}^{-1}$) were recorded in dependence of the time after the addition of 40 eq. of glucono-delta-lactone (GdL) to the solution (Figure 4.5). It has to be noted that although the

concentration of **4Na** clearly lies below the critical gelation concentration (cgc) aggregates are formed upon decrease of the pH value that might decrease the optical density of the absorbance spectra due to scattering effects. As the experimental set up lacks the possibility to stir the sample during the experiment, the formed aggregates slowly deposit at the bottom of the cuvette causing a gradient in the solution. Therefore, the experiment had to be terminated after 2 h. The high excess of GdL was used since an increased amount of GdL leads to a faster decrease of the pH value in the solution and thus faster gelation, as shown in chapter 3.3.2.3.

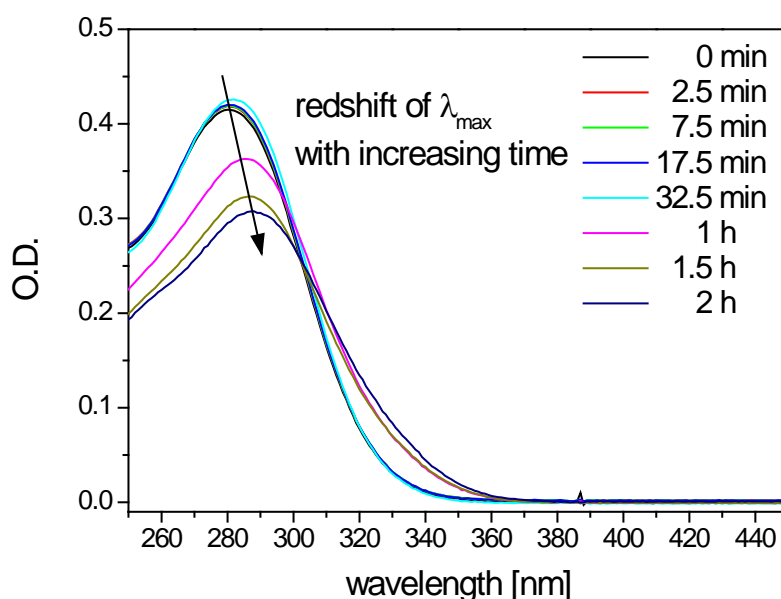


Figure 4.5: Time-dependent UV-Vis absorbance measurements of an aqueous solution of **4Na** ($c = 10^{-5} \text{ mol L}^{-1}$) after the addition of 40 eq. of glucono-delta-lactone (GdL) to decrease the pH value.

With increasing time a decrease of the O. D. can be observed that is attributed to the scattering effects. Additionally, a red shift of the respective absorbance maxima occurs with increasing time. Before the addition of GdL the maximum in the spectrum can be found at $\lambda_{\text{max}}(t=0) = 280 \text{ nm}$, whereas it shifts to 282 nm, 285 nm, 287 nm, and 288 nm after 17.5 min, 32.5 min, 1 h, 1.5 h, and 2 h, respectively with increasing time after the addition. Thus, this red shift is correlated to the formation of aggregates. This observation is supported by the fact that in films of **4**, that solely consist of aggregated molecules, the respective absorbance maxima can be found at an even higher wavelength of $\lambda_{\text{max}}(\text{film}) = 306 \text{ nm}$.

4.1.2 Photoluminescence studies in solution, bulk and hydrogel state

For the PL studies solutions with a concentration of 10 g L^{-1} were used. Usually the excitation wavelength is chosen to be equal to the respective absorbance maximum of the sample. In this study the excitation wavelength was set to $\lambda_{\text{exc}} = 300 \text{ nm}$ for the performed PL measurements

in solution, as this value is close to the respective absorbance maxima of the dissolved and solid state samples. For solutions of **4** in DMSO and DMF as well as for a solution of **4Na** in desalted water no PL could be detected in the wavelength range from 310 to 700 nm with the used set up. The absorbed energy is probably emitted in non-radiative pathways due to quenching effects of the solvent and vibrational energy losses.

Most chromophoric systems only show PL behavior in dissolved state, while upon aggregation the PL is quenched.^{345,346} Only thirteen years ago systems that show *aggregation-induced emission* independent on their PL behavior in solution were found.^{347,348} Since then, aggregation-induced emission and *aggregation-induced emission enhancement* (AIEE) of multiple supramolecular assemblies have been intensely studied.^{323,349–353} As such systems are interesting candidates for various applications in sensors or in electro-optical devices such as organic light-emitting diodes (OLEDs), it is important to test the solid state PL properties of compounds that show no PL in solution. Recently, a review article about supramolecular organogelators that show luminescence upon gel formation was published showing the interest in and the importance of that field of research.^{354–356} Mainly organogelators have been in the focus of interest. However, as they might be especially useful in medical applications such as *in vitro* and *in vivo* imaging, supramolecular hydrogels that show aggregation-induced emission might be even more interesting. Apart from the publication of our group¹⁰² so far only a few other supramolecular hydrogelators with enhanced emission upon gel formation have been published.^{61,81,243}

Therefore, the PL properties of **4** in film from DMSO solution, as well as in the hydrogel state are investigated proving that **4** shows bright blue emission upon aggregation. Both spectra showed a harmonic overtone of the excitation beam at 600 nm when exciting the samples with a wavelength of 300 nm. To avoid the presence of the harmonic overtone in the range of the emission signal the excitation wavelength was set to $\lambda_{\text{exc}} = 330$ nm and the PL spectra were recorded from 340 nm to 650 nm. In the case of the hydrogel, except from the shift of the harmonic overtone from 600 nm to 660 nm, no change of the PL spectrum could be observed when changing the excitation wavelength from 300 nm to 330 nm. Each sample was measured ten times and the respective average spectra were calculated to reduce the signal-to-noise ratio. In Figure 4.6 the normalized spectra of both samples are compared.

The PL spectra of the film and the hydrogel of **4** are very similar, although both samples are prepared differently and possess a different macroscopic appearance, a different morphology on the micrometer scale as proven by SEM imaging, and a different molecular arrangement as shown by XRD measurements. This is only possible if despite the large differences between the film and the hydrogel the underlying chromophoric system and the emitting excited states are

the same in both samples. This is very unusual, as it was reported for different chromophoric systems that the aggregate morphology strongly influences the corresponding PL properties.^{81,243,357} Especially the planarity of the molecules, the intermolecular π - π -distance, and the rotation of the amide unit in respect to the aggregation direction are known to play a role on the overlap of the respective molecular orbitals and thus the emission. The respective maximum in the PL spectrum of the film can be found around 450 nm, while the respective maximum of the hydrogel PL spectrum is slightly shifted to higher wavelength of about 455 nm. This might be explained by the different solvents used for the preparation, namely DMSO in case of the films and water in case of the hydrogels. In both samples a slight shoulder at around 398 nm can be observed.

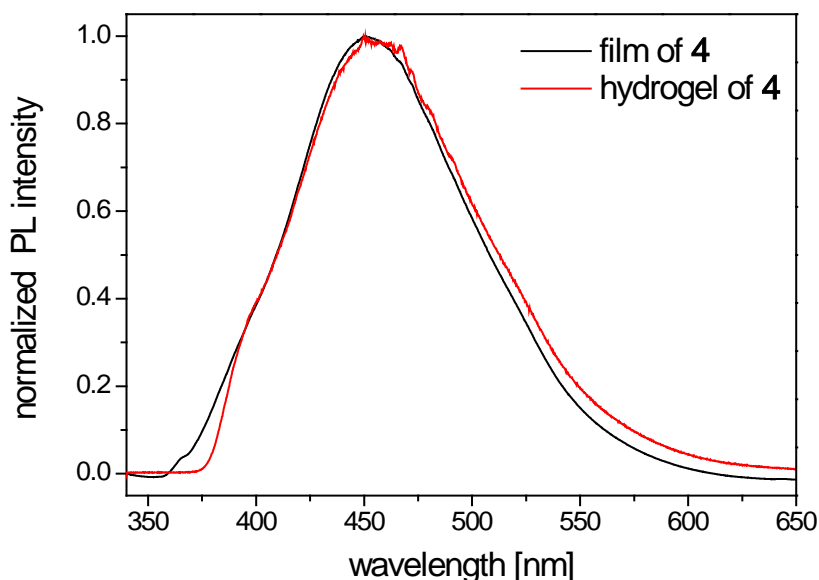


Figure 4.6: Normalized PL spectra of a film and hydrogel of **4** at an excitation wavelength of $\lambda_{\text{exc}} = 330$ nm.

Zhang *et al.* prepared a single crystal of compound **4** and published the respective structure.²¹⁰ This single crystal of **4** shows a slightly different PL spectrum compared to the spectra presented here, as the respective emission maximum is blue-shifted to 446 nm with no shoulder at smaller wavelength.¹ It is reasonable to assume that molecules are arranged in a higher order in the single crystal compared to the film and hydrogel sample. Therefore, the red shift of the respective emission maximum and emergence of a shoulder in the spectra of the film and the hydrogel are probably due to structural defects of those samples and a higher flexibility of the side arms of **4**.

¹ The PL spectra of the single crystal was not included in the publication, but was kindly provided in the frame of a private communication by Zhang and co-workers.

In the literature compound **4** has also been used as ligand in metal complexes and metal organic frameworks (MOFs).^{198–203,210,268,358} It was shown that the luminescence of a lanthanide metal–organic framework with **4** as ligand is blue shifted in respect to the pure compound **4** in solid state.²⁰³ Nevertheless, due to the similarity of both spectra the luminescence was attributed to ligand-based emission with π^* - π -transitions in both cases. The blue shift of the complex was explained by rigidification of the ligand and thus reduced energy loss by radiationless decay. This also supports the assumption that in the hydrogel the side arms are more flexible than in the film and especially in the single crystal.

For structurally related BTA molecules similar PL behavior could be observed upon aggregation that was attributed to either intraligand π^* - π or π^* -n-transitions.^{204,205,209} One example even describes AIEE upon heating above a certain temperature comparable to the *lower critical solution temperature* (LCST) phenomenon of polymers. The heat-induced blue shift of the absorption maximum suggests a face-to-face-stacking of the BTA chromophores resulting in H-type aggregates.²⁶²

Only few examples have been reported to self-assemble in H-type aggregates and show fluorescence, as usually H-aggregates induce radiationless decay.^{355,356} It is rather reasonable that the emission is induced from defects in the well-ordered columnar H-aggregates. One BTA compound that showed AIEE consisted of both, H-type and J-type aggregates.²¹⁶ The emission was enhanced upon transition of H-type to J-type aggregates and therefore, it was assumed that the energy was transferred within the stacks from the H-aggregates which acted as some kind of “antenna” to the J-aggregates that acted as emitter. The studies of Markovitsi and co-workers furthermore showed that the triplet exciton transport in well-ordered columnar mesophases can be hindered by structural defects leading to an emission with a large Stokes shift.³⁵⁹ These effects are mainly used to prepare novel opto-electronic materials, *e. g.* by incorporating a fluorophore as emitter in a naphthalene based hydrogel to induce a blue shift of the PL of the hydrogel.^{169,360,361}

By bridging two BTA cores with a diacetylene unit it could be shown that the PL at 450 nm exhibits a strong charge-transfer (CT) character, where the dendritic side arms act as “antennas” for the light absorption and the self-assembled BTA-cores act as emitter for the aggregation-enhanced blue luminescence.³⁶² Such a charge transfer from the molecular periphery to the central benzene core was also reported for other BTA based self-assembly systems.³¹

Summarizing, the results in the literature suggest that compound **4** shows aggregation-induced emission due to π^* - π or π^* -n transitions with a CT from the side arms to the self-assembled benzene cores. The PL enhancement is only possible due to a rigidification of the

side arms, which leads to reduced vibrational energy losses. In order to confirm these assumptions time-dependent PL studies upon gel formation and theoretical calculations have been performed.

4.1.3 Photoluminescence studies upon gel formation

While in aqueous solutions of **4Na** no photoluminescence could be detected, hydrogels of **4** exhibit blue luminescence upon irradiation with UV light. This leads to the conclusion that during gel formation the chromophoric system is slowly formed. As the hydrolysis of GdL results in a very slow and homogenous decrease of the pH value in the whole solution.^{98,103,363} this gelation method is ideal to monitor the formation of the chromophoric system upon gel formation in dependence of time. After the addition of 4 eq. of GdL to a solutions of **4Na** (10 g L^{-1}) an increase of the intensity of the blue luminescence can be observed with the naked eye upon irradiation with UV light at 366 nm (Figure 4.7a). The combination of time-dependent PL measurements and GdL-assisted gelation can further give quantitative insight in the formation of the chromophoric system upon aggregation (Figure 4.7b).

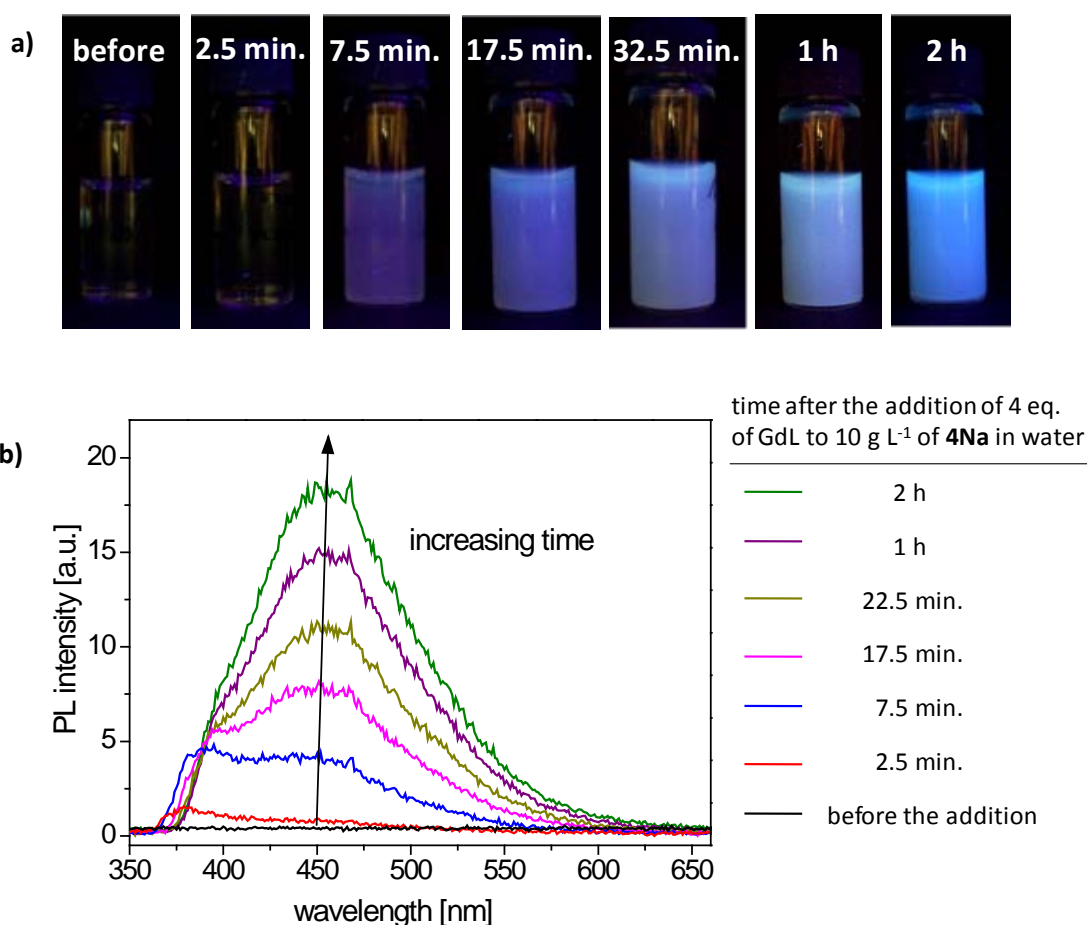


Figure 4.7: a) Optical images of a solution of **4Na** (10 g L^{-1}) after the addition of 4 eq. of GdL under irradiation with UV light at 366 nm; and b) the respective PL spectra using an excitation wavelength of $\lambda_{\text{exc}} = 330 \text{ nm}$.

To exclude any influence of the added GdL and its hydrolysis products on the PL properties, an aqueous solution with a GdL concentration similar to that present during the gelation process was prepared. No PL intensity of this GdL solution could be detected proving that the origin of the PL intensity in Figure 4.7 is indeed due to the formation of aggregates of **4** upon decrease of the pH value.

Already after 2.5 min a first peak at about 380 nm can be detected in the PL spectrum, which is consistent with the observation of first aggregates in DLS measurements and TEM images (chapter 3.3.2.3). After 7.5 min a second peak evolves at about 450 nm in the PL spectrum, while a violet to blue luminescence can be observed in the optical images that were irradiated with UV light at 366 nm. The PL intensities of both peaks increase with increasing time and show a slight red shift. As the peak at about 450 nm grows much faster than the peak at about 380 nm, already after 17.5 min the maximum PL intensity of the respective spectra can be found at about 453 nm, while the peak at lower wavelength is only visible as shoulder of the main peak.

To get further insight into the formation of the chromophoric system upon decrease of the pH value and resulting gel formation, calculations using density functional theory (DFT) and time-dependent DFT (TDDFT) were performed.

4.2 Theoretical calculations

With increasing technological progress computational studies have become more and more important to understand aggregation processes, such as the gel formation mechanisms of various supramolecular gels.⁶⁴ Although the self-assembly of 1,3,5-benzene tricarboxamides (BTAs) has been investigated intensely in the last decades,^{132,134,135} only a few theoretical calculations giving insight into the supramolecular aggregation process and the molecular arrangements have been published yet.^{139,149,151,357,364,365}

The density functional theory (DFT) and the time-dependent DFT (TDDFT) calculations of the monomer, dimer, trimer, and tetramer forms of **4** together with the respective highest occupied molecular orbital (HOMO) and lowest unoccupied molecular orbital (LUMO) were performed by Rodrigo Q. Albuquerque. Detailed description of the used programs and algorithms can be found in chapter 9.4.6 and in the literature.¹⁰²

The optimized geometry of the monomer form of **4** with the respective HOMO and LUMO are presented in Figure 4.8. While the HOMO is rather located at one side arm of the relatively planar molecule, the LUMO can be found at the benzene core. Such a distribution of the

respective HOMO and LUMO is also known from other computational studies on BTA derivatives^{357,364} and compounds with a similar structural concept for molecular aggregation.¹⁴⁸

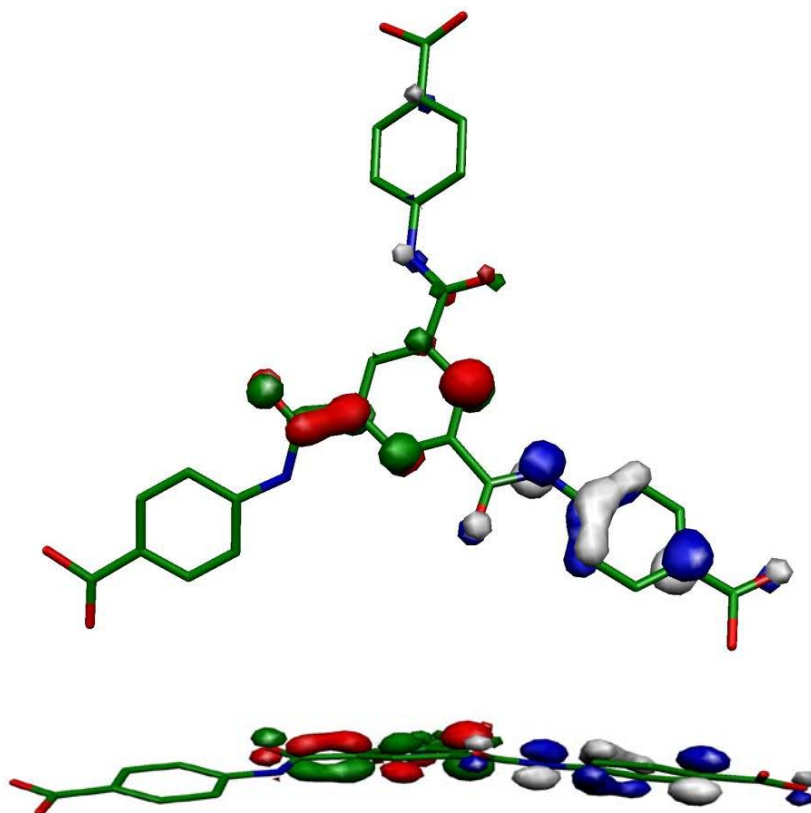


Figure 4.8: DFT-Optimized geometries and electron densities of the HOMO (blue/white) and LUMO (red/green) orbitals of the monomer of **4** (top and side view). The atom labels are: carbon (green), nitrogen (blue), oxygen (red). The hydrogens are omitted for clarity. Reproduced from reference 102 with permission from *The Royal Society of Chemistry*.

When optimizing the geometry of the respective dimer (two molecules of **4**) one has to keep in mind, that in general two different interaction modes are possible: i) the formation of a dimer mainly by interactions of the lateral moieties leading to a “side-by-side” dimer; and ii) the formation of a “on-top” dimer by stacking of the molecules with triple hydrogen bonding between the amide units. The experimental findings presented in chapter 3 and in the literature^{see for example: 132,134,135,267} show the preference of one-dimensional aggregates in the bulk and hydrogel state leading to the assumption that the “on-top” dimer is more favorable. This can be explained by the fact that in the “on-top” dimer triple hydrogen bond formation is possible between the amide units of adjacent molecules, while only one self-complementary hydrogen bond is present between the lateral carboxylic acid moieties in the “side-by-side” dimer.

In Figure 4.9 the optimized geometry of the tetramer form of **4** (four stacked molecules) is shown.

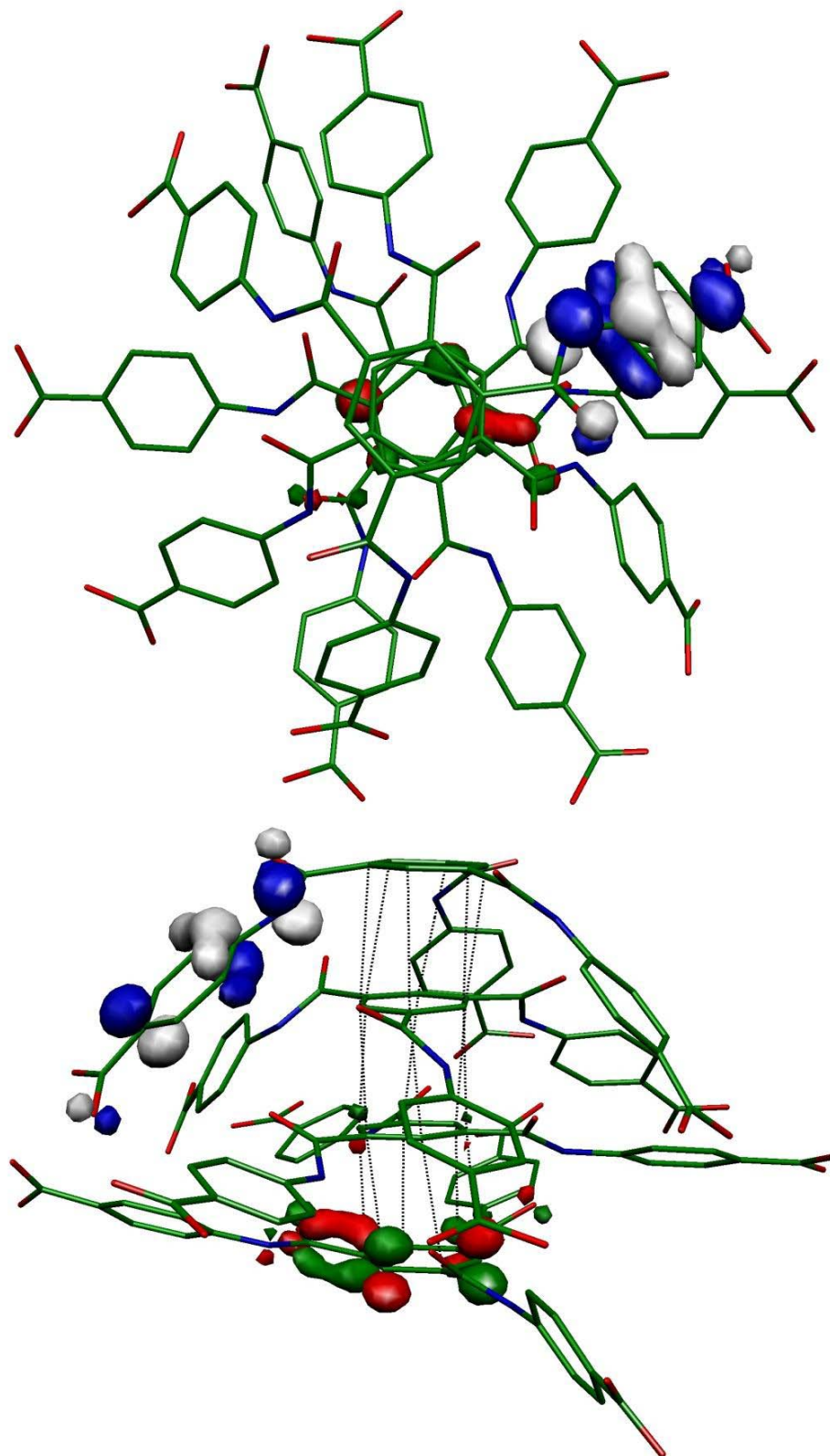


Figure 4.9: DFT-Optimized geometries and electron densities of the HOMO (blue/white) and LUMO (red/green) orbitals of the tetramer of **4** (top and side view). The atom labels are: carbon (green), nitrogen (blue), oxygen (red). The hydrogens are omitted for clarity. The black dotted lines represent the stacking of the aromatic cores. Reproduced from reference 102 with permission from *The Royal Society of Chemistry*.

The rotation of the adjacent molecules by an angle of 60° (*abab...* conformation) and the twisting of the amide units out of the molecular plane enable the formation of triple hydrogen bonding between two adjacent molecules. Such a staggered *abab...* conformation is also reported for other BTA based assemblies.^{134,135,210}

Interestingly, the cores in the optimized geometry are not directly located above each other as indicated by the black dotted lines in Figure 4.9. This induces a helicity in the molecular arrangement (see also chapter 3.4) and might prevent a face-to-face (H-type) aggregate formation. The helicity of the columnar stacks is transferred to the superstructures upon further aggregation, as in SEM images of hydrogel samples and films of **4** twisted and helical fibers can be observed (chapter 3.3.2).

The calculated core-core distance of the central benzenes in the geometry optimized tetramer of **4** is about 0.328 nm, which is in the range of reported π - π -distances for similar systems.^{132,134,135,138,139,214} The performed XRD studies on wet and dried hydrogels of **4** (chapter 3.3.2.3) give a core-core-distance of about 0.347 nm that is slightly higher compared to the calculated distance. This might be due to the fact that the used calculation technique overestimates the π - π -interactions and therefore leads to lower core-core-distances.

Furthermore, also a bending of the side arms in the optimized geometry of the tetramer can be observed due to π - π -interactions between the respective phenylene spacers in the periphery of the molecule. However, one has to keep in mind that the overestimation of these interactions is further pronounced as only aggregates with a few molecules are simulated. It is reasonable to assume that in elongated aggregates with a much higher number of molecules this bending effect of the side arms will play a minor role and occur only at the end of a stack. Furthermore, it has to be noted that in bulk or hydrogel samples no isolated columns of stacked molecules could be observed. This indicates that additionally “side-by-side” interactions between columns occur in the samples, which further stabilize and rigidify the side arms.

Similar to the monomeric form of **4** the HOMO in the tetramer is mainly located at the side arm of one molecule, while the LUMO can be found at a central benzene core. The calculations thereby indicate that the HOMO and the LUMO are located at different ends of the short stack. In the literature for BTA self-assemblies charge transfer from the periphery to the central core of one molecule³¹ as well as along the columnar stack are reported.³⁶²

Due to the location of the LUMO at the benzene core the energy levels of the excited states are shielded from the solvent molecules. Therefore, environmental differences, such as the presence of a solvent and the morphology of the superstructures, do not significantly influence the PL behavior. This effect should be even more pronounced with increasing number of

molecules in the molecular stack and therefore, clearly explains the similarity of the obtained spectra from films and hydrogels of **4**, despite the different morphologies and chemical environments of the samples.

The energy values of the lowest excited states S_1 and T_1 for the monomer, the two possible dimers, the trimer, and the tetramer form of **4** were calculated and are presented in Table 4.1. The respective energy values decrease with increasing number of molecules in the aggregate and also the singlet triplet splitting decreases. This red shift of the calculated excited states might be explained by the formation of triple hydrogen bonds between the amide units as well as π - π -interactions of the benzene cores in the formed anisotropic aggregates. Experimentally this red shift could also be observed during the PL study upon gel formation with GdL (Figure 4.7, chapter 4.1.3). Thereby, the first observed peak at about 380 nm might be assigned to the formation of “on-top” dimers. The second peak at about 450 nm that evolves with increasing time and is then slightly red shifted might be assigned to the formation of columnar aggregates with a higher number of molecules.

Table 4.1: Calculated energy values of the lowest excited singlet (S_1) and triplet states (T_1) of the monomer and different aggregates of **4**.

| number of molecules | (n) | S_1 energy [eV] | T_1 energy [eV] |
|----------------------|-----|-------------------|-------------------|
| monomer | (1) | 3.79 | 3.02 |
| “side-by-side” dimer | (2) | 3.67 | 2.97 |
| “on-top” dimer | (2) | 3.28 | 2.94 |
| trimer | (3) | 2.65 | 2.63 |
| tetramer | (4) | 2.45 | 2.44 |

As the energy values of the “side-by-side” dimer are similar to the calculated ones for the monomeric form, it is unreasonable to assume that the observed red shift in the experiments upon gel formation is due to “side-by-side” interactions and dimerization. This further supports the assumption that the chemical environment and hydrogen bond formation between lateral carboxylic acid moieties does not significantly influence the PL behavior. However, dimerization of supramolecular columns of **4** lead to a rigidification and stabilization of the whole aggregate, which results in an increased emission due to less non-radiative energy loss.

The calculated energy levels describe the lowest excitation from the HOMO to the LUMO. As the electrons are transferred from the side arms at one end of the stack to the benzene

core of the molecule at the other end of the stack these lowest excited states have a strong charge transfer (CT) character. In the literature similar computational studies for other self-assembly systems based on intermolecular hydrogen bonds are described that confirm such CT characteristics for supramolecular aggregates.^{148,357,362} As the orbitals of the lowest excited states show a poor overlap and therefore a low oscillator strength, it is assumed that transitions of higher-lying excited states occur, *e. g.* from (HOMO – x) to (LUMO + y). Such excitations still exhibit CT character, but possess a much larger oscillator strength.³⁶⁴

The CT character in supramolecular assemblies of BTA derivatives is especially interesting, as it is known from different studies that a macrodipole is present in the BTA columns due to the rotation of the amide units out of the plane of the benzene core.^{139,150,151} The calculations presented here reveal that in the optimized geometry of the tetramer form of **4** all three amide units of a BTA molecule point in one direction causing a macrodipole in the stack (Figure 4.9). A novel molecular dynamics simulation study concerning the self-assembly of BTA derivatives in *n*-nonane as realistic solvent revealed that BTA aggregates are more stable, if only two amide units point in the same direction, while the third is directed to the opposite.¹⁴⁹ Nevertheless, a macrodipole is present in such stacks although its total strength is weakened.

In the computed tetramer of **4** the CT is directed in the opposite direction of the macrodipole. Therefore, it might be assumed that the macrodipole and the anisotropic assembly into molecular columns are additionally stabilized by the CT. As already discussed earlier, it is important to note that the aggregates in the investigated films and hydrogels of **4** consist of stacks that contain a significantly higher number of molecules than the tetramer simulated here. Thus, the energy levels calculated from the experimentally determined absorption and PL spectra might be even lower than the energy levels of the tetramer.³⁵⁷ Furthermore, also defects and less ordered domains in the columnar assembly of **4** must be considered as they might act as emitter for the radiation and therefore cause the observed red shift. In order to fully determine the origin of the PL of hydrogels and films of **4**, fluorescence decay and lifetime measurements are necessary which are currently performed in an ongoing study in cooperation with Prof. Anna Köhler from Experimental Physics II of the University of Bayreuth.

4.3 Considerations regarding the proposed structural model

Due to the pH-sensitivity of the gelator system of **4**, by decreasing the pH value from alkaline to acidic, molecules are slowly transferred from the sodium salt **4Na** to the fully protonated state of **4**. This leads to the formation of a hydrogel with bright blue luminescence upon irradiation with UV light at 366 nm.

Compound **4Na** as well as compound **4** show no luminescence in the dissolved state, but blue luminescence can be observed in films and hydrogels of **4**. Thus, this system clearly shows aggregation and gelation-induced emission. As the emission spectra of films and hydrogels of **4** are very similar, it is assumed that the chromophoric system, that forms during aggregation, is rather independent of the environment. In accordance to the literature the emission is assigned to either a π^* -n or a π^* - π -transition.^{203–205,209} The comparison with the emission spectra of the single crystal of **4**²¹⁰ indicates that a rigidification of the side arms in a more tightly and ordered structure leads to a blue shift of the emission. Furthermore, it has to be noted that the BTA molecules are planar in the single crystal due to the formation of a layered structure, while in the hydrogel columnar aggregates are present that are usually characterized by a twist of the amide unit out of the molecular plane. Intense spectroscopic studies about benzanilides showed that the angle of the amide unit in respect to the benzenes can strongly influence the spectroscopic properties of such compounds.^{366,367}

Time-dependent PL studies during gel formation showed the presence of an emission signal at 380 nm during the first minutes of the experiments. In combination with TDDFT calculations this signal was assigned to the emission of “on-top” dimers. With increasing gel formation a second red shifted signal at about 450 nm evolves and increases, which was assigned to the formation of enlarged stacks of **4**. The structural model of the hydrogel proposed in chapter 3.4 was supported by the optimized geometries of short stacks of **4**. The “on-top” aggregation is favored by triple hydrogen bond formation between adjacent molecules, as proposed in chapter 3.2.2.2 when discussing the infra-red spectroscopy results. Therefore, adjacent molecules in the stack are rotated by 60° and the amide units are twisted out of the plane of the benzene core leading to a macrodipole in the columnar aggregates. The calculated core-core distance is about 0.33 nm. Considering the slight overestimation of π - π -interactions by the calculation technique the calculated core-core distance is in good agreement with experimental findings for hydrogels of **4**. Interestingly, the benzene cores in the optimized geometry of the tetramer of **4** are not arranged in a face-to-face mode, but slightly shifted against each other, which might be the origin of the helicity in the self-assembled aggregates. The distribution of the HOMO and LUMO in the optimized geometries of the tetramer of **4** indicates a charge transfer from the periphery of the molecule to a central benzene core of the

stack. This might be the reason for the observed large Stokes shift. Due to the poor overlap of the respective orbitals and the resulting low oscillator strength, it is reasonable to assume that also transitions of higher excited states contribute to the emission.

Summarizing, the combination of time-dependent PL studies during gel formation and DFT calculations are a very powerful tool to give insight in the formation of first aggregates and the chromophoric system. Unfortunately, it is rather difficult and time-consuming to simulate larger systems with many atoms. Therefore, only tetramers of **4** could be calculated. Furthermore, one should keep in mind that the first aggregates are probably build up from charged, partially charged and uncharged molecules as the three carboxylic acid moieties are subsequently protonated. Due to the complexity of this problem, this situation could not be simulated using DFT and TDDFT calculations. The recent publication of Balasubramanian and co-workers highlights the importance of molecular dynamics (MD) simulations on BTA molecules in realistic solvents to understand supramolecular polymerization mechanisms.¹⁴⁹ They furthermore propose that coarse grain models will be inevitable to extend the MD simulations of single columnar aggregates to the self-assembly of fibers and other superstructures.

Further spectroscopic investigations such as fluorescence decay and life-time measurements are conducted in cooperation with Prof. Anna Köhler from the department of Experimental Physics II of the University of Bayreuth. This current study shall help to evaluate the origin of the luminescence and to better understand the energy transport processes for this water-based, pH-sensitive BTA derivative.

5 Dye adsorption and release studies: towards a pH-sensitive supramolecular drug delivery system

In this chapter the pH-sensitive hydrogelator system **4/4Na** is investigated regarding its adsorption properties from aqueous rhodamine B solutions, which acts as model drug. The adsorption data were analyzed according to the isothermal models developed by Langmuir and Freundlich and with respect to the adsorption kinetics. Furthermore, the hydrogel was loaded with the dye by “encapsulation”, *i.e.* gel formation in presence of rhodamine B. The release behavior was investigated in water at different initial dye concentrations and correlated to Fickian diffusion. Moreover, the release of the model compound in biologically relevant media, such as phosphate buffered saline (PBS), simulated body fluid (SBF), simulated gastric fluid (SGF) and simulated intestinal fluid (SIF) was studied in view of the application of this hydrogel as controlled drug delivery system.

5.1 Requirements for controlled drug delivery systems

Although there are many advantages of so called “smart” supramolecular hydrogels for the application in the field of controlled drug delivery, every hydrogelator system must fulfill certain requirements for its successful development as state of the art medical product,³¹ such as i) good biocompatibility and nontoxicity; ii) responsiveness of the hydrogel to an external stimuli in a physiological relevant range; iii) sufficient stability against mechanical and thermal stress; iv) high surface area and porosity; and v) a high loading efficiency through adsorption or encapsulation of the drug molecules. In the following, it is shown that the hydrogelator **4** fulfills these basic criteria and is therefore an interesting candidate for controlled drug delivery applications.

5.1.1 Biocompatibility and nontoxicity

Assays for antiproliferative and cytotoxic properties of the gelator **4** and the gelator sodium salt **4Na** were carried out by a CellTiter-Blue cell viability assay with HUVEC (human umbilical vein endothelial), K-562 (human immortalized myelogenous leukaemia) and HeLa (human cervix carcinoma) cell lines, respectively. Both tested compounds did not show any antiproliferative effect on HUVEC or K-562 cells (GI_{50} values $> 50 \mu\text{g mL}^{-1}$) or any cytotoxic effect on HeLa cells (CC_{50} values $> 50 \mu\text{g mL}^{-1}$).

Furthermore, antimicrobial properties were tested using a broadband screening *via* agar diffusion assay with five different strains of bacteria and fungi. For compound **4** dimethyl sulfoxide (DMSO) was used as solvent. The antimicrobial control experiments showed activity of pure DMSO against *escherichia coli* (14 mm zone of growth inhibition), *pseudomonas aeruginosa* (16 mm zone of growth inhibition) and *penicillium notatum* (14 mm zone of growth inhibition). Therefore, the slight activity of compound **4** against *escherichia coli* (12 mm zone of growth inhibition) is probably caused by the solvent DMSO. Interestingly, compound **4** in DMSO showed no activity against the *pseudomonas aeruginosa* and *penicillium notatum*, which might indicate a cytoprotective effect of compound **4** from the effect of the solvent DMSO. The sodium salt **4Na** was tested in aqueous solution and neither the solvent water nor the compound did show any activity against the tested bacteria and fungi.

Summarizing, it can be stated that the gelator **4** and the gelator sodium salt **4Na** could be used for biomedical applications without undesirable side effects.

5.1.2 Responsiveness of hydrogels of **4**

For biomedical application the hydrogels should be responsive to a physiological relevant trigger. Hydrogels of **4** are formed by a change of pH from slightly basic to slightly acidic values.^{102,267} The sodium salt of the gelator **4Na** can be dissolved in water and depending on the amount of gelator salt this results in a pH value between 7 and 9. From the titration curves shown in chapter 3.3.1.1 a sol-gel transition pH of about 6.2 can be deduced. Stable gels can be formed when a final pH value of about 4 to 5 is realized. The hydrogel media then can be exchanged to desalted water with a pH value of about 6 without gel destruction. An interesting approach would be to use the different pH values in the gastrointestinal tract to deliver bioactive molecules in a controlled manner to the intestine. Due to the low pH values present in the stomach the gel should stay intact. When the pH increases in the intestinal tract the gel should slowly dissolve and therefore release an adsorbed drug molecule. Thus, this responsive hydrogel system is not only suitable for biomedical application due to its transition near neutral pH value, but is especially interesting for the use as a controlled drug delivery system with oral administration. For the detailed study regarding the gel stability and release of a model compound in biologically relevant media see chapter 5.5.

Furthermore, the hydrogels are highly thermally stable. Down to a gelator concentration of 2 g L⁻¹ the hydrogel shape is kept intact even when heating the sample to 100 °C.¹⁰² This clearly illustrates that the multiple non-covalent interactions strongly stabilize the formed nanofibers, thus resulting in a stable network.

5.1.3 Mechanical stability of hydrogels of **4**

The mechanical characterization, as shown by rheological measurements in the literature, confirms the gel state at acidic pH values with the storage modulus G' (4000 Pa) being an order of magnitude higher than the loss modulus G'' (230 Pa).²⁶⁷ In frequency sweep experiments the storage modulus showed a plateau over a wide range of frequencies at a gelator concentration of 10 g L^{-1} . Above the critical oscillatory torque (also “yield stress”) of about $1100 \text{ } \mu\text{Nm}$ the gel started to flow irreversibly. The indentation measurements discussed in chapter 3.3.3.3 prove that the mechanical stability of the gel can be increased by increasing the gelator concentration. Samples prepared with a gelator concentration of 10 g L^{-1} rather break than flow at a compression stress at break of 150 mN. Furthermore, the experiments regarding the sample preparation (chapter 3.3.3) show that it is possible to handle small gel samples using tweezers without destruction.

5.1.4 Specific surface area

While being sufficiently stable, the hydrogels at the same time need a high specific surface area to ensure high adsorption capacities. This is often achieved by using very porous structures. The specific surface area is usually determined by the adsorption method developed by Brunauer, Emmett and Teller (BET measurement).³⁴⁴ In general nitrogen gas is used for this method. However, as the accuracy of the method can be enhanced by using krypton, the latter gas was used here. BET measurements can only be performed on dried systems. This is ensured by applying an outgas temperature of $150 \text{ } ^\circ\text{C}$ on the sample prior to the measurement. The specific surface area of a bulk sample of **4** after crystallization and of the sodium salt **4Na** were determined to be $14 \text{ m}^2 \text{ g}^{-1}$ and $17 \text{ m}^2 \text{ g}^{-1}$, respectively. As the hydrogel is formed by solidifying the whole solvent volume at a concentration of 10 g L^{-1} , it is expected that the specific surface area is much higher in the hydrogel state than in the bulk samples. As the hydrogel cannot be measured in the wet state, it was dried by blotting the excess of solvent with paper pulp and subsequent drying under high vacuum at r. t.. It is known from literature that the porosity and gas adsorption properties in a metal organic framework containing **4** as a ligand can be drastically decreased by removal of solvent molecules *via* conventional vacuum drying due to the loss of the integrity of the structure.¹⁹⁹ By removing the solvent molecules under high vacuum, at least the macroscopic dimensions of the gel samples of **4** remain intact, while air-dried samples are completely collapsed (Figure 5.1). This phenomenon might be explained by the conditions present under high vacuum that lead to the sublimation of the water at r. t..

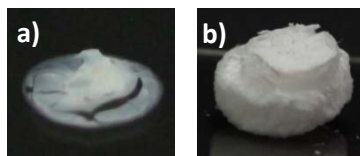


Figure 5.1: Optical images of washed hydrogels of **4** prepared from 10 g L^{-1} of **4Na** and 4 eq. of glucono-delta-lactone (GdL), respectively; a) dried under ambient conditions and b) dried under high vacuum (4×10^{-3} mbar).

Unfortunately, the gel dried under high vacuum (xerogel) has also different properties compared to the original wet hydrogel, indicated by the very brittle nature of the xerogel. In SEM images of the dried gel nearly no pores can be detected, suggesting that the single fibers and fiber bundles converge upon drying. This assumption can also be supported by the XRD pattern of the xerogel compared to the wet gel (chapter 3.3.2). Upon drying the signal at $2\theta = 4.02^\circ$ ($\sim 2.2 \text{ nm}$) in the wet hydrogel shifts to larger angles ($2\theta = 5.92^\circ$) and smaller distances in real space ($\sim 1.5 \text{ nm}$). This shift to smaller distances in the dried state might be caused by fibers that are more closely connected than in the original wet state, thus leading to smaller or closed pores and lower specific surface area values. Using an outgas temperature of 150°C prior to the measurement a specific surface area of *ca.* $17 \text{ m}^2 \text{ g}^{-1}$ could be achieved for the dried hydrogel, which is slightly higher than the specific surface area of the crystalline bulk sample with $14 \text{ m}^2 \text{ g}^{-1}$. This clearly shows that the specific surface area can indeed be increased by forming a hydrogel compared to the original bulk compound after crystallization. By increasing the outgas temperature to 250°C , the value could nearly be doubled to about $30 \text{ m}^2 \text{ g}^{-1}$. These values are in good agreement with other porous organic materials based on the 1,3,5-benzene tricarboxamide core, which were reported to be between 14 and $34 \text{ m}^2 \text{ g}^{-1}$, dependent on the exact molecular structure of the compound.¹⁹⁶

The fact that the outgas temperature influences the measured specific surface area indicates that some strongly bound water might remain at the surface of the xerogel and is not completely removed even at 150°C . This loss of water at temperatures above the boiling point of free water can also be observed in thermal gravimetric analyses (TGA) of the bulk compounds of **4** and **4Na** as discussed in chapter 3.2.2. While the bulk samples show a weight loss of 5.7% (**4**) and 15.4% (**4Na**), the dried hydrogel samples of **4** show a weight loss of 9.6% between 25°C and 300°C . As this weight loss occurs before the decomposition of the respective samples, it is associated with the loss of water adsorbed at the surface. The molecular ratio of compound **4** as bulk material and water deduced from these TGA-investigations is about 1 to 1.9. This is in good agreement with the values found in the elemental analysis of compound **4** ($\mathbf{4} \cdot 1.5 \text{ H}_2\text{O}$). To make sure that the amount of water

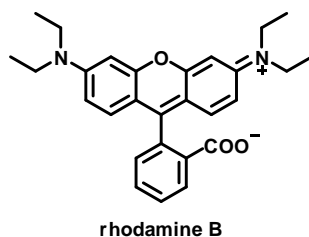
detected in the elemental analysis was not due to insufficient drying after synthesis, the sample was kept under reduced pressure at 100 °C for 24 h prior to the elemental analysis.

By performing experiments with a moisture analyzer it was shown that bulk samples of **4** could take up between 4.4 % and 8.7 % of water depending on the humidity during storage (chapter 3.2.2). The water uptake of the sodium salt **4Na** was even higher (9.4 %). The water uptake is limited and reaches distinct saturation values for different levels of humidity. Thus, the compounds do not show the typical hygroscopic behavior that leads to liquefaction, as it is observed for sugar or salts such as NaCl. Hydrogels of **4** consist of fibers that are built by entangled fibrils which are formed by the anisotropic alignment of the trigonal-shaped molecules. Considering such a hierarchical structure of the hydrogel, it can be assumed that the large surface area of the hydrogel fibers is highly decorated with carboxylic acid moieties. With such a “polycarboxylic acid functionalization” of the fiber surface the hydrogel should be able to form strong hydrogen bonds with solvent molecules such as water or other small organic guest molecules, or might even act as an anchor group for metal ions. Hence, the high uptake of water of compound **4** in bulk combined with the morphological structure and large specific surface area of the hydrogel leads to the hypothesis that hydrogels of **4** have a high adsorption potential either for waste water treatment applications or the adsorption of drug molecules for drug delivery applications.

As hydrogels of **4** fulfill the basic requirements, such as biocompatibility, non-toxicity, responsiveness in a physiological relevant range, high mechanical strength, thermal stability, and high surface area, this system seems to be a promising candidate for the application in the field of controlled drug delivery.

5.2 Adsorption of rhodamine B using pre-formed hydrogels

Adsorption is not only used for the loading of a carrier system with bioactive molecules or drugs, but it is also important for waste water purification. Rhodamine B is a standard compound used in textile industry and due to its good solubility in water and multiple functional groups, it can act as a model compound for the adsorption onto a pre-formed hydrogel (Scheme 5.1).



Scheme 5.1: Chemical structure of rhodamine B.

Because of the unique combination of properties of hydrogels of **4**, the adsorption capacity of the system and the release behavior regarding rhodamine B as model compound were investigated and the results are discussed in the following.

5.2.1 Sample preparation and experimental set up

When determining the adsorption capacity of a system, the results can vary depending on the used method of evaluation and the chosen parameters, such as concentration of the dye solution, mass and volume of the adsorbent and time. Therefore knowledge of the experimental parameters is very important to be able to compare results. In the literature the *adsorption capacity* is given as quotient of the mass of adsorbed dye in mg and the mass of the adsorbent or gelator in g (mg g^{-1}).^{for example see: 25,87,281,284,285} However, the ratio of the adsorbed mass of dye to the initial mass of dye in solution in percent (%) is an important value to characterize the system as well. As no consistent terminology for this value could be found in the literature, in this work it is given at the adsorption equilibrium as the *decolorization efficiency* d_e of the system. Figure 5.2 gives a schematic overview of the adsorption process and the used technical terms and variables.

With the gelator system investigated in this work it seemed furthermore to be useful to give the ratio of the molar amount of dye in the supernatant solution to the molar amount of gelator **4** in the hydrogel. This molar ratio directly gives the number of dye molecules that might be adsorbed by one gelator molecule and is displayed with eq. (equivalents) as unit. This molar ratio is especially interesting as the molar masses of the gelator **4** and the sodium salt **4Na** are different, but the molar amount and therefore the number of gelator molecules are constant. The concentrations of the dye solutions used for the generation of the calibration curve and those used for the adsorption studies were chosen regarding the molar ratio in eq. of dye and gelator. Nevertheless, for comparison reasons the adsorption capacity is also given as mass ratio in mg g^{-1} . As for the gel preparation the gelator concentration of 10 g L^{-1} refers to the water soluble sodium salt **4Na**, the amount of **4Na** in the system is also used for the calculation of the adsorption capacity.

The linear fit of the calibration curve was calculated with the intercept set to zero and can be expressed by:

$$\text{O.D.}_{553\text{nm}} = 223.1 \text{ L g}^{-1} c_{\text{sol}} \quad (5.1)$$

with $\text{O.D.}_{553\text{nm}}$ being the optical density at 553 nm of four measurements and c_{sol} being the dye concentrations of the rhodamine B solutions.

It has to be noted that above a concentration of 10^{-4} M ,¹ rhodamine B forms aggregates due to intermolecular π - π -interactions.²⁷⁷ The dye concentrations for the calibration curve were chosen in the range where optical densities at 553 nm obtained by UV-Vis measurements increase linearly with concentration. This concentration range was also used for the rhodamine B solutions applied in the adsorption studies.

5.2.1.2 Preparation of defined gel samples

To get defined gel samples with constant dimensions and geometries for the adsorption experiments, polydimethylsiloxane (PDMS) molds were made by mixing a silicon elastomer with a curing agent. Subsequently the mixture was filled in a Teflon mold (form D in Figure 5.4a) and left to stand at r. t. for 3 days for hardening. The resulting PDMS molds have 25 cylindrical wells with well defined dimensions (height: 0.5 cm, \varnothing : 0.5 cm) for the gel formation (Figure 5.4b). Thus, each well comprises a volume of *approx.* 0.1 mL. As the PDMS molds are flexible, it is easy to remove the gelled samples with a small spatula.

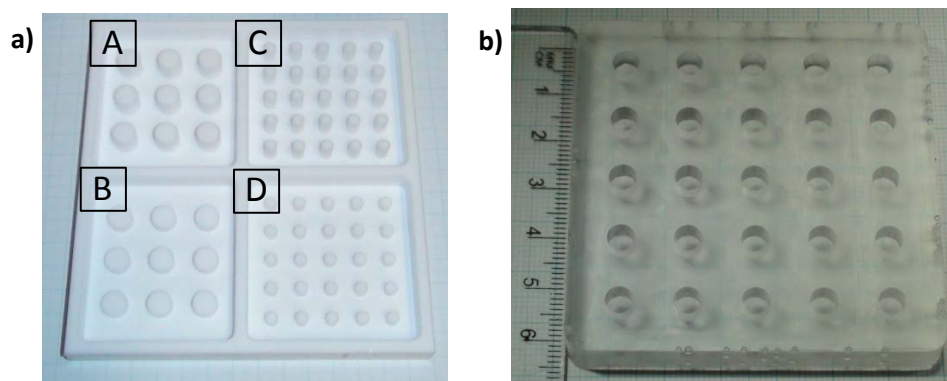


Figure 5.4: a) Teflon mold with four different geometries; b) PDMS mold formed in Teflon mold D with 25 defined wells for gel sample preparation.

All hydrogels were prepared from aqueous solutions of **4Na** with a concentration of 10 g L^{-1} . Addition of 4 eq. of glucono-delta-lactone (GdL) to the gelator sodium salt solution resulted in the decrease of the pH value and thus gelation. The **4Na** solution with freshly added GdL was filled in each of the wells of the PDMS mold (Figure 5.5).

¹ This corresponds to a rhodamine B concentration of $0.047902 \text{ g L}^{-1}$.

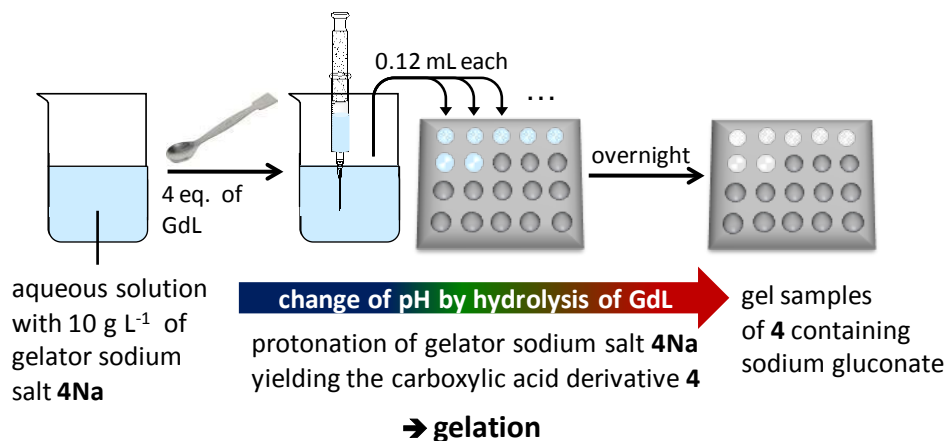


Figure 5.5: Preparation of defined gel samples in the wells of a PDMS mold by addition of 4 eq. of glucono-delta-lactone (GdL) to an aqueous solution of **4Na** ($c = 10 \text{ g L}^{-1}$) and gelation overnight.

Preliminary tests regarding the influence of mechanical agitation on the adsorption kinetics were performed with gel samples prepared from 0.10 mL of **4Na** solution. However, after gelation the removal of the samples was quite difficult. Thus, for all other performed tests gel samples with a volume of 0.12 ml were prepared. These gels had a cylindrical shape with a hemispherical cap due to the surface tension of water and could be removed easily (Figure 5.6).

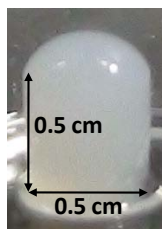


Figure 5.6: Optical image showing the shape of a typical hydrogel sample prepared from 0.12 mL of a **4Na** solution with a concentration of 10 g L^{-1} and 4 eq. of GdL.

Thus, if not stated otherwise, one sample comprises 1.2 mg of the gelator sodium salt **4Na** and 1.35 mg of GdL. After gelation overnight gel samples of **4** containing sodium gluconate were obtained due to the hydrolysis of GdL.

Each gel sample was removed from the well using a spatula and put in 5 mL of desalted water, respectively (Figure 5.7). The resulting sodium gluconate was removed from the gel samples by a repeatedly applied washing process with desalted water. Size and shape of the hydrogels were fully retained during this process.

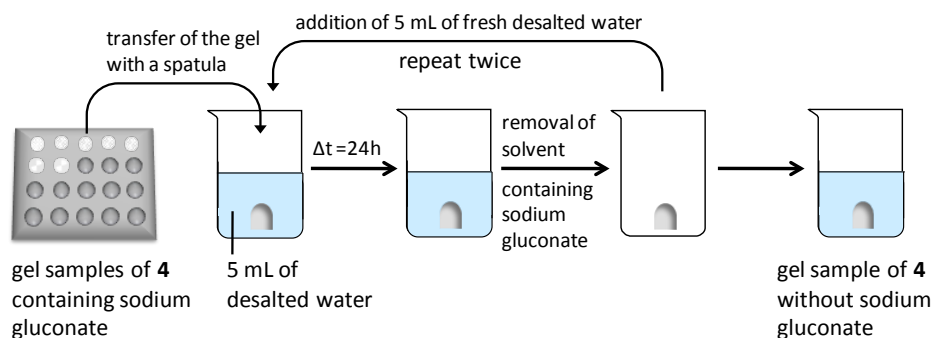


Figure 5.7: Washing procedure for freshly prepared hydrogels of **4** containing sodium gluconate.

5.2.1.3 Experimental concept and calculations

The gel samples, that were prepared as described above, were put into 5 mL of aqueous rhodamine B solutions with distinct concentrations. The sample set up and the dye concentrations were chosen in a way that the maximum amount of rhodamine B in the supernatant solution was within the range of the calibration curve. If not stated otherwise, each experiment was performed three times to be able to calculate reliable average and standard deviation values. After certain time intervals approximately 0.3 mL of the supernatant solution were removed for the UV-Vis measurements. Afterwards, the volume of solution was put back into the sample. The loss of liquid due to residues in the syringe or the cuvette was negligible compared to the total volume of the sample.

If not stated otherwise, adsorption experiments were performed with gel samples prepared with 0.12 mL of a **4Na** solution with a concentration of 10 g L^{-1} . Thus, one typical gel sample consists of 1.2 mg of **4Na**, which corresponds to 0.00189 mmol of **4Na** or **4**, respectively. The initial molar amount of rhodamine B is given as equivalents (eq.) in relation to this molar amount of **4** in the gel. Figure 5.8 exemplarily shows the optical images and absorption spectra of a dye solution with 0.05 eq. of rhodamine B, which corresponds to a rhodamine B concentration of 0.00907 g L^{-1} using a volume of 5 mL. The images and the spectra were recorded 6 h, 24 h, 48 h, 72 h and 240 h after the addition of a washed gel sample to the dye solution.

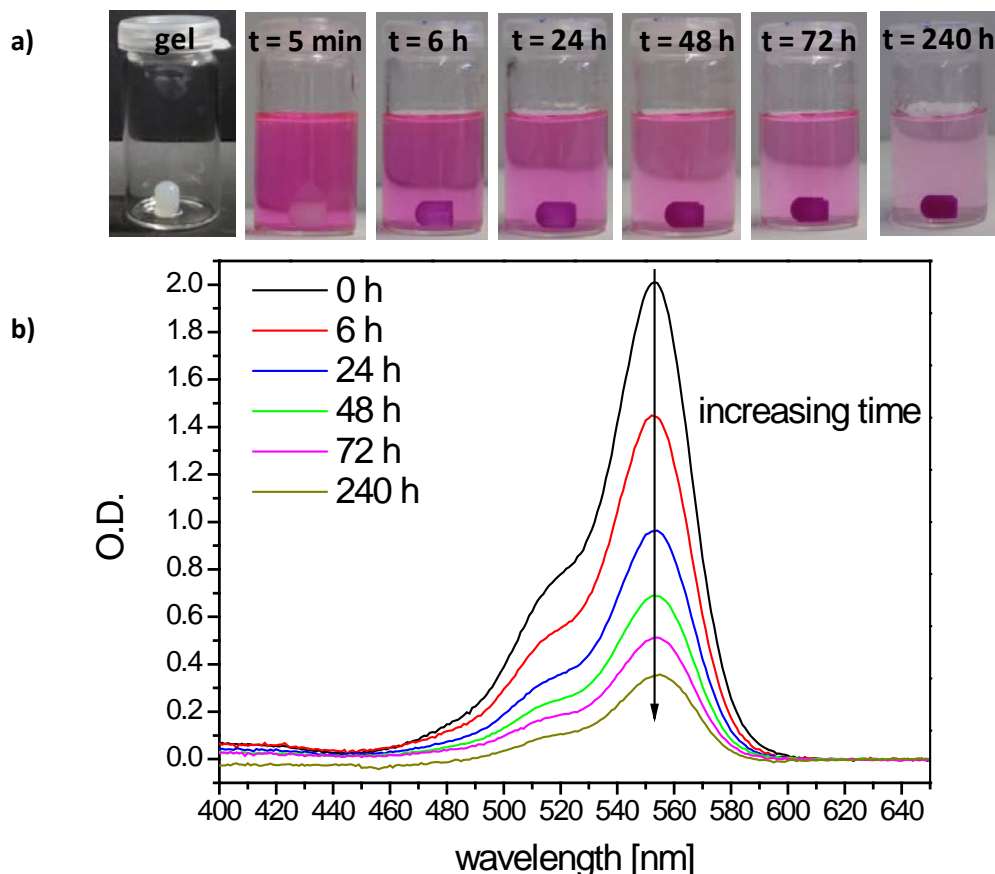


Figure 5.8: a) Optical images and b) absorption spectra of a rhodamine B solution with an initial dye concentration of 0.00907 g L^{-1} after the addition of a washed gel sample ($c(\mathbf{4Na}) = 10 \text{ g L}^{-1}$, $V = 0.12 \text{ mL}$).

With increasing time the optical density decreases in the supernatant solution. This is in accordance with the optically visible decolorization of the solution and the colorization of the gel sample. Besides this change of color no visible changes of the hydrogel appearance during the adsorption experiment, such as shrinkage or swelling behavior, were observed.

The concentration of rhodamine B in solution at distinct times t ($c(t) = [\text{g L}^{-1}]$) can be calculated by using the average value of the optical density at 553 nm at the time t ($\text{O.D.}_{553\text{nm}}(t)$) and the slope of the calibration curve:

$$c(t) = \frac{\text{O.D.}_{553\text{nm}}(t)}{223.1 \text{ Lg}^{-1}} \quad (5.2)$$

As the volume of the supernatant solution is known to be 5 mL , the amount of dye in solution in mg at time t can be calculated:

$$m_{\text{sol}}(t) = c(t) \cdot V_{\text{sol}} \quad (5.3)$$

The initial amount of dye in solution is known in mg ($m_{\text{sol}}(t_0)$) and mol ($n_{\text{sol}}(t_0)$). Thus, the amount of rhodamine B adsorbed into the gel at time t ($m_{\text{ads}}(t)$ and $n_{\text{ads}}(t)$) can be easily calculated using equation 5.4 and the molar mass of rhodamine B ($M = 479.02 \text{ g mol}^{-1}$).

$$m_{\text{ads}}(t) = m_{\text{sol}}(t_0) - m_{\text{sol}}(t) \quad (5.4)$$

The *adsorption capacity* at time t ($q_t = [\text{mg g}^{-1}]$) can be expressed as the amount of adsorbed dye in mg at time t ($m_{\text{ads}}(t)$) per gram of gelator **4Na** ($m(\mathbf{4Na})$) in the gel sample.

$$q_t = \frac{m_{\text{ads}}(t)}{m(\mathbf{4Na})} \quad (5.5)$$

The *decolorization efficiency* d_e can be given in percentage as ratio of the adsorbed mass of dye to the initial amount of dye present in solution. This value is especially interesting at the adsorption equilibrium for $t = t_e$:

$$d_e = \frac{m_{\text{ads}}(t_e)}{m_{\text{sol}}(t_0)} \quad (5.6)$$

Furthermore, the ratio of the molar amount of adsorbed dye at t ($n_{\text{ads}}(t)$) and the molar amount of compound **4** present in a gel sample ($n(\mathbf{4}$ in gel)) gives the molar ratio of adsorbed dye at t in eq..

5.2.1.4 Influence of mechanical agitation on the adsorption kinetics

It is known from the literature^{293,368} that mechanical agitation yields higher adsorption rates when the adsorption is a diffusion-controlled process. As in waste water treatment the adsorption or decolorization time plays a crucial role and high adsorption rates must be achieved, agitation of the sample might offer an advantage compared to static conditions. A preliminary test was performed with four washed hydrogel samples, each prepared from a solution of 10 g L^{-1} of the gelator sodium salt **4Na** at a volume of 0.10 mL.

Each of the four rhodamine B solutions had a volume of 5 mL and a concentration of 0.00756 g L^{-1} (0.05 eq. relative to the amount of 0.00157 mmol of **4** in the gel sample). While two samples were mechanically agitated using an orbital shaker at 200 rpm, the other two were left to stand without any disturbances. Absorbance spectra were recorded after 1 d, 2 d, 3 d, 4 d, and 7 d and the data were processed as described above to calculate the adsorption capacity q in mg g^{-1} . Figure 5.9 shows the adsorption curve in dependence of the time. The initial slope of the curve represents the adsorption rate. The steeper the curve evolves the faster the adsorption takes place. It can be clearly seen that the mechanical agitation of the hydrogels leads to a higher adsorption rate and faster adsorption compared to the undisturbed samples. This indicates that the adsorption of rhodamine B from solution into hydrogels of **4** is a diffusion-controlled process.²⁸⁸

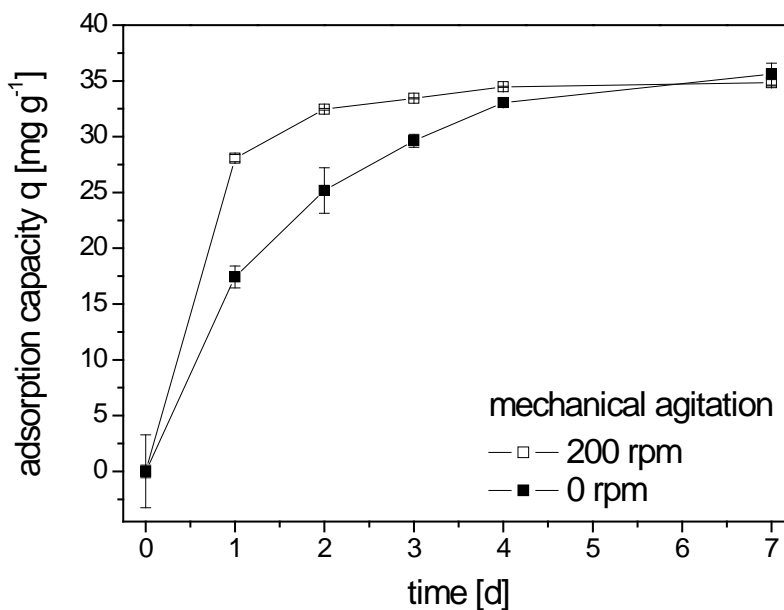


Figure 5.9: Absolute adsorption capacity q in mg of dye per g of **4Na** versus time for mechanical agitated (open squares) and undisturbed (filled square) rhodamine B solutions with an initial dye concentration of 0.00756 g L^{-1} (0.05 eq. , 37.8 mg g^{-1}) after addition of a washed hydrogel sample ($c(\mathbf{4Na}) = 10 \text{ g L}^{-1}$, $V = 0.10 \text{ mL}$).

Due to the enhanced adsorption rate, mechanically agitated samples reach the maximum plateau value after approximately three days, while undisturbed samples reach this value only after *ca.* seven days. This maximum adsorption capacity is also often described as the adsorption capacity in equilibrium. As it is the same for both experiments, it can be stated that agitation only influences the adsorption rate, but not the adsorption capacity (as long as the mechanical integrity of the hydrogel samples is assured).

As the deviation of the two mechanically agitated samples was much greater than for the undisturbed samples, further experiments in this study were carried out under static conditions. Furthermore, it became clear that for a quantitative analysis of the initial adsorption rate and to obtain reliable results with a high reproducibility, a higher resolution of the data points within the first 24 h is necessary. Thus, in the following study also data points within the first day were recorded. As already mentioned above, the removal of the gel samples prepared with a volume of 0.10 mL was quite difficult. Thus, all other tests were performed with gel samples prepared from 0.12 mL of **4Na** solution.

5.2.2 Time-dependent adsorption studies with different initial dye concentrations

To fully evaluate the adsorption potential of hydrogels of **4** regarding rhodamine B, a detailed time-dependent study using dye solutions with six different concentrations were performed. The received data sets were analyzed regarding the isothermal models from Langmuir and Freundlich, and the adsorption kinetics were investigated regarding the pseudo first and second order kinetic models.

5.2.2.1 Adsorption studies with different initial rhodamine B concentrations

The hydrogel samples were prepared, as described above with a concentration of **4Na** of 10 g L^{-1} and a volume of 0.12 mL, and washed three times prior to the experiments. The initial rhodamine B concentrations of the supernatant solutions are displayed in Table 5.1. They were chosen to achieve molar ratios of the dye in the supernatant solution to the gelator in the hydrogel of 0.005 eq. to 0.200 eq..

Table 5.1: Initial rhodamine B contents in the supernatant solutions for the concentration dependent adsorption studies.

| initial molar ratio dye/gelator ^a [eq.] | initial ratio of dye : gelator 4 molecules | initial dye concentration $c_{\text{sol}}(t_0)$ [g L^{-1}] |
|--|--|---|
| 0.200 | 1 : 5 | 0.03630 |
| 0.100 | 1 : 10 | 0.01815 |
| 0.050 | 1 : 20 | 0.00907 |
| 0.020 | 1 : 50 | 0.00363 |
| 0.010 | 1 : 100 | 0.00181 |
| 0.005 | 1 : 200 | 0.00091 |

^a: calculated from a gelator (**4Na**) concentration of 10 g L^{-1} at a gel volume of 0.12 mL and a volume of 5 mL of the supernatant solution, which are the usual testing conditions for the concentration dependent adsorption studies.

The rhodamine B solutions were prepared by a dilution series. For each concentration three individual experiments were performed to get an average value and the respective standard deviations of the adsorption capacity q and the decolorization efficiency d_e . The absorbance spectra were recorded 1 h, 3 h, 6 h, 24 h, 48 h, 72 h, and 240 h after the addition of the washed hydrogel samples to the dye solutions. The data were processed as described above to get the adsorption capacity q in mg of adsorbed dye to one gram of gelator **4Na** in dependence of the time (Figure 5.10).

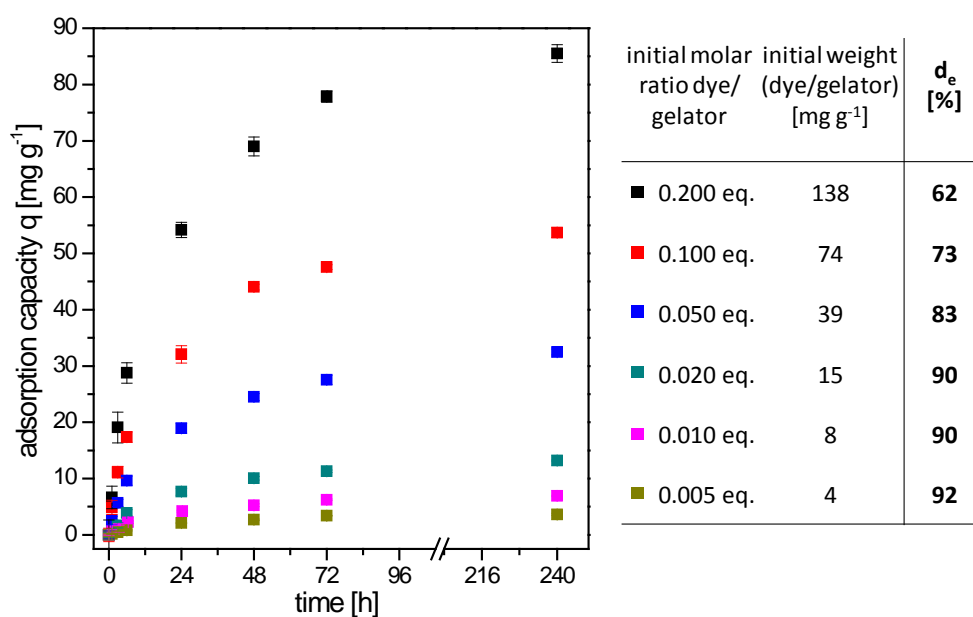


Figure 5.10: Adsorption capacity q in mg g^{-1} of hydrogels of **4** versus time and the decolorization efficiency at equilibrium d_e after 10 days.

With increasing time the adsorption capacity increases for all tested initial dye concentrations until a saturation value is reached after ten days. This saturation value is highly dependent on the initial concentration and gives the maximum adsorption capacity or adsorption capacity in equilibrium for a distinct initial dye concentration (Table 5.2).

Table 5.2: Adsorption capacities q_e and decolorization efficiencies d_e at the adsorption equilibrium (10 days after the addition of the hydrogel sample to solutions comprising different initial rhodamine B concentrations).

| initial molar ratio dye/gelator [eq.] | adsorption capacity q_e [mg g ⁻¹] | decolorization efficiency d_e [%] |
|---------------------------------------|---|-------------------------------------|
| 0.005 | 3.6 ± 0.2 | 92 |
| 0.010 | 6.9 ± 0.1 | 90 |
| 0.020 | 13.2 ± 0.1 | 90 |
| 0.050 | 32.5 ± 0.5 | 83 |
| 0.100 | 53.7 ± 0.9 | 73 |
| 0.200 | 85.5 ± 1.5 | 62 |

Below an initial rhodamine B concentration of 0.02 eq. at least 90 % of the dye is removed from the solution. This is especially interesting for the application of this hydrogel system in waste water treatment processes, as it is important to remove small amounts of a toxic dye efficiently and reliable even in dilute solutions. In this dilute concentration regime it seems that the adsorption capacity q after 10 days shows a linear dependency on the initial amount of dye, although more data points are necessary in this regime to proof this dependency (Table 5.2).

For the highest initial concentration of 0.20 eq. (138 mg g⁻¹) an adsorption capacity q_e of 85.5 mg g⁻¹ could be achieved, which correlates to a decolorization efficiency d_e of 62 % of the initial amount of dye. It should be noted that at or above an initial concentration of 0.05 eq. the relative amount of removed dye, which is given as the decolorization efficiency d_e , slowly decreases, while the amount of adsorbed dye and the adsorption capacity q_e still increases. This trend indicates that the adsorption capacity q_e might be further enhanced by using higher initial dye concentration. However, this will probably lead to lower decolorization efficiencies and thus a higher concentration of remaining dye in the supernatant solution at the end of the experiment. This is especially a disadvantage when the loading process is thought to be transferred to the adsorption of expensive drug molecules. Nevertheless, an adsorption capacity q_e of 85.5 mg g⁻¹ is extraordinary, as it correlates to a molar ratio of 0.113 eq.. This means that one dye molecule is bound by approximately nine gelator molecules. That is especially remarkable, as the observed fibers in the SEM images consist of multiple fibrils (Figure 3.25, chapter 3.3.2.3). As a result many gelator molecules are enclosed inside the fibers and are not in contact with the solution at all.

As the idea to use low molecular weight (lmw) hydrogels for the adsorption of toxic dyes is rather new, there exist only a few examples in the literature. And most of these deal with the adsorption of dyes onto native and dried hybrid hydrogels or metallo-xerogels (Table 5.3).^{25,83,123,124,275,287,292}

Thus, studies regarding the adsorption capacities for true lmw hydrogelators that solely consist of organic molecules are very rare. One example uses a slightly different adsorption concept as discussed here, as the dye crystal violet is completely removed from the water phase by addition of a toluene phase with subsequent gelation of the organic phase by change of pH and applying a temperature profile.⁷⁰ Due to this phase selective gelation the dye is transferred to the organic solvent and completely removed from the water. The dried hydrogel was able to remove 97 % of crystal violet from a 0.01 mM dye solution, which correlates to an adsorption capacity of about 6.3 mg g⁻¹.

Table 5.3: Overview of adsorption studies using lmw hydrogelators and different dye solutions and the respective reported and calculated¹ adsorption capacities q in mg g^{-1} .

| | hydrogelator based on | dye | adsorption capacity [mg g^{-1}] | reference | |
|--|--|---|--|-----------|-----|
| dried organic-inorganic hybrid hydrogels | terpyridine and Zn^{2+} , Cu^{2+} ions | basic blue 41 | 141.0 | 287 | |
| | | crystal violet | 115.7 | | |
| lmw xerogels | lithocholic acid and $\text{C}_{12}\text{DMAO}^{\text{a}}$ | bromocresol green | 86.9 | 123 | |
| | | crystal violet | 63.0 | | |
| | | naphtol blue black | 84.0 | | |
| | | pyrene | 2.8 | | |
| hybrid hydrogels | polydopamine-coated clay and Fe^{3+} | vitamin B12 | ~ 17 | 83 | |
| | | crystal violet | ~ 6.3 | | |
| | | crystal violet | ~ 6.3 | | |
| hybrid hydrogels | polydopamine-coated clay and Fe^{3+} | rhodamine 6G | ~ 150 | 124 | |
| | | safranin-T | 484.2 | | |
| | | brilliant cresyl blue | 494.2 | | |
| hybrid hydrogels | melamine and Ag(I) | rose Bengal | 18.6 | 275 | |
| | | eosin Y | 19.6 | | |
| | | methyl orange | 19.8 | | |
| organic lmw hydrogels | isophtalic acid bisaromates | methylene blue | ~ 450 ¹ | 288 | |
| | | methyl violet 2B | ~ 550 ¹ | | |
| | | pyrenemethylamine | ~ 240 ¹ | | |
| | C_2 -symmetric 1,4-diamide benzene | methylene blue | 40 - 50 | 289 | |
| | | hydrazide-functionalized dibenzylidene sorbitol | methylene blue (pH = 12) | ~ 820 | 290 |
| | N-terminally protected tripeptides | acid blue 25 (pH = 2) | acid blue 25 (pH = 2) | ~ 700 | 87 |
| | | | naphtol blue black (pH = 2) | ~ 1050 | |
| reactive blue 4 | | | 9.8 | | |
| litocholate with different monovalent cations (e. g. CsCl) | direct red 80 | direct red 80 | 10.6 | 291 | |
| | | rhodamine B | 7.4 | | |
| litocholate with different monovalent cations (e. g. CsCl) | rhodamine 6G | methylene blue | 1100 | 291 | |
| | | rhodamine 6G | 1350 | | |

^a C_{12}DMAO : dodecyldimethylamine oxide; ^b AAm: acrylamide, AMPSNa: 2-acrylamide-2-methylpropanesulfonic acid sodium salts.

¹ The marked adsorption capacities were calculated from the results given in the respective publications.

Rodriguez-Llansola *et al.* investigated the adsorption capacity of an isophthalic based bisaromatic hydrogelator regarding methylene blue, methyl violet 2B and pyrenemethylamine solutions.²⁸⁸ Under the used experimental conditions, efficiencies of 98 %, 97 % and 62 % could be achieved, respectively. From these efficiencies and the given experimental data, adsorption capacities of *approx.* 450 mg g⁻¹, 540 mg g⁻¹, and 240 mg g⁻¹, respectively, could be calculated. Interestingly, the adsorption capacity could be significantly enhanced to *ca.* 800 mg g⁻¹ for methylene blue and methyl violet 2B by forming the pH-sensitive gel in presence of the respective dye.

The most potent low molecular weight hydrogelator in terms of dye adsorption over a broad range of pH values was only found recently by Babatunde *et al.*²⁹⁰ Depending on the pH value of the solution either methylene blue, acid blue 25 or naphthol blue black was selectively adsorbed. At the optimum pH value up to 700 to 1050 mg g⁻¹ of respective dye could be removed from the solution due to strong dye-gelator interactions. This is in the range of a stoichiometric ratio between gelator and dye molecules.

Also interesting is the work of Adhikari *et al.* regarding the adsorption properties of N-terminally protected dipeptides, as in this study rhodamine B was used as model compound.⁸⁷ At an initial dye concentration of 0.479 g L⁻¹ only an adsorption capacity of 7.4 mg g⁻¹ could be achieved. With the hydrogel system **4**, that is investigated in the present study, at the highest tested initial rhodamine B concentration (0.200 eq., 0.03630 g L⁻¹) an adsorption capacity of 85.5 mg g⁻¹ could be realized, which is about 11 times higher than the reported value in the literature.

Summarizing, this comparison of adsorption capacities with other hydrogel systems reveals that the adsorption potential of hydrogels of **4** is sufficiently high for its use in waste water treatments. Nevertheless, other dyes that are common as dyeing agents in textile industry have to be tested regarding their adsorption onto preformed hydrogels of **4**. A promising indication that also other dyes might be adsorbed is the decolorization of a methylene red solution as proof of concept. Furthermore, Noah Al Nakeeb investigated the adsorption potential of hydrogels of **4** regarding aqueous iron salt solutions in his bachelor thesis.³⁶⁹ Unfortunately, the qualitative analysis of the iron ions in solution was challenging, as staining agents had to be used to enhance the optical density of the ions. Additionally, the oxidation states of the iron ions in the test samples seemed to change due to oxidation and reduction reactions with the gelator molecules. Therefore, no conclusive statement regarding the adsorption of iron ions could be drawn yet.

In the following, the adsorption data obtained from the concentration- and time-dependent rhodamine B studies will be processed and evaluated in detail regarding the adsorption isotherm models and adsorption kinetic models.

5.2.2.2 Isothermal models

For the mathematical representation of the adsorption process from a dye solution mainly two isothermal models are used: the Langmuir model and the Freundlich isotherm.^{25,271,276,286,370} Both models provide fits for the *equilibrium isotherm*, that describes the adsorption capacity in the equilibrium state q_e in dependence of the dye concentration at equilibrium C_e (Figure 5.11). As in this study the equilibrium state is reached after ten days, the corresponding data are used to calculate the isothermal models. To evaluate which model describes the adsorption of rhodamine B on hydrogels of **4** best, in the following both models are explained in more detail.

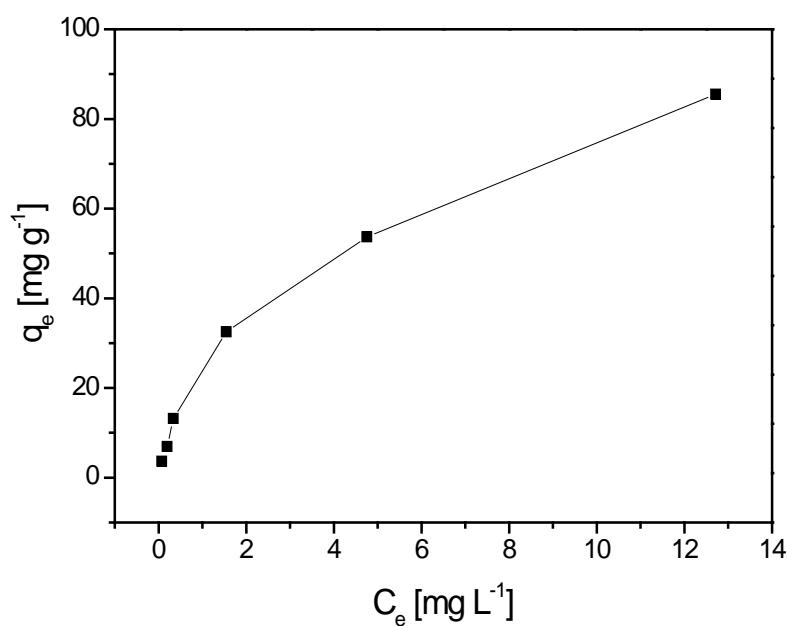


Figure 5.11: Equilibrium isotherm of the concentration dependent adsorption of rhodamine B onto hydrogels of **4** after 10 days (q_e : adsorption capacity at equilibrium; C_e : final equilibrium concentration).

Langmuir model

The Langmuir isothermal method is based on the assumption that the free energy of adsorption is independent of the surface coverage.³⁷⁰ From this assumption the following predictions can be made. For low concentrations there should be a linear dependence of adsorption and concentration, while for high concentrations a saturation of the surface with a monolayer is expected. Thus, if adsorption of rhodamine B onto hydrogels of **4** follows the Langmuir model, the curve in Figure 5.11 should show saturation for high concentrations. The

saturation effect occurs when the equilibrium constant q_e is equal to the Langmuir constant Q_L , which is related to the maximum adsorption capacity of the system. It should be noted that these assumptions are valid for high adsorbate concentrations near saturation. The Langmuir model can mathematically be expressed as:

$$\frac{C_e}{q_e} = \frac{1}{(Q_L \cdot b)} + \frac{1}{Q_L} \cdot C_e \quad (5.7)$$

with C_e being the final equilibrium concentration in [mg L^{-1}], q_e the adsorption capacity at equilibrium in [mg g^{-1}], Q_L the Langmuir constant of the adsorption capacity in [mg g^{-1}], and b the Langmuir constant related to the energy of adsorption in [L mg^{-1}].

By plotting the ratio of C_e/q_e versus the final equilibrium concentration C_e , the data points should show a linear correlation (Figure 5.12). The data for the adsorption of rhodamine B onto gels of **4** can be linearly fitted with a correlation coefficient r_L^2 of 0.9664.

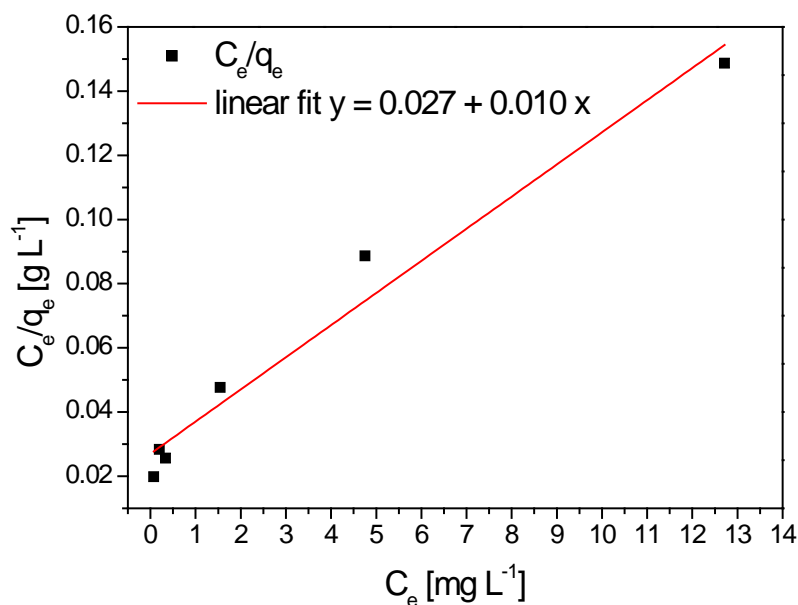


Figure 5.12: Langmuir isotherm for the adsorption of rhodamine B onto hydrogels of **4** (q_e : adsorption capacity at equilibrium; C_e : final equilibrium concentration).

From the slope of the linear fit the Langmuir constant regarding the maximum adsorption capacity Q_L can be calculated. The intercept, on the other hand, gives the Langmuir constant b related to the energy of adsorption (Table 5.4). The correlation factor of the fit r_L^2 shows that the adsorption data fit well to the Langmuir model.

Table 5.4: Characteristic Langmuir constants calculated from the linear fit of the Langmuir isotherm.

| constant | description | value |
|--------------------------------|--|--------|
| Q_L [mg g ⁻¹] | Langmuir constant related to the maximum adsorption capacity | 100 |
| b [L mg ⁻¹] | Langmuir constant related to the energy of adsorption | 0.370 |
| R_L | separation factor | 0.175 |
| r_L^2 | correlation factor of the linear fit | 0.9663 |

Using the Langmuir constant b and the highest initial dye concentration C_0 in [mg L⁻¹] the dimensionless separation factor can be calculated:

$$R_L = \frac{1}{1 + b \cdot C_0} \quad (5.8)$$

This separation factor gives some information about the type of adsorption (Table 5.5).²⁵ With the separation factor being 0.175, adsorption of rhodamine B onto hydrogels of **4** is favorable and nearly irreversible.

Table 5.5: The separation factor R_L .

| separation factor R_L | type of adsorption |
|-------------------------|--------------------|
| $R_L > 1$ | unfavorable |
| $R_L = 1$ | linear |
| $0 < R_L < 1$ | favorable |
| $R_L = 0$ | irreversible |

This means that there are strong interactions between the dye and the gelator molecules and it might be expected that practically no adsorbed dye molecules will be released by a washing procedure with desalted water.¹

¹ The removal of the dye into desalted water from gels loaded with dye by adsorption is investigated in chapter 5.2.3 in dependence of the applied temperature.

Freundlich model

The Freundlich model was developed as an empirical relationship and is based on the assumption that the probability of the adsorption energy of a bond lying between ΔG and $\Delta G + d \Delta G$ is proportional to the exponent of $(- \Delta G/RT)$. This means that the adsorbent, which is the hydrogel in this study, has different adsorption sites with several adsorption energies.^{271,370} From this assumption several predictions can be made. The most important one is that the surface can be infinitely covered with guest molecules. Thus, if adsorption follows the Freundlich model, the equilibrium isotherm presented in Figure 5.11 should show an increase of the adsorption capacity q_e with increasing final equilibrium concentration C_e without a saturation effect.

The following equation gives the mathematical expression of the Freundlich isotherm:

$$\log(q_e) = \log(K_F) + \frac{1}{n_F} \cdot \log(C_e) \quad (5.9)$$

with q_e being the adsorption capacity at equilibrium in [mg g^{-1}], C_e the final equilibrium concentration in [mg L^{-1}], K_F the Freundlich constant in [$\text{mg}^{1-1/n} \text{g}^{-1} \text{L}^{-1/n}$] related to the capacity of adsorption, and n_F the Freundlich constant related to the adsorption intensity.

It is important to note that with n_F equal to one the Freundlich isotherm is mathematically equivalent to the Langmuir isotherm. While for $n_F < 1$ the bond energy increases with increasing surface density, for $n_F > 1$ the bond energy decreases with increasing surface density. The latter case is the most common one and expresses that there is a decreasing *adsorbent-adsorbate* (hydrogel-adsorbed dye) interaction with increasing surface density. This model was found to be only valid for low concentrations and to be erratic at high concentrations or near saturation.

By plotting the logarithm of q_e versus the logarithm of the final equilibrium concentration C_e there should be a linear correlation of the data points, if the Freundlich isotherm is valid (Figure 5.13). The slope is equal to the inverse Freundlich constant n_F , while the Freundlich constant related to the adsorption capacity K_F can be calculated from the intercept.

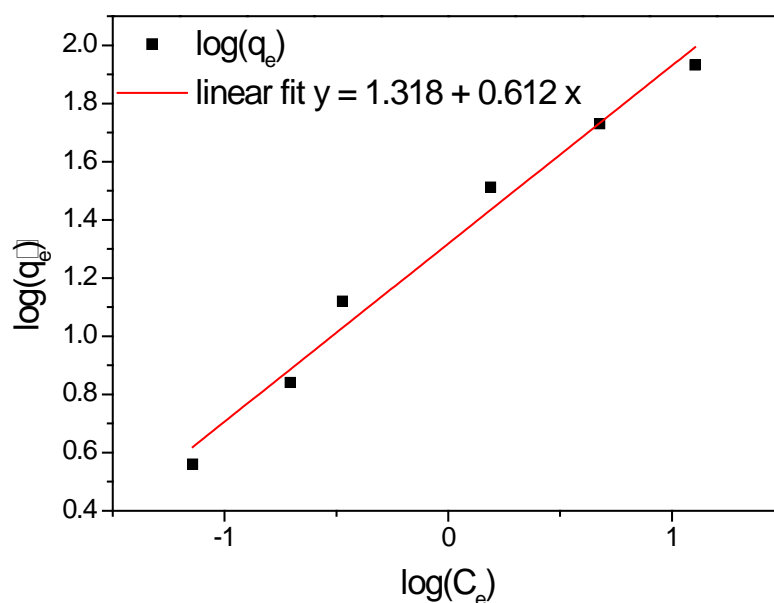


Figure 5.13: Freundlich isotherm for the adsorption of rhodamine B on hydrogels of **4** (q_e : adsorption capacity at equilibrium; C_e : final equilibrium concentration).

The adsorption data could be fitted very well according to the Freundlich model with a correlation coefficient r_F^2 of the linear fit of 0.9793. The Freundlich constants K_F and n_F were calculated and are depicted in Table 5.6.

These data show that the Freundlich isothermal model also fits the adsorption data obtained from the concentration-dependent adsorption studies. The Freundlich constant n_F is higher than one. This indicates that with increasing surface density the adsorbent-adsorbate interactions decrease.

Table 5.6: Characteristic Freundlich constants calculated from the linear fit of the Freundlich isotherm.

| constant | description | value |
|--|---|--------|
| K_F [$\text{mg}^{1-1/n} \text{g}^{-1} \text{L}^{-1/n}$] | Freundlich constant related to the adsorption capacity | 21 |
| n_F | Freundlich constant related to the adsorption intensity | 1.6 |
| r_F^2 | correlation factor of the linear fit | 0.9793 |

Comparison of both isothermal models

Summarizing, the adsorption data fit both the Langmuir and the Freundlich isothermal model. The maximum adsorption capacity calculated with the Langmuir model ($Q_L = 100 \text{ mg g}^{-1}$)

should be handled with care, as the Langmuir model is based on the assumption that a saturation can be observed for high concentrations. This, however, is not true for the Freundlich isotherm. Nevertheless, it can be stated that the adsorption of rhodamine B from solution onto hydrogels of **4** is favorable, but that the adsorbent-adsorbate interactions decrease with increasing surface density. Therefore, a less favorable adsorption is expected for high concentrations.

5.2.2.3 Adsorption kinetics

The investigation of the adsorption kinetics is important, as the kinetics determines the uptake rate of the dissolved guest molecule. Therefore, it influences the residence time that is required for the completion of the adsorption reaction. If a suitable model is found for the adsorption kinetics, it furthermore can help to predict the equilibrium adsorption capacity for not-tested initial concentrations. Therefore a good understanding of the kinetics is important for applications, such as waste water treatment and adsorption and delivery of drug molecules.

The different kinetic models are either adsorption reaction models (based on chemical reaction kinetics) or adsorption diffusion models (based on diffusion kinetics).³⁷¹ The two most used models to describe liquid-solid adsorption are based on adsorption reaction models and will be presented in more detail in the following: the pseudo 1st order and the pseudo 2nd order model.³⁷² When dealing with pseudo kinetic models the reaction rate is calculated on basis of the adsorption capacity, while “real” or non-pseudo kinetics are based on the concentration of the solution.

Pseudo first order kinetics

The pseudo 1st order kinetic model or Lagergren-plot was the first pseudo kinetic model that has been developed.³⁷³ The model can be mathematically expressed in a linear form as shown in the following equation:

$$\log(q_e - q_t) = \log(q_e) - \frac{K'}{2.303} \cdot t \quad (5.10)$$

with q_e being the equilibrium adsorption capacity in [mg g^{-1}], q_t the adsorption capacity at time t in [mg g^{-1}], K' the rate constant for pseudo 1st order adsorption in [h^{-1}], and t the time in hours [h]. The boundary conditions for this equation are $t = 0$ to $t = t_e$ and $q_t = 0$ to $q_t = q_e$.

This linearized pseudo 1st order equation clearly shows that the equilibrium adsorption capacity q_e must be known before the equation can be solved. The equilibrium adsorption capacity can either be extrapolated from experimental data for t versus infinite, or be evaluated by a trial and error process.²⁸⁵ For the adsorption study shown here the equilibrium adsorption capacity was chosen to be equal to the adsorption capacity after ten days, as at this

time the equilibrium state should have been reached. When the analyzed data are not measured at the equilibrium, the pseudo 1st order kinetic model fails, as many examples in the literature show.³⁷² Furthermore, it has to be noted that the pseudo 1st order model is not valid for the whole range of adsorption. As the reaction rate changes with time, there is no linear dependence of the adsorption capacity on the reaction time during the whole adsorption process. Therefore, the model is limited to intervals of the reaction time. The data presented here are limited to the first 72 h of the experiment, as with increasing time adsorption becomes less favorable and is thus slower. The chosen limitation of the experimental data might lead to an underestimation of the calculated adsorption capacities in equilibrium q_{e1} , even when the data can be fitted linearly with a high correlation coefficient r_1^2 . The graphical presentation of the pseudo 1st order kinetic model of the time-dependent adsorption of rhodamine B onto hydrogels of **4** is shown in Figure 5.14.

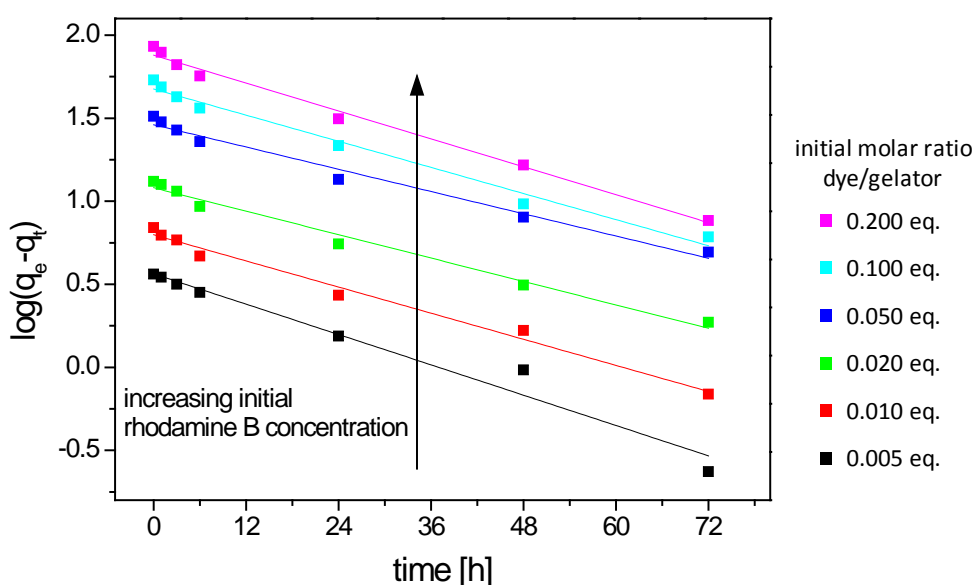


Figure 5.14: Plot of the pseudo 1st order kinetic data for the first 72 h of the adsorption experiment with increasing initial rhodamine B concentrations.

From the slope of the curves the rate constant K' can be derived. The intercept gives the calculated value for the adsorption capacity in equilibrium q_{e1} . The results of all six initial rhodamine B concentrations with the correlation coefficient of the linear fit r_1^2 are given in Table 5.7. The high correlation coefficient for all tested dye concentrations (r_1^2 close to one) shows that a linear fit of the data is reasonable. The average value of all six calculated rate constants K' is $0.030 \pm 0.003 \text{ h}^{-1}$. The small value of the standard deviation clearly shows that the adsorption rates are in the same range for all six different initial rhodamine B concentrations. This indicates that the kinetics of the adsorption process is independent of the

amount of dye in solution. Unfortunately, the calculated q_{e1} values underestimate the experimental data, especially for high initial rhodamine B concentrations. Thus, the pseudo 1st order kinetic model is not suitable to describe the data set obtained by the adsorption study of rhodamine B from aqueous solutions onto hydrogels of **4**.

Table 5.7: Results of the pseudo 1st order kinetic model with the rate constant for adsorption K' , the calculated value for the adsorption capacity at equilibrium q_{e1} , and the correlation coefficient of the linear fit r_1^2 in dependence on the initial molar ratio of dye to gelator. For comparison reasons the absolute adsorption capacities derived from the adsorption experiments after ten days q_e are additionally displayed.

| initial molar ratio dye/gelator [eq.] | K' [h ⁻¹] | q_{e1} [mg g ⁻¹] | r_1^2 | q_e [mg g ⁻¹] ^a |
|--|----------------------------|-----------------------------------|---------|---|
| 0.200 | 0.032 | 75.9 | 0.9895 | 85.5 ± 1.5 |
| 0.100 | 0.030 | 47.4 | 0.9819 | 53.7 ± 0.9 |
| 0.050 | 0.026 | 28.9 | 0.9798 | 32.5 ± 0.5 |
| 0.020 | 0.027 | 12.1 | 0.9828 | 13.2 ± 0.1 |
| 0.010 | 0.030 | 6.3 | 0.9855 | 6.9 ± 0.1 |
| 0.005 | 0.035 | 3.7 | 0.9649 | 3.6 ± 0.2 |

^a experimental results from chapter 5.2.2.1, table 5.2.

Pseudo second order kinetics

For the pseudo 2nd order kinetic model no parameters must be known beforehand. Thus, good results can be obtained for many different applications.³⁷¹ The model is based on the assumption that chemical adsorption is the rate limiting step and that adsorption can occur onto two different adsorption sites at the surface. It might be envisioned that one of these adsorption sites is a carboxylic acid group of the gelator **4** at the surface of the hydrogel fibers (type I), while the second type of adsorption site (type II) might be another rhodamine B molecule that is already bound to the gel *via* a type I adsorption site. As the mathematical description of this situation is very complex, the differential equation of the pseudo 2nd order kinetic model can be solved by five different linearized forms.²⁷⁸ The most used type of linearization was firstly presented by Ho (see equation 5.11).^{278,284,372}

$$\frac{t}{q_t} = \frac{1}{K'' \cdot q_{e2}^2} + \frac{1}{q_{e2}} \cdot t \quad (5.11)$$

with t being the time in [h], q_t the adsorption capacity at time t in [mg g⁻¹], K'' the rate constant for pseudo 2nd order adsorption in [g mg⁻¹ h⁻¹], and q_{e2} the calculated adsorption capacity from the pseudo 2nd order model in [mg g⁻¹].

The initial adsorption rate h for $q_t/t \rightarrow 0$ in $[\text{mg g}^{-1} \text{h}^{-1}]$ can be calculated using equation 5.12.

$$h = K'' \cdot q_{e2}^2 \quad (5.12)$$

This linearized form was used to investigate the kinetic data obtained in the study presented here, as in the literature it has been proved to give reliable predictions for the calculated adsorption capacities q_{e2} ,²⁷⁸ to be independent of the underlying adsorption mechanism,³⁷⁴ to be usually valid for the whole range of the adsorption kinetics,³⁷² and to be suitable for many different adsorption systems, such as activated carbon, brown seaweed, wood, peat, and hydrogel-clay nanocomposites.^{25,278,284–286,372} The graphical presentation of equation 5.11 for the different initial rhodamine B concentrations is presented in Figure 5.15.

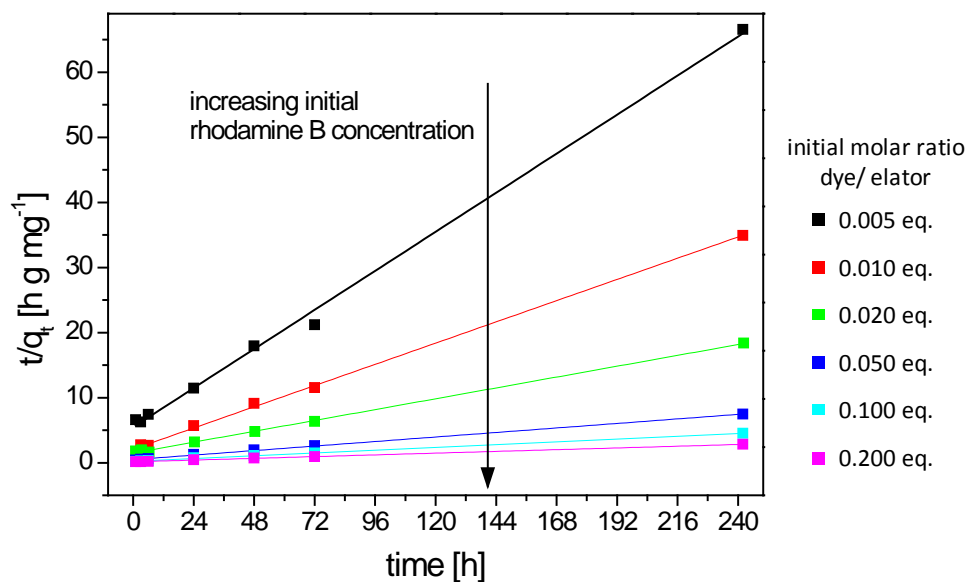


Figure 5.15: Plot of the pseudo 2nd order kinetic data of the adsorption experiment with increasing initial rhodamine B concentrations.

With increasing initial rhodamine B concentration the slope of the respective linear fit decreases and the value for the intercept increases. While the slope of the graphs gives the reciprocal calculated value for the adsorption capacity in equilibrium q_{e2} , the rate constant for the pseudo 2nd order model can be calculated using the intercept and the calculated value for q_{e2} . The reciprocal value of the intercept gives the respective initial adsorption rate h for the different initial rhodamine B concentrations. The characteristic values for the pseudo 2nd order model K'' , q_{e2} , h , and the correlation coefficients r_2^2 of the linear fits are given in Table 5.8 for the different initial rhodamine B concentrations.

As the correlation coefficient r_2^2 is close to one for all tested rhodamine B concentrations, the linear fit of the data according to the pseudo 2nd order kinetic model is reasonable. The

correlation coefficients are even higher than the correlation coefficients r_1^2 obtained from the fits of the pseudo 1st order model. The determined q_{e2} values slightly overestimate the experimental determined values in equilibrium. This deviation could be due to rounding errors and the linearization of the differential kinetic equation.

Table 5.8: Results of the pseudo 2nd order kinetic model with the rate constant for adsorption K'' , the calculated value for the adsorption capacity at equilibrium q_{e2} , the initial adsorption rate h , and the correlation coefficient of the linear fit r_2^2 in dependence of the initial molar ratio of dye to gelator. For comparison reasons the absolute adsorption capacities derived from the adsorption experiments after ten days q_e are additionally displayed.

| initial molar ratio dye/gelator [eq.] | K'' [g mg ⁻¹ h ⁻¹] | q_{e2} [mg g ⁻¹] | h [mg g ⁻¹ h ⁻¹] | r_2^2 | q_e [mg g ⁻¹] ^a |
|--|--|-----------------------------------|--|---------|---|
| 0.200 | 0.0008 | 90.1 | 6.9 | 0.9995 | 85.5 ± 1.5 |
| 0.100 | 0.0013 | 56.8 | 4.2 | 0.9991 | 53.7 ± 0.9 |
| 0.050 | 0.0017 | 34.5 | 2.1 | 0.9989 | 32.5 ± 0.5 |
| 0.020 | 0.0032 | 14.4 | 0.7 | 0.9987 | 13.2 ± 0.1 |
| 0.010 | 0.0089 | 7.4 | 0.5 | 0.9987 | 6.9 ± 0.1 |
| 0.005 | 0.0114 | 4.0 | 0.2 | 0.9970 | 3.6 ± 0.2 |

^a experimental results from chapter 5.2.2.1, table 5.2.

It is known from the literature that the adsorption rate of the pseudo 2nd order model K'' depends on the initial dye concentration.³⁷² An increase of the value for K'' with decreasing initial rhodamine B concentration is also observed for the data set presented here. In consequence, the initial adsorption rate h is also dependent on the initial dye concentration. Both adsorption rates are very slow compared to adsorption rates given in the literature, as their values are both given in dependence of the time in hours. In the literature the adsorption rates of the pseudo 1st as well as for the pseudo 2nd order model are usually given in minutes.^{278,279,284,285,372} This clearly shows that adsorption and hence loading of the gels of **4** with rhodamine B is very slow and needs rather days than hours or minutes. Thus, for the loading of the gels no “flow through” process, but only a “fixed bed” system can be used to achieve complete loading of the sample. Nevertheless, it has to be noted here that most of the adsorption takes place within the first 24 h. So if no equilibrium of adsorption is needed the loading of the gel with sufficient high amounts of rhodamine B can be achieved in 24 h or less.

Comparison of both pseudo kinetic models

At a first glance it seems that the pseudo 1st as well as the pseudo 2nd kinetic model can be applied, as the correlation coefficients of both are close to one. While the pseudo 1st order model underestimates the adsorption capacities in equilibrium especially for high initial

rhodamine B concentrations, the pseudo 2nd order model slightly overestimates them. However, the pseudo 2nd order fits the experimental data better than the pseudo 1st order model, as the correlation coefficients of the linear fits are closer to one and the calculated adsorption capacities in equilibrium describe the experimental values better than the pseudo 1st order model. The more favorable pseudo 2nd order kinetic model indicates that chemisorption, *i.e.* the adsorption step of the dye rhodamine B onto hydrogels of **4**, is the rate controlling step.^{25,371,372} Thus, the adsorption rate should be related to the number of adsorption sites on the surface of the hydrogel, while film diffusion and intraparticle diffusion processes should play a minor role.²⁵ Furthermore, a very stable complex between the rhodamine B and the gelator **4** should be formed. The adsorption rates K'' and h are dependent on the initial rhodamine B concentration and are in general very low. This slow adsorption indicates that during chemisorption, which is considered to be the rate limiting step, a stable dye-gelator complex is formed. Unfortunately, this hinders a fast and efficient loading of the gel of **4** with rhodamine B. As the interactions between adsorbent and adsorbate strongly influence the adsorption kinetics as well as the stability of the formed complex, these findings are only valid for adsorption of rhodamine B onto hydrogels of **4**, and not for other dyes or small molecules.

In the following, the stability of the rhodamine B-gelator complex formed during adsorption is investigated regarding the temperature of the surrounding accepting media. Furthermore, another loading method, *i.e.* gelation in the presence of the dye, and the subsequent release behavior of the dye is presented in detail in chapter 5.3.

5.2.3 Thermal stability of adsorbed dye-gel systems

To test the thermal stability of the dye-gelator complex after adsorption the release of rhodamine B in water at r. t. and 40 °C was investigated.

For these experiments hydrogel samples of **4** were prepared as described above, with 10 g L⁻¹ of gelator sodium salt **4Na**, 4 eq. of GdL in respect to the molar amount of **4Na** and a volume of 0.12 mL, and subsequently washed. Rhodamine B solutions with an initial concentration of 0.05 eq. in respect to the molar amount of gelator **4** in a gel sample were prepared by dilution of a stock solution. The washed gels were each put in 5 mL of the rhodamine B solution and left to stand at r. t. for 10 days. As already shown in Table 5.2 (chapter 5.2.2.1) the adsorption capacity and decolorization efficiency after 10 days were 32.5 mg g⁻¹ and 83 %, respectively.

Afterwards, each loaded gel sample was transferred to 5 mL of desalted water, respectively, and either left to stand at r. t. or 40 °C. Each experiment was performed in

triplicate to get an average value for the residual adsorbed amount of rhodamine B in the gel. The UV-Vis spectra measured at distinct times were treated as described above (chapter 5.2.1.3), to get the cumulative amount of released rhodamine B in dependence of the amount of the gelator (cumulative release in $[\text{mg g}^{-1}]$; Figure 5.16).

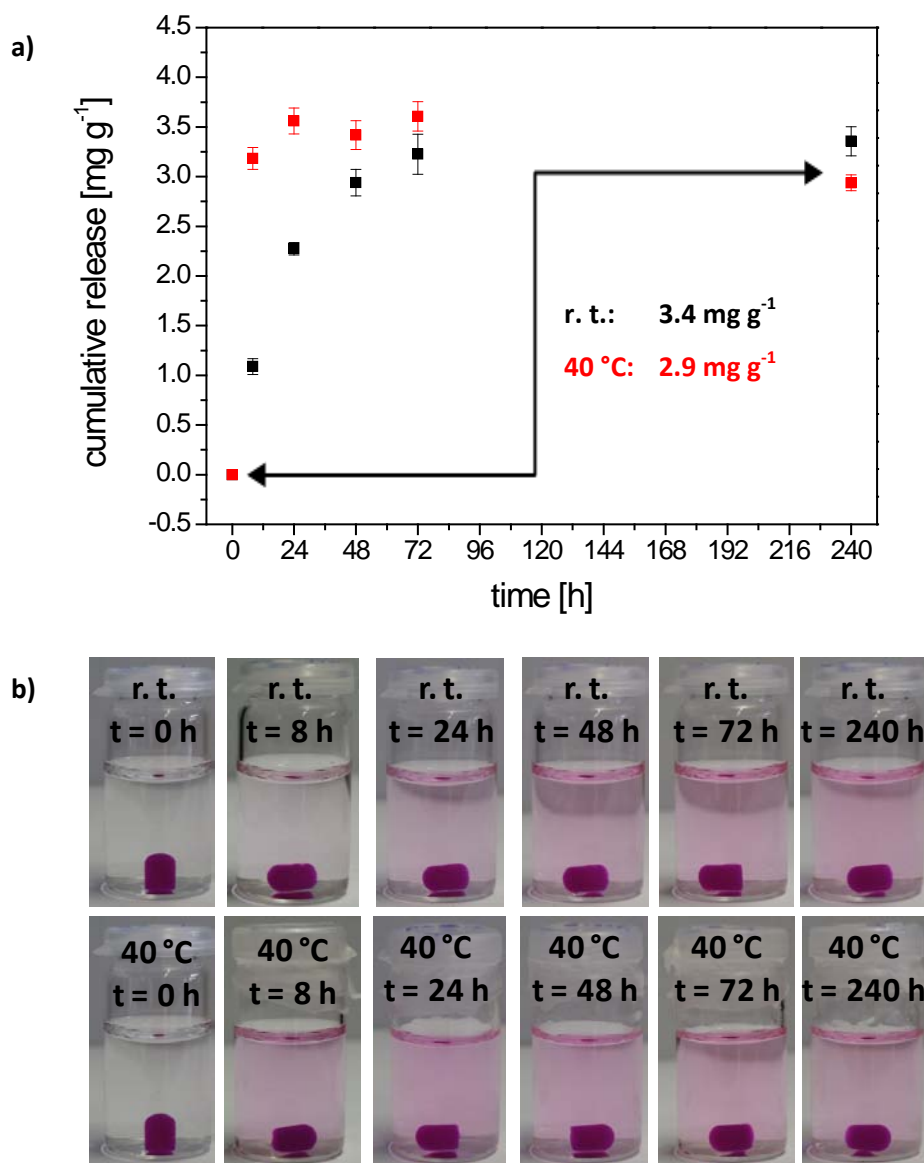


Figure 5.16: a) Cumulative release of rhodamine B from a hydrogel of **4** loaded by adsorption (initial dye concentration: 0.05 eq., adsorption time: 10 days) in water at r. t. (black squares) and at 40 °C (red squares); b) The optical images show the slight color increase of the accepting media with increasing time.

The cumulative release of rhodamine B versus the time can be described as the desorption curve and the initial slope represents the desorption rate. A qualitative analysis reveals that the dye is released much faster from gel samples stored at 40 °C compared to the samples at r. t.. While the data points for the experiment at 40 °C already reach a saturation value after

approximately 24 h, the control study at r. t. reaches a plateau only after 72 h. This indicates that desorption rates increase with increasing temperatures. The fluctuation of the values for samples stored at 40 °C is larger than the standard deviation of the average of the three samples that were measured. These fluctuations lead to values of the cumulative release that decrease and increase again. However, this should be impossible by using the above described experimental set up, where the removed solution for the UV-Vis measurements is put back to the sample afterwards. A possible explanation might lie in the fact that the samples were removed from the heated water bath for the spectroscopic investigation. Although the absorbance spectra should not be influenced by the temperature, the dye adsorption and desorption is an equilibrium reaction and therefore temperature-dependent. Thus, the exact temperature of the accepting media at which the sample for the UV-Vis measurement was taken might influence the results. Nevertheless, these fluctuations are still small compared to the total amount of released rhodamine B.

The experiments for both temperatures give saturation values for the cumulative release in the same range, about $3.4 \pm 0.1 \text{ mg g}^{-1}$ for the samples at r. t. and about $2.9 \pm 0.1 \text{ mg g}^{-1}$ for the samples at 40 °C. It has to be noted that at the end of the adsorption process the fluid phase of the gel also contains dissolved rhodamine B molecules. Thus, the concentration of dissolved dye in the gel at the beginning of this release experiment should be the same as the concentration of the supernatant solution in the adsorption process after 10 days. Using this consideration, the amount can be calculated. In relation to the amount of the gelator in the gel, it is about 0.15 mg g^{-1} . This is in the same order of magnitude as the standard deviation of the cumulative release and therefore can be neglected.

Remarkably, only 9 % or less of the initially adsorbed amount of rhodamine B are released, independent of the temperature of the accepting media. These results further support the thesis that during the adsorption process a very stable complex between the dye and the gelator is formed. The ability of the gel to form stable complexes with guest molecules even above body temperature is promising for controlled drug delivery applications. In the literature for adsorbed drug molecules often a “burst release” is described, which means that most of the loaded drug molecules are released within the first minutes of the experiment.³⁷⁵

Summarizing, it can be stated that the dye-gelator-complex formed during adsorption is very stable with over 90 % of the adsorbed dye remaining in the gel even at elevated temperatures. The release kinetics can be enhanced by increasing the temperature of the accepting media, while there is no influence on the cumulative released amount. Due to this stability of the dye-gel-system, the release of the adsorbed dye can probably only be triggered

by dissolution of the gel *via* change of the pH value. This might be interesting for the controlled release of adsorbed drugs in the gastrointestinal tract with its different pH values.

Altogether, hydrogels of **4** show a high adsorption potential even at low rhodamine B concentrations, and the formed host guest complexes are very stable regarding the release at different temperatures of the accepting media. To overcome the disadvantage of the slow adsorption within days, in the following, a study is presented that uses a different loading method, *i. e.* the *in situ* adsorption and encapsulation, accomplished by gel formation in the presence of the dye rhodamine B.

5.3 Hydrogel formation in the presence of rhodamine B with *in situ* adsorption

Although hydrogels of **4** exhibited a high adsorption potential towards the dye rhodamine B in the concentration- and time-dependent studies, the adsorption kinetics were very slow. Thus, the maximum adsorption capacity for the different tested concentrations was only reached after days. This time-consuming adsorption might be a disadvantage when trying to use this hydrogel system in controlled drug delivery applications. For industrial uses the loading of the gel should be achieved in a very simple and fast process with high loading capacities and a low excess of guest molecules.

A common loading approach of responsive supramolecular hydrogels is the hydrogel formation in presence of a specific guest molecule.^{70,80,115,116,129,241,288,305,306} Thus, the guest molecules are not only adsorbed at the surface of the gel, but can also be entrapped in smaller voids and pores of the gel or between gel fibers. This should lead to higher loading capacities compared to the adsorption capacities of preformed hydrogels. Moreover, the loading of the gel can be achieved as fast as the gelation of the gel.

In this chapter, the hydrogel formation of gels of **4** in presence of different amounts of the model compound rhodamine B is investigated. The loading capacities in dependence of the initial dye concentration were determined by studying the time-dependent release behavior of loaded gels in desalted water. The kinetic data were fitted in accord with the generalized Fickian diffusion model. Furthermore, the release behavior of gels, formed in the presence of dye, was determined in biologically relevant media, such as phosphate buffered saline (PBS), simulated body fluid (SBF), simulated gastric fluid (SGF), and simulated intestinal fluid (SIF).

these amounts were so small that they could not be weighed in without a massive experimental error, a dilution series of rhodamine B solutions with distinct concentrations was prepared. Please note that when preparing the gel samples, the respective rhodamine B solutions had higher concentrations (g L^{-1}) than the solutions used for the adsorption studies, although they have the same molar ratio of dye to gelator (eq.). This is due to the fact that for the supernatant solutions used in the adsorption studies the respective amount of rhodamine B was dissolved in 5 mL of desalted water, while in the release studies the same amount of rhodamine B was dissolved in 0.12 mL (the volume of one gel sample). Therefore, the concentrations of the solutions used to prepare the gels loaded with rhodamine B are much higher than the solutions with the same equivalents used for the adsorption experiments. The concentrations of the used rhodamine B solutions are given in Table 5.9.

Table 5.9: Concentrations of the rhodamine B solutions used for the preparation of hydrogels with encapsulated and *in situ* adsorbed dye for the release studies.

| initial molar ratio dye/gelator [eq.] ^a | c(dye) [g L ⁻¹] | initial weight dye/gelator [mg g ⁻¹] ^a |
|---|--------------------------------|--|
| 1.00 | 7.56207 | 756 |
| 0.50 | 3.78103 | 378 |
| 0.40 | 3.02483 | 302 |
| 0.30 | 2.26862 | 227 |
| 0.20 | 1.51241 | 151 |
| 0.10 | 0.75621 | 76 |
| 0.05 | 0.37810 | 38 |

^a assuming a gelator (**4Na**) concentration of 10 g L^{-1} at a gel volume of 0.12 mL, which are the usual testing conditions for the concentration dependent release studies.

To these aqueous dye solutions the gelator sodium salt **4Na** and glucono-delta-lactone (GdL) were added (Figure 5.18). All hydrogels were prepared with a concentration of 10 g L^{-1} of **4Na** and 4 eq. of GdL in respect to the molar amount of the gelator sodium salt. The dye solution with the gelator and GdL was then transferred to the wells of the PDMS-mold that were also used for the preparation of the hydrogels for the adsorption experiments (chapter 5.2.1.2).

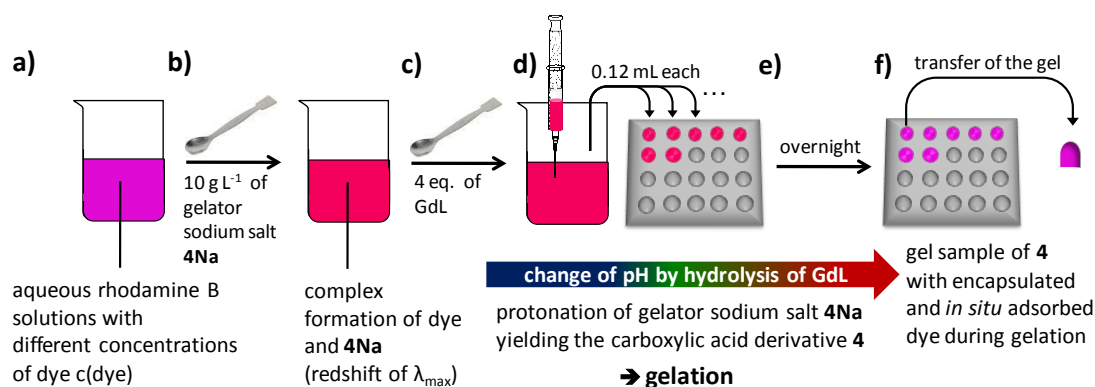


Figure 5.18: Preparation of defined gel samples in presence of rhodamine B as guest molecule: a) Preparation of solutions with different rhodamine B concentrations; b) Addition of the gelator sodium salt **4Na**, which resulted in a change of color of the solution; c) Addition of the glucono- δ -lactone (GdL) to decrease the pH value; d) Filling of the wells of the PDMS-mold with 0.12 mL of the dye solution with **4Na** and GdL; e) Gel formation overnight; f) Transfer of each hydrogel into 5 mL of the accepting media.

Each well was filled with 0.12 mL and left to stand at r. t. overnight. After the gel formation was completed the hydrogels were transferred into 5 mL of the accepting solution, respectively. In contrast to the gel samples prepared for the adsorption studies, no washing steps to remove the sodium gluconate were applied for hydrogels prepared in the presence of dye, as this procedure would already have initiated the release of rhodamine B. By using hydrogel samples, prepared as described above, with a constant volume and shape as well as a constant volume of the accepting solution of 5 mL, the surface to volume ratio is kept constant for all experiments. Thus, the influence of the initial rhodamine B concentration in the gel on the release of dye in desalted water and the influence of the type of the accepting media at a constant initial rhodamine B concentration can be investigated.¹

Interestingly, upon addition of the gelator sodium salt to the rhodamine B solutions, a change of color could be observed (Figure 5.19). This change of color corresponds to a red shift of the absorbance maximum from 553 nm without **4Na** to 558 nm with **4Na**.

¹ The findings of these experiments can be found in chapter 5.3.2 and chapter 5.5, respectively.

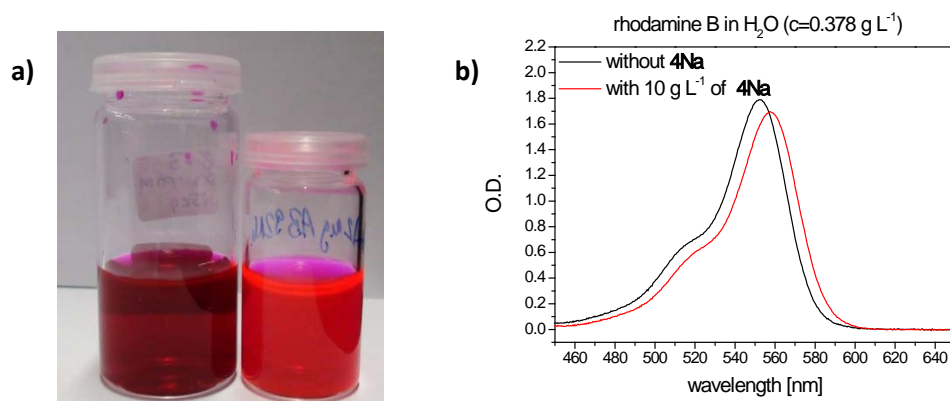
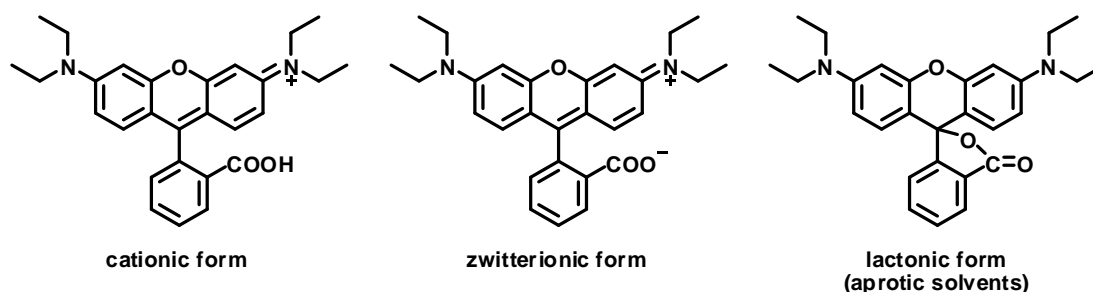


Figure 5.19: a) Rhodamine B solutions for the release studies with a concentration of 0.378 g L^{-1} (0.05 eq.). Left: without the gelator sodium salt **4Na**; and right: with a concentration of 10 g L^{-1} of **4Na**; b) Absorbance spectra of the rhodamine B solutions shown in a) without (black line) and with 10 g L^{-1} of **4Na** (red line).

It is known from the literature that the solvent plays a crucial role on the molecular structure of rhodamine B in solution and thus its absorbance spectrum. Not only the pH value of the solvent can change the conformation of the rhodamine B structure, but also the dye concentration as well as the viscosity, polarity, and polarizability of the solvent. Depending on these factors rhodamine B can adopt three different structures, a lactone form in aprotic solvents and a zwitterionic or a cationic form in protic solvents, such as water (Scheme 5.2).²⁷³



Scheme 5.2: Molecular structures of rhodamine B.

While the zwitterionic structure has its absorbance maximum at 552.5 nm , and is present in aqueous solutions with a pH value above 3.1 , the cationic form shows the highest optical density around 557 nm and is present below pH values of 3.1 .^{273,277} Due to the shift of the absorbance maxima upon addition of the gelator sodium salt **4Na** to the rhodamine B solution, it might be assumed that the structure of rhodamine B changes from the zwitterionic to the cationic form. As an aqueous gelator sodium solution itself is rather alkaline than acidic and has its pK_a value around 6.2 , it is not reasonable to assume that the structural change results from the pH value and the formation of a cationic structure of rhodamine B. It is therefore suspected that either the sodium ions act as a bridge between the carboxylates of the gelator

sodium salt **4Na** and the carboxylate moieties of the zwitterionic rhodamine B or more likely that the carboxylate groups of **4Na** interact with the positively charged amino moieties of the rhodamine B *via* electrostatic forces. Thus, the change of color and the red shift in the adsorption spectra ought to be induced by a complex formation between **4Na** and rhodamine B and the electrostatic interactions between those two molecules. For the dye methylene blue a blue shift of the absorbance spectra was observed upon combined release with a tetrapeptide-based hydrogelator, which was also explained by strong interactions between the dye and the gelator resulting in complex formation.⁸⁰

Upon gelation, the color of the rhodamine B, that is encapsulated in the gels, changes back to its original color. Due to hydrolysis of the GdL and the formation of protons in the solution, the sodium carboxylate moieties of the gelator **4Na** get protonated below a pH value of 6.2 to form the gelator **4**. Thus, the complex between the gelator sodium salt **4Na** and the rhodamine B is destroyed as the salt **4Na** is changed to the uncharged molecule **4**. At complete hydrolysis of GdL a final pH of around 4 is reached in the gel. This pH value is still above the pK_a value of rhodamine B, so that no formation of the cationic species is observed. Thus, the rhodamine B molecules released from the gels in desalted water are still in their zwitterionic form and have an absorption maximum at 553 nm. Therefore, the calibration curve developed for the adsorption experiments is also valid for the concentration-dependent release studies into desalted water.

5.3.1.2 Influence of the rhodamine B concentration on gel formation

Although the complex formation of the sodium salt **4Na** with rhodamine B does not completely prevent the gel formation, the rhodamine B content in the solution influences the mechanical stability of the formed aggregates. A visual inspection of the gel samples suggested that with increasing rhodamine B content in the initial solution the mechanical stability decreases (Figure 5.20).



Figure 5.20: Optical images of gels prepared with 10 g L^{-1} of **4Na** and 4 eq. of GdL in presence of different amount of rhodamine B after 8 days in desalted water.

Stable gels are formed in the presence of rhodamine B, only if the initial dye concentration is 0.50 eq. ($c = 3.78103 \text{ g L}^{-1}$) or lower. This correlates to a molecular ratio of one dye molecule to two gelator molecules. Above an initial dye concentration of 0.50 eq. the formed gels are either destroyed at the attempt to remove them from the wells (0.60 eq.) or no gel formation occurs but only the formation of a red precipitate (0.80 eq. and 1.0 eq.).

This influence of the initial rhodamine B concentration on the mechanical stability of the gel samples indicates that strong non-covalent interactions, such as π - π -stacking between the aromatic moieties and hydrogen bonding between the carboxylic acid moieties, are present between the gelator **4** and the dye. The change of mechanical stability upon encapsulation of guest molecules during gelation is known in the literature. It was suggested that the guest molecules act as impurities within the fibrillar structures that can either enhance or weaken the supramolecular interactions between the gelator molecules.^{116,305} This leads to the conclusion that rhodamine B molecules are not only adsorbed on the surface of the fibers, but are also incorporated in between fibers and in the columnar stacks formed by the gelator.

Due to the instability of hydrogels formed in the presence of rhodamine B concentrations higher than 0.50 eq. ($c = 3.78103 \text{ g L}^{-1}$), release studies were performed with hydrogels loaded with 0.05 eq. 0.10 eq. 0.20 eq., 0.30 eq., 0.40 eq., and 0.50 eq. of rhodamine B.

5.3.1.3 Experimental concept and calculations

The hydrogels formed in the presence of different amounts of rhodamine B were put in 5 mL of desalted water each and absorption spectra of the accepting solutions were recorded after 1.5 h, 3 h, 6 h, 24 h, 48 h, 72 h, and 240 h. The spectra were processed similar to the data obtained from the adsorption studies and the average maximum intensity at 553 nm of three individually performed experiments was calculated. Using the calibration curve developed in chapter 5.2.1.1, the rhodamine B concentration of the accepting solution in g L^{-1} at time t ($c_{\text{sol}}(t) = [\text{g L}^{-1}]$) can be obtained (equation 5.2, chapter 5.2.1.3). From this and from the fact that the volume of the accepting media is known to be 5 mL for all performed release experiments, the amount of rhodamine B in the solution in mg ($m_{\text{sol}}(t) = [\text{mg}]$) can be calculated (equation 5.3, chapter 5.2.1.3). The molar amount of rhodamine B in solution ($n_{\text{sol}}(t) = [\text{mol}]$) is consequently calculated by dividing the mass of rhodamine B in the supernatant solution by the molar mass of rhodamine B ($M = 479.02 \text{ g mol}^{-1}$).

In the literature the *cumulative release* at time t ($M_{\text{rel}}(t) = [\text{mg g}^{-1}]$) is usually given in mg of dye per gram of gelator. As the mass of the gelator sodium salt in one gel sample is known to be 1.2 mg the cumulative release at t ($M_{\text{rel}}(t) = [\text{mg g}^{-1}]$) can be calculated using equation 5.13.

$$M_{\text{rel}}(t) = \frac{m_{\text{sol}}(t)}{m_{\text{gel}}(4\text{Na})} \quad (5.13)$$

The initially encapsulated amount of rhodamine B ($m(t_0) = [\text{mg}]$) is known to be 0.4537 mg, 0.3630 mg, 0.2722 mg, 0.1815 mg, 0.0907 mg, and 0.0454 mg for 0.50 eq., 0.40 eq., 0.30 eq., 0.02 eq., 0.01 eq., and 0.05 eq., respectively.

Therefore, the encapsulated amount of rhodamine B at time t ($m_{\text{encaps}}(t) = [\text{mg}]$) can be calculated for a distinct initial dye concentration by equation 5.14. This amount gives the mass of rhodamine B that is still present in the gel after a certain time t .

$$m_{\text{encaps}}(t) = m(t_0) - m_{\text{sol}}(t) \quad (5.14)$$

For comparison purposes the *encapsulated amount of dye after a certain time t* is often expressed in mg of dye remaining encapsulated in the gel at time t per gram of gelator ($M_{\text{encaps}}(t) = [\text{mg g}^{-1}]$).

$$M_{\text{encaps}}(t) = \frac{m_{\text{encaps}}(t)}{m_{\text{gel}}(4\text{Na})} \quad (5.15)$$

The *loading efficiency $l(t)$* for a specific initial dye concentration in percent gives the relative amount of encapsulated dye at a time t in relation to the initially encapsulated amount $m(t_0)$. Often only the loading efficiency at the equilibrium state with $t = t_e$ is presented (l_e).

$$l_e = \frac{m_{\text{encaps}}(t_e)}{m(t_0)} \quad (5.16)$$

Similar concentration dependent release studies were performed in the bachelor thesis of Noah Al Nakeeb using high-performance liquid chromatography (HPLC) as analytical tool to detect the amount of rhodamine B present in the supernatant solutions.³⁶⁹ Although the analysis with HPLC is experimentally less elaborate, the method underestimates the released amounts of rhodamine B in solutions and is thus less sensitive at low rhodamine B concentrations than UV-Vis spectroscopy. Nevertheless, the obtained results showed the same trends as the results presented here.

5.3.2 Release of rhodamine B in water at $r. t.$

The release behavior of hydrogels of **4** prepared in the presence of six different rhodamine B concentrations was investigated dependent on the initial dye concentration and the time. The cumulative release as well as the loading efficiency after ten days was determined in dependence of the initial dye concentration and the generalized Fickian diffusion model was used to analyze the kinetic data. Furthermore, the subsequent release in water after the

equilibrium is reached after ten days is investigated by complete exchange of the accepting media.

5.3.2.1 Release behavior at different initial rhodamine B concentrations in water

The hydrogels prepared in presence of rhodamine B had a dye content of 0.50 eq. (378 mg g^{-1}), 0.40 eq. (302 mg g^{-1}), 0.30 eq. (227 mg g^{-1}), 0.20 eq. (151 mg g^{-1}), 0.10 eq. (76 mg g^{-1}), and 0.05 eq. (38 mg g^{-1}), respectively and were each put in 5 mL of desalted water as accepting media at r. t.. From the UV-Vis absorbance spectra of the supernatant solution the cumulative release was calculated as described above. The cumulative release for all six different concentrations is plotted versus the time in Figure 5.21.

Figure 5.21 clearly shows that for all concentrations the amount of rhodamine B in the solution increases with increasing time, showing a saturation effect after ten days. This indicates that at the end of the experiment the equilibrium of desorption is reached. Interestingly, the cumulative release after ten days is still very low compared to the initial amount of encapsulated dye. This means that most of the dye content is not released in desalted water, but is strongly bound to the gel fibers or encapsulated within the gel structure.

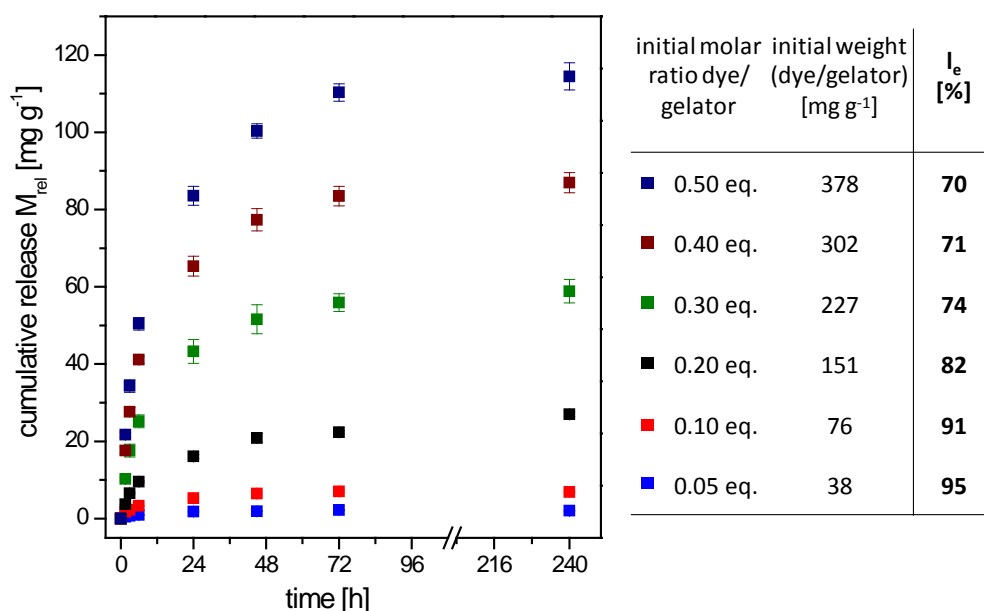


Figure 5.21: Cumulative release M_{rel} versus time of hydrogels loaded with different initial amounts of rhodamine B during gelation and the respective loading efficiency at equilibrium I_e after 10 days.

The data for the cumulative release, the encapsulated amount of dye, and the loading efficiency after 10 days (in equilibrium state) are given in Table 5.10.

Table 5.10: Cumulative release M_{rel} and encapsulated amount M_{encaps} of rhodamine B as well as the loading efficiency I_e at the desorption equilibrium (after 10 days in desalted water) of hydrogels of **4** loaded with different initial amounts of rhodamine B.

| initial molar ratio dye/gelator [eq.] ^a | initial weight (dye/gelator) [mg g ⁻¹] | cumulative release encapsulated amount loading efficiency | | |
|--|--|---|--|--------------|
| | | $M_{rel}(10\text{ d})$ [mg g ⁻¹] | $M_{encaps}(10\text{ d})$ [mg g ⁻¹] | I_e [%] |
| 0.50 | 378 | 114 ± 3 | 264 ± 3 | 70 |
| 0.40 | 302 | 87 ± 3 | 215 ± 3 | 71 |
| 0.30 | 227 | 59 ± 3 | 168 ± 3 | 74 |
| 0.20 | 151 | 27.0 ± 0.6 | 124.2 ± 0.6 | 82 |
| 0.10 | 76 | 6.8 ± 0.2 | 68.8 ± 0.2 | 91 |
| 0.05 | 38 | 2.0 ± 0.1 | 35.8 ± 0.1 | 95 |

^a calculated from a gelator (**4Na**) concentration of 10 g L⁻¹ at a gel volume of 0.12 mL, which are the usual testing conditions for the concentration dependent release studies.

As expected, the cumulative release of dye in equilibrium increases with increasing initial rhodamine B concentration. But also the encapsulated amounts increase, which means that by loading the gel through gel formation in the presence of rhodamine B a very high dye concentration can be reached in the gels even after washing them with desalted water. The loading efficiency gives the relative amount of dye remaining encapsulated in the gel. With increasing initial dye concentration the loading efficiency after ten days decreases. This means that, although the absolute encapsulated amount of dye after ten days increases with initial dye, it does not increase linearly. For small initial dye contents (< 0.10 eq.) over 90 % of the rhodamine B is still attached to the gel after ten days in desalted water. However, for the highest possible rhodamine B concentration in which stable gels could be formed, still 70 % of the initial dye is bound to the gel. Thus, only an excess of dye of 30 % is needed to get an encapsulated amount of 264 mg g⁻¹. This correlates to a molar ratio of dye and gelator of 0.35 eq. Thus, one dye molecule is bound by only three gelator molecules.

There are numerous examples in the literature where drug molecules, bioactive agents or model compounds are encapsulated in a hydrogel scaffold and the release behavior is investigated.^{for example see: 36,83,88,115–117,300,305,306} The most potent example is the encapsulation of around 800 mg g⁻¹ of the dye 1-pyrenemethylamine by a pH-sensitive tripeptide-based hydrogel. This dye concentration corresponds to a nearly equimolar ratio of dye and gelator. While most publications show a proof of principle of the encapsulation of guest molecules, only a few of these examples deal with the influence of the initial concentration of the guest molecule on the encapsulation and release behavior.^{116,305} Depending on the interactions between the guest and gelator molecules, with increasing guest molecule concentration the

released amount and the release rate can be either enhanced¹¹⁶ or decreased.³⁰⁵ Friggeri *et al.* already showed in 2004 that the release behavior of quinoline derivatives, that are interesting for their use as antimalarial and antileishmanial drugs, is mainly influenced by the interactions between the gelator and the entrapped molecules.¹¹⁵ In the study presented here, the rhodamine B molecules weaken the gel network, as they seem to interact strongly with the gelator molecules and disrupt the interactions between the gelator molecules.

The possibility to encapsulate guest molecules *via* a change of the pH value near neutral conditions is promising for the further use of thermo-labile bioactive molecules or enzymes. In the literature only a few pH-sensitive supramolecular hydrogelators have been proven to be able to encapsulate⁷⁰ and also release guest molecules in a controlled manner.^{88,306} Independent of the encapsulation method, many low molecular weight hydrogels release 50 % or more of the encapsulated molecules into water within the first hours of the experiment ("burst release").^{54,67,85,88,117,129} A peptide-based hydrogel with encapsulated vitamin B₆ and B₁₂ showed release rates in plain water that were determined by the size of the bioactive molecule and diffusion. Within the first three days 70 to 100 % of the respective vitamin were released.⁶⁷ A guanosine based hydrogel released 68 % of encapsulated rhodamine 6G even within the first hours in water.¹²⁹ Using supramolecular hydrogel capsules with a mechanical toughness similar to that of polymer gels, hydrophilic dyes, such as fluorescein and rhodamine 110 were released completely after 60 min, while only 33 % of the hydrophobic dye pyrene butyric acid were released.¹¹² A ferrocenoyl phenylalanine-based hydrogelator releases 60 % of the encapsulated model compounds methylene blue and rhodamine B within the first 12 h.⁵⁴

Summarizing, the release of only 5 to 30 % of the hydrophilic dye rhodamine B shown here is very rare and highly interesting as it corresponds to loading capacities of 70 to 95 % even after 10 days in water. The release behavior of a guest molecule can further be influenced by the degradation of the gel.^{37,38,76,79} Depending on the interactions between gelator and guest molecules the release might be faster than or as fast as gel degradation.¹¹⁵ The release behavior of hydrogels of **4** during gel degradation is addressed in chapter 5.5.

5.3.2.2 Release kinetics

In the literature there exist many different equations to describe the controlled release of a drug. About 50 years ago Higuchi described the release of a drug from a thin ointment film in the skin.³⁷⁶ Despite the complex situation and many assumptions that had to be made to describe the release conditions, the resulting equation was very simple. In combination with Fick's law of diffusion³⁷⁷ this equation could be further developed to fit the conditions of drug release from polymer films. Analogous to Higuchi, he described a one-dimensional drug transport mechanism and found proportionality between the cumulative released amount of

the drug and the square root of time ($t^{1/2}$). Because of their mathematical simplicity, the equations of Higuchi and Fick have been often misused to describe the release from polymers that show swelling or dissolving behavior. Thus, a generalized expression of the Fickian diffusion model was developed.^{28,378}

$$\frac{M_t}{M_e} = kt^n \quad (5.17)$$

where M_t is the amount of released dye at time t in [mg], M_e is the amount of released dye in [mg] in equilibrium state, t is the time in [h], k is the rate constant relating to the properties of the hydrogel matrix and the drug in [h^{-1}], and n is the dimensionless release exponent characterizing the transport mechanism.⁸⁵

In this study, the data after 10 days are considered to be the equilibrium data. Due to the boundary conditions, this equation is only valid for small times or for approximately the first 60 % of the total drug release.^{25,28,85,379} In the literature a peptide-saccharide based supramolecular hydrogel was used as carrier for controlled drug delivery that showed Fickian diffusion behavior in the first two hours of the experiments, but slower release thereafter.³⁶ It was assumed that the diffusion of drug molecules from deeper inside the gel medium needed more time for the release or that hydrophobic interactions between the drug and the gel matrix slowed the release after two hours. Therefore, it is important to choose a reasonable time range for the calculations performed according to the Fickian model.

The double logarithmic presentation of equation 5.17 should give a linear correlation between $\log(M_t/M_e)$ and $\log(t)$, as shown in Figure 5.22. As time range $t = 1.5$ h to $t = 24$ h was chosen. The intercept gives the logarithm of the rate constant k , while the slope gives the release exponent n . The initial dye concentration should not influence k or n , as the rates of diffusion-controlled release only depends on the solute concentration difference.¹¹⁶ The values for k and n as well as the correlation coefficients of the linear fits R^2 for all investigated initial rhodamine B concentrations are given in Table 5.11. Due to the scattering of the data points in the data sets for the different initial rhodamine B concentrations, the correlation coefficients R^2 differ between 0.9413 and 0.9901. Despite these deviations, the correlation coefficients are sufficiently high to state that the linear fits are reasonable.

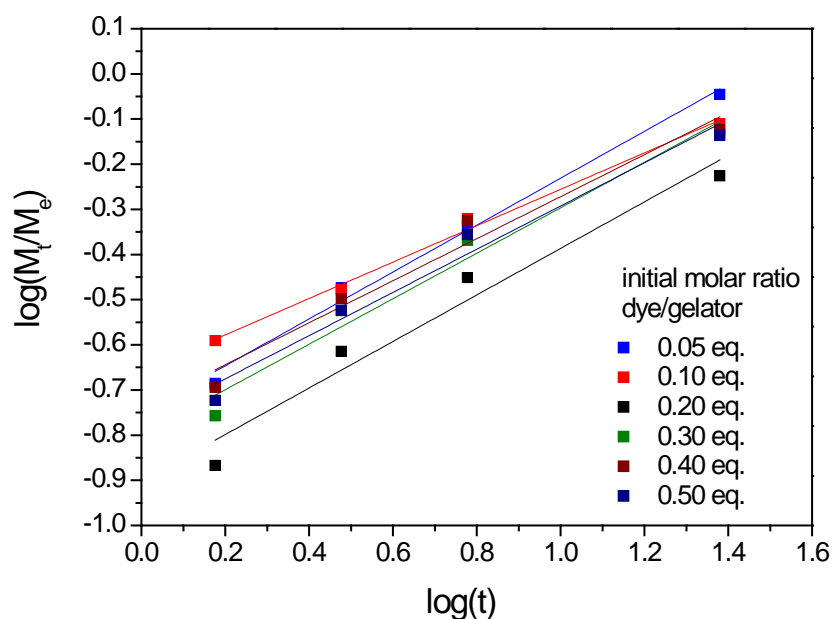


Figure 5.22: Double logarithmic presentation of the release kinetics of different amounts of encapsulated rhodamine B from hydrogels of **4** in accordance with the generalized Fickian diffusion model within the given time range of $t = 1.5$ h to $t = 24$ h.

Although the initial dye concentration should not influence the values for k and n , Table 5.11 shows that the value for the rate constant k and the release exponent n vary between 0.13 h^{-1} and 0.22 h^{-1} and 0.40 and 0.52 , respectively. Interestingly, the deviations of both constants are related, as the higher the k value, the lower the value for n . The average of both values gives $k = 0.17 \pm 0.03 \text{ h}^{-1}$ and $n = 0.48 \pm 0.04$.

Table 5.11: Release characteristics of encapsulated rhodamine B from hydrogels of **4** with different initial dye concentrations according to the generalized Fickian model.

| initial molar ratio dye/gelator [eq.] | $k \text{ [h}^{-1}\text{]}$ | n | R^2 |
|--|-----------------------------|------|--------|
| 0.50 | 0.17 | 0.48 | 0.9663 |
| 0.40 | 0.18 | 0.47 | 0.9567 |
| 0.30 | 0.16 | 0.50 | 0.9582 |
| 0.20 | 0.13 | 0.52 | 0.9413 |
| 0.10 | 0.22 | 0.40 | 0.9901 |
| 0.05 | 0.18 | 0.52 | 0.9879 |

As already mentioned above, most release studies with low molecular weight hydrogelators found an enhanced release of the encapsulated molecules within a few hours. Therefore, usually higher values for the rate constant k are reported and thus given in min^{-1} .^{25,28,36,85,88} The slow release of rhodamine B in case of hydrogels of **4** might be due to two different reasons. Either, it indicates that there is a strong interaction between the gelator and the dye molecules, or that hydrogels of **4** are composed of a dense 3D-network with small pores, so that the dye molecules that should be released from the network need to diffuse in a more zig-zag like way.¹¹⁶

The release exponent n gives information about the transport mechanism depending on the geometry of the used release matrix. For the polymer films described by Fick the transport is in accordance with the Fickian model, *i. e.* unhindered diffusion, if $n \leq 0.5$. It is anomalous or non-Fickian if $n > 0.5$, and if $n = 1$ it is a relaxation controlled transport (Case II). In the literature most release data of small guest molecules from supramolecular hydrogels are investigated by this classification.^{25,36,85,88,116} Peppas and co-workers transferred this principle of the transport mechanism to other matrix geometries, such as cylinders and spheres.^{28,378}

As the hydrogel samples used here are rather cylindrical than film-like or spherical, the following assignment for n is valid:

| | |
|---------------|---|
| $n \leq 0.45$ | Fickian diffusion |
| $n > 0.45$ | Anomalous or non-Fickian transport |
| $n = 0.85$ | Case II (relaxation controlled transport) |

With the average value and standard deviation of n being 0.48 ± 0.04 , it can be stated that the release of rhodamine B from hydrogels of **4** is in accordance with the Fickian model in the given time range for a cylindrical geometry. Thus, the release of the dye is purely diffusion controlled. In combination with the fact that the majority of the initial encapsulated amount of rhodamine B is still in the gel after ten days, this suggests that only the rhodamine B molecules that are dissolved in the aqueous phase of the gel and do not interact with the gel fibers are released.

5.3.2.3 Anew release in water after reaching the equilibrium state after ten days

As shown previously, the cumulative release of encapsulated rhodamine B from hydrogels of **4** reaches a saturation value after ten days in desalted water at r. t.. This saturation is considered to be the equilibrium state. To test if this release is due to dissolved dye molecules in the aqueous phase of the hydrogel that do not interact with the gel matrix or if also dye molecules that are adsorbed at the surface of the hydrogel are dissolved and released from the gel, the following experiment was carried out. Analogous to the previously performed release studies,

a hydrogel of **4** was prepared in the presence of 0.05 eq. (38 mg g^{-1}) of rhodamine B. This initial rhodamine B concentration was chosen exemplarily as it was also used to test the stability of the hydrogel loaded *via* adsorption (chapter 5.2.5). After monitoring the cumulative release at r. t. after 2 h, 4 h, 6 h, 24 h, 48 h, 72 h, and 240 h in desalted water (first release sequence), the accepting media was completely exchanged by 5 mL of fresh desalted water, and again the release behavior was monitored (second release sequence). The experiment was performed in triplicate to obtain an average value and a standard deviation for the cumulative release and the loading efficiency. The UV-Vis spectroscopic measurements and calculations were carried out as described above. The cumulative release in dependence of the time and optical images of a sample are presented in Figure 5.23.

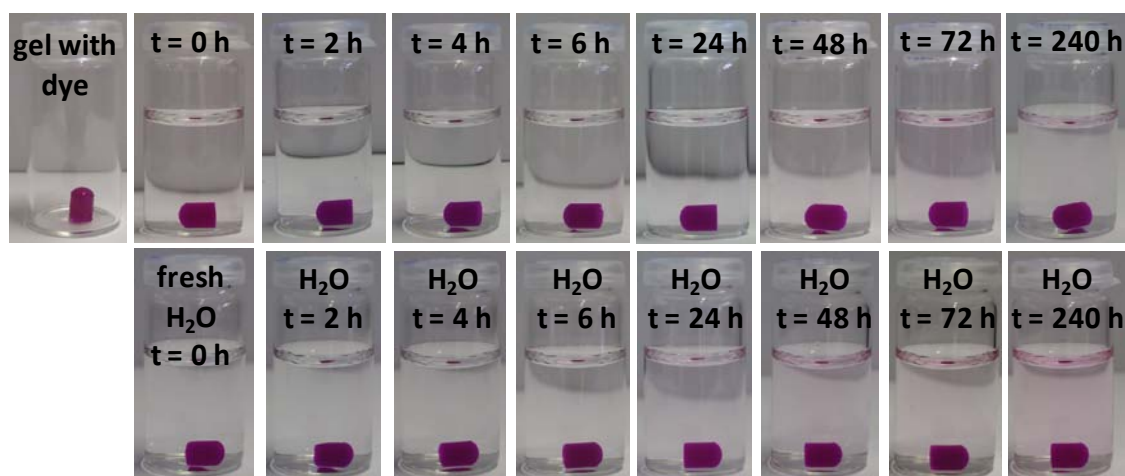
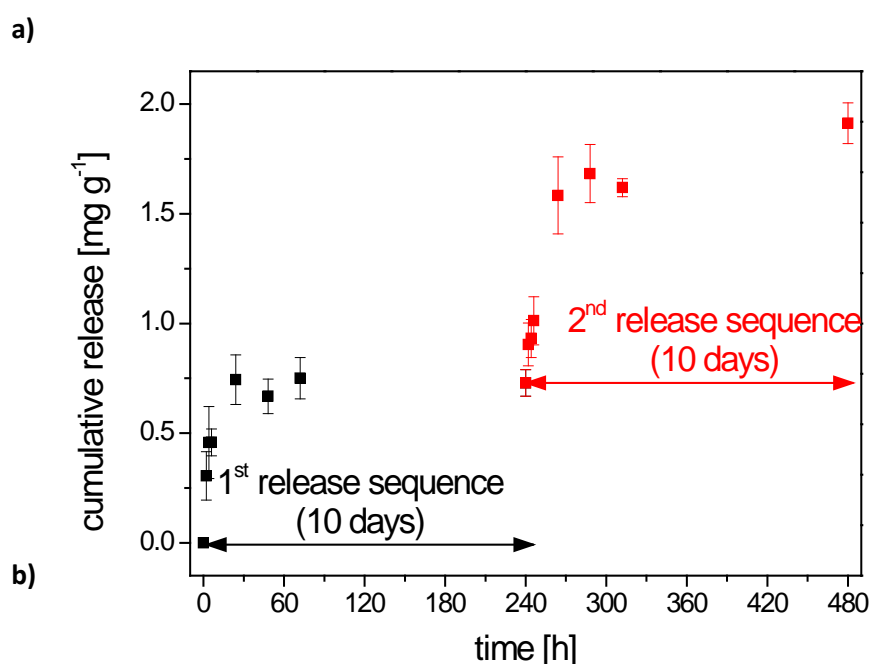


Figure 5.23: a) Cumulative release of a hydrogel of **4**, loaded with 0.05 eq. of rhodamine B during gelation, for 10 days in desalted water (black squares) and for another 10 days after complete exchange of the accepting media with fresh desalted water (red squares); b) optical images of the respective sample during the two release sequences.

By changing the accepting media after ten days an anew release can be observed. Due to the low absolute amounts of released dye (*ca.* $0.73 \pm 0.06 \text{ mg g}^{-1}$ within the first release sequence and *ca.* $1.18 \pm 0.10 \text{ mg g}^{-1}$ within the second release sequence) the fluctuations of the average values are very high, but they lie within the standard deviation of the average value. It has to be noted that dissolved rhodamine B molecules are present in the fluid phase of the gel after the first ten days. The concentration of dissolved dye in the gel at the beginning of the second sequence should be same as the concentration of the accepting solution after the first ten days. To derive its influence on the cumulative release of the second sequence, the amount is calculated in relation to the amount of the gelator in the gel. The obtained value is about 0.02 mg g^{-1} , which is negligible in comparison to the standard deviation of the cumulative release.

The overall release after 20 days is $1.9 \pm 0.1 \text{ mg g}^{-1}$. The cumulative releases correspond to loading capacities of 98 % and 95 % after the first and the second release sequence, respectively. In the concentration dependent study described in chapter 5.3.2.1 a loading efficiency of 95 % was determined already after the first 10 days. Thus, it must be assumed that the experimental fluctuations are higher than the standard deviation of three measurements. Nevertheless, it can be said that upon changing the accepting media, an anew release can be observed. As the influence of the dissolved dye molecules in the gel after ten days is negligible, it must be assumed that the release in the second release sequence is mainly due to desorption of dye molecules from the surface of the hydrogel. Consequently, the equilibrium of bound dye molecules can indeed be shifted in favor of the release due to change of the solvent. This might be interesting for flow-through systems where low but continuous release of a specific guest molecule is needed.

As already known from the adsorption studies the initial amount of 0.05 eq. of rhodamine B was adsorbed up to an adsorption capacity of 83 % (32.5 mg g^{-1}). Subsequent release in desalted water at r. t. gave a cumulative release of 3.4 mg g^{-1} (see chapter 5.2.2.1 and 5.2.3). This release was attributed to the sensitive balance of adsorption and desorption onto the hydrogel surface. For the hydrogel samples prepared in the presence of rhodamine B this equilibrium can also be observed. However, the overall cumulative release is still lower after 20 days than the released 3.4 mg g^{-1} of dye in ten days during the adsorption study. This is attributed to the fact that, when preparing the hydrogel in presence of the dye, the dye molecules are encapsulated in closed pores of the gel, between gel fibers, or maybe even be incorporated in columnar stacks formed by the BTA-based gelator.

This makes the loading method *via* hydrogel formation in presence of the dye very interesting, as not only high loading capacities can be achieved, but also very stable hydrogel-

rhodamine B systems are obtained. In the following chapter, a comparison of these results with the results from the adsorption studies is presented to evaluate the differences and advantages of each method.

5.4 Comparison of the different loading techniques

In the previous chapters the results of the adsorption and release studies regarding rhodamine B in desalted water at r. t. were discussed in detail. The advantages and disadvantages of both loading methods are pointed out in the following. For the investigation of the adsorption behavior preformed hydrogels with a volume of 0.12 mL and a gelator concentration of 10 g L^{-1} of **4Na** were stored for ten days in 5 mL of a rhodamine B solution with a distinct dye concentration, respectively (Figure 5.2, chapter 5.2.1). The decolorization efficiency d_e in percent gives the amount of adsorbed rhodamine B after 10 days in respect to the initial amount of dye, while the adsorption capacity q_e gives the amount of adsorbed dye after 10 days in mg per gram of gelator **4Na**. For the release studies hydrogels with a volume of 0.12 mL and a gelator concentration of 10 g L^{-1} of **4Na** were formed in presence of distinct amounts of rhodamine B (Figure 5.17, chapter 5.3.1). The loading efficiency l_e in percent gives the amount of still adsorbed and encapsulated dye after 10 days in respect to the initial amount of dye and is comparable to d_e from the adsorption studies. The amount of dye, that is still encapsulated in the gel after ten days ($M_{\text{encaps}}(10\text{d})$), is given in mg per gram of the gelator **4Na**. This value is comparable to the adsorption capacity q_e from the adsorption studies. The tested amounts of dye that were used for both experiments were initially 0.05 eq., 0.10 eq., and 0.20 eq. of rhodamine B. The results of both loading methods are compared in Table 5.12.

Table 5.12: Comparison of the results from the adsorption of rhodamine B onto preformed hydrogels of **4** after 10 days and the release of rhodamine B from hydrogels prepared in the presence of the dye after ten days. The initial molar ratio of dye to gelator were 0.20 eq., 0.10 eq., and 0.05 eq., respectively.

| initial molar ratio dye/gelator [eq.] | adsorption study | | | release study | | |
|--|---|--|---|------------------------------------|---|---|
| | decolorization efficiency d_e [%] | adsorption capacity q_e [mg g^{-1}] | ratio of dye : gelator 4 molecules after 10 d | loading efficiency l_e [%] | encapsulated amount $M_{\text{encaps}}(10 \text{ d})$ [mg g^{-1}] | ratio of dye : gelator 4 molecules after 10 d |
| 0.20 | 62 | 86 | 1 : 9 | 82 | 124 | 1 : 6 |
| 0.10 | 73 | 54 | 1 : 14 | 91 | 69 | 1 : 11 |
| 0.05 | 83 | 32 | 1 : 23 | 95 | 36 | 1 : 21 |

From this comparison it is obvious that despite the same initial molar ratio of dye to gelator, the decolorization efficiency d_e *via* adsorption is for all concentrations lower than the loading efficiency l_e obtained in the release experiments. Consequently, this trend is also observed for the adsorption capacity q_e and the encapsulated amount M_{encaps} , respectively. The molar ratio of dye to gelator after ten days shows that in case of the loading by forming the hydrogels in presence of rhodamine B, one dye molecule can be bound by less gelator molecules compared to preformed hydrogels that adsorb the dye.

From the adsorption studies it was derived that for low initial rhodamine B concentrations there is a linear dependence between the initial dye concentration and the adsorbed amount of dye after ten days, while for higher initial dye concentrations a saturation value is approached. As the adsorption data fit well both Langmuir and Freundlich isotherm model, it can be stated that the adsorption is favorable, but a maximum adsorption capacity of 100 mg g^{-1} was predicted due to decreasing dye-gelator interactions with increasing surface density. This clearly states that the adsorption capacity is limited, even when the initial dye concentration is significantly enhanced. Furthermore, the adsorption kinetics follows the pseudo 2nd order model for all tested initial concentrations with a low initial adsorption rate h and a very low adsorption rate K'' , which means adsorption is completed in the range of several days. Thus, an application in flow-through systems is probably not suitable, while the application in fixed-bed systems is interesting. The adsorption of rhodamine B with subsequent release in water at r. t. and 40°C showed that the desorption rate, but not the amount of maximum desorbed dye, is dependent on the temperature. The adsorbed rhodamine B molecules are thought to be bound strongly to the gel surface, as 90 % of the dye remains in the gel within ten days.

The hydrogels formed in presence of different amounts of initial rhodamine B can encapsulate high amounts of dye within the time of gelation, which is around 8 h. This is very fast compared to the time that the adsorption process needs for the loading of preformed hydrogels. Furthermore, a much higher loading can be achieved for the same amount of initial dye. This can be attributed to the incorporation of dye molecules in the gel network and not only on the hydrogel surface. The only limitation is the mechanical stability of the gels formed in presence of rhodamine B, as above an initial concentration of 0.5 eq. (378 mg g^{-1}) no self-supporting networks can be obtained. Nevertheless, this maximum encapsulated amount of 264 mg g^{-1} corresponds to a dye to gelator ratio of 1 : 3 with a loading efficiency of still 70 %.

In summary, hydrogels of **4** have a high adsorption potential regarding rhodamine B, even at very low dye concentrations. However, a higher absolute encapsulated amount of dye and higher loading efficiencies can be achieved in less time by forming hydrogels in the presence of

rhodamine B. Thus, further release studies in biologically relevant media were performed with hydrogels prepared in the presence of rhodamine B.

5.5 Release of *in situ* adsorbed rhodamine B in biologically relevant media

Gels of **4** might be interesting for the application in controlled drug delivery, as they are highly stable in different organic solvents as well as in aqueous sodium chloride solution or aqueous solutions with a pH value lower than 6.2 (chapter 3.3.3.4). Especially the pH-responsiveness might be promising for the oral administration of drugs. For the controlled drug release it is important to test the stability of loaded hydrogels in different biologically relevant media. As mentioned above, the hydrogel formation in presence of the model compound rhodamine B led to higher loading capacities in shorter time than hydrogels loaded *via* adsorption of the dye from solution. Hence, hydrogels prepared in presence of 0.05 eq. (37.8 mg g^{-1}) of rhodamine B were exemplarily used for the release studies in biologically relevant media.

In the literature only a few examples of supramolecular hydrogels are known that were loaded with a guest molecule to study its subsequent release in biologically relevant media. In these few examples mainly phosphate buffered saline (PBS) is used as the accepting media.^{3,36,305,306}

In the following a stability and release study of hydrogels of **4** formed in the presence of rhodamine B is presented in phosphate buffered saline (PBS) and simulated body fluid (SBF), both with a pH value of 7.4. Additionally, the stability and the release behavior is tested in fasted-state simulated gastric fluid (SGF) and fasted-state simulated intestinal fluid (SIF) at body temperature.

5.5.1 Release of rhodamine B upon dissolution in PBS (pH = 7.4) at r. t.

Phosphate buffered saline (PBS) is a salt solution with a pH value of 7.4, that consists of sodium chloride, potassium chloride, dibasic sodium phosphate (Na_2HPO_4), and monobasic potassium phosphate (KH_2PO_4). It is isotonic and non-toxic, and therefore used as a standard buffer in biochemistry to rinse cell cultures, to treat immobilized proteins or enzymes, or to conduct immuno-histochemical assays.^{79,380} Mixing PBS with hyaluronic acid yields simulated synovial fluid, which simulates joint fluid.²⁹⁷

As PBS has a pH value above 6.2, which leads to a slow dissolution of gel samples of **4**, it was chosen as accepting media to investigate the release behavior upon dissolution. The hydrogels with a volume of 0.12 mL and a gelator concentration of 10 g L^{-1} of **4Na** were

prepared in presence of a rhodamine B amount of 0.05 eq. (37.8 mg g^{-1}). The dissolution tests were performed in 5 mL of PBS at r. t. in triplicate.

In chapter 3.3.3.4 it was already shown that pure hydrogels of **4** with a volume of 0.3 mL and a gelator concentration of 10 g L^{-1} dissolved within 3 days in 3 mL of PBS at r. t.. It is expected that the surface area to volume ratio of the hydrogel sample as well as the volume of the dissolution media might influence the dissolution behavior. Therefore, dissolution of pure hydrogels with only a volume of 0.12 mL in 5 mL of PBS should dissolve much faster than the previous tested samples. As the pure hydrogels were prepared as described above but without addition of the dye, additionally the potential influence of the dye on the dissolution process can be evaluated in this study.

Figure 5.24 shows the pure hydrogel directly after the addition to PBS, as well as after 2 h, 4 h, 6 h, and 24 h. Within the first 6 h of the dissolution test the shape of the hydrogel slowly changes and the volume decreases. After 24 h no traces of the hydrogel sample can be found in the solution. Due to the pH value of 7.4 of the buffer solution, it is assumed that the gelator molecules **4** are deprotonated and transferred into their respective sodium salts **4Na**, which show good solubility in aqueous solutions.

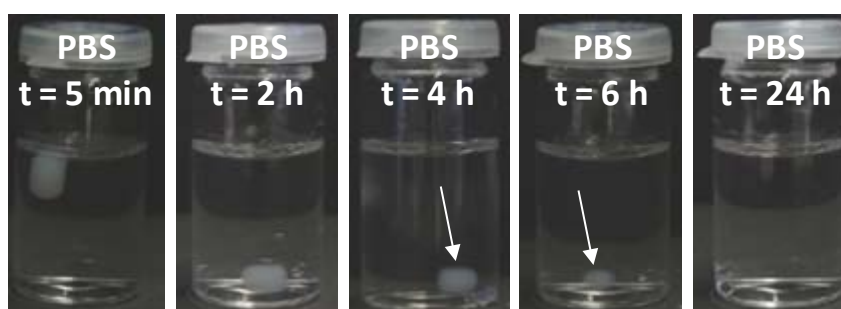


Figure 5.24: Optical images of a pure hydrogel of **4** (prepared with 0.12 mL of a **4Na** solution with a concentration of 10 g L^{-1} and 4 eq. of GdL) after the addition to 5 mL of PBS at r. t. (small hydrogel samples are indicated by an arrow for clarity).

The UV-Vis spectra of the pure PBS showed no absorbance in the measured range between 200 nm and 700 nm. Upon dissolution of the hydrogel it is expected to find an absorbance maximum around 280 nm, similar to the one obtained for the concentration series of **4Na** in water (chapter 4.1.1). Upon complete dissolution of the hydrogel sample the concentration of **4Na** is about 0.234 g L^{-1} , which corresponds to a molar concentration of $3.70 \cdot 10^{-4} \text{ mol L}^{-1}$. However, this concentration exceeds the detection limit of the used spectrometer. Therefore, a detailed analysis of the dissolution of the pure hydrogels *via* UV-Vis spectroscopy could not be performed. The optical images of a hydrogel of **4**, loaded with 0.05 eq. of dye, shortly after the addition to PBS at r. t. and after 2 h, 4 h, 6 h, and 24 h are shown in Figure 5.25.

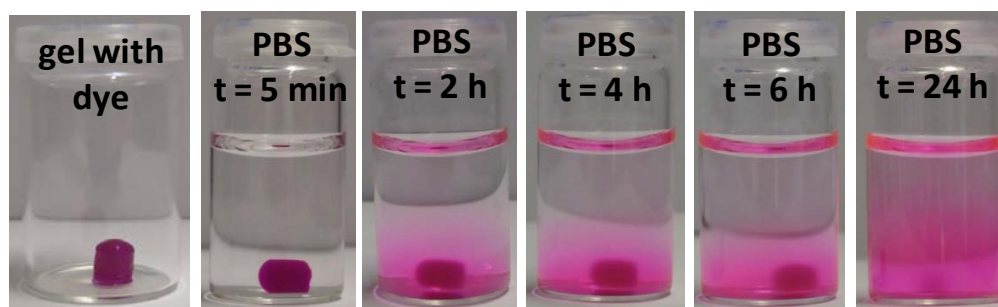


Figure 5.25: Optical images of a hydrogel of **4** prepared in the presence of 0.05 eq. of rhodamine B (with 0.12 mL of a **4Na** solution with a concentration of 10 g L^{-1} and 4 eq. of GdL) after the addition to 5 mL of PBS at r. t..

These images show that the dye is released when the gel dissolves. Within the first 6 h the shape of the hydrogel blurs and the rhodamine B diffuses into the solution. After 24 h the hydrogel samples is completely dissolved, but due to the slow diffusion process a dye gradient in the solution still can be found at this time. Therefore the samples used for the UV-Vis investigations were shortly stirred prior to the sampling to ensure homogenous distribution of the dye within the buffer solution. The UV-Vis spectroscopic measurements were performed in triplicate at r. t. to determine the time-dependent release 2 h, 4 h, 6 h, and 24 h after the addition to the PBS solution. The absorbance spectra for one sample are exemplarily shown in Figure 5.26.

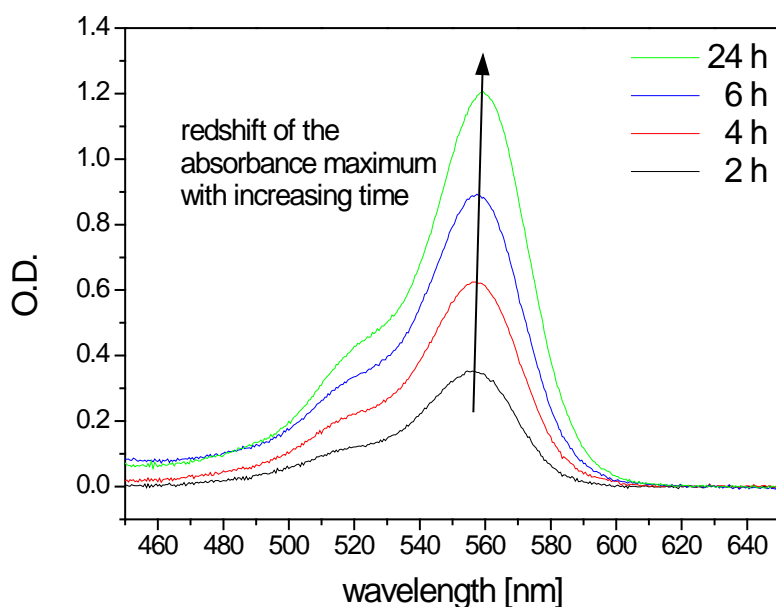


Figure 5.26: UV-Vis absorbance spectra of a hydrogel of **4** formed in the presence of 0.05 eq. of rhodamine B in 5 mL of PBS at r. t..

The optical density increases with increasing time, indicating a higher rhodamine B concentration in the solution. Interestingly, also a red shift of the absorbance maxima from 556.0 nm after 2 h to 557.0 nm after 4 h, 557.5 nm after 6 h and 559.5 nm after 24 h can be observed. To exclude any influence of the pH or the salt content of the buffer solution on the optical properties of rhodamine B, a calibration curve of rhodamine B in PBS was developed, similar to that prepared for rhodamine B in water (chapter 5.2.1.1). Rhodamine B solutions with six different concentrations (0.03630 g L^{-1} , 0.01815 g L^{-1} , 0.00907 g L^{-1} , 0.00363 g L^{-1} , 0.00181 g L^{-1} , 0.00091 g L^{-1}) were prepared in triplicate by a dilution series in PBS. The absorbance spectra were set to zero at 625 nm as manual baseline correction. The resulting spectra of one concentration series are exemplarily shown in Figure 5.27.

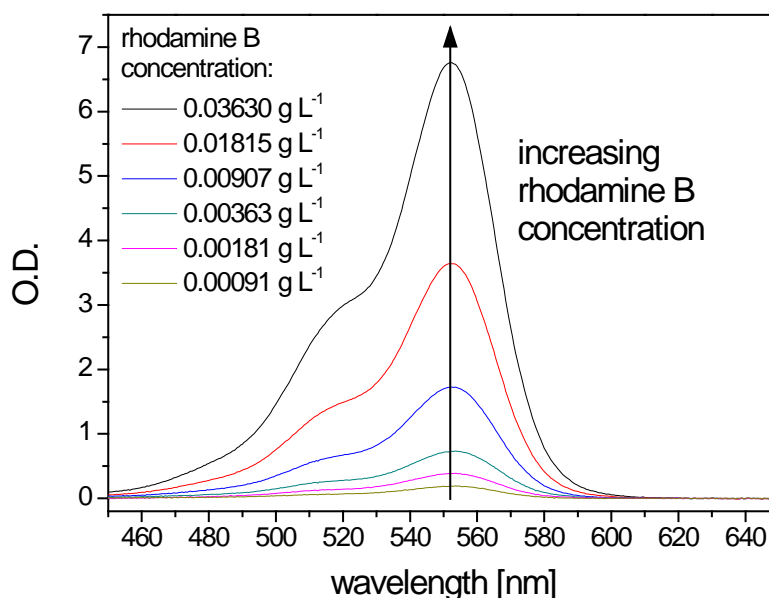


Figure 5.27: Absorbance spectra of six different rhodamine B concentrations in PBS at r. t..

These absorbance spectra also show that with increasing rhodamine B concentration the optical density increases. Furthermore, as the absorbance maximum is constantly at 553 nm for every measured concentration, any influence of the solvent PBS on the molecular and electronic structure of the dye can be excluded. The calibration curve obtained from these spectra has a good linear correlation with a coefficient r^2 of 0.9973 and a regression equation of $y = (198.8 \pm 1.5) \cdot x$ (for the calibration graph see chapter 9.4.10).

As the pK_a value of rhodamine B is around 3.1, the rhodamine B molecules should be present in their zwitterionic form with a maximum optical densities at 552.5 nm during the whole experiment in PBS. However, due to the slightly basic pH value of 7.4 of PBS, compound **4** is deprotonated and the gelator sodium salt **4Na** is formed during dissolution. The red shift

observed in Figure 5.27 might therefore be explained by the complex formation of rhodamine B with the gelator sodium salt **4Na**. As already discussed in chapter 5.3.1.1, when describing the gel formation in presence of rhodamine B, this complex formation can be detected by a slight red shift of the absorbance maxima to 559 nm. A similar behavior could be observed during the combined release of methylene blue and a tetrapeptide-based hydrogelator, where the interactions between the dye and the gelator molecules caused a blue shift compared to the spectrum of the “free” dye.⁸⁰

To prove that the red shift indeed occurs due to the complete transformation of **4** to **4Na** during dissolution and the subsequent complex formation with rhodamine B, reference solutions were prepared. Therefore, it was calculated which amounts should be present in the solutions obtained from the release study after 24 h. One dissolved gel sample consists of 1.2 mg of **4Na**, 4 eq. of hydrolyzed GdL (1.35 mg of GdL), 0.05 eq. of rhodamine B (0.045 mg), and 0.12 mL of water. These amounts are dissolved in 5 mL of PBS during the experiment. Three reference samples were prepared containing these amounts of the gelator sodium salt **4Na**, of hydrolyzed GdL, of rhodamine B, desalted water, and 5 mL of PBS. Additionally, three reference samples were prepared with only 0.05 eq. of rhodamine B (0.045 mg) in 5 mL of PBS ($c(\text{dye}) = 0.00907 \text{ g L}^{-1}$). A typical absorbance spectrum from the samples of the release study at 24 h and from the two types of reference samples are presented in Figure 5.28, respectively.

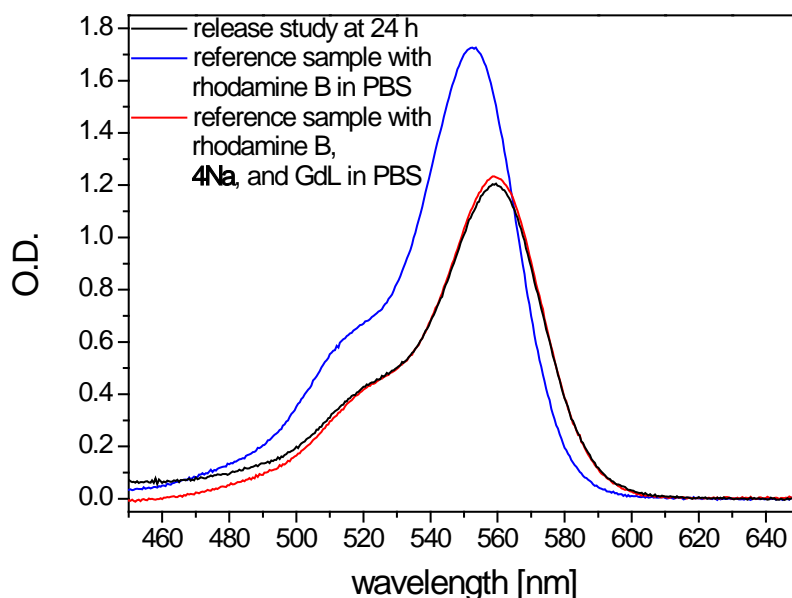


Figure 5.28: A typical absorbance spectrum from a solution obtained from the release study in PBS at 24 h (black), from rhodamine B solutions in PBS with a dye concentration of 0.00907 g L^{-1} (blue), and from the reference solutions in PBS containing rhodamine B, **4Na**, and GdL (red), respectively.

The reference sample with only rhodamine B has its absorbance maximum at 553 nm and has a higher optical density than the spectrum obtained from the release study at 24 h. However, the spectrum of the second set of reference samples, that also considers the amount of gelator sodium salt **4Na** and GdL, agrees very well with the spectra obtained from the release experiment in terms of the wavelength and the optical density of the absorbance maxima. It therefore can be stated that during the dissolution of the gel sample the gelator **4** is transferred into the water soluble sodium salt **4Na**, which interacts with the dissolved rhodamine B molecules resulting in a red shift of the absorbance maxima to 559 nm.

Altogether, it can be stated that under the same testing conditions the hydrogels prepared in the presence of rhodamine B dissolve qualitatively as fast as the pure hydrogels (within 24 h). Upon dissolution, the rhodamine B concentration in solution increases. A quantitative time-dependent analysis *via* UV-Vis spectroscopy is difficult, as the absorbance maxima shift from 553 nm (solely rhodamine B in PBS) to 559 nm at complete dissolution of the gel. This leads to the conclusion that the observed red shift of the absorbance maximum is due the dissolution of the hydrogel and the involved formation of gelator sodium salt molecules **4Na**, which are able to form a complex with the dye molecules. The increasing red shift with increasing time is accounted to the increasing number of deprotonated gelator molecules upon dissolution of the gel.

In the literature few examples of supramolecular hydrogels deal with the release of a guest molecule in PBS. Naskar *et al.* showed that tetrapeptide-based hydrogels could release the anti-cancer drug doxorubicin in PBS buffer solutions with a pH value of either 7.4 or 6.5.³⁰⁶ The gels were stable in both buffer solutions. Dependent on the exact structure of the gelator, they released 85 % to 90 % of the model compound within 45 h at pH 7.4. In the buffer with the lower pH value the release rates were slightly slower. In another study, ciprofloxacin was encapsulated into a tripeptide-based hydrogelator *via* change of pH.³⁰⁵ The encapsulation of the drug led to more stable hydrogels. These released the antibiotic agent within 2 to 3 days, while the pure hydrogel without drug disintegrated completely in PBS at 37 °C. The release rate could thus be tuned by the amount of encapsulated drug. This publication is also one of the rare examples that investigated the cytotoxicity and the activity of the hydrogel-drug system. For docetaxel-loaded peptide-polysaccharide hybrid hydrogels the release rate in PBS at 37 °C was tuned by the fraction of polysaccharide present in the gel.³⁶ While the pure peptide hydrogel completely precipitated within two days, the addition of the polysaccharide led to stable gels with a release of around 34 % in the first 52 h. In a taxol-derived hydrogelator with sustained activity of the drug, the release was triggered *via* enzymatic cleavage in PBS, resulting in release rates of 0.13 % to 0.046 % per hour.³

5.5.2 Release of rhodamine B upon dissolution in SBF (pH = 7.4) at 37 °C

For the parenteral application route drug delivery systems are injected intramuscularly, intravenously or subcutaneously. To be able to test the release behavior *in vitro*, the properties of human blood plasma must be simulated. In the literature for this purpose simulated body fluid (SBF) with a pH value of 7.4 is usually used.²⁹⁷ The composition of the SBF, used in this study, is an improved version of the composition published in 2003.³⁸¹ It consists of sodium chloride, sodium bicarbonate, potassium chloride, potassium phosphate dibasic trihydrate, magnesium chloride hexahydrate, calcium chloride, sodium sulfate, and tris(hydroxymethyl) aminomethane. Originally, it was used to investigate the surface changes of glass-ceramic implants for potential use as artificial vertebrae, ileum, tooth roots or the middle-ear bone. It is now also the standard fluid for the *in vitro* investigation of the apatite-forming ability of implant materials.²⁹⁷

In this study washed hydrogels of **4** with a volume of 0.12 mL and a gelator concentration of 10 g L⁻¹ of **4Na** were tested regarding their dissolution behavior in 5 mL of SBF at r. t. and at 37 °C. Furthermore, the release of encapsulated rhodamine B from such hydrogels was monitored at 37 °C *via* optical images and UV-Vis spectroscopy. In Figure 5.29 optical images of the pure hydrogels are shown directly after the addition to SBF at r. t. and 37 °C, as well as after 2 h, 4 h, 6 h, and 8 h.

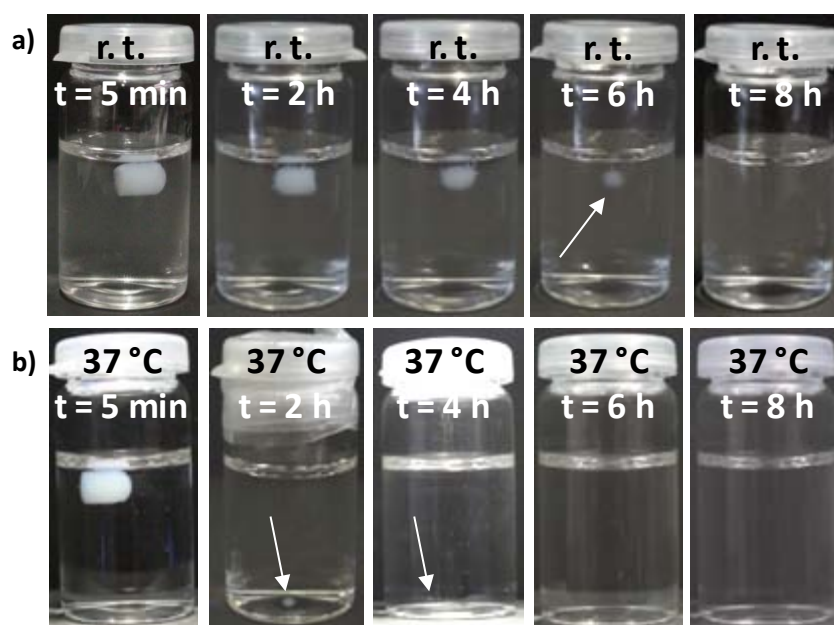


Figure 5.29: Optical images of a pure hydrogel of **4** (prepared with 0.12 mL of a **4Na** solution with a concentration of 10 g L⁻¹ and 4 eq. of GdL) after the addition to 5 mL of SBF a) at r. t. and b) at 37 °C (small hydrogel samples are indicated by an arrow for clarity).

The dissolution behavior of the gel in SBF at r. t. is similar to that in PBS and completed within 8 h. As the pH value of the SBF buffer is 7.4, like the pH value of PBS, this is not surprising. The increase of the solution temperature to body temperature results in a faster dissolution of the pure hydrogel. Within 4 h to 6 h the hydrogel has completely vanished. This low stability of the gel in SBF at 37 °C makes it obvious that the gel is not suitable as template for apatite-formation in implant research. As this furthermore indicates the great importance of the temperature regarding the dissolution and release behavior, further tests were only performed at 37 °C to simulate the body temperature.

The optical images of a hydrogel of **4** loaded with 0.05 eq. of rhodamine B shortly after the addition to SBF at 37 °C and after 2 h, 4 h, 6 h, 8 h, and 24 h are shown in Figure 5.30.

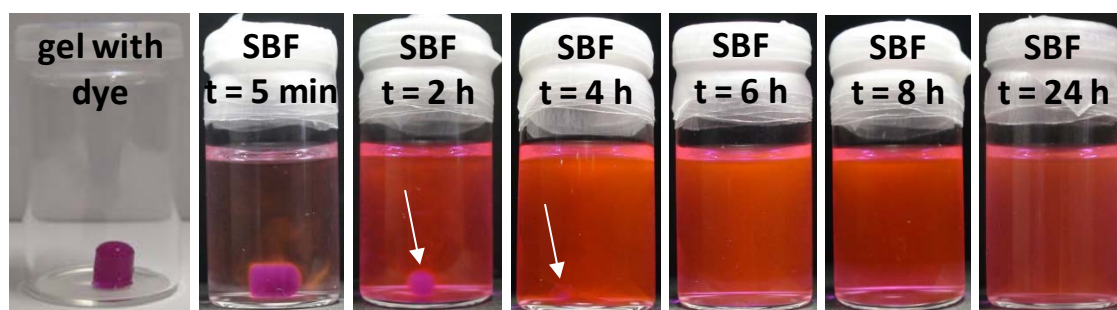


Figure 5.30: Optical images of a hydrogel of **4** prepared in the presence of 0.05 eq. of rhodamine B (with 0.12 mL of a **4Na** solution with a concentration of 10 g L^{-1} and 4 eq. of GdL) after the addition to 5 mL of SBF at 37 °C (small hydrogel samples are indicated by an arrow for clarity).

The hydrogel also dissolves within 4 h to 6 h releasing all the encapsulated rhodamine B. For the UV-Vis spectroscopic measurements three identical samples were prepared and measured after the same time intervals to investigate the quantitative release (Figure 5.31).

The respective maxima of the optical density in the different spectra increase with increasing time until a maximum is reached after 4 h. This indicates that the hydrogel is already completely dissolved at 4 h. This might be explained by the fact that the samples prepared for the spectroscopic analysis were shortly stirred prior to each measurement to ensure a homogenous distribution of the dye in the solution. Obviously, this mechanical agitation led to a faster dissolution of the gel and a faster release of the dye, compared to the samples prepared for the optical analysis, that were left to stand without such agitation and dissolved within 4 h to 6 h.

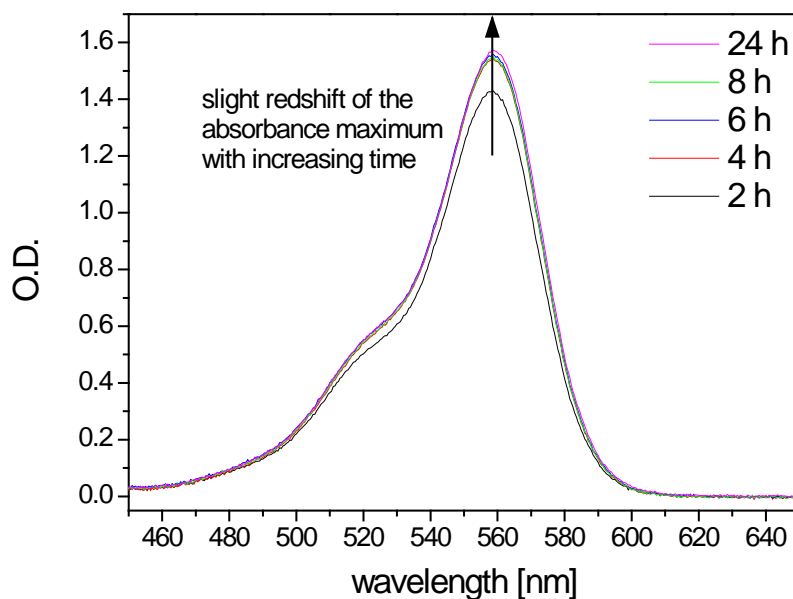


Figure 5.31: UV-Vis absorbance spectra of a hydrogel of **4** formed in the presence of 0.05 eq. of rhodamine B in 5 mL of SBF at 37 °C.

The respective absorbance maxima in the spectra recorded after 2 h, 4 h, 6 h, and 8 h can be found at 558.5 nm, while the spectra after 24 h have their maxima at 559.5 nm. As the accuracy of the spectrometer is around 0.5 nm, and the determination of the exact position of the maxima is furthermore affected by the signal to noise ratio of the spectra, a detailed analysis of this shift between 8 h to 24 h is not reasonable. As already discussed for the samples dissolved in PBS, the red shift of all obtained spectra in SBF compared to the spectra of rhodamine B in water ($\lambda_{\max} = 553 \text{ nm}$) might be explained by the interaction of rhodamine B with molecules of **4Na** that are formed during dissolution.

To confirm this assumption, a reference sample was prepared containing the same amount of rhodamine B in SBF that was encapsulated in the hydrogels. Furthermore, a rhodamine B solution including also 1.2 mg of **4Na** was compiled. The amount of hydrolyzed GdL in the solution had no influence on the absorbance spectrum in the relevant wavelength range. It was therefore neglected to keep the reference solution as simple as possible. The comparison of the spectra from the release study and of the reference samples is displayed in Figure 5.32.

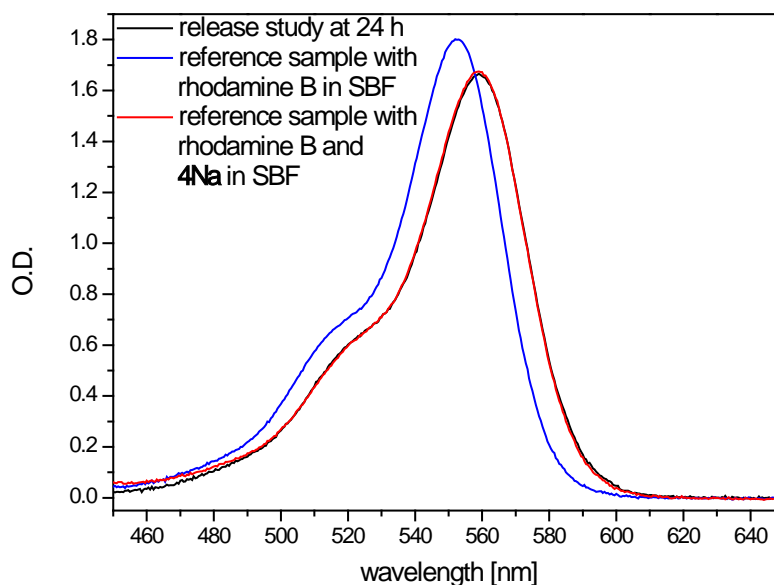


Figure 5.32: A typical absorbance spectrum from a solution obtained from the release study in SBF at 24 h (black), from the rhodamine B solution in SBF with a dye concentration of 0.00907 g L^{-1} (blue), and from the reference solution in SBF containing rhodamine B and **4Na** (red), respectively.

The adsorption maximum of the sample with only rhodamine B in SBF can be found at 552.5 nm. Therefore, a calibration curve with only varying the concentration of rhodamine B in SBF would not allow for a quantitative analysis of the obtained data. The spectra of the reference sample, that also contains **4Na**, matches the spectra obtained from the release study at 24 h within their deviations. Therefore, it can be stated that the whole amount of encapsulated rhodamine is released during the dissolution of the gel in SBF. The released dye molecules form a complex with **4Na** molecules, which causes a red shift of the absorbance maximum.

5.5.3 Release of rhodamine B in simulated gastric fluid containing pepsin (pH = 1.6) at 37 °C

The simulation of the conditions in the gastro-intestinal tract is very complicated, as it is one of the largest organs in the human body and has very different milieus. When simulating the conditions in the stomach, it is very important to differentiate between the fasted and the fed state, as the ingestion of food can drastically change the conditions in the stomach minutely. To be able to neglect the type and amount of ingested food as well as the progression of digestion, the studies performed here concentrate on the fasted state. At the fasted state the pH value in the stomach is about 1.6, which indicates that the hydrogels of **4** should be stable. However, the stomach also produces large amounts of pepsin, an enzyme that is able to

hydrolyze most peptide linkages such as amide bonds. As the hydrogelator **4** consists of three amide bonds between the core and the phenylene side arms, the hydrogel might as well dissolve due to enzymatic bond cleavage.

Thus, at first it was tested if gels of **4** are stable in the milieu of the stomach, so that they might act as a protective matrix for acid labile drugs. Washed hydrogels, analogous to those used in the adsorption studies, were prepared and put in 5 mL of simulated gastric fluid containing pepsin (SGF) at 37 °C (Figure 5.33).

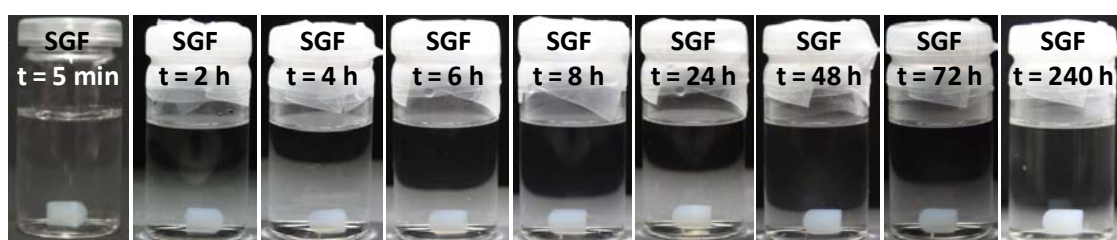


Figure 5.33: Optical images of a pure hydrogel of **4** (prepared with 0.12 mL of a **4Na** solution with a gelator concentration of 10 g L⁻¹ and 4 eq. of GdL) after the addition to 5 mL of SGF at 37 °C.

These pictures clearly show that no dissolution, shrinking or swelling of the gel samples within ten days at 37 °C can be observed. This is promising, as now it can be stated that the pepsin in the stomach does not hydrolyze the amide bonds of the gelator. It seems that the formation of fibers, as well as the steric hindrance of the phenylenes in the side arms, protects the hydrogen bonds from enzymatic cleavage.

Furthermore, the stability and release behavior of hydrogels of **4**, formed in the presence of 0.05 eq. of rhodamine B, was tested in 5 mL of SGF at body temperature. The optical images show a slight colorization of the supernatant solution during the first days (Figure 5.34).

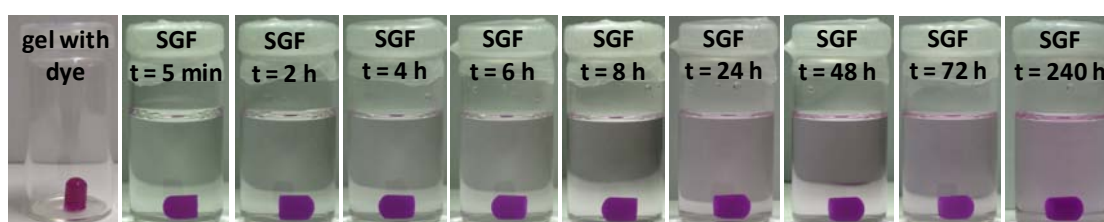


Figure 5.34: Optical images of a hydrogel of **4** prepared in the presence of 0.05 eq. of rhodamine B (with 0.12 mL of a **4Na** solution with a concentration of 10 g L⁻¹ and 4 eq. of GdL) after the addition to 5 mL of SGF at 37 °C.

This indicates that the hydrogels, that encapsulate rhodamine B, are also stable in SGF and only release small amounts of the dye. To investigate this release more quantitatively, UV-Vis spectra were recorded analogous to the measurements performed in water, PBS, and SBF.

As expected, with increasing time an increase of the respective absorbance maximum can be observed (Figure 5.35). However, no shift of the maxima occurs, probably because no gelator sodium salt **4Na** is formed during the experiment. One also has to keep in mind that only very low amounts of dye are released during this experiment. This leads to a low signal to noise ratio in the time-dependent spectra making the analysis of the data difficult. Nevertheless, it can be seen that the respective absorbance maxima of the spectra are at 556 nm, while in water they could be found at 553 nm. This is explained by the low pH value of 1.6 in SGF. According to the pK_a value of rhodamine B ($pK_a = 3.1$) the rhodamine B molecules should be present in their cationic state at that pH value, which leads to this red shift. In the literature values of the absorbance maxima in acidic aqueous media of 557 nm and 558 nm are mentioned.^{273,277} In our experiments the maximum was found at 556 nm. Such deviations might occur when different spectrometers and experimental parameters, such as response time and data interval, are used. To obtain comparable and coherent results, in this study the same spectrometer and experimental parameters were used for all performed adsorption and release experiments.

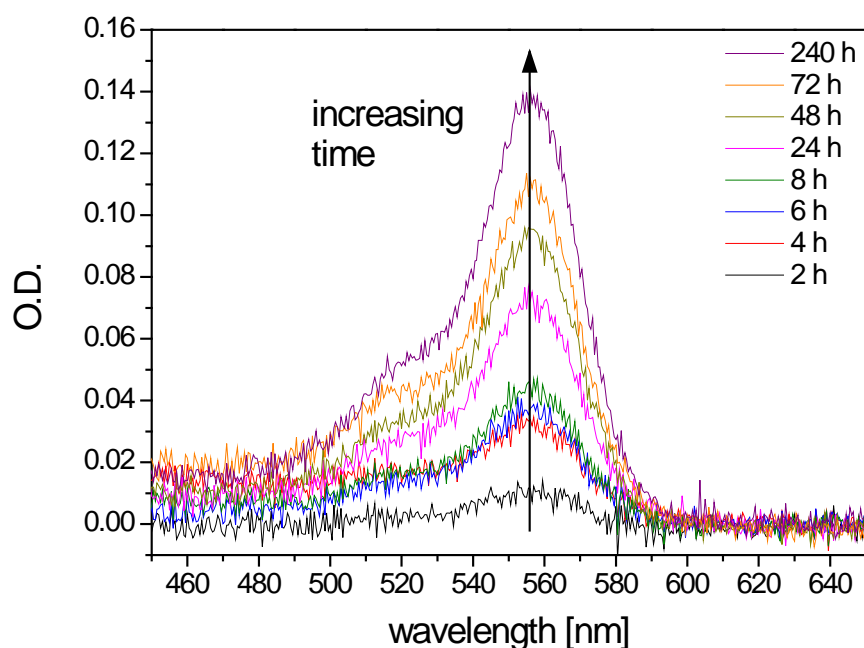


Figure 5.35: UV-Vis absorbance spectra of a hydrogel of **4** formed in the presence of 0.05 eq. of rhodamine B in 5 mL of SGF at 37 °C.

A calibration curve of rhodamine B in SGF with six different concentrations was developed. The UV-Vis spectra of three independently prepared dilution series were measured and the respective maximum of the optical density at 556 nm was plotted versus the concentration (Figure 5.36).

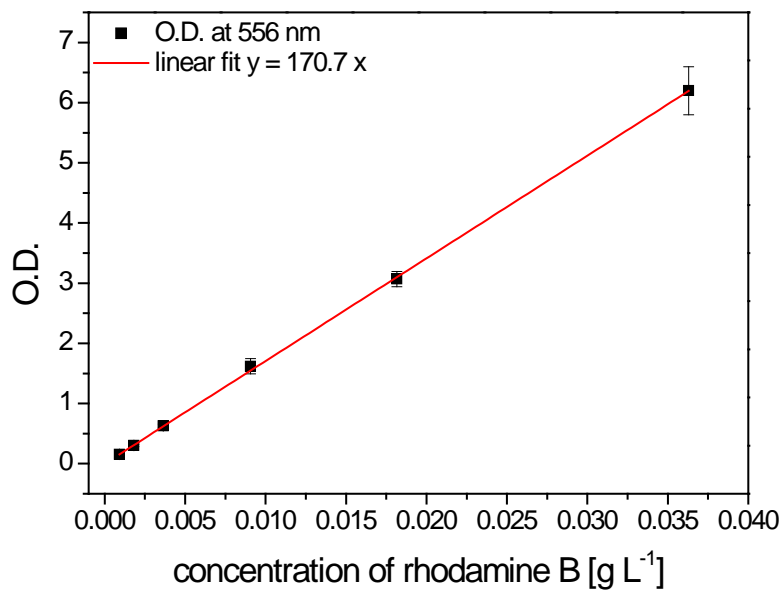


Figure 5.36: Calibration graph with 6 different rhodamine B concentrations in SGF. Each data point is the average obtained from three independently prepared dilution series.

A linear fit with the intercept set to zero resulted in a regression curve with a correlation coefficient of $r^2 = 0.99967$ and a regression equation of

$$\text{O.D.}_{556\text{nm}} = (170.7 \pm 4.0) \text{Lg}^{-1} \cdot c_{\text{sol}} \quad (5.18)$$

with $\text{O.D.}_{556\text{nm}}$ representing the average optical density at 556 nm and c_{sol} the concentration of rhodamine B in SGF in g L^{-1} .

This calibration equation was used to calculate the cumulative release of rhodamine B in mg g^{-1} , the encapsulated amount of dye in mg g^{-1} , and the loading efficiency in % for the time-dependent release study in SGF. The data were processed and calculated analog to the data obtained from the release study in water. The cumulative release versus time for hydrogels of **4**, prepared in the presence of 0.05 eq. of rhodamine B, in SGF at 37 °C and in water at r. t. is shown in Figure 5.37.

As expected, the cumulative release increases with increasing time until it reaches a saturation value after 10 days. It is assumed that at this time the equilibrium state has been reached. Interestingly, although the study in SGF was performed at a higher temperatures compared to the study in water, the desorption rate in water is slightly higher leading to saturation already after 24 h. Usually an increase in temperature leads to higher desorption rates, as the diffusion process is enhanced. This leads to the conclusion that in these experiments the pH value and the salt concentration of the solution have a much higher influence on the release behavior than the temperature.

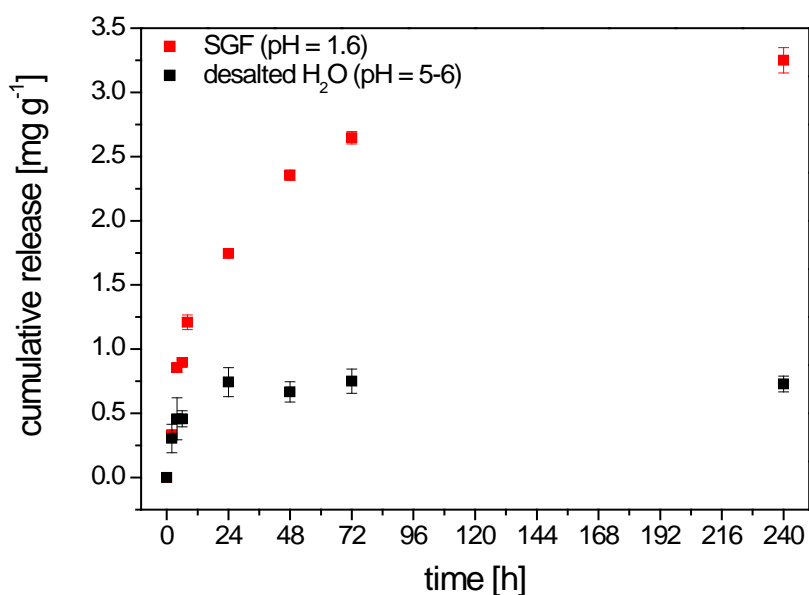


Figure 5.37: Cumulative release versus time of hydrogels formed in the presence of 0.05 eq. in desalted water with a pH value of 5 to 6 at r. t. (black) and in SGF with a pH value of 1.6 at 37 °C (red).

Furthermore, despite the same initial rhodamine B amount, that was encapsulated in the hydrogels, the cumulative release after 10 days is higher in SGF than in water. This suggests that the lower pH value and the higher temperature slightly favor the release of rhodamine B in SGF compared to the release in water. Despite this enhanced release in SGF, the loading efficiency after ten days is still above 90 % (Table 5.13). This means that the vast majority of the encapsulated model compound is protected from dissolution in the milieu of the stomach.

Table 5.13: Results of the release studies of hydrogels of **4** prepared in the presence of 0.05 eq. of rhodamine B after 10 days in water at r. t. and SGF at 37 °C, respectively.

| | cumulative release (10 d) [mg g ⁻¹] | encapsulated amount (10 d) [mg g ⁻¹] | loading efficiency (10 d) [%] |
|--------------------------|---|--|-------------------------------------|
| H ₂ O (r. t.) | 0.7 | 37.1 | 98 |
| SGF (37 °C) | 3.2 | 34.6 | 91 |

However, when simulating the conditions in the stomach not only the composition of the gastric acid and the physical properties, such as the pH value, the osmotic pressure, the buffer capacity and the surface tension, must be adapted but also the residence times, the volume, and the hydrodynamics must be considered.^{297,298}

The residence times in the stomach are strongly dependent on the amount of ingested food and can vary between a few minutes in the fasted state to half a day for a big meal. One has to keep in mind that even when the medicine is taken in fasted state, it is usually administered with a glass of water, that as well changes the composition, condition and residence time in the gastro-intestinal tract. The residence time in the stomach can be best decreased by administering the drug delivery system without food, but with a sufficient amount of liquid. Knowing this, it is expected that the amount of the released molecules in the stomach would be even lower than 9 %, as the hydrogel is probably passed to the upper small intestinal within half a hour. In the fasted state the volume of the gastric acid is about 50 mL, and might extend to around 300 mL due to the dilution when administering the drug system with a glass of water. Thus, it might be interesting to repeat this release studies under standard testing conditions that also take into account the volume of the gastric acid and the hydrodynamics present in the stomach. Nevertheless, the findings of the study presented here clearly show that the hydrogels of **4** are stable in fasted state SGF at body temperature over ten days, which exceeds the expected residence time in the stomach manifold. Furthermore, only small amounts of the model compound rhodamine B are released in that time making this system a promising candidate for a stable transport matrix in acidic media.

In the following, the system is investigated regarding its dissolution and release properties in simulated intestinal fluid (SIF) in the fasted state at 37 °C. The aim is to verify that the gel system is able to selectively release the encapsulated model compound under the conditions of the intestinal tract and is thus suitable for the use of oral administration of drug molecules.

5.5.4 Release of rhodamine B in simulated intestinal fluid (pH = 6.5) at 37 °C

While it is widely known that there is an acidic milieu in the stomach, people often think that the intestine is alkaline. This is only partially true as the intestine can be divided in several sections. The upper small intestine or duodenum as well as the jejunum have a slightly acidic pH value in the fasted state between 4.9 and 6.4. The proximal small intestine or ileum has a slightly alkaline pH in the fasted state between 6.8 and 8.0.^{31,298} In the fed state the pH value in the upper small intestine is about 5.2 and gradually increases to 7.5 in the ileum. Obviously the pH value in the upper small intestine is also dependent on the type and amount of ingested food as well as the time after ingestion of the food. The large intestine and the colon have a more alkaline milieu – with pH values between 7.8 and 8.0 – that is rather independent of the food intake. As the transition pH value between gel and sol of hydrogels of **4** is about 6.2, the gels should get dissolved even in the upper small intestine. For simplicity and to be able to

neglect food ingestion, the following experiments were carried out in fasted state simulated intestinal fluid with a pH value of 6.5.

The optical images of pure hydrogels of **4** in SIF at 37 °C show that the gels slowly dissolve within 72 h (Figure 5.38).

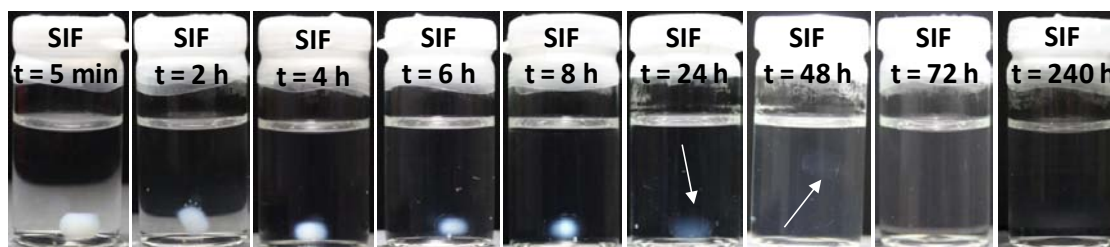


Figure 5.38: Optical images of a pure hydrogel of **4** (prepared with 0.12 mL of a **4Na** solution with a concentration of 10 g L^{-1} and 4 eq. of GdL) after the addition to 5 mL of SIF at 37 °C (small hydrogel samples are indicated by an arrow for clarity).

At this time the gels are rarely seen in the solution as they turn transparent before they completely dissolve. This might be due to two different reasons: i) The transparency of the gel might be caused by a match of the refractive index of the gel and the SIF upon diffusion of the fluid into the gel. ii) At first, the superstructures of the gel, such as fiber bundles, are disassembled. This leads to a weak transparent gel that is then thought to be disintegrated into single molecules. In the literature it is known from different crosslinked polymer networks with an azo-aromatic moiety that they either dissolve *via* a surface erosion process, where the polymer network diminishes in size from the surface to the core, or by a process where a colorless dissolution front moves through the polymer network.²³ These different types of dissolution processes are explained to be related to the crosslink density and the additional entanglement of the polymer chains. The entanglement leads to a stabilization of the polymer network even after all azo cross-links have been cleaved.

The hydrogels of **4** prepared in the presence of rhodamine B are dissolved within 72 h, just like the pure gel samples, and the encapsulated rhodamine B is released. After 48 h the gel in the solution can be hardly recognized as the gel has the same color as the solution, indicating that the dye concentration in the gel and the solution is the same (Figure 5.39). This might be explained by the fact that at this time the superstructure of the gel is already completely dissolved, and only weakly connected fibrils are present that are not able to bind large amounts of the dye.

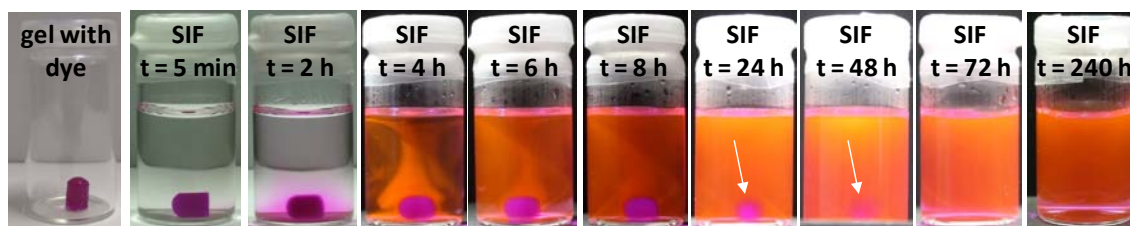


Figure 5.39: Optical images of a hydrogel of **4** prepared in the presence of 0.05 eq. of rhodamine B (with 0.12 mL of a **4Na** solution with a concentration of 10 g L^{-1} and 4 eq. of GdL) after the addition to 5 mL of SIF at $37 \text{ }^\circ\text{C}$ (small hydrogel samples are indicated by an arrow for clarity).

This dissolution and release pattern is also supported by the obtained UV-Vis spectra of the solutions (Figure 5.40).

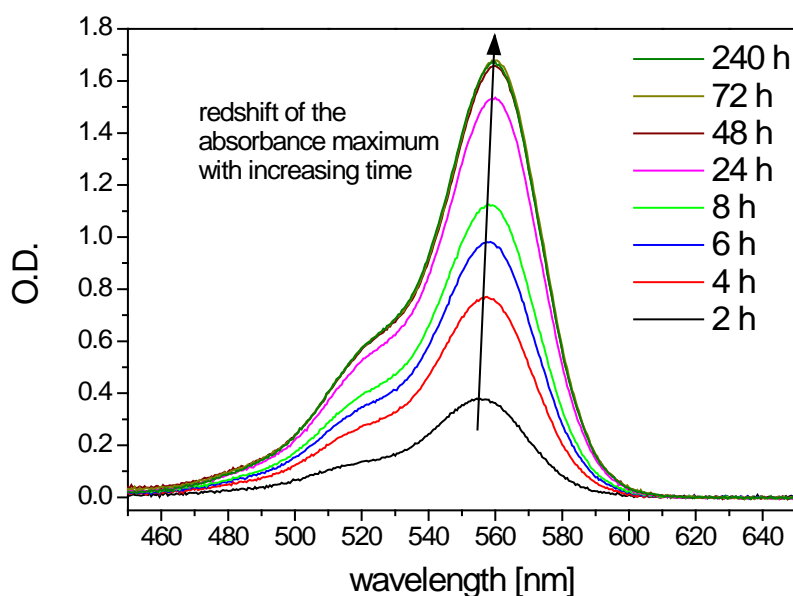


Figure 5.40: UV-Vis absorbance spectra of a hydrogel of **4** formed in the presence of 0.05 eq. of rhodamine B in 5 mL of SIF at $37 \text{ }^\circ\text{C}$.

With increasing time the intensity of the optical density increases until the maximum is reached after 48 h. As already discussed for the release of rhodamine B in PBS and SBF, a slight red shift of the absorbance maxima can be observed from 554.5 nm after 2 h to 559 nm after 240 h. This again indicates an interaction between the dye molecules and the gelator sodium salt **4Na**, that is formed during the dissolution process.

Similar to the results obtained from UV-Vis measurements of pure rhodamine B in PBS (Figure 5.27, chapter 5.5.1), the pure dye in SIF showed no red shift. Instead, a linear correlation between the respective absorbance maxima at 553 nm and the dye concentration of the solution was found. In the presence of 1.2 mg of **4Na** in 5 mL of SIF with the same rhodamine B concentrations also a linear correlation between the rhodamine B concentration

and the respective maximum optical density of the different spectra could be observed. The respective absorbance maximum however had shifted from 553 nm to 559 nm due to the interactions between the dye and the sodium salt **4Na**. Both calibration curves are presented in Figure 5.41 with their respective linear correlation equations.

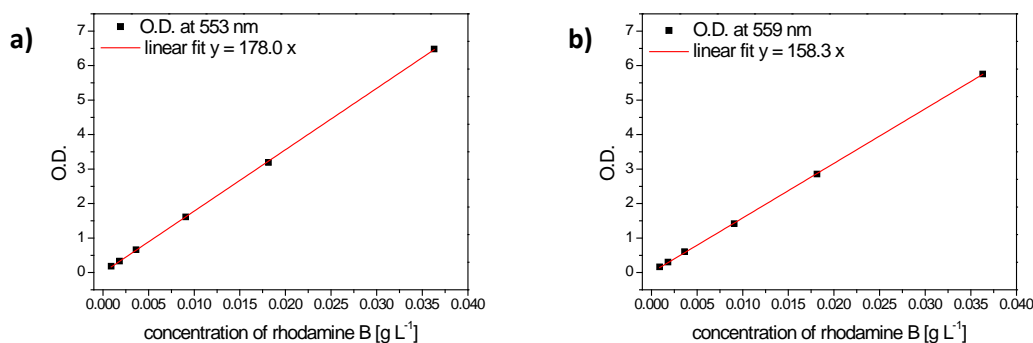


Figure 5.41: Calibration graph with 6 different rhodamine B concentrations in SIF a) without and b) in presence of 1.2 mg of **4Na**. The correlation coefficient r^2 is 0.9994 for both linear fits.

With the calibration curve in presence of **4Na**, the amount of rhodamine B after 240 h in SIF can be calculated, proving that all dye is released. As during the release of rhodamine B upon dissolution of the gel, the rhodamine B concentration as well as the gelator sodium salt concentration changes, a detailed analysis of the time-dependent spectroscopic data would require a 3D-calibration curve that changes the amount of dye and **4Na** independently. However, this time-consuming work would highly exceed the benefit of the analysis. A quantitative comparison of the results obtained in SIF with the release data in SBF (chapter 5.5.2), that was also performed at 37 °C, clearly shows that the dissolution of gels of **4** is faster in SBF (~ 24h) than in SIF (48 - 72 h). This can be explained by the slightly lower pH value of SIF that leads to a slower dissolution of the gels.

The bioabsorption of nutrition and drug molecules, administered *via* the oral route, mainly takes place in the small intestine, as in the large intestine or colon there is usually not enough water present. While the overall residence time of ingested food in the gastro-intestinal tract can vary from 2 to 6 h for gases and up to 80 h for high density materials, it is mainly constant for liquids and solids in the small intestine and ranges from 1 to 3 h. Thus, usually pharmaceuticals are digested and adsorbed within the first three hours after ingestion. Therefore, dissolution should take place in the upper small intestine within the first hour. Usually this cannot be achieved and a dissolution rate of 85 % within the first 30 min is considered sufficient.^{297,298}

It was shown that a Fmoc-FF-peptide-based hydrogel is stable in 10 mM PBS-HCl buffer with pepsin at a pH value of 2.0, that was used as simplified SGF, and in 10 mM PBS with

trypsin at a pH value of 7.4, that was used as simplified SIF.³⁶ In both buffers less than 1.5 % of degradation occurred after 24 h of incubation, which indicated their resistance to enzymatic digestion. It was furthermore shown that the presence of β -mannose promotes the release of the encapsulated drug docetaxel, which might make this system suitable for targeting the colon, as the mannose exists there. This is one of the rare examples in the literature that considers the stability and release of a supramolecular hydrogel in milieus that are similar to those in the gastro-intestinal tract.

For the hydrogel system presented here, it could be shown that the gel dissolves in SIF within 72 h, but that the main amount of the dye is already released within the first 24 h. For a successful oral drug delivery system this is still too slow, but the general behavior, *i. e.* the stability in SGF and the dissolution in SIF, is promising. The dissolution and release rate can also be influenced by the volume and the hydrodynamics that were not considered in this study. As the volume of the fluid in the upper small intestine is greater than the 5 mL used for the studies here, it is expected that the dissolution rate is slightly increased by increasing the volume of the accepting media. Also the hydrodynamics of the gastro-intestinal tract are known to influence the mixing of the components and the effective boundary thickness which leads to an increased dissolution and biosorption rate. Furthermore, it can also be influenced by the size of the administered hydrogel or probably by the gelator concentration. Therefore, it is possible to tune the release rate for hydrogels of **4** to fit the required conditions.

For the bioabsorption in the gastro-intestinal tract not only the dissolution behavior is important but many other factors, such as the hydrophobicity of the drug molecules that affects the transport through the intestinal membrane. Therefore, further tests with an actual drug using standard dissolution and release conditions should be performed. This should give further details on the possible application of hydrogels of **4** as controlled drug delivery system through oral administration. The results obtained in this study are, however, very encouraging.

5.6 Achievements and further investigations towards a pH-sensitive drug delivery system

Summarizing, hydrogels of **4** show a good potential for the application as a new controlled drug delivery system, especially for the oral administration of drugs. The gels fulfill the basic requirements for a successful drug delivery system, such as: i) good biocompatibility and nontoxicity; ii) responsiveness of the hydrogel to a change of the pH value in a physiological relevant region; iii) sufficient stability against mechanical and thermal stress; iv) high surface area and porosity; and v) a high loading efficiency due to adsorption and/or encapsulation of the drug molecules.

The detailed studies regarding the adsorption capacity of hydrogels of **4** with regard to the model compound rhodamine B showed that the adsorbed amount of dye is strongly dependent on the initial dye concentration. While for low initial dye concentration a linear dependence on the adsorption capacity can be found, for higher initial concentrations a saturation effect can be observed. At most, an absolute amount of 86 mg g^{-1} of rhodamine B were adsorbed from an aqueous solution with an initial dye amount of 138 mg g^{-1} , which was the highest initial dye concentration tested in this study. The adsorption data fit well both the Langmuir and the Freundlich isotherm model. These models predict that although the adsorption is favorable, a maximum adsorption capacity of $Q_L = 100 \text{ mg g}^{-1}$ is reached for high initial dye concentrations. This saturation effect with increasing surface density is ascribed to decreasing adsorbent-adsorbate interactions, *i. e.* with increasing amount of adsorbed molecules the adsorption becomes less favorable. The adsorption kinetics follows the pseudo-second order model for all tested initial concentrations, which indicates chemisorption as the rate limiting step. The initial adsorption rate h and the adsorption rate K'' are very slow with complete adsorption within ten days. Although agitation of the hydrogel samples in the dye solutions increases the adsorption rate, it still takes up to three days to achieve the equilibrium state of adsorption. Thus, the application of the hydrogels regarding their adsorption potential is mainly interesting for fixed-bed systems. As the adsorption capacity at low initial concentrations is very high (over 90%), the system might be interesting for filtration applications.

The adsorption of rhodamine B with subsequent release in water at r. t. and 40°C shows that adsorbed dye molecules are strongly bound at the hydrogel surface at both temperatures, as 90 % of dye remains in the gel. The desorption rate, but not the maximum amount of desorbed dye is dependent on the temperature of the solution. Although the adsorption potential of hydrogels of **4** is very promising, the limited maximum adsorption capacity for high

initial dye concentrations and especially the adsorption rate is a great disadvantage for the industrial use of this system.

Therefore, the loading of the hydrogel by preparing it in presence of distinct amounts of the model compound rhodamine B was investigated. It could be shown that the loading *via* encapsulation of the guest molecules has several advantages over the loading method *via* adsorption onto a preformed hydrogel. First, the loading can be achieved within the time of gelation, which is 8 h for the gelation method used here. Second, higher loading capacities can be achieved, when using the same initial amount of the dye for the adsorption experiments, as the dye is not only adsorbed at the surface of the preformed gel fibers, but can also be incorporated into the gel fibers and in between the gelator molecules. Third, the overall maximum loading capacity is only limited by the mechanical stability of the gel, that decreases upon encapsulation of high amounts of rhodamine B. The influence of the dye on the mechanical stability of the gel samples proves that the guest molecules are incorporated in the gel structure as some kind of impurity. This furthermore suggests that the bondage between dye and gel is very strong. For the formation of stable gels the highest possible molar ratio of dye molecules to gelator molecules is 1 : 2 (0.5 eq., 378 mg g⁻¹). This is very promising as only one example was found in the literature that describes a nearly equimolar encapsulation of a guest molecule, namely 1-pyrenemethylamine, in a low molecular weight hydrogelator.²⁸⁸ The time-dependent release study in water at r. t. of gels with different encapsulated amounts of rhodamine B showed that even after ten days a maximum remaining encapsulated amount of 264 mg g⁻¹ could be achieved, which corresponds to a dye to gelator ratio of 1 : 3 and a loading efficiency of still 70 %. The release kinetics is in accordance with the generalized Fickian diffusion model and shows a non-hindered diffusion of the dye molecules.

The release studies in biologically relevant media were performed with hydrogels of **4** formed in the presence of a distinct amount of rhodamine B (0.05 eq., 38 mg g⁻¹). In phosphate buffered saline (PBS) with a pH value of 7.4 – a standard fluid in biochemistry for *e. g.* rinsing cell cultures – all the dye is released at r. t. within 24 h upon dissolution of the gel sample. To simulate the condition of the human blood plasma and to test the surface changes of potential implant materials *in vitro*, simulated body fluid (SBF) with a pH value of 7.4 is used. The pure hydrogel samples of **4** dissolve within 8 h at r. t. and within 6 h at 37 °C in SBF, showing that an increase in temperature increases the dissolution and thus release rate. Due to this fast dissolution all encapsulated dye is release within 6 h at body temperature, making this material unsuitable as template for the growth of tissue or bone material.

Far more promising is the use of this hydrogel system as controlled drug delivery matrix for the oral administration of drugs. Hydrogels of **4** have been proven to be stable in fasted state

simulated gastric fluid (SGF) at a pH value of 1.6 at 37 °C over days, even though pepsin was present which is able to hydrolyze amide bonds. It seems that the amide bonds of the gelator are protected against enzymatic hydrolysis due to steric hindrance by the fiber formation and the bulky phenyl units in the side arms of the gelator. Furthermore, only about 9 % of the encapsulated model compound rhodamine B was released in SGF at 37 °C over ten days, indicating that it is possible to protect an encapsulated molecule from the acidic milieu of the stomach.

Contrary to the stability of the gel in fasted state SGF, it slowly dissolves in fasted state simulated intestinal fluid (SIF) at 37 °C. Although it is often stated that the complete intestinal tract is alkaline, the milieu of the upper small intestine, which is simulated here, has a pH value of 6.5 at the fasted state. Nevertheless, hydrogels of **4** dissolve within 72 h. Interestingly, the release of the encapsulated model compound is already completed within 48 h, supposedly because the superstructure of the gel is already dissolved at that time. Although this release rate is still too slow for a successful oral drug delivery system, the general dissolution and release behavior of gels of **4** in simulated gastro-intestinal fluids is promising. The release rate will probably be enhanced by the larger volume of SIF that is present in the gastro-intestinal tract, as well as the hydrodynamics of the digestive system. Furthermore, the increasing pH value in the proximal small intestine and the large intestine will additionally promote the dissolution of the gels. Moreover, by changing the volume, shape, and gelator concentration of the administered gel the dissolution and release behavior can be adjusted to fit the requirements of oral drug administration.

Concluding, the hydrogel system presented here showed promising results as a controllable drug delivery system for oral administration. Therefore, further tests should be conducted to promote the realization of a successful medical product. First of all, further release studies should be conducted with pharmaceutical active compounds under standard testing conditions that also simulate the hydrodynamics of the gastro-intestinal tract and the respective volumes of the fluids. Furthermore, it also would be interesting to test the gel stability and release behavior under fed-state conditions, as the administration of especially hydrophobic drugs in combination with food usually leads to higher resorption rates in the small intestine.

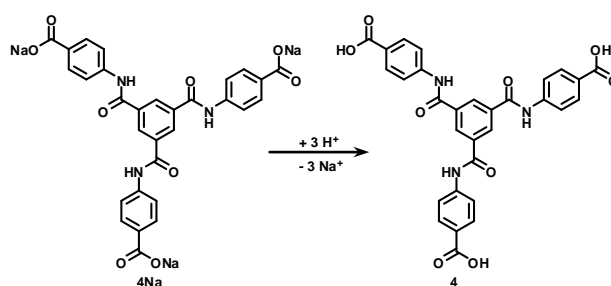
In chapter 3.3.3.4 it was shown that hydrogels of **4** are stable in most organic solvents and can therefore be transferred into organogels. This quality might be especially interesting for poorly water soluble drugs, as the drug can be dissolved in an organic solvent and subsequently be adsorbed at the gel surface. By exchanging the organic solvent again with

water, the gel is transferred back to a hydrogel and can be used as a drug delivery system in biological systems without the negative effect of an organic co-solvent.

Furthermore, it might be interesting to use hydrogels of **4** as template for the preparation of metal nanoparticles or clusters, as the gel itself consists of polycarboxylate-coated fibers. As carboxylate moieties are known to act as anchoring groups and to complex metal oxides and metal ions, the growth of nanoparticles within the gel network should be possible. Especially the incorporation of silver clusters is of interest, as they possess anti-inflammatory and antibacterial properties and are thought to be promising in applications, such as wound treatment, sensing, and catalytic nanoreactors.³⁸² In the literature only few low molecular weight hydrogelators are known that enable the formation of nanoparticles within the gel network.^{69,383,384}

6 “Electrogelation” – controlled formation of hydrogel films on conductive substrates

Electrochemistry is a useful tool for the application of multiple coatings on various substrates. In this chapter “*electrogelation*” processes, namely hydrogel film formation on conductive substrates *via* the electrolysis of water, and the resulting films are investigated in detail. Therefore, solutions of the pH-sensitive gelator sodium salt **4Na** are used. By the proton formation at the anode molecules of **4Na** are transformed to the carboxylic acid derivative **4** (Scheme 6.1).



Scheme 6.1: Transformation of the gelator sodium salt **4Na** to the carboxylic acid derivative **4**.

Using a 9-volt battery as power supply, an indium tin oxide (ITO)-covered glass substrate as anode and a stainless steel slide as counterelectrode, it can be shown in principle that hydrogel films of this hydrogelator system can be produced *via* electrogelation at a **4Na** concentration of only 1 g L^{-1} (Figure 6.1).

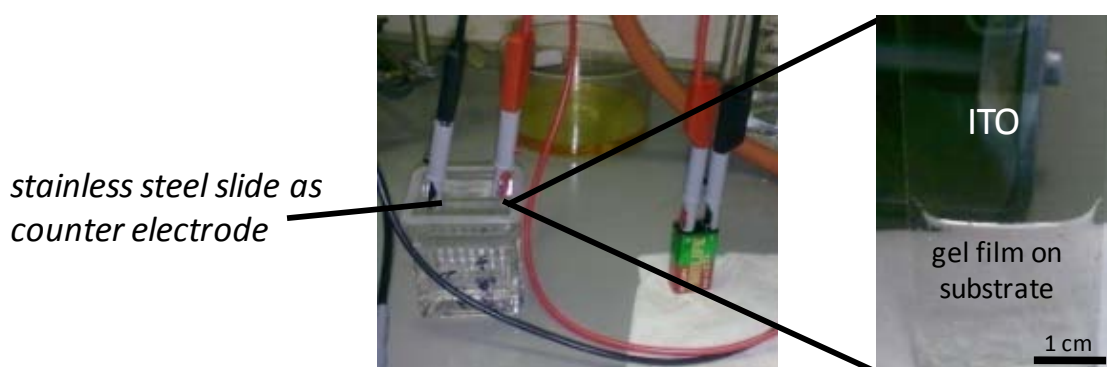


Figure 6.1: Optical image of the proof-of-principle experiment of the electrogelation process with a 9-volt battery.

In the following, the parameters that might influence the controlled formation of hydrogel films are discussed. These are in particular the distance between the working and the counter electrode, the applied voltage, the gelator **4Na** concentration, the concentration of sodium chloride (NaCl), which acted as background electrolyte, and the time for gelation. For the optimization of the electrogelation parameters a more defined set up was used, which is explained in detail in the following together with the underlying concept of this study.

6.1 Concept and set up

Using the electrolysis of water the pH value can be varied in the vicinity of the electrodes. While hydroxide ions (OH⁻) are formed at the cathode, protons (H⁺) are produced at the anode. As a consequence, the pH value in the aqueous solution close to the anode is reduced. This decrease of the pH value leads to a transfer of the gelator sodium salt **4Na** to the carboxylic acid derivative **4** that forms the actual hydrogel film.

In chapter 3.3.3.1 it was shown that the critical gelation concentration (cgc) of this system for the preparation of bulk gel samples is very low (2 g L⁻¹). As for the electrogelation process the cgc might be even lower, the conductivity of a **4Na** solution is expected to be very low and to even decrease upon the transformation to the uncharged gelator molecule. To exclude any influence that might arise due to such a variation of the conductivity during the experiments, NaCl is added to the gelator solution as background electrolyte. However, it should be noted that chloride ions in solution might be oxidized to chlorine when an electrical field is applied.³¹³



As chlorine is partially soluble in water, this leads to the *in situ* formation of hydrochloric acid and hypochlorous acid.



As hypochlorous acid (HClO) can act as an oxidizing agent, it might affect the surface of the electrodes. Therefore, the requirements for the substrate should not only include conductivity, but also sufficient stability against electrochemical and chemical oxidation.

For the optimization study of the electrogelation parameters, which is described in the following, a standard potentiostat was employed and set to potential-controlled mode for all performed experiments. While for the technical applications of the electrolysis of water, which are mainly to gain oxygen and hydrogen, usually a potential of 1.9 V is used, the formation of protons already occurs at a lower potential of about 1.2 V.

A three-electrode set up with a silver wire as pseudo-reference electrode is used for the experiments (Figure 6.2). Thus, a constant potential can be adjusted, which induces a controlled electrical field and a constant proton formation at the anode.

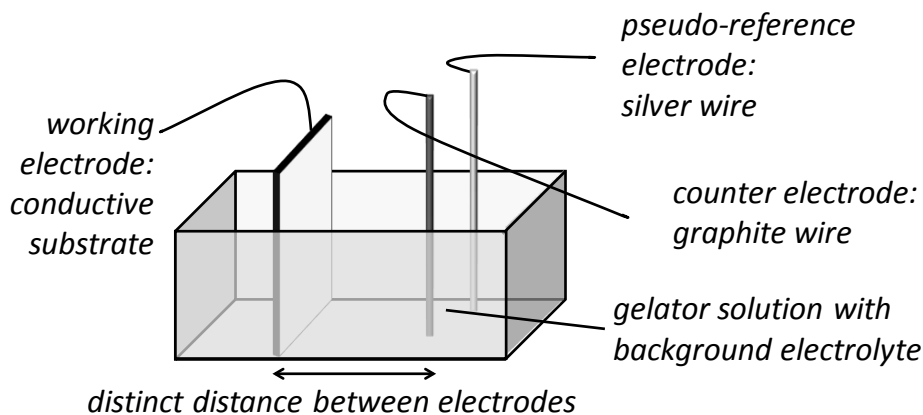


Figure 6.2: Schematic representation of the three-electrode set up for the electrogelation process with the hydrogelator system of **4**.

While a graphite wire is chosen as cathode or counter electrode, in principle every conductive substrate exhibiting enough stability might be used as anode or working electrode. Suitable materials might be oxidized ceramics, noble metals or any other material with a sufficiently high conductivity and oxidation potential. In this study the anode materials were chosen regarding the following aspects: i) stability in aqueous solutions with a pH range from slightly alkaline to basic; ii) stability against electrochemical oxidation at the applied potentials; iii) stability against chemical oxidation due to the *in situ* formation of chlorine and hypochlorous acid from the background electrolyte NaCl; and iv) the type of material. The surface roughness, the functionalization of the surface, and the presence of surface charges might alter the interactions between the gelator molecules and the surface. Thus, the type of material might promote or hinder the anchoring of molecules of **4** on the substrate.

Considering this, indium tin oxide (ITO)-covered as well as gold (Au)-covered glass slides seemed perfectly suitable for the hydrogel film formation *via* electrogelation. The ITO-covered substrates have the advantage of easy handling, strong attachment of the ITO-cover on the underlying glass slide, and transparency, which allows for characterization of the films *via* transmission UV-Vis and fluorescence spectroscopy. Furthermore, the functionalization of the surface with oxide moieties might be a good anchor for the carboxylic acid groups of the gelator. On the contrary, Au-covered substrates exhibit a lower surface roughness compared to ITO surfaces, which is especially important for atomic force microscopy (AFM) investigations. Taking these considerations into account, ITO-covered glass slides were used

for the screening of the electrogelation parameters of the dried films and Au-covered slides were used for more advanced AFM investigations. A rectangular chamber for thin layer chromatography (TLC) was employed in the electrogelation set up, as the working electrode could be easily fixed in a defined distance to the counter electrode (Figure 6.3).

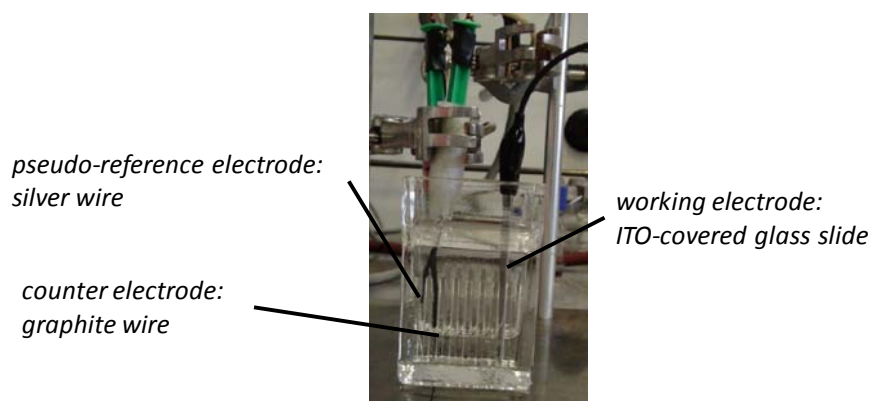


Figure 6.3: Custom-made three-electrode set up in a conventional TLC-chamber.

6.2 Hydrogel film formation and characterization of the dried films

Various parameters of the electrogelation process were systematically varied and their influence on the resulting hydrogel films was investigated. Besides finding the optimum distance between the working and the counter electrode, the influence of the applied potential, the concentration of the gelator sodium salt **4Na** and the background electrolyte NaCl as well as the gelation time were considered. For all performed experiments the three-electrode set up with 25 x 25 mm ITO-covered glass substrates as working electrode were used.

The characterization of the wet films is rather difficult, as the gel films dry quickly after the removal from the gelator solutions. Therefore, the thickness of the films could not be evaluated in wet state using a standard profilometer for height determination. To investigate the influences of the various parameters on the growth rate of the gel films, the thickness of the respective gel films was measured in dried state. However, the presence of NaCl in the gelation medium as background electrolyte leads to the formation of small salt crystals upon drying. To avoid the formation of these sodium chloride crystals, the substrates were dipped into desalted water directly after the gelation process, washing away the sodium and chloride ions. Besides determining the film thickness in dried state, UV-Vis and fluorescence spectroscopic measurements as well as scanning electron microscopy (SEM) studies were performed.

6.2.1 Influence of the distance between working and counter electrode

To evaluate the influence of the distance between the working and the counter electrode a solution of **4Na** (1 g L^{-1}) with the background electrolyte NaCl (10 mM) was prepared. The potential was set to 2.0 V for 10 min for three different films and the distances between the working electrodes were varied to be 1 cm, 2 cm, and 3 cm, respectively.

The evaluation of the influence of the distance between the electrodes is especially important as a graphite wire and not a graphite plate or sheet was used as counter electrode. Between two parallel orientated electrodes a homogeneous electrical field is present, that varies only in its strength depending on the distance between the two electrodes. However, if the counter electrode is rather a point or one-dimensional source, the homogeneity of the electrical field is also strongly influenced by the distance between the electrodes. The ITO-covered glass substrates were only partially submerged into the gelator solution so that a sharp edge between the hydrogel film and the uncovered substrate occurred at the liquid-air-interface. The optical images presented in Figure 6.4a-c show the front view of the obtained films in the wet state with the hydrogel films at the lower half of the substrate. At an electrode distance of 1 cm the submerged part of the substrate is only partially covered with the hydrogel film, while the samples obtained with an electrode distance of 2 cm and 3 cm seem to be equally homogeneous. This indicates that only above a certain distance of the electrodes a sufficient homogeneous electrical field is obtained that again results in a homogeneous formation of protons at the submerged substrate surface. To achieve a homogeneous hydrogel film formation, the distance between the working and the counter electrode was set to 3 cm for further experiments.

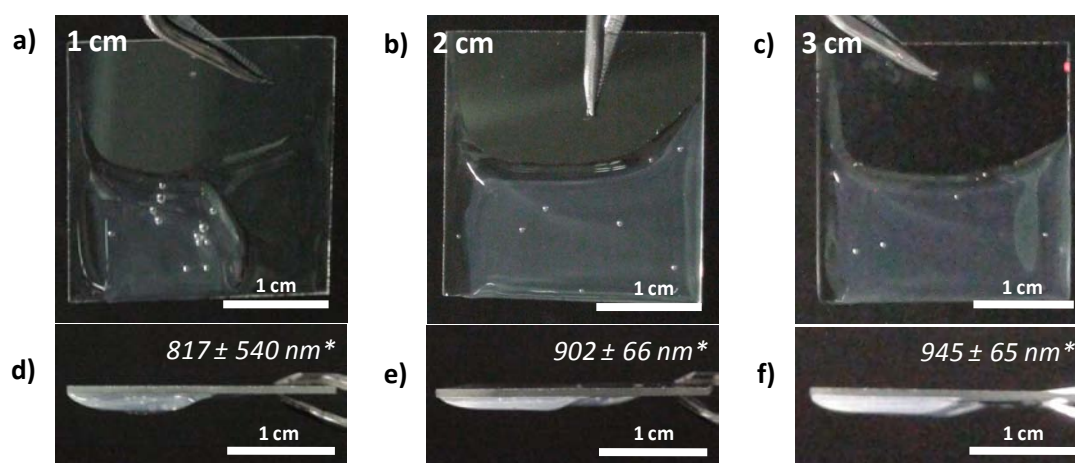


Figure 6.4: Optical images showing the front (a-c) and side view (d-f) of hydrogel films on ITO-covered glass substrates in the wet state, prepared *via* electrogelation using a distance between the counter and the working electrode of 1 cm (a and d), 2 cm (b and e), and 3 cm (c and f), an applied potential of 2.0 V, a **4Na** concentration of 1 g L^{-1} , a NaCl concentration of 10 mM, and a gelation time of 10 min. (*: The average thickness of the dried film was calculated from $n = 9$ measurements per film.)

The side view images of the wet hydrogel films on the glass substrates in Figure 6.4d-f show no film delamination under gravitational stress when inverting the samples reveal. Thus, the hydrogels are self-supporting and strongly bound to the substrate surface. The thicknesses of the wet films were estimated to be around 1.5 mm to 2.0 mm. The exact measurement of the film thicknesses in wet state using a standard profilometer was not possible as drying of the samples occurred very fast and falsified the results. Therefore, the hydrogel films were washed with desalted water and dried under ambient conditions before determining the film thicknesses at nine spots that were evenly distributed over the film. The calculated average thicknesses of the dried films as well as the respective standard deviations are given as inset in Figure 6.4d-f. For the hydrogel film prepared with an electrode distance of 1 cm the standard deviation is extremely high (817 ± 540 nm) due to the inhomogeneity of the film. This renders a comparison with the other films unreasonable. The average thicknesses of the dried films prepared with an electrode distance of either 2 cm or 3 cm are comparable within their standard deviations (902 ± 66 nm and 945 ± 67 nm, respectively). This leads to the assumption that the distance between the electrodes has only a negligible influence on the film thickness as long as a homogeneous electrical field is present in the solution which ensures homogeneous proton and hence film formation. However, it is important to note that the average thickness of the dried films is significantly lower than the estimated thickness in wet state. The loss of water upon drying the films is accompanied by a collapse of the network, which reduces the thickness by about three orders of magnitude.

It should be noted that in all three films small gas bubbles can be detected independent of the electrode distance (Figure 6.4). This might be explained by the applied potential of 2.0 V. In technical applications usually a potential of 1.9 V or higher is used to obtain oxygen and hydrogen from the electrolysis of water. Besides the formation of oxygen at the anode, the above mentioned electrochemical decomposition of the background electrolyte NaCl might additionally result in the formation of hydrogen (H_2) and chlorine (Cl_2). These gases are only soluble in water at low concentrations. It seems that at the applied potential of 2.0 V, the growth of the hydrogel film and the formation of gas is so accelerated that gas bubbles are trapped inside the gel film.

In the following, experiments with different applied potentials are presented to evaluate the influence of the potential on the hydrogel film formation *via* the electrolysis of water.

6.2.2 Influence of the applied potential

Three hydrogel film samples were prepared *via* electrogelation by applying potentials of 1.25 V, 1.5 V, and 2.0 V, respectively. Apart from that, the electrogelation parameters were

analogous to the ones described above with a **4Na** solution (1 g L^{-1}) containing NaCl (10 mM), a gelation time of 10 min, and an electrode distance of 3 cm.

As electrolysis of water and thus proton formation occurs above a potential of 1.2 V, electrogelation should in principle be observed for all three chosen applied potentials. This is confirmed by the optical images presented in Figure 6.5. While for the sample prepared with 1.25 V the film is barely visible (Figure 6.5a), at 1.5 V and 2.0 V significant film formation can be observed (Figure 6.5b and c). For films prepared with 1.25 V, 1.5 V, and 2.0 V a film thickness in dried state of $14 \pm 6 \text{ nm}$, $284 \pm 76 \text{ nm}$, and $947 \pm 65 \text{ nm}$ were obtained, respectively (see insets in Figure 6.5). The measurement of the film thicknesses in dried state confirmed that with increasing applied potential a significant increase of the film thickness can be realized, probably resulting from an increased proton formation rate.

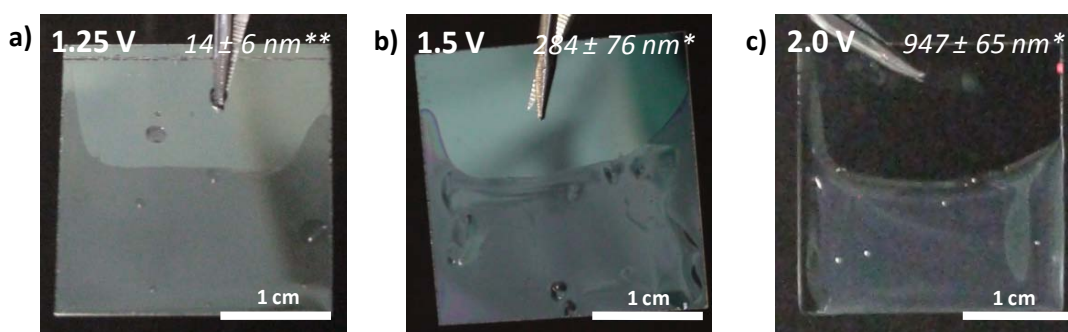


Figure 6.5: Optical images showing hydrogel films on ITO-covered glass substrates in the wet state, prepared *via* electrogelation using an applied potential of 1.25 V (a), 1.5 V (b), and 2.0 V (c), a **4Na** concentration of 1 g L^{-1} , a NaCl concentration of 10 mM, a gelation time of 10 min, and an electrode distance of 3 cm.

(*: The average thickness of the dried film was calculated from $n = 9$ and **: $n = 4$ measurements per film.)

When using a potential of 1.25 V, the thickness of the dried film could only be measured at four different spots with a standard profilometer due to the limited resolution of the used method and the morphology respectively surface roughness of the film. The average thicknesses for the dried films obtained by applying a potential of 1.5 V and 2.0 V were calculated using nine measured values. At an applied potential of 2.0 V gas bubbles are enclosed in the hydrogel film. This is not the case for films prepared with lower applied potentials which is assigned to be a combination of two complementary reasons: i) Only low amounts of gas are produced at the surface of the anode which are still completely soluble in the aqueous solution; and ii) the formation of the hydrogel network is too slow to entrap the produced gas.

To exclude any influence of the potential on the morphology of the hydrogel network a scanning electron microscopy (SEM) study was performed on the dried films. Typical SEM

images of the film prepared with an applied potential of 1.25 V are presented in Figure 6.6 showing a persistent, but very thin fiber network. It has to be noted that although a coherent network is formed, the substrate is not completely covered with gel fibers so that the underlying ITO cover is visible. The diameters of what seems to be single fibers range from about 20 nm to 30 nm, while they grow several microns in length scale. However, as these fibers intertwine, twist and converge to form larger bundles with diameter of about 70 nm and higher, it is difficult to determine the actual diameter and length of the underlying structures. Nevertheless, the measured thickness of the dried film of about 14 ± 6 nm seems to correspond to the diameter of a single fiber. These findings are in good accordance with the morphologies observed for bulk gel samples presented in chapter 3.3.2.

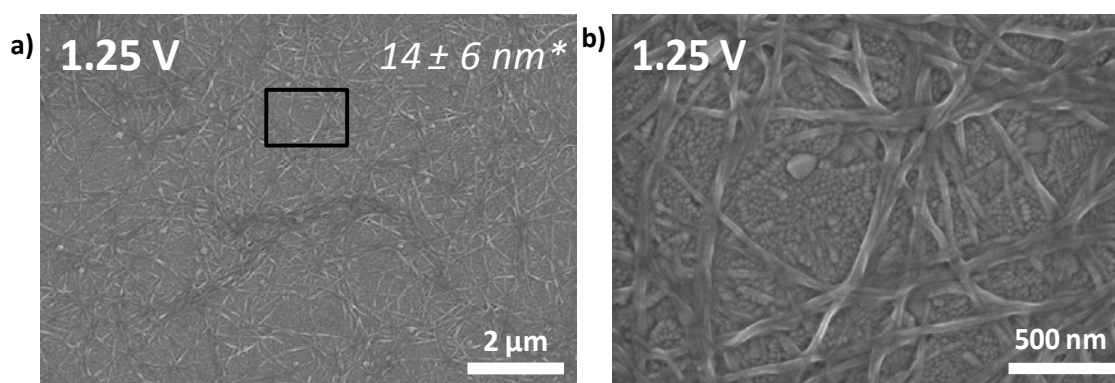


Figure 6.6: Typical SEM images of a dried hydrogel film on a ITO-covered glass substrate, prepared *via* electrogelation using an applied potential of 1.25 V, a **4Na** concentration of 1 g L^{-1} , a NaCl concentration of 10 mM, a gelation time of 10 min, and an electrode distance of 3 cm. Note: The black rectangle in a) marks the magnified region which is shown in b).

(*: The average thickness of the dried film was calculated from $n = 4$ measurements per film.)

The SEM images of gel films prepared by applying a potential of 1.5 V show a dense fiber network (Figure 6.7).

Single fibers in the range of 20 nm to 30 nm can be found that entangle to form superstructures similar to those observed in films prepared with 1.25 V. Although no gas bubbles could be observed on a macroscopic scale, in the SEM images small circular holes with diameters in the range of 100 nm to 150 nm can be observed (indicated by black arrows in Figure 6.7). These pores might be the result of gas transport processes from the anode to the interface of the hydrogel and the gelator solution.

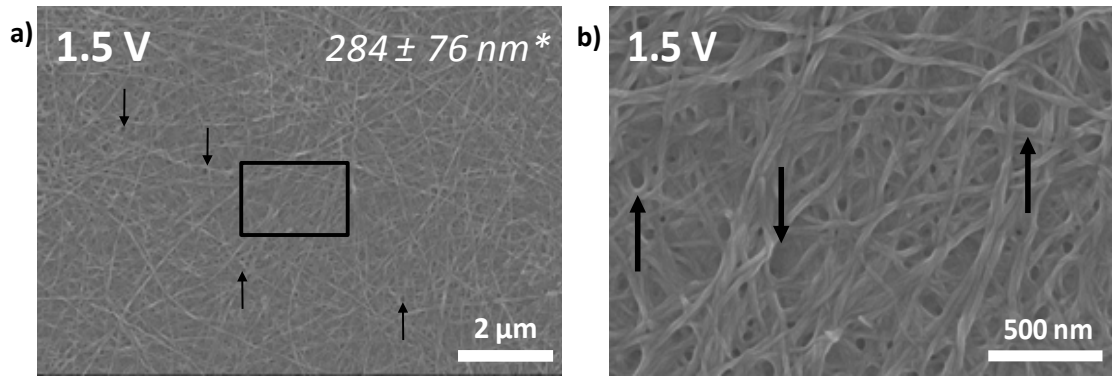


Figure 6.7: Typical SEM images of a dried hydrogel film on a ITO-covered glass substrate, prepared *via* electrogelation using an applied potential of 1.5 V, a **4Na** concentration of 1 g L^{-1} , a NaCl concentration of 10 mM, a gelation time of 10 min, and an electron distance of 3 cm. Note: The black rectangle in a) marks the magnified region which is shown in b), while the arrows indicate circular channels. (*: The average thickness of the dried film was calculated from $n = 9$ measurements per film.)

SEM images of films prepared with an applied potential of 2.0 V show a fiber network very similar to the one obtained from films prepared with 1.5 V in respect to the diameters of single fibers and the formation of fiber bundles (Figure 6.8).

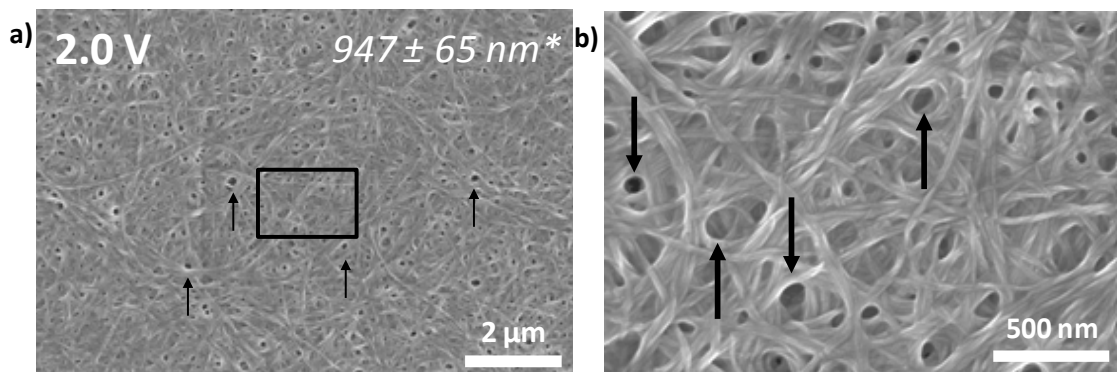


Figure 6.8: Typical SEM images of a dried hydrogel film on a ITO-covered glass substrate, prepared *via* electrogelation using an applied potential of 2.0 V, a **4Na** concentration of 1 g L^{-1} , a NaCl concentration of 10 mM, a gelation time of 10 min, and an electrode distance of 3 cm. Note: The black rectangle in a) marks the magnified region which is shown in b), while the arrows indicate circular channels. (*: The average thickness of the dried film was calculated from $n = 9$ measurements per film.)

However, the hydrogel film prepared with 2.0 V seems to be more porous due to the presence of more circular holes in the range of 50 nm to 150 nm. Since the gas formation is highly increased during electrogelation at a potential of 2.0 V, these findings support the assumption that the pores arise from the gas transport through the film and act as some kind of gas channel. Nevertheless, one should keep in mind that the hydrogel film collapses upon drying due to the loss of water. This leads to a significant decrease of the film thickness and might also influence the morphology and especially the porosity of the fiber network.

The UV-Vis and photoluminescence (PL) spectra obtained from the dried hydrogel films prepared with increasing applied potentials show an increase in optical density (O.D.) and PL intensity, respectively (Figure 6.9a and b). The respective maximum of the O.D. of the films can be found at about 310 nm. This is within the range of the absorbance maximum of about 306 nm found for the films of **4** prepared from DMSO (chapter 4.1.1). At an applied potential of 2.0 V the limit of the UV-Vis set up led to an erratic spectra at high optical densities which makes the evaluation of the maximum difficult. However, a red shift of the tail of the absorbance spectra with increasing applied voltage during film preparation can be observed.

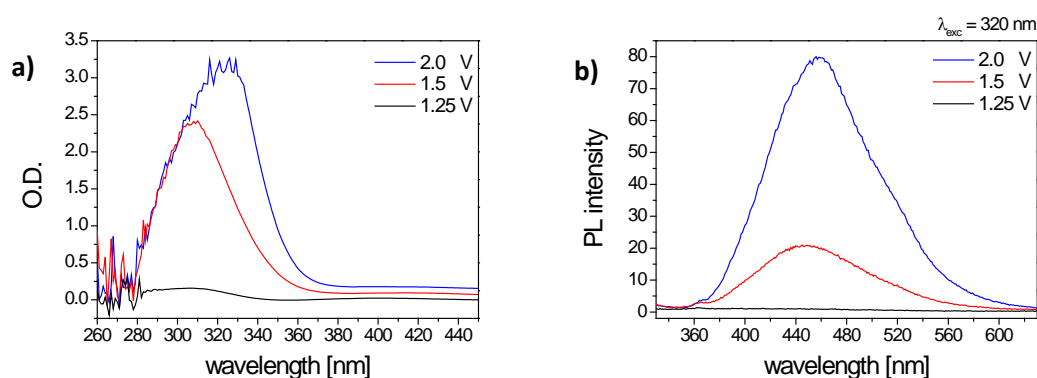


Figure 6.9: a) UV-Vis spectra and b) PL spectra of dried hydrogel films prepared *via* electrogelation using an applied potential of 1.25 V, 1.5 V, and 2.0 V, respectively, a **4Na** concentration of 1 g L^{-1} , a NaCl concentration of 10 mM, a gelation time of 10 min, and an electrode distance of 3 cm.

To avoid the presence of a harmonic overtone in the PL spectra of the films, as observed for films of **4** in chapter 4.1.2, the dried hydrogel films were excited at $\lambda_{exc} = 320$ nm. Due to the low absorbance observed for films prepared with 1.25 V, no PL intensity could be detected with the used PL set up. For the two other films an increase in PL intensity can be observed with increasing applied potential, which probably correlates to the increased optical densities of the films. The respective maxima of the PL intensity were found at about 450 nm and 455 nm for films prepared with 1.5 V and 2.0 V, respectively. As already discussed in chapter 4, a more rigid and ordered arrangement of molecules of **4** might lead to a blueshift of the respective PL spectrum. The blue shift of the respective PL maxima with decreasing applied potential might therefore indicate that at a lower applied potential the formation of the chromophore is more ordered and molecules are stronger rigidified. This is very reasonable, as lower applied potential results in a lower proton formation rate at the anode and thus slower gel formation. This should give the molecules more time to align in a higher ordered fashion.

Further tests were carried out using an applied potential of 1.5 V to avoid the inclusion of gas bubbles within the gel film during electrogelation, while simultaneously obtaining a sufficiently coverage of the substrate within 10 min.

6.2.3 Influence of the gelator concentration

In chapter 3.3.3.1, the critical gelation concentration (cgc) of bulk gel samples was determined to be 2.0 g L^{-1} . Above this concentration of **4Na** in solution, a stable and self-supporting fiber network, which is able to resist gravitational flow upon inversion of the test tube, is formed within the whole volume of the sample.

The hydrogel film samples prepared *via* electrogelation were prepared with a **4Na** concentration of only 1 g L^{-1} as described above. This clearly lies below the cgc of bulk gel samples of **4**. It can be explained by the fact that for the hydrogel film preparation not the whole volume of the gelator solution is solidified. The transfer from the water soluble sodium salt **4Na** to the gelator molecule **4** only occurs in the vicinity of the anode leading to a deposition of **4** on the substrate. Due to diffusion processes, the supply of **4Na** molecules at the anode from the solution is assured. The effective **4Na** concentration at the anode is therefore not only dependent on the initial **4Na** concentration in solution, but also on the diffusion of **4Na**. Thus, it might be assumed that there is no cgc for the electrogelation process, as long as the diffusion rate of **4Na** is high enough.

To test this hypothesis and to evaluate how the gelator concentration influences hydrogel film formation, samples with four different initial gelator concentrations were prepared using an applied potential of 1.5 V, a NaCl concentration of 10 mM, a gelation time of 10 min, and a distance between the working and the counter electrode of 3 cm, respectively.

In Figure 6.10 the optical images for the films prepared with an initial **4Na** concentration of 0.1 g L^{-1} , 0.5 g L^{-1} , 1.0 g L^{-1} , and 2.5 g L^{-1} are presented.

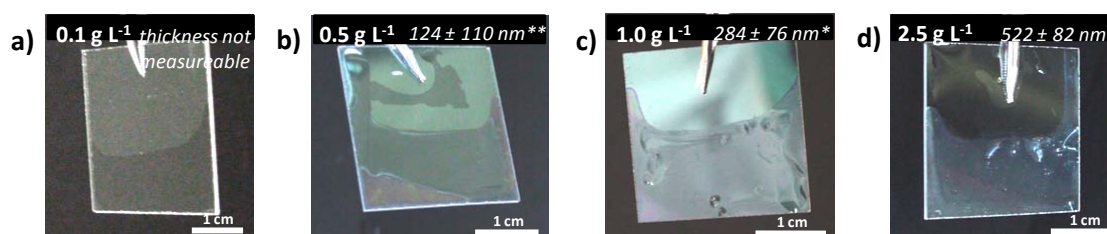


Figure 6.10: Optical images showing hydrogel films on ITO-covered glass substrates in the wet state, prepared *via* electrogelation using a **4Na** concentration of 0.1 g L^{-1} (a), 0.5 g L^{-1} (b), 1.0 g L^{-1} (c), and 2.5 g L^{-1} (d), an applied potential of 1.5 V, a NaCl concentration of 10 mM, a gelation time of 10 min, and an electrode distance of 3 cm.

(*: The average thickness of the dried film was calculated from $n = 9$ and **: $n = 5$ measurements per film.)

The inclusion of gas bubbles in the gel layer could not be observed for any of the samples indicating that the gas formation of the anode is indeed mainly dependent on the applied potential.

At a **4Na** concentration of 0.1 g L^{-1} no film formation could be observed macroscopically (Figure 6.10a). Consequently, also the measurement of the film thickness in dried state gave no results. This leads to the conclusion that under the applied conditions no gel film is formed and that there is a cgc for the electrogelation process using the described set up. By increasing the initial **4Na** concentration to 0.5 g L^{-1} hydrogel films are formed on the substrate. However, the obtained film is barely visible in the optical images in the wet state (Figure 6.10b). The average thickness of the dried sample was determined to be $124 \pm 110 \text{ nm}$. As the standard deviation is nearly as high as the average value itself, it seems that the dried hydrogel film is rather inhomogeneously distributed on the substrate with thick and thin parts. Moreover, it should be noted that the thickness could only be measured at five different spots, which is probably due to this high height deviation.

For the samples prepared with a **4Na** concentration of 1.0 g L^{-1} and 2.5 g L^{-1} , respectively, no significant differences between the wet hydrogel films could be observed in the optical images (Figure 6.10c and d). The average thicknesses of the dried films calculated from nine measured values are given as inset in the optical images and show a significant increase of the film thickness in dried state with increasing **4Na** concentration. Comparing the samples obtained using 0.5 g L^{-1} and 1.0 g L^{-1} , there seems to be a linear dependence of the dried film thickness and the gelator concentration. However, this assumption is not supported when also considering the sample prepared with 2.5 g L^{-1} . If a linear dependence would be valid, an average thickness of about 680 nm in dried state would be expected.

SEM studies on the dried hydrogel films prepared with different initial **4Na** concentrations were performed to give further insight into the influence of the gelator concentration on the morphology of the resulting dried films. For the sample prepared with a **4Na** concentration of only 0.1 g L^{-1} most SEM images show only the bare substrate surface and no fiber network or film formation. Only in a few SEM images a partial coverage of the submerged substrate with organic material can be observed (Figure 6.11).

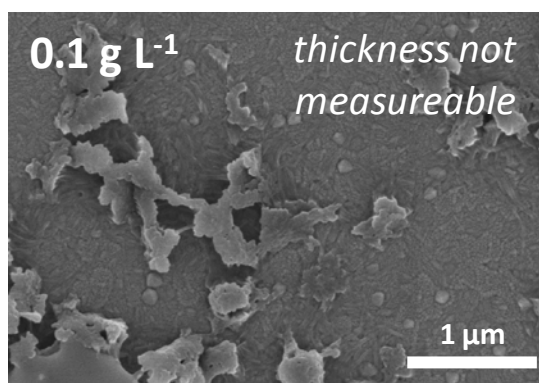


Figure 6.11: SEM image of a dried ITO-covered glass substrate treated with the electrogelation process using a **4Na** concentration of 0.1 g L^{-1} , an applied potential of 1.5 V, a NaCl concentration of 10 mM, a gelation time of 10 min, and an electrode distance of 3 cm. Note: A typical SEM image would only display the ITO-covered substrate surface and is therefore not shown here.

This also supports the assumption that there is a *cgc* for the electrogelation process under the applied conditions. The few deposited aggregates are in the range of several hundreds of nanometers and no obvious anisotropy of the structures can be observed. For samples prepared using a **4Na** concentration of 1 g L^{-1} at a rather low applied voltage of 1.25 V, single fibers and fiber bundles could be observed on the substrate surface (Figure 6.6, chapter 6.2.2). The resulting morphology at a **4Na** concentration of 0.1 g L^{-1} and an applied potential of 1.5 V does not resemble that morphology of single fibers and fiber bundles at all, as only rather large clusters can be observed. These findings indicate that a low proton formation rate (1.25 V, 1 g L^{-1} of **4Na**) still enables the formation of a fiber network, while at a low gelator concentration (1.5 V, 0.1 g L^{-1} of **4Na**) the limited diffusion of **4Na** to the surface of the anode hinders the formation of ordered aggregates. As the diffusion of protons is much faster in aqueous media than the diffusion of organic molecules, such as **4Na** or **4**, it might be even possible that the observed aggregates were formed in the solution and deposited on the substrate, when removing the substrate from the solution.

SEM imaging of dried hydrogel films prepared with a **4Na** concentration of 0.5 g L^{-1} revealed that there is no characteristic SEM image for the sample due to a rather inhomogeneous distribution of the hydrogel fibers. While some parts of the submerged substrate are covered with a network of fibers that consists of several layers (Figure 6.12a), only single fiber strands are deposited on other parts of the substrate (Figure 6.12b).

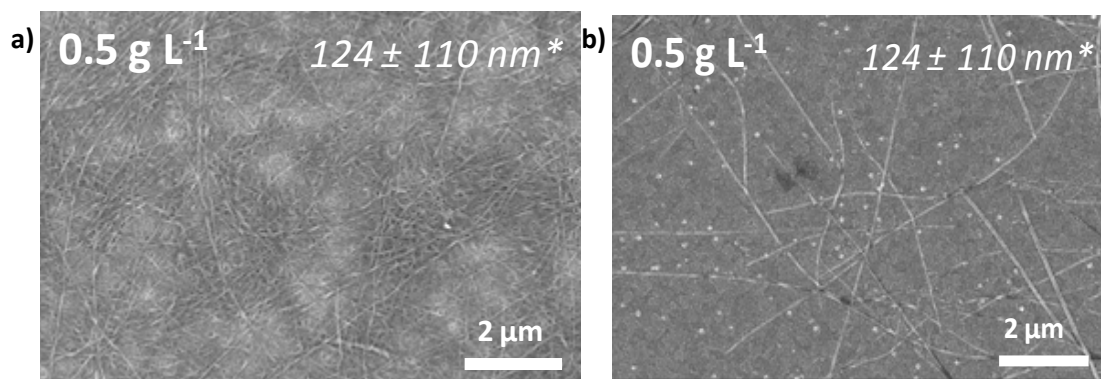


Figure 6.12: SEM images of a dried hydrogel film on an ITO-covered glass substrate, prepared *via* electrogelation with a **4Na** concentration of 0.5 g L^{-1} , an applied potential of 1.5 V, a NaCl concentration of 10 mM, a gelation time of 10 min, and an electrode distance of 3 cm.

(*: The average thickness of the dried film was calculated from $n = 5$ measurements per film.)

This lateral inhomogeneity of the fiber deposition clearly explains the difficulties when measuring the thicknesses of the dried film and the large resulting deviation of the average thickness. Both fiber networks consist of twisted and entangled fibers that form bundles and superstructures in the range of 50 nm to about 120 nm, whereas the diameters of the underlying anisotropic structures are in the range of 20 nm to 30 nm. Thus, apart from the inhomogeneities, the hydrogel network is built up similar to the networks produced using a **4Na** concentration of 1 g L^{-1} as already discussed in chapter 6.2.2 (Figure 6.7).

It was shown that using a **4Na** concentration of 1 g L^{-1} and an applied potential of 1.5 V homogeneous hydrogel films can be prepared over the whole submerged substrate surface. It thus can be stated that for the electrogelation process 1 g L^{-1} is the critical gelation concentration of the gelator sodium salt **4Na**. However, one has to keep in mind that this cgc is only valid for the described conditions, such as the three-electrode set up, the applied potential of 1.5 V, the NaCl concentration of 10 mM, the gelation time of 10 min, and the electrode distance of 3 cm. As shown in chapter 6.2.2, the applied potential significantly influences the growth rate of the gel film. This makes it reasonable to assume that at a higher applied potential the cgc for electrogelation might be lower than 1.0 g L^{-1} .

Further increase of the **4Na** concentration to 2.5 g L^{-1} results in a dense network of fibers with morphologies comparable to the one obtained for samples with 1.0 g L^{-1} (Figure 6.13). Solely the average thickness of the dried gel film is increased compared to the samples with lower initial gelator sodium salt concentrations. This can be explained by the fact that at a higher initial **4Na** concentration, diffusion processes are less significant and thus are not rate-limiting.

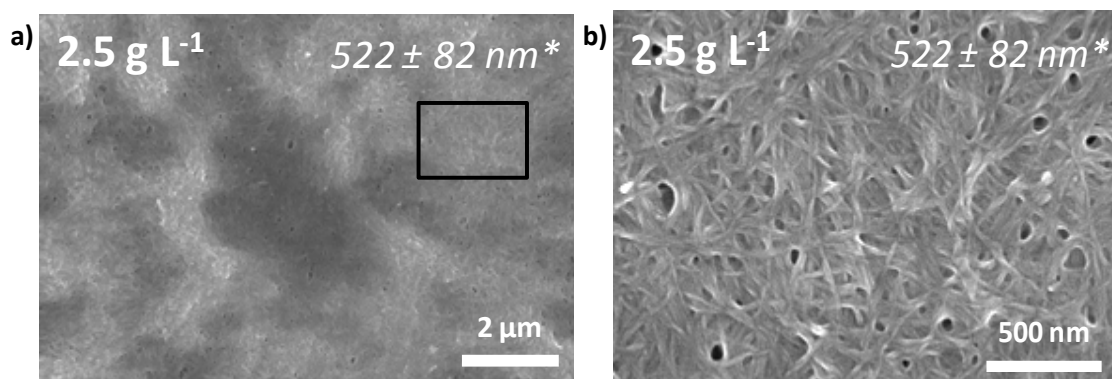


Figure 6.13: Typical SEM images of a dried hydrogel film on a ITO-covered glass substrate, prepared *via* electrogelation with a **4Na** concentration of 2.5 g L^{-1} , an applied potential of 1.5 V, a NaCl concentration of 10 mM, a gelation time of 10 min, and an electrode distance of 3 cm. Note: The black rectangle in a) marks the magnified region which is shown in b).

(*: The average thickness of the dried film was calculated from $n = 9$ measurements per film.)

The increasing average thickness of the dried hydrogel films with increasing initial **4Na** concentration can also be detected using UV-Vis and PL spectroscopy (Figure 6.14a and b). For samples prepared with 0.1 g L^{-1} of **4Na**, no absorbance between 260 nm and 450 nm can be detected with a standard UV-Vis spectrometer. Therefore, no PL can be measured upon excitation with $\lambda_{\text{exc}} = 320 \text{ nm}$. Samples prepared with 0.5 g L^{-1} of **4Na** show slight absorbance with a maximum at about 303 nm. However, the respective absorbance is too low to enable PL that is detectable with a standard photometer upon excitation with $\lambda_{\text{exc}} = 320 \text{ nm}$.

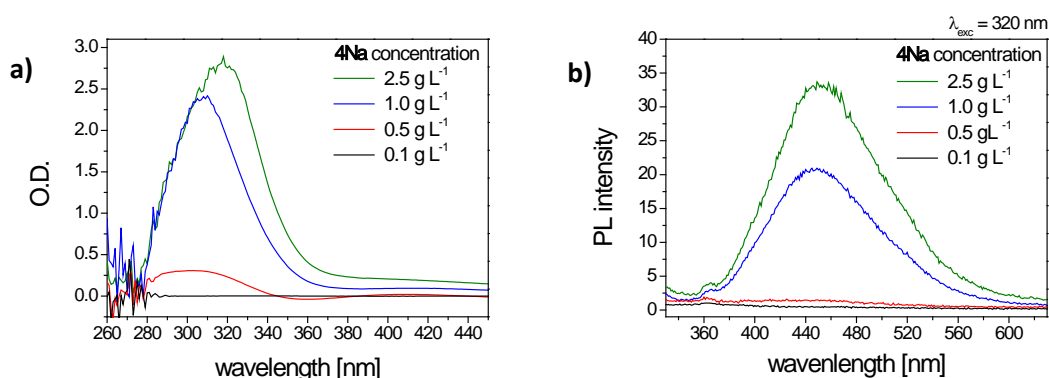


Figure 6.14: a) UV-Vis spectra and b) PL spectra of dried hydrogel films prepared *via* electrogelation using a **4Na** concentration of 0.1 g L^{-1} , 0.5 g L^{-1} , 1 g L^{-1} , and 2.5 g L^{-1} , respectively, an applied potential of 1.5 V, a NaCl concentration of 10 mM, a gelation time of 10 min, and an electrode distance of 3 cm.

With increasing initial **4Na** concentration, the respective O.D. of the dried films as well as the PL intensity increases. While for the absorbance spectra a red shift of the respective maxima from about 303 nm to about 308 nm and 318 nm can be observed with increasing **4Na**

concentration, the respective maxima of the PL spectra of the different films can all be found at a wavelength of about 450 nm.

These findings are in good agreement with the results obtained from the spectroscopic studies of the bulk hydrogel samples discussed in chapter 4 and of the hydrogel films prepared *via* the electrogelation process using different applied potentials (chapter 6.2.2).

For the further optimization of the electrogelation parameters a **4Na** concentration of 1 g L^{-1} was chosen as standard, as this is the lowest concentration at which homogeneous hydrogel films are formed under the applied condition.

6.2.4 Influence of the concentration of the background electrolyte

As shown above, only low amounts of the gelator sodium salt **4Na** are necessary for the electrogelation process. Already an initial **4Na** concentration of 1 g L^{-1} leads to the formation of homogeneous hydrogel films under the applied conditions. It must be noted that this concentration is further reduced during electrogelation due to the transformation of **4Na** into its protonated form **4**, which is then deposited on the anode as hydrogel network. Due to these facts, the conductivity of the initial **4Na** solution is very low and should further decrease during the gelation process. Therefore, sodium chloride was added to the gelator sodium salt solution as background electrolyte. In the electrogelation experiments described above, the NaCl content was set to 10 mM to ensure a stable conductivity in the gelator solution during the whole electrogelation process. To evaluate the influence of the sodium chloride content on the electrogelation process, hydrogel films were prepared *via* electrogelation using a NaCl concentration of 10 mM, 100 mM, 250 mM, and 500 mM, respectively.

The hydrogel films were prepared applying the standard gelation parameters, such as a **4Na** concentration of 1 g L^{-1} , an applied voltage of 1.5 V, a gelation time of 10 min, and an electrode distance of 3 cm. The gel films were immediately washed with desalted water after gelation to remove the NaCl ions before drying and to prevent NaCl crystal formation. The optical images of the wet hydrogel films prepared using NaCl concentrations of 100 mM, 250 mM, and 500 mM did not significantly differ from the sample prepared in the presence of 10 mM of NaCl (Figure 6.10c, chapter 6.2.3). Therefore, they are not shown here.

The respective average thicknesses of the obtained gel films were determined in dried state using nine measurement spots per film. The average values as well as the respective standard deviations are displayed in Table 6.1.

Table 6.1: Thickness of the dried films in dependence of the NaCl concentration

| NaCl concentration [mM] | thickness of dried film ¹ [nm] |
|-------------------------|---|
| 10 | 284 ± 76 |
| 100 | 647 ± 221 |
| 250 | 525 ± 66 |
| 500 | 682 ± 231 |

¹ average of 9 measurements

With increasing amount of the background electrolyte in the gelator solution from 10 mM to 100 mM, the average thickness of the dried film as well as the standard deviation increases significantly. Interestingly, these values are in good accordance with the average thickness and standard deviation of films prepared with a NaCl content of 500 mM, while the values slightly decrease for samples prepared with 250 mM of NaCl. It seems that the NaCl content in the initial gelator solution has only a minor effect on the dried film thickness, if the concentration is 100 mM or higher.

The rather large fluctuations of the standard deviations in dependence of the background electrolyte concentration might indicate differences in the roughness of the hydrogel film surface. Therefore, SEM studies of gel films prepared *via* electrogelation were conducted to further evaluate the influence of the background electrolyte on the morphology.

A typical SEM image of a dried hydrogel film prepared with a NaCl concentration of 10 mM was discussed earlier in this work (Figure 6.7, chapter 6.2.2). It shows a dense network formed by twisted and entangled fibers. The underlying anisotropic structures have diameters in the range of 20 nm to 30 nm.

In a typical SEM image of a dried gel film prepared using a background electrolyte concentration of 100 mM also underlying structures with diameters in the range of 20 nm to 30 nm are observed (Figure 6.15). These fibers entangle and intertwine as well, which leads to the formation of bundles with diameters in the range of 50 nm to 120 nm. However, the resulting morphology of this superstructure is quite different and much more porous compared to the morphology obtained using a NaCl content of 10 mM. Instead of a dense network, pores in the range of several hundreds of nanometers are also present. It might be suspected that this porosity originates from the enhanced conductivity of the gelator solution and thus the faster proton transport from the anode into the gelator solution.

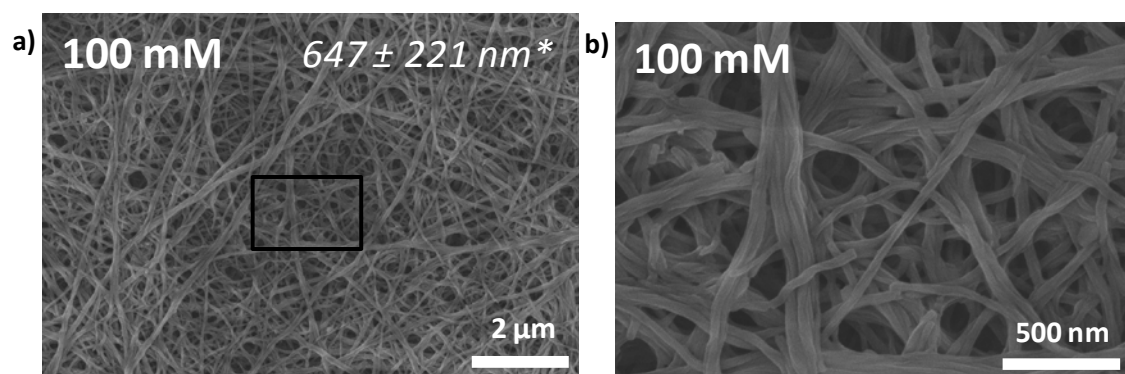


Figure 6.15: Typical SEM images of a dried hydrogel film on a ITO-covered glass substrate, prepared *via* electrogelation with a NaCl concentration of 100 mM, an applied potential of 1.5 V, a **4Na** concentration of 1 g L^{-1} , a gelation time of 10 min, and an electrode distance of 3 cm. Note: The black rectangle in a) marks the magnified region which is shown in b).

(*: The average thickness of the dried film was calculated from $n = 9$ measurements per film.)

For the washed and dried samples prepared with an even higher amount of the background electrolyte, such as 250 mM and 500 mM, also porous morphologies can be observed (Figure 6.16 and Figure 6.17). A direct correlation between the amount of background electrolyte and the pore size in dried state could not be found. While the pore size significantly increases with increasing the amount of NaCl from 10 mM to 100 mM, which is an increase by an order of magnitude, the change in the pore size is rather negligible, when changing the NaCl content from 100 mM to 250 mM or 500 mM.

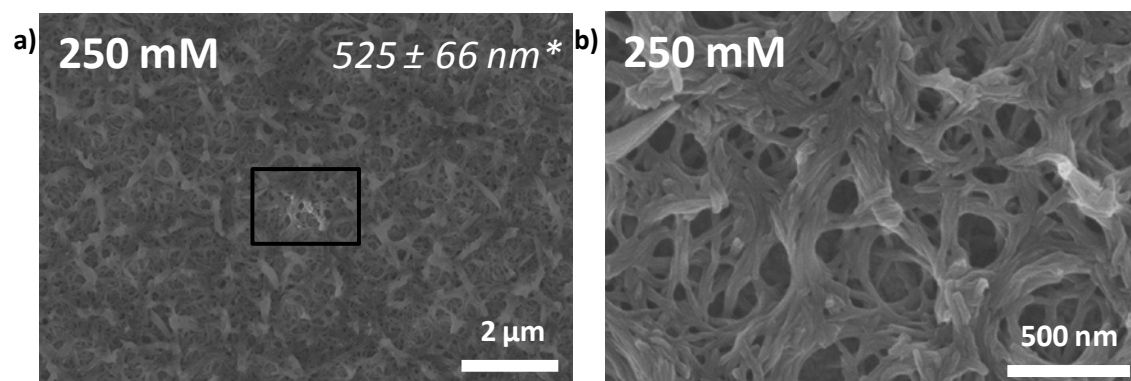


Figure 6.16: Typical SEM images of a dried hydrogel film on a ITO-covered glass substrate, prepared *via* electrogelation with a NaCl concentration of 250 mM, an applied potential of 1.5 V, a **4Na** concentration of 1 g L^{-1} , a gelation time of 10 min, and an electrode distance of 3 cm. Note: The black rectangle in a) marks the magnified region which is shown in b).

(*: The average thickness of the dried film was calculated from $n = 9$ measurements per film.)

Although the porosity as well as the determined average thickness is not significantly influenced when the NaCl content is 100 mM or higher, slight differences in the morphology of the different films as well as the respective standard deviations can be determined.

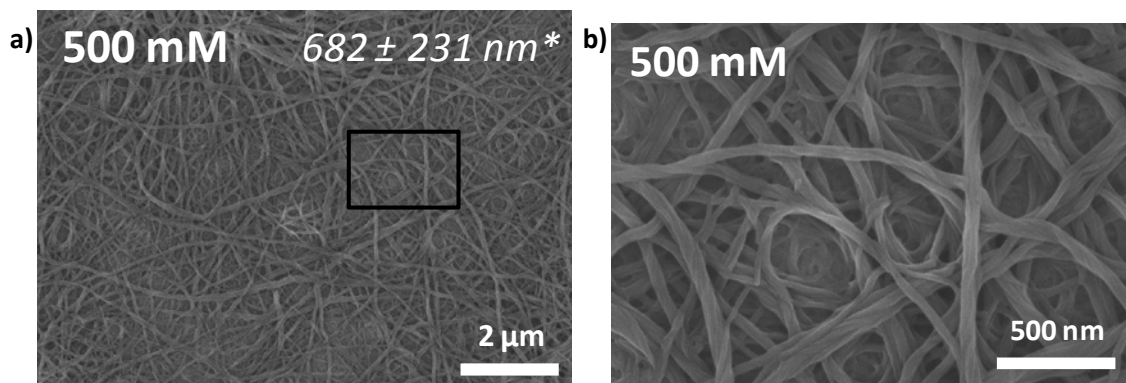


Figure 6.17: Typical SEM images of a dried hydrogel film on a ITO-covered glass substrate, prepared *via* electrogelation with a NaCl concentration of 500 mM, an applied potential of 1.5 V, a **4Na** concentration of 1 g L⁻¹, a gelation time of 10 min, and a distance between the working and the counter electrode of 3 cm. Note: The black rectangle in a) marks the magnified region which is shown in b).

(*: The average thickness of the dried film was calculated from n = 9 measurements per film.)

These differences might arise from the washing procedure and the subsequent drying step after electrogelation. One might imagine that if the gel film partially dried before the washing step, the formation of NaCl crystals in the pores of the hydrogels prevents a complete collapse of the gel fibers and therefore, the formation of a dense network. However, if the gel is thoroughly washed before any drying might have occurred, the gel fibers collapse as also observed for bulk samples leading to a thinner and denser hydrogel film. The investigated gel films in the study presented here were immediately washed after gelation preventing partial drying of the film and thus NaCl crystal formation.

However, to fully eliminate any artifacts in the SEM images due to partial drying of the respective films before the washing procedure, further tests varying the time between the removal of the substrate from the gelator solution and the washing procedure should be performed.

As the spectroscopic studies (UV-Vis and PL spectroscopy) of the dried films prepared with different initial NaCl concentrations did not show any significant influence of the background electrolyte on the respective spectra, they are not displayed in this work.

Summarizing, the formation of the fiber network itself as well as the found diameters of the underlying structures and the fiber bundles seem not to be influenced by the amount of NaCl present in the gelator solution. The pore size significantly increases for samples prepared with a NaCl concentration of 100 mM or higher compared to the sample prepared with only 10 mM.

6.2.5 Influence of the gelation time

In this chapter, the influence of the gelation time on the hydrogel films prepared *via* the electrolysis of water is investigated. For these experiments the optimized parameters found previously in this study, such as an applied potential of 1.5 V, a gelator sodium salt

concentration of 1 g L^{-1} of **4Na**, a NaCl background electrolyte concentration of 10 mM, and a distance of the electrodes of 3 cm, were used.

The optical images of wet hydrogel samples obtained with gelation times of 1 min, 2 min, 5 min, and 10 min indicate an increase in the film thickness with increasing gelation time (Figure 6.18). The calculated average film thicknesses in the dried state given in Figure 6.18 support this observation.

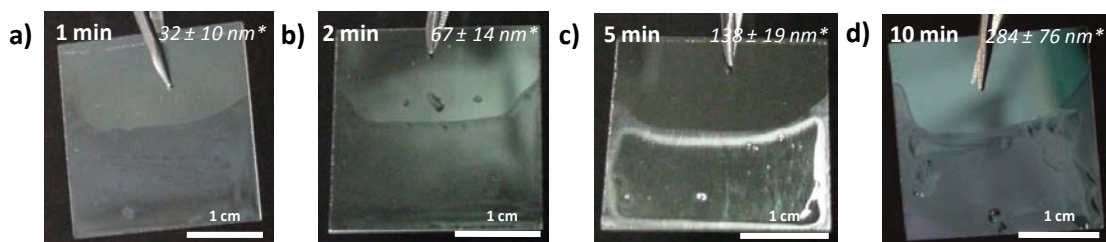


Figure 6.18: Optical images showing hydrogel films on ITO-covered glass substrates in the wet state, prepared *via* electrogelation using a gelation time of 1 min (a), 2 min (b), 5 min (c), and 10 min (d), an applied potential of 1.5 V, a **4Na** concentration of 1 g L^{-1} , a NaCl concentration of 10 mM, and an electrode distance of 3 cm.

(*: The average thickness of the dried film was calculated from $n = 9$ measurements per film.)

With increasing gelation time not only the calculated average thickness in dried state, but also the respective standard deviations increase significantly. In Figure 6.19, the average thicknesses in dried state are plotted versus the gelation time.

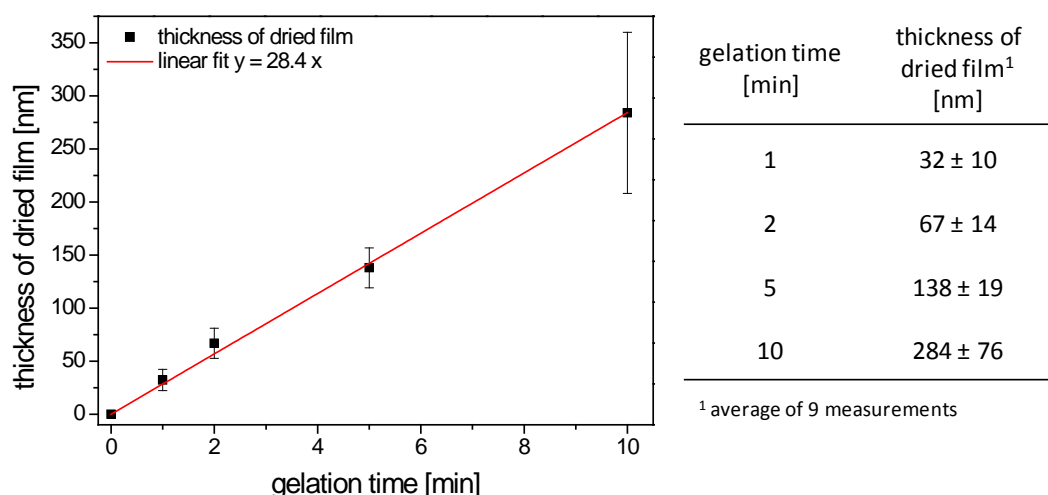


Figure 6.19: Thickness of the dried films (average of nine measurements) plotted versus the gelation time with a linear regression curve with a correlation constant of $r^2 = 0.9983$.

The data can be fitted well to a linear regression curve with the intercept set to zero. The resulting regression equation is $y = 28.4 x$ with a correlation constant of $r^2 = 0.9983$. However, it is important to note that this equation only describes the relation between the gelation time and the film thickness in dried state. It is known that the gel network collapses upon drying by about three orders of magnitude (see chapter 6.2.1), but there are no indications that this collapse proceeds linearly. Therefore, no conclusions can be drawn regarding the growth rate in the hydrated or wet state.

Considering, that the electrogelation method is dependent on the diffusion of the formed protons and the gelator sodium salt molecules **4Na**, one would expect that with increasing film thickness the film growth is hindered. The formation of a thick and dense fiber network at the anode should limit the transport of the protons from the anode surface to the interface of the film with the gelator solution. Furthermore, with proceeding gelation the **4Na** concentration in the gelator sodium salt solution decreases resulting in a lower film growth rate with increasing gelation time.

However, the linear fit describes the found data very well. This might be explained by the fact that the collapse of the films upon drying counteracts the expected non-linear film growth. Furthermore, at gelation times of 10 min or less the **4Na** concentration might be still sufficiently high and the respective film thicknesses might not be high enough to hinder the diffusion.

To exclude any influence of the drying process and the corresponding collapse of the gel network, the thickness of gel films is determined *in situ* in cooperation with the group of Prof. Georg Papastavrou from the department of Physical Chemistry II of the University of Bayreuth. The combination of an electrochemical atomic force microscopy (AFM) cell and colloidal probe AFM techniques additionally enables the *in situ* determination of the mechanical properties of the films on Au-covered substrates without any artifacts from transferring or drying the samples. A manuscript including these results is currently prepared for publication.

Typical SEM images of the washed and dried hydrogel films after an applied gelation time of 1 min and 2 min, respectively, are displayed in Figure 6.20. While after only 1 min the surface of the substrate is only partially covered with fibers, after 2 min already a dense fiber network similar to the one observed after 10 min can be seen (compare with Figure 6.7). The respective diameters of underlying fibers are in the range of about 20 nm to 30 nm for both samples.

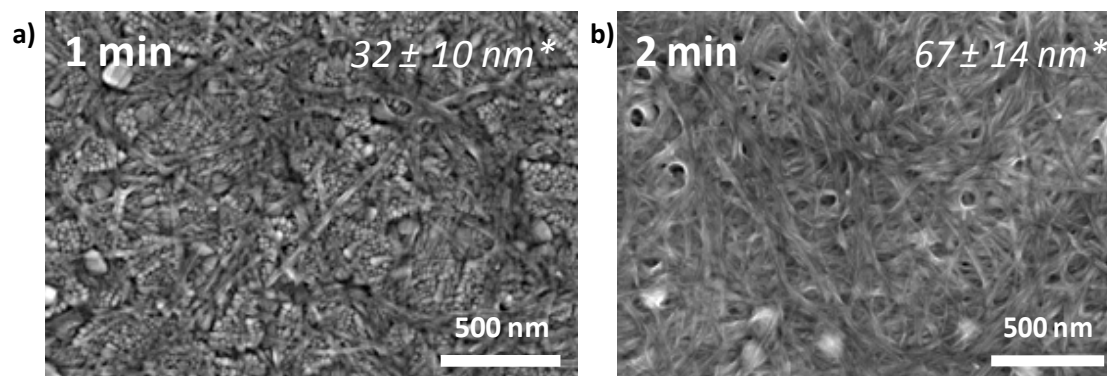


Figure 6.20: Typical SEM images of a dried hydrogel film on a ITO-covered glass substrate, prepared *via* electrogelation using a gelation time of 1 min (a) and 2 min (b), an applied potential of 1.5 V, a **4Na** concentration of 1 g L^{-1} , a NaCl concentration of 10 mM, and an electrode distance of 3 cm. (*: The average thickness of the dried film was calculated from $n = 9$ measurements per film.)

The washed and dried hydrogel samples were also investigated using UV-Vis and PL spectroscopy (Figure 6.21a and b).

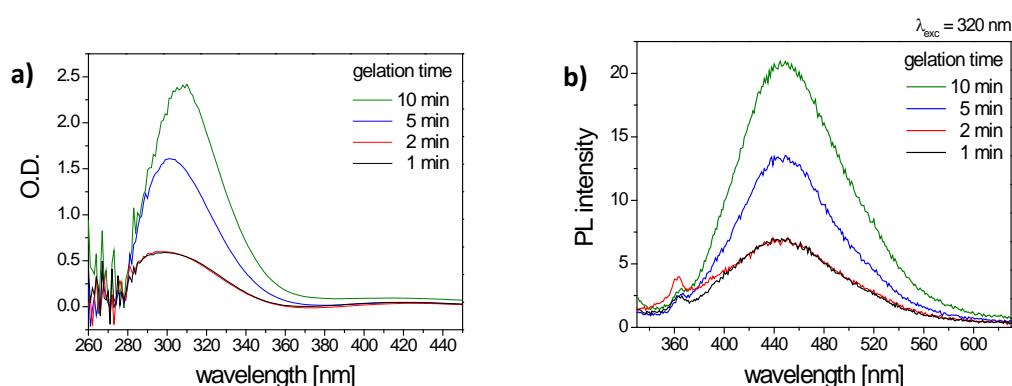


Figure 6.21: a) UV-Vis spectra and b) PL spectra of dried hydrogel films, prepared *via* electrogelation using a gelation time of 1 min, 2 min, 5 min, and 10 min, respectively, an applied potential of 1.5 V, a **4Na** concentration of 1 g L^{-1} , a NaCl concentration of 10 mM, and an electrode distance of 3 cm.

While for the samples with a gelation time of 1 min and 2 min, the respective spectra were very similar, for longer gelation times an increase of the respective intensities with gelation time could be observed. This corresponds very well to the findings presented earlier that indicate an increasing absorbance and PL intensity with increasing film thickness. However, it seems that the resolution of these spectroscopic investigations is too low to distinguish between the thickness of the film after 1 min (about 32 nm) and after 2 min (about 67 nm). The respective maxima of the absorbance spectra are between wavelengths of about 300 nm to 310 nm, which is in good accordance with the results from dried hydrogel films of **4** prepared *via* electrogelation with different initial **4Na** concentrations (Figure 6.14) and prepared by drying a DMSO solution of **4** (chapter 4). With increasing gelation time, a slight

redshift of the maximum and the tail at higher wavelength occurs. These properties are similar to the ones for films prepared with different applied potentials (Figure 6.9, chapter 6.2.2).

The PL spectra were recorded using an excitation wavelength of $\lambda_{\text{exc}} = 320$ nm and show a maximum at about 450 nm, respectively. The intensities of the spectra coincide very well with the intensities of the respective absorbance spectra. Thus, these findings are in good agreement with the luminescence properties of dried hydrogel films of **4** discussed earlier.

Summarizing, the gelation time is an excellent parameter to precisely control the thickness of the gel film without changing the morphology and porosity of the fiber network.

6.3 Tunable gel film properties *via* electrogelation and possible fields of application

In the previous chapters, it could be shown that several external parameters influence the formation of hydrogel films of **4** on conductive substrates using the change of the pH value *via* the electrolysis of water. Thus, the gel film properties can be precisely controlled by tuning these parameters.

The average thickness of the dried gel films is thereby influenced by the applied potential, the gelator **4Na** concentration, and the gelation time.

As long as the applied potential exceeds the minimum potential for the electrolysis of water of about 1.2 V, it directly influences the proton formation rate and thus the “speed” of gelation. The higher the applied potential, the faster the gelation proceeds. This, however, leads to undesirable side-effects, such as the inclusion of gas bubbles within the gel film at applied potentials of about 2.0 V.

As the electrogelation can only proceed as long as gelator molecules diffuse to the interface between the anode with the gel film and the solution, the gelator sodium salt (**4Na**) concentration determines the growth rate of the hydrogel film as well. Above the critical gelation concentration (cgc) of 0.5 g L^{-1} continuous and homogeneous hydrogel networks can be obtained. This is remarkable considering the cgc of bulk gel samples of 2 g L^{-1} . Above 1 g L^{-1} , with increasing **4Na** concentration the influence of the gelator concentration on the thickness in dried state slightly decreases.

For the gelation time a linear dependence on the dried film thickness was found. However, this might be different for thicknesses in wet state or for gelation times higher than 10 min. using the applied conditions.

The morphology of the samples can be evaluated regarding two major criteria: the formation of a fiber network with underlying anisotropic structures, and the porosity of the dried films.

Apart from the sample with a very low **4Na** concentration (0.1 g L^{-1}), the arrangement of the fiber network was not significantly altered by any of the applied parameters. Even the diameters of the underlying structures were found to be in the range of 20 nm to 30 nm for all prepared samples. These findings are very reasonable considering that the molecular structure of the gelator molecule is the same and thus also the functional moieties responsible for spontaneous self-assembly into supramolecular aggregates.

The analysis of the porosity of the films is rather difficult as only dried samples can be investigated by SEM studies. Due to drying effects and the collapse of the gel network upon the loss of water, it is not possible to deduce any reliable information about the porosity in the wet state from the images in the dried state. Nevertheless, porous films in dried state can be obtained either by increasing the applied potential or by increasing the concentration of the background electrolyte. When using a potential of 2.0 V, few pores are formed probably due to the gas formation upon the electrolysis of water and the electrochemical decomposition of NaCl to hydrogen and chlorine gas. Highly porous films can be obtained by increasing the NaCl concentration in the gelator solution above 100 mM. However, it is not clear why these pores are formed, as there seems to be no direct correlation between the number and size of the pores and the NaCl concentration. As the pores are not circular as observed for the ones obtained by applying an enhanced potential, it is reasonable to assume that the formation of gas from the electrochemical decomposition of NaCl plays a negligible role. It is suspected that either the enhanced conductivity of the solution leads to a faster proton transport and thus the formation of a more porous network or that drying effects occur. It might be possible that the formation of NaCl crystals upon drying prevents the complete collapse of the gel. However, as all samples were washed immediately in desalted water after the removal from the gelator solution, this should not be the case in the study presented here.

While parameters, such as the applied potential, the **4Na** concentration, the concentration of the background electrolyte, and the gelation time influence the formation of the gel network significantly, the distance between the electrodes has a rather negligible influence on the thickness of the gel film. Due to the application of a wire as counter electrode, solely for low distances the homogeneity of the electrical field and thus the gel formation is influenced.

The spectroscopic investigations, *i. e.* UV-Vis and photoluminescence (PL) spectroscopy show a dependence of the respective maximum intensity with the film thickness. The absorbance maxima of the films can be found at about 300 nm to 310 nm, which is consistent with the findings of films of **4** prepared from a DMSO solution (chapter 4.1.1, Figure 4.4).

Furthermore, a redshift of the maxima and the tails at higher wavelength can be observed with increasing film thickness.

The analysis of the PL spectra shows that the maxima of the dried films are located between 450 nm and 455 nm. The blueshift of the PL maxima is associated with a decrease of the applied potential and thus slower gel formation. Moreover, it indicates a more ordered structure of the underlying chromophore. These results are in good accordance with the findings of the PL study on wet bulk hydrogel samples and the corresponding theoretical calculations presented in chapter 4.

In the study presented here, only the properties in dried state were investigated. In cooperation with the group of Prof. Georg Papastavrou (Physical Chemistry II) of the University of Bayreuth, also *in situ* studies regarding the thickness of the wet gel films and the respective mechanical properties were performed using AFM techniques. The combination of an electrochemical cell with the AFM set up enabled to interrupt the electrogelation process at distinct times and to evaluate the thickness and the Young's modulus without any drying effects or transfer of the sample out of the gelator solution. As standard conditions for these experiments Au-covered glass substrates, applied potentials of 1.25 V, **4Na** concentrations of 1 g L^{-1} and background electrolyte concentration of 10 mM were used. By adjusting the gelation time the hydrogel film thickness in wet state can be precisely controlled down to the nm-level. These *in situ* tests for gelation times up to 2 min seem to indicate that in wet state no linear dependence between the film thickness and gelation time is valid, but a decrease of the growth rate occurs for longer gelation times. Independent of the gelation time or respectively the thickness of the gel film, the Young's modulus for wet gel films prepared by electrogelation was found to be about 640 kPa, which is in the range of Young's moduli determined for polymer and multi-layered polyelectrolyte films. These findings are even more remarkable considering that solely so-called "weak" and non-covalent interactions are present in the formed gel network of **4**. Upon drying, the Young's modulus increases four orders of magnitude to about 7 GPa. Compared to the mechanical properties of bulk gel samples prepared *via* the diffusion of HCl vapor, gelator concentration of about 50 g L^{-1} are necessary to achieve such high mechanical stability in wet state. The results of these investigations are currently summarized as full paper planned for publication.

Summarizing, many parameters can be adjusted to precisely control the formation of thin hydrogel films of **4** *via* the electrogelation method and thus tune the properties of the resulting films. This makes this technique in combination with the hydrogel system ideal for several fields of applications. As hydrogel films are only formed on the conductive substrates, patterned hydrogel films can be easily prepared by using patterned substrates. The

photoluminescence properties of the gelator system presented in chapter 4 and the biocompatibility and high adsorption potential discussed in chapter 5 additionally open up possible applications in sensing and biomedical active coatings. The unique combination of possible processing techniques and gel properties encourages further studies in various scientific fields.

7 Summary

In this thesis the pH-sensitive aggregation behavior of low molecular weight (lmw) compounds based on the 1,3,5-benzene tricarboxamide (BTA) self-assembly motif is investigated in aqueous systems to elucidate their potential to form supramolecular hydrogels.

The content of this thesis covers four main subjects, which are illustrated in Figure 7.1: the investigation of the *self-assembly behavior of pH-sensitive BTAs in aqueous solutions* to identify new lmw hydrogelators (highlighted in green); the *spectroscopic and theoretical study¹ of a supramolecular chromophore* formed via the self-assembly of a BTA derivative (highlighted in yellow); the investigation of the *adsorption and release behavior of a supramolecular hydrogel* for the application in controlled drug delivery (highlighted in red); and the study of the *“electrogelation” method for the formation of defined supramolecular hydrogel films* on conductive substrates (highlighted in blue).

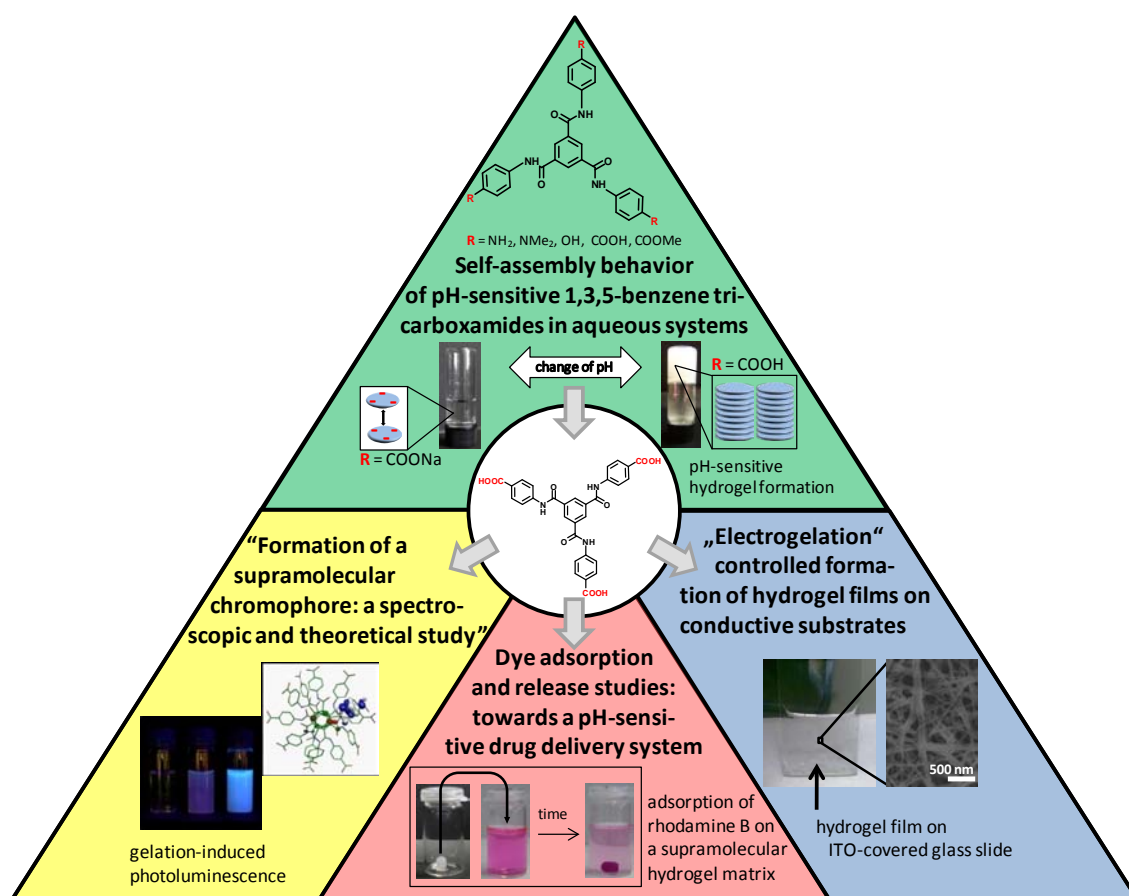


Figure 7.1: Illustration of the four different chapters of this thesis.

¹ The theoretical calculations were performed in cooperation with Rodrigo Q. Albuquerque and are published in *Soft Matter*.¹⁰²

Self-assembly behavior of pH-sensitive 1,3,5-benzene tricarboxamides in aqueous solutions

In the first subject of this thesis a structural concept was developed that enables the *pH-sensitive aggregation of BTA derivatives (1,3,5-benzene tricarboxamides) in aqueous media*. This concept includes the hydrophobic shielding of the BTA core with the amino moieties from water molecules and the introduction of pH-sensitive groups in the periphery of each side arm that can either act as Bronsted bases or acids (Figure 7.2). Four BTA derivatives with pH-sensitive peripheral substituents and a non pH-sensitive reference compound were selected and studied in this thesis.

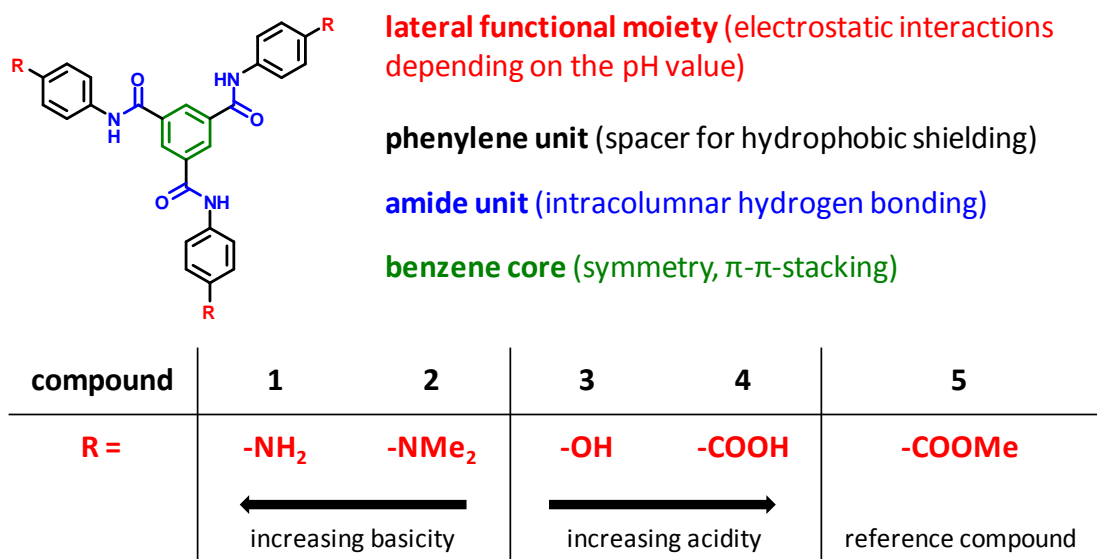


Figure 7.2: Structural concept and chemical structures of the BTA-based compounds investigated regarding their pH-sensitive aggregation in aqueous solutions.

In case of the amino derivative **1**, no pH-sensitive self-assembly could be observed. Compounds **2**, **3**, and **4** showed *pH-sensitive aggregation and dissolution behavior* at different pH values. Their pH-sensitive aggregation behavior was investigated in detail revealing that compounds **2** and **3** do form superstructures but do not form stable gels. However, compound **4** forms stable supramolecular hydrogels by transforming the respective sodium salt **4Na** into the carboxylic acid derivative **4**. The reference compound **5**, which cannot be charged by protonation or deprotonation of the lateral groups, did consequently not show any pH-sensitivity.

As compound **4** shows supramolecular hydrogel formation upon change of pH, this thesis focuses on this BTA derivative. *Different gelation methods* were tested for compound **4** and the *properties of the resulting gels* were compared. These preparation methods include: i) gel

formation by addition of acidic acid solutions; ii) diffusion of hydrochloric acid gas; and iii) the addition of glucono-delta-lactone (GdL), a slow proton donating agent.

Upon addition of aqueous acid solutions only inhomogeneous gels are obtained. Thus, this method was not further used in this thesis. The diffusion of hydrochloric acid gas or the addition of GdL to **4Na** solutions leads to macroscopically homogenous hydrogels. For both gelation methods, stable gels can be obtained above a critical gelation concentration (cgc) of 2 g L^{-1} . Even at this low gelator concentration the hydrogels are thermal stable up to the boiling point of water without any signs of gel destruction or melting. The mechanical stability of the gels was investigated using indentation measurements revealing that gels prepared by diffusion of hydrochloric acid gas show a gradient of the mechanical stability with a more stable layer at the gel/air interface. Gels prepared using the hydrolysis of GdL show a homogeneous mechanical stability. The mechanical stability increased with increasing gelator concentration. Thus, the addition of GdL is a highly potent gelation method for the preparation of homogeneous and stable gels of **4**. These gels are also stable against dissolution in different aqueous acidic solutions and in various organic solvents miscible with water. In addition by a complete exchange of the solvent, the hydrogel can be transformed to a stable organogel.

Electron microscopy techniques were performed at different stages of the gel formation as well as on dried hydrogels to propose a *structural model for the pH-sensitive formation of the supramolecular hydrogel of 4*. While the negatively charged molecules of the gelator salt **4Na** are molecularly dissolved due to electrostatic repulsion, upon decrease of the pH value the anisotropic aggregation is assumed to occur stepwise. It is proposed that at the beginning of the gelation process partially charged molecules aggregate to form supramolecular stacks with evenly distributed surface charges which seem to form helical superstructures upon further protonation.

Formation of a supramolecular chromophore: a spectroscopic and theoretical study

In the second section of this thesis the spectroscopic properties of the hydrogelator system **4/4Na** are discussed in detail revealing that aggregation-induced emission enhancement (AIEE) in water occurs. In combination with theoretical calculations performed by Prof. Rodrigo Q. Albuquerque these findings were used to verify the proposed columnar aggregation model. The major results of this chapter are published in *Soft Matter*.¹⁰²

Neither the carboxylic acid derivative **4** nor the respective sodium salt **4Na** show photoluminescence in solution, while films and supramolecular hydrogels of **4** show a blue luminescence upon irradiation with UV-light. Thus, this system clearly shows *aggregation and gelation-induced emission* enhancement. As the photoluminescence (PL) spectra of the drop-casted, dried film and the wet hydrogel prepared with GdL are very similar, it is assumed that

the chromophoric system in both samples is the same. The emission in the bulk and gel state is assigned to a π^* -n or π^* - π -transition with a charge transfer (CT) character.

Time-dependent PL studies during gel formation with GdL showed that a red shift of the PL maxima can be observed with increasing gelation time. In combination with *theoretical calculations* it could be shown that at the beginning of the gelation the maximum of the PL spectrum can be assigned to stacked dimers. The red shift of the PL maxima with increasing gelation time can thus be explained by the growth of molecular stacks. The theoretical calculations and optimized geometries of tetrameric stacks of **4** complement the experimental findings very well and support the proposed structural model at the early stage of aggregation.

Dye adsorption and release studies: towards a pH-sensitive supramolecular drug delivery system

While the first and the second section of this work mainly deal with fundamental studies regarding the supramolecular self-assembly and hydrogel formation, the third section focuses on the possible application of the pH-sensitive hydrogelator **4**. Detailed adsorption and release studies elucidate the potential of this hydrogel system for the application as biomaterial in controlled drug delivery, particularly using oral administration. Furthermore, the possible use of the hydrogels as adsorption material for dyes in waste water treatment is discussed.

It is demonstrated that hydrogels of **4** fulfill the *basic requirements* for matrix materials in drug release applications, such as biocompatibility and non-toxicity,¹ responsiveness in a physiological relevant pH range, sufficient mechanical and thermal stability, and a high specific surface area.

The *concentration and time-dependent adsorption* of the model dye rhodamine B on preformed hydrogels of **4** was intensely studied. The dye solutions are effectively decolorized demonstrating that the hydrogel has a high adsorption potential even at very low rhodamine B concentrations. This renders this system particularly interesting for applications in waste water treatment. The *adsorption data* fit both the Langmuir and the Freundlich *isothermal model* indicating that the adsorption is favorable, but at high dye concentrations a less favorable adsorption can be expected. The adsorption rates are dependent on the initial rhodamine B concentration and are very low with complete adsorption within several days. Thus, for the application of the hydrogel in waste water treatment fixed-bed systems should be used, which allow longer adsorption times. The *adsorption kinetics* can be described with the pseudo 2nd order kinetic model indicating that chemisorption, *i.e.* the actual adsorption step, is the rate limiting process.

¹ The biocompatibility and non-toxicity tests were performed by the Hans-Knöll Institute in Jena.

The *stability of the formed dye-gelator complexes* was tested at different temperatures revealing that the dye molecules are strongly bound to the gel surface. Although the release kinetics is enhanced at elevated temperatures, over 90 % of the adsorbed rhodamine B remains in the gel independent of the applied temperature.

Besides the adsorption of a dye after gelation, also the *in situ* adsorption during the formation of the gel is an interesting loading technique. *Hydrogels of 4* can be *formed in the presence of rhodamine B* as guest molecules. Strong interactions between the dye and the gelator molecules enable the preparation of stable hydrogels if the dye to gelator ratio is 0.5 or below. This suggests that rhodamine B is not only adsorbed on the gel surface, but is also incorporated between the fibers. Thus, the *loading* of the hydrogels with rhodamine B is *more efficient and faster* when preparing the gels in presence of the dye instead of adsorbing the dye on preformed gels. Dependent on the initial amount of encapsulated rhodamine B, 70 % to 95 % of the dye remains in the gel even after 10 days in water. The release is very slow and follows the generalized Fickian model within the given boundary conditions. This suggests that only dye molecules that are still dissolved in the aqueous phase are washed out of the gel, while molecules that are adsorbed or incorporated remain within the gel network.

For the application of a matrix material in controlled drug delivery systems, the release of the model compound must be triggered by specific physiological conditions. Therefore, the *dissolution and release behavior* of pure hydrogels of **4** and hydrogels formed in the presence of rhodamine B were monitored *in biologically relevant media*. For these tests buffer solutions with different pH values and compositions were chosen, such as phosphate buffered saline (PBS, pH = 7.4), simulated body fluid (SBF, pH = 7.4), fasted state simulated gastric fluid (SGF, pH = 1.6), and fasted state simulated intestinal fluid (SIF, pH = 6.5).

PBS and SBF are important biological fluids for cell culturing and tissue engineering. At room temperature their slightly alkaline pH value causes hydrogel dissolution and consequently complete release of the dye, for PBS within 24 h and for SBF within 8 h. By increasing the temperature of SBF to body temperature (37 °C), the dissolution of the gel and the release of the encapsulated dye can be completed within 6 h. For an application of the gel as scaffold material in tissue engineering the dissolution is too fast, as stabilities in the range of several weeks are required. Thus, further stabilization of the gel would be required.

Interestingly, the hydrogels do not dissolve in SGF at 37 °C, although pepsin, an enzyme that can hydrolyze amide units and might destroy the gelator molecule, was present. Only low amounts of the dye are released within 10 days supporting the assumption that this hydrogel system might be used to protect labile drugs from the acidic milieu in the stomach. The pH-sensitivity of the hydrogelator allows for stable gels in strong acidic solutions, while they

dissolve above a pH value of 6.2. Thus, dissolution of the gels can be observed in fasted state SIF within 72 h at body temperature. The dye is already completely released within 48 h, probably due to the dissolution of the entire superstructures in the gel. The stability of the gels in SGF in combination with their release behavior in SIF renders this hydrogelator a promising matrix material for controlled drug delivery applications with oral administration.

Electrogelation – controlled formation of hydrogel films on conductive substrates

The fourth section of this thesis focuses on the use of a unique gelation method, called “electrogelation”, to prepare defined hydrogel films of **4** on conductive substrates. This gelation technique utilizes the decrease of the pH value in the vicinity of an anode due to the electrolysis of water.

For the systematic screening of the electrogelation parameters, an *experimental set up was developed* consisting of three-electrodes. Indium tin oxide (ITO)-covered glass substrates were used as working electrode, while a graphene wire acted as counter electrode, and a silver wire as pseudo-reference electrode.

For the used set up *important parameters* to control the electrogelation process were selected and systematically varied: i) electrode distance; ii) applied potential; iii) gelator concentration; iv) concentration of the background electrolyte; and v) gelation time. The influence of these parameters on the gel properties in dried state, such as the dried film thickness, the morphology and the spectroscopic properties, was investigated in detail. This study revealed that changing one gelation parameter can influence several properties and that one specific property, such as the film thickness in dried state, is controlled by several parameters. Thus, using the findings of this study, the electrogelation technique provides a simple method to prepare defined gel films by optimizing these parameters.

The gelation technique has not only potential for the controlled preparation of hydrogel coatings of compound **4**, but might also be transferred to other pH-sensitive low molecular weight hydrogelators. In cooperation with Prof. Georg Papastavrou and his group (Physical Chemistry II, University of Bayreuth) the mechanical properties of hydrogel films prepared by electrogelation are currently investigated *in situ* by atomic force microscopy techniques.

Summarizing, the results of the four sections of this thesis reveal that particularly the BTA derivative **4** is a highly interesting low molecular weight compound for the self-assembly in aqueous media and the formation of supramolecular hydrogels. Due to the unique combination of properties, the presented pH-sensitive hydrogelator is not only interesting for fundamental research studies, but might also find application in sensors based on the photoluminescence effects, as an adsorption material, as a matrix material for the controlled delivery of drugs, and for the preparation of functional coatings on conductive substrates.

8 Zusammenfassung

Der Fokus dieser Arbeit liegt auf der Untersuchung von pH-sensitiven, niedermolekularen 1,3,5-Benzoltricarboxamiden (BTAs) und ihrer Fähigkeit supramolekulare Hydrogele zu bilden.

Die Arbeit umfasst vier Hauptkapitel, die in Abbildung 8.1 dargestellt sind: Die Untersuchung des *Selbstassemblierungsverhaltens von pH-sensitiven BTAs in wässrigen Lösungen*, um neue niedermolekulare Hydrogelatoren zu identifizieren (grün hinterlegt); die *spektroskopische und theoretische Studie¹ eines supramolekularen Chromophores*, der durch Selbstassemblierung eines BTA-Derivates gebildet wird (gelb hinterlegt); die Untersuchung des *Adsorptions- und Freisetungsverhaltens eines supramolekularen, pH-sensitiven Hydrogels* für eine mögliche Anwendung im Bereich der kontrollierten Wirkstofffreisetzung (rot hinterlegt); und die Studie der *„Elektrogelations“-Methode zur Herstellung von definierten, supramolekularen Hydrogelfilmen* auf leitfähigen Trägermaterialien (blau hinterlegt).

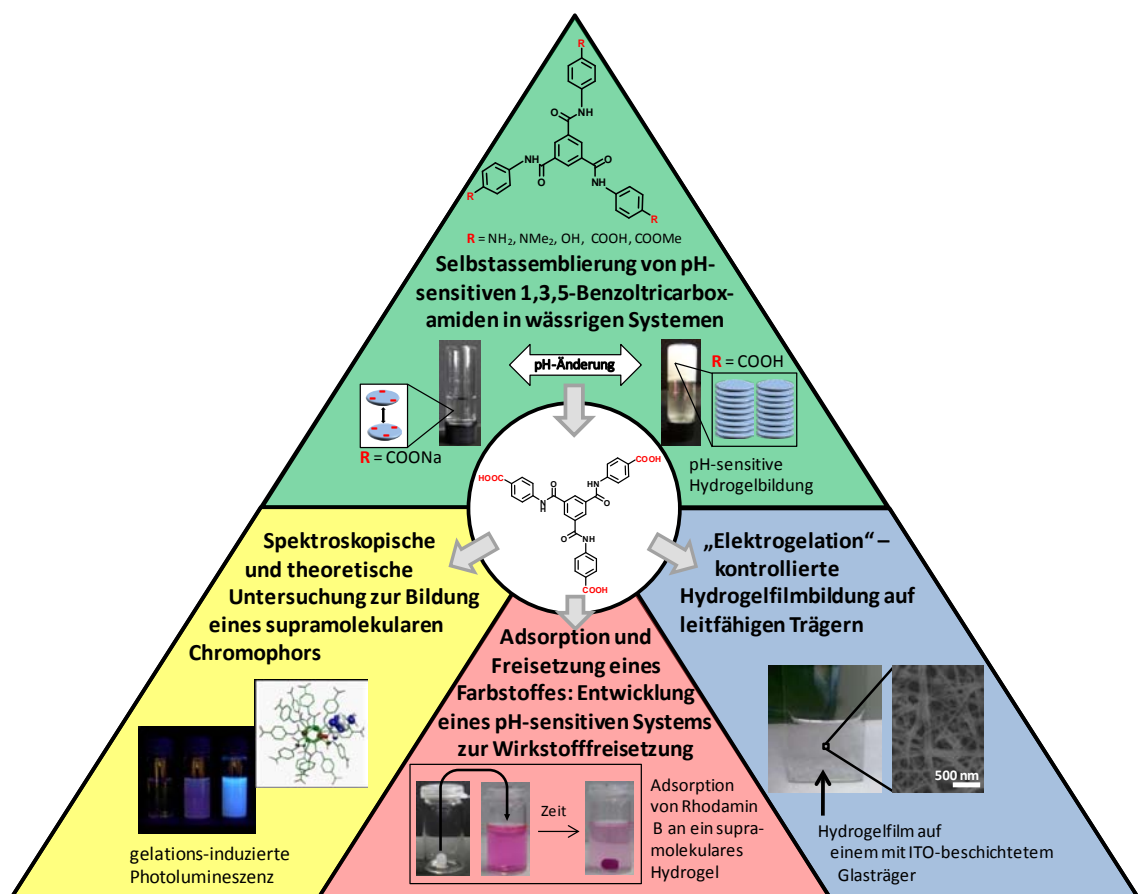
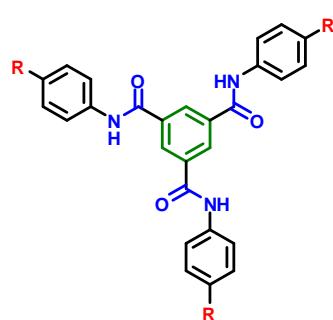


Abbildung 8.1: Darstellung der vier Hauptkapitel in dieser Arbeit.

¹ Die theoretischen Berechnungen wurden in Zusammenarbeit mit Rodrigo Q. Albuquerque durchgeführt und sind in *Soft Matter* veröffentlicht.¹⁰²

Selbstassemblierungsverhaltens von pH-sensitiven 1,3,5-Benzoltricarboxamiden (BTAs) in wässrigen Lösungen

Der erste Teil dieser Arbeit beschäftigt sich mit der Entwicklung eines strukturellen Konzeptes, das die *pH-sensitive Aggregation von BTA-Derivaten in wässrigen Medien* ermöglicht. Dieses Konzept umfasst die hydrophobe Abschirmung des BTA-Kerns mit den Amid-Gruppen von Wassermolekülen und die Einführung von pH-sensitiven, lateralen Gruppen in jedem BTA-Seitenarm, die entweder als Brönsted-Säuren oder -Basen reagieren können (Abbildung 8.2). Vier BTA-Derivate mit pH-sensitiven peripheren Substituenten und eine nicht pH-sensitive Referenzverbindung wurden in dieser Arbeit untersucht.



laterale funktionelle Gruppe (elektrostatische Wechselwirkungen abhängig vom pH-Wert)

Phenyl-Einheit (hydrophobe Abschirmung)

Amid-Gruppe (intrakolumnare Wasserstoffbrücken)

Benzol-Kern (Symmetrie, π - π -Wechselwirkungen)

| Verbindung | 1 | 2 | 3 | 4 | 5 |
|------------|-------------------------|-------------------|------------------------|-------|--------------------|
| R = | -NH ₂ | -NMe ₂ | -OH | -COOH | -COOMe |
| | ← ansteigende Basizität | | → ansteigende Azidität | | Referenzverbindung |

Abbildung 8.2: Strukturelles Konzept und Strukturformeln der BTA-Verbindungen, deren pH-sensitives Aggregationsverhalten in Wasser untersucht wurde.

Im Falle des Amino-Derivates **1** konnte keine pH-sensitive Selbstassemblierung beobachtet werden. Die Verbindungen **2**, **3** und **4** zeigten ein *pH-sensitives Aggregations- und Auflöseverhalten* bei verschiedenen pH-Werten. Bei der Untersuchung ihres pH-abhängige Aggregationsverhaltens zeigte sich, dass die Verbindungen **2** und **3** Überstrukturen bilden, aber nicht in der Lage sind stabile Gele zu formen. Bei Verbindung **4** hingegen bilden sich stabile supramolekulare Hydrogele durch die Umwandlung des entsprechenden Natriumsalzes **4Na** in das Carbonsäurederivat **4**. Die Referenzverbindung **5** kann nicht durch Protonierung oder Deprotonierung der lateralen Gruppen in einen geladenen Zustand versetzt werden und zeigt daher auch keine pH-sensitive Aggregation.

Da Verbindung **4** bei der Änderung des pH-Wertes supramolekulare Hydrogele ausbildet, liegt der Fokus dieser Arbeit auf diesem BTA-Derivat. *Verschiedene Gelationsmethoden* wurden

für Verbindung **4** getestet und die Eigenschaften der entstandenen Gele verglichen. Folgende Herstellungsmethoden wurden verwendet: i) Zugabe von wässrigen Säurelösungen, ii) Diffusion von Chlorwasserstoffgas, und iii) Zugabe von Glucono-delta-Lacton (GdL), einem langsamen Protonendonator.

Die Zugabe von wässrigen Säurelösungen führt zur Bildung inhomogener Gele. Daher fand diese Methode in der vorliegenden Arbeit keine weitere Verwendung. Durch die Diffusion von Chlorwasserstoffgas und die Zugabe von GdL zu einer Lösung von **4Na** können makroskopisch homogene Gele erhalten werden. Für beide Gelationsmethoden beträgt die kritische Gelatorkonzentration 2 g L^{-1} . Auch bei einer solch niedrigen Gelatorkonzentration sind die Gele thermisch sehr stabil. Beim Erhitzen bis zum Siedepunkt von Wasser zeigen sie keine Zersetzungs- oder Schmelzerscheinungen. Die mechanische Stabilität der Gele wurde mittels Indentationsmessungen untersucht. Diese zeigten, dass mit Chlorwasserstoffgas hergestellte Gele eine graduelle mechanische Stabilität besitzen, da die oberste Gelschicht an der Grenzfläche zur Luft stabiler ist. Mit GdL präparierte Gele weisen demgegenüber eine homogene mechanische Stabilität auf. Diese steigt mit zunehmender Gelatorkonzentration an. Die Zugabe von GdL ist daher eine sehr elegante Methode zur Herstellung homogener und stabiler Gele. Die Gele zeigen außerdem eine hohe Beständigkeit in verschiedenen wässrigen Säuren und vielen organischen Lösungsmitteln. Zusätzlich können die Hydrogele durch einen kompletten Austausch des Gelationsmediums in stabile Organogele überführt werden.

An verschiedenen Stufen der Gelbildung und an vollständig gelierten und getrockneten Gelen wurden elektronenmikroskopische Untersuchungen durchgeführt, um ein *Strukturmodell für die pH-sensitive Bildung des supramolekularen Hydrogels* zu entwickeln. Während die negativ geladenen Moleküle des Gelatorsalzes **4Na** wegen der elektrostatischen Abstoßung molekular gelöst vorliegen, geht man davon aus, dass das Absenken des pH-Wertes schrittweise zur Bildung anisotroper Aggregate führt. Das vorgeschlagene Modell sieht vor, dass zu Beginn der Gelation die teilweise geladenen Moleküle zu supramolekularen Säulen oder Stapeln aggregieren, deren Ladungen gleichmäßig über die Oberfläche verteilt sind. Diese scheinen bei fortschreitender Protonierung helikale Überstrukturen zu bilden.

Spektroskopische und theoretische Untersuchung eines supramolekularen Chromophores

Im zweiten Teil dieser Arbeit werden die spektroskopischen Eigenschaften des Hydrogelatorsystems **4/4Na** detailliert diskutiert. Diese zeigen, dass eine gesteigerte Emission des Systems im aggregierten Zustand (*aggregation-induced emission enhancement, AIEE*) auftritt. In Kombination mit den theoretischen Berechnungen von Prof. Rodrigo Q. Albuquerque wurden diese Ergebnisse verwendet, um das vorgeschlagene Strukturmodell zu unterstützen. Die wichtigsten Ergebnisse dieses Kapitels sind in *Soft Matter* veröffentlicht.¹⁰²

Weder das Säurederivat **4** noch das entsprechende Natriumsalz **4Na** zeigen Lumineszenz in Lösung, während bei den Filmen und Hydrogelen der Verbindung **4** unter UV-Bestrahlung eine blaue Emission beobachtet werden kann. Dieses System zeigt daher eindeutig eine *aggregations- und gelations-induzierte Emissionsverstärkung*. Da sich die Photolumineszenzspektren des getrockneten Films und des nativen (nassen) Hydrogels stark ähneln, kann angenommen werden, dass ein ähnlicher Chromophor in den beiden Proben vorliegt. Die Emission im Feststoff und im Gel wird einem π^* -n- oder π^* - π -Übergang zugeordnet, der die Charakteristik eines Ladungstransportes (*charge transfer*) aufweist.

Die *zeitabhängigen Photolumineszenzuntersuchungen* während der Gelbildung mit GdL zeigen eine Rotverschiebung der Photolumineszenzmaxima mit zunehmender Gelationszeit. In Kombination mit den *theoretischen Berechnungen* konnte das Photolumineszenzmaximum zu Beginn der Gelation einem aufeinander gestapelten Dimer zugeordnet werden. Weiterhin wird angenommen, dass die Rotverschiebung mit zunehmender Gelationszeit das Wachstum der molekularen Stapel anzeigt. Die theoretischen Berechnungen und die optimierten Geometrien von tetrameren Stapeln der Verbindung **4** passen sehr gut zu den experimentellen Ergebnissen und unterstützen das vorgeschlagene Strukturmodell in der Anfangsphase der Aggregation.

Adsorptions- und Freisetungsverhaltens eines supramolekularen, pH-sensitiven Hydrogels

Während sich die ersten beiden Teile dieser Arbeit hauptsächlich mit grundlegenden Fragestellungen zur supramolekularen Selbstassemblierung und Hydrogelbildung beschäftigen, liegt der Fokus des dritten Teils auf der möglichen Nutzung des identifizierten pH-sensitiven Hydrogelators **4**. Detaillierte Adsorptions- und Freisetzungsstudien zeigen das Potential des Hydrogelators für die Anwendung als Biomaterial in der kontrollierten Wirkstofffreisetzung, vor allem bei oraler Einnahme. Weiterhin wird der mögliche Nutzen der Hydrogele als Adsorptionsmittel für toxische Farbstoffe bei der Abwasseraufbereitung diskutiert.

Es konnte gezeigt werden, dass Hydrogele der Verbindung **4** *grundlegende Voraussetzungen* für die Anwendung als Matrixmaterial im Bereich der Wirkstofffreisetzung erfüllen. Solche Voraussetzungen sind Biokompatibilität, nicht-toxisches Verhalten,¹ die Adressierbarkeit des Gels innerhalb eines physiologisch relevanten pH-Bereichs, ausreichende mechanische und thermische Stabilität sowie eine hohe spezifische Oberfläche.

Für die Untersuchung der *konzentrations- und zeitabhängigen Adsorption* an gebildeten Hydrogelen der Verbindung **4** wurde Rhodamin B als Modellverbindung verwendet. Die Farbstofflösungen werden effektiv entfärbt und die Hydrogele zeigen ein hohes Adsorptionspotential. Dies gilt auch für niedrige Rhodamin B-Konzentrationen. Diese

¹ Die Tests zur Bestimmung der Biokompatibilität und des toxischen Verhaltens wurden vom Hans-Knöll Institut in Jena durchgeführt.

Eigenschaft macht das System für Filteranwendungen im Bereich der Wasseraufbereitung interessant.

Die *Adsorptionsdaten* können durch die beiden *isothermen Modelle* von Langmuir und Freundlich beschrieben werden. Diese zeigen auf, dass die Adsorption des Farbstoffes begünstigt ist. Bei hohen Farbstoffkonzentrationen muss jedoch mit einer weniger starken Adsorption gerechnet werden. Die Adsorptionsgeschwindigkeiten sind abhängig von der anfänglich eingestellten Rhodamin B-Konzentration, aber insgesamt sehr niedrig. Eine vollständige Adsorption ist innerhalb weniger Tage erreicht. Daher sollten für die Anwendung der Hydrogele im Bereich der Wasseraufbereitung Festbettsysteme („*fixed-bed*“ systems) verwendet werden, da diese längere Adsorptionszeiten erlauben. Die *Adsorptionskinetik* kann mit dem kinetischen Modell der pseudo-zweiten Ordnung (*pseudo 2nd order model*) beschrieben werden. Dies deutet darauf hin, dass die Chemisorption, also der eigentliche Adsorptionsschritt, der geschwindigkeitsbestimmende Faktor ist.

Die *Stabilität der gebildeten Farbstoff-Gelator-Komplexe* wurde bei verschiedenen Temperaturen getestet. Die Untersuchungen zeigten, dass die Farbstoffmoleküle stark an die Oberfläche des Gels gebunden sind. Obwohl durch eine Erhöhung der Temperatur die Freisetzung beschleunigt wird, verbleiben unabhängig von der eingestellten Temperatur über 90 % des adsorbierten Rhodamin Bs im Gel.

Neben der Adsorption eines Farbstoffes nach vollendeter Gelation ist auch die *in situ*-Adsorption während der Gelbildung eine interessante Beladungstechnik. *Hydrogele* der Verbindung **4** können *in Anwesenheit von Rhodamin B als Gastmolekül gebildet* werden. Starke Wechselwirkungen zwischen den Farbstoff- und Gelatormolekülen ermöglichen die Bildung stabiler Gele, wenn das molekulare Verhältnis von Farbstoff zu Gelator 0,5 oder weniger beträgt. Das deutet darauf hin, dass Rhodamin B nicht nur an der Geloberfläche adsorbiert, sondern auch zwischen den Fasern eingeschlossen und eingebaut wird. Daher können Hydrogele *effizienter und schneller mit Rhodamin B beladen* werden, wenn sie in Anwesenheit des Farbstoffes hergestellt werden, anstatt den Farbstoff an bereits gebildete Gele zu adsorbieren. Abhängig von der zu Beginn eingelierten Rhodamin B-Menge verbleiben nach 10 Tagen in Wasser 70 % bis 95 % des Farbstoffes im Gel. Die Freisetzung ist sehr langsam und folgt innerhalb der gegebenen Grenzbedingungen dem verallgemeinerten Fick'schen Modell. Das weist daraufhin, dass nur Farbstoffmoleküle, die in der wässrigen Phase des Gels gelöst sind, freigesetzt werden, während eingeschlossene Farbstoffmoleküle im Gel verbleiben.

Für die Anwendung eines Matrixmaterials in kontrollierten Wirkstofffreisetzungssystemen muss die Freisetzung der Modellverbindung von spezifischen physiologischen Bedingungen ausgelöst werden. Daher wurde das *Auflöse- und Freisetzungverhalten* in *biologisch*

relevanten Medien von unbeladenen Hydrogelen der Verbindung **4** und von Hydrogelen, die in Anwesenheit von Rhodamin B hergestellt wurden, untersucht. Für diese Tests wurden Pufferlösungen mit verschiedenen pH-Werten und Zusammensetzungen verwendet: Phosphatgepufferte Salzlösung (PBS, pH = 7,4), simulierte Körperflüssigkeit (SBF, pH = 7,4), simulierte Magensäure im nüchternen Zustand (SGF, pH = 1,6), und simulierte Darmflüssigkeit im nüchternen Zustand (SIF, pH = 6,5).

PBS und SBF sind wichtige biologische Flüssigkeiten für das Kultivieren von Zellen und die Züchtung von Gewebe (*tissue engineering*). Bei Raumtemperatur führt ihr leicht alkalischer pH-Wert zur Auflösung des Gels und zur Freisetzung des gesamten Farbstoffes innerhalb von 24 h in PBS, beziehungsweise 8 h in SBF. Durch eine Erhöhung der Temperatur von SBF auf Körpertemperatur (37 °C) kann die Auflösung des Gels und die Freisetzung des eingeschlossenen Farbstoffes innerhalb von 6 h erreicht werden. Das Gel ist daher nicht für eine Anwendung als Gerüstmaterial bei der künstlichen Herstellung von Gewebe geeignet, da hierbei Stabilitäten im Bereich von mehreren Wochen benötigt werden. Für eine Anwendung müssten zusätzliche Stabilisierungsprozesse realisiert werden.

Interessanterweise werden die Gele in SGF bei 37 °C trotz der Anwesenheit von Pepsin nicht aufgelöst. Da das Enzym Pepsin Amidbindungen hydrolysieren kann, könnte es die Gelatormoleküle zersetzen und so zu einer Auflösung des Gels beitragen. Innerhalb von 10 Tagen werden jedoch nur geringe Mengen des Farbstoffes freigesetzt. Dieses Verhalten stärkt die Annahme, dass die Hydrogel-Matrix labile Wirkstoffe vor dem sauren Milieu des Magens schützt. Durch die pH-Sensitivität des Hydrogelators sind die Gele in starken Säuren stabil, während sie sich in Lösungen mit einem pH-Wert von über 6.2 langsam auflösen. In SIF im nüchternen Zustand kann daher bei Körpertemperatur ein Auflösen der Gele innerhalb von 72 h beobachtet werden. Der Farbstoff ist bereits nach 48 h komplett freigesetzt, vermutlich durch die Auflösung der Überstrukturen des Gels. Die Stabilität der Gele in SGF in Kombination mit ihrem Freisetzungsverhalten in SIF macht diesen Hydrogelator zu einem vielversprechenden Matrixmaterial für die Anwendung in der kontrollierten Wirkstofffreisetzung bei oraler Einnahme.

Elektrogelation – kontrollierte Hydrogelfilmbildung auf leitfähigen Trägern

Der vierte Teil dieser Arbeit fokussiert sich auf eine einzigartige Gelationsmethode, die so genannte „Elektrogelation“. Diese Methode kann dazu verwendet werden, definierte Hydrogelfilme der Verbindung **4** auf leitfähigen Trägern herzustellen. Dabei wird die Absenkung des pH-Wertes durch die Elektrolyse von Wasser in der Nähe einer Anode genutzt.

Für die systematische Untersuchung der Elektrogelationsparameter wurde ein *experimenteller Aufbau* mit drei Elektroden verwendet. Indium-Zinnoxid (ITO)-beschichtete

Glasträger fanden dabei Verwendung als Arbeitselektrode, während ein Graphendraht als Gegenelektrode und ein Silberdraht als Pseudo-Referenzelektrode diente.

Für den verwendeten Aufbau konnten *wichtige Parameter* identifiziert werden, die den Elektrogelationsprozess steuern: i) der Abstand der Elektroden; ii) das angelegte Potential; iii) die Gelatorkonzentration; iv) die Konzentration des Hintergrundelektrolyten; und v) die Gelationszeit. Der Einfluss dieser Parameter auf die Geleigenschaften im getrockneten Zustand, wie zum Beispiel auf die Filmschichtdicke, die Morphologie und die spektroskopischen Eigenschaften, wurde genau untersucht. Die Studie zeigte, dass die Änderung eines Parameters mehrere Eigenschaften gleichzeitig beeinflussen kann. Auf der anderen Seite kann eine bestimmte Eigenschaft, wie zum Beispiel die Filmdicke im getrockneten Zustand, von mehreren Parametern bestimmt werden. Mit Hilfe dieser Ergebnisse können definierte Gelfilme durch Elektrogelation hergestellt werden, indem die identifizierten Parameter entsprechend optimiert werden.

Diese Gelationsmethode hat nicht nur großes Potential für die kontrollierte Herstellung von Gelbeschichtungen der Verbindung **4**, sondern sie könnte auch für andere pH-sensitive niedermolekulare Hydrogelatoren verwendet werden. In Kooperation mit Prof. Georg Papastavrou und seiner Gruppe (Physikalische Chemie II, Universität Bayreuth) werden derzeit die mechanischen Eigenschaften der mit Elektrogelation hergestellten Gelfilme *in situ* am Rasterkraftmikroskop untersucht.

Zusammenfassend zeigen die Ergebnisse dieser Arbeit, dass vor allem das BTA-Derivat **4** eine sehr interessante niedermolekulare Verbindung für die Studie des Selbstassemblierungsverhaltens in wässrigen Medien und der Bildung supramolekularer Hydrogele ist. Aufgrund der einzigartigen Kombination vielversprechender Eigenschaften ist der vorgestellte pH-sensitive Hydrogelator nicht nur als Modellverbindung für Fragestellungen der Grundlagenforschung attraktiv. Ebenso könnte das untersuchte Hydrogelator-System in verschiedenen Bereichen Anwendung finden, wie zum Beispiel in Photolumineszenz-basierten Sensoren, als Adsorptionsmittel, als Matrixmaterial für die kontrollierte Wirkstofffreisetzung oder auch für die funktionale Beschichtung leitfähiger Oberflächen.

9 Experimental part

9.1 Materials

All chemicals were used as received without further purification and purchased from Aldrich and Acros, if not stated otherwise. Solvents were distilled prior to usage. Desalted water was obtained by a standard ion exchange set up. For the preparation of the simulated body fluids ultrapure water (Milli-Q) was used, which was obtained from a Milli-Q plus purification system (Millipore GmbH) with a QPAK®2 filter (pore size: 0.2 μm , purity: 0.0549 $\mu\text{m}/\text{cm}$). For UV-Vis (ultraviolet-visible) absorption measurements spectroscopic grade solvents were used. For nuclear magnetic resonance (NMR) measurements deuterated solvents were employed.

9.2 Standard characterization methods

Nuclear magnetic resonance (NMR) experiments

^1H NMR and ^{13}C NMR spectra were recorded on a Bruker AC 300 MHz spectrometer at 25°C at 300 MHz and 100 MHz, respectively. All samples were either dissolved in DMSO- d_6 or in D_2O , which also acted as internal reference.

Mass spectroscopy (MS)

MS was carried out on a Finnigan MAT 8500 apparatus (EI, 70 eV) using direct injection mode.

Elemental analysis

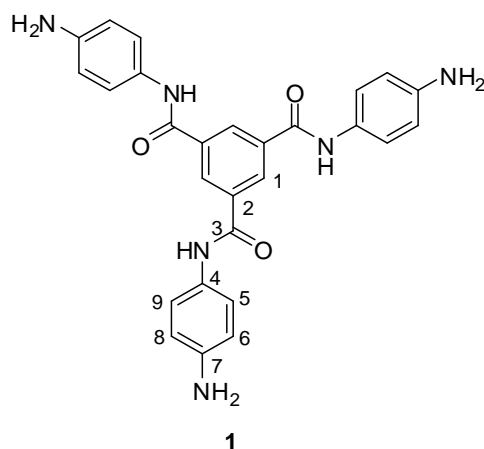
Elemental analysis (C, H, N) was carried out with an EA 3000 (HEKAtech) by Birgit Brunner at the Department of Chemical Engineering (Prof. A. Jess) of the University of Bayreuth. The theoretical amounts of the elements C, H, N, and O were calculated using Isis Draw.

Thermal analysis

The DSC/TGA measurement for compound **1** was performed on a simultaneous thermal analytical apparatus TGA/SDTA 851e Modul (Mettler Toledo). The analysis of the data was carried out using the Stare Default-DB V9.10 A-ICTA software. The thermal properties of compounds **2** – **5**, and **4Na** were investigated using a NETZSCH Simultane Thermoanalysenapp. STA 409. The crucible consisted of Alox and as reference substance kaolin was used. Independent of the used set up the flow rate of nitrogen was set to 75 $\text{cm}^3 \text{min}^{-1}$. Each sample was heated from 25 °C to 650 °C with a heating rate of 10 K min^{-1} .

9.3 Synthesis

9.3.1 *N,N',N''*-Tris(4-aminophenyl)-1,3,5-benzene tricarboxamide **1**



Step 1: *N,N',N''*-Tris(4-nitrophenyl)-1,3,5-benzene tricarboxamide

To a solution of 4-nitroaniline (19.37 g, 140.24 mmol) in *N*-methyl-2-pyrrolidone (NMP, 200 mL), pyridine (100 mL) and LiCl (0.10 g) were slowly added at r. t. under constant stirring. The solution was cooled with an ice-water bath. 1,3,5-benzenetricarbonyl trichloride (11.63 g, 43.82 mmol) was dissolved in NMP (25 mL) and slowly added to the cooled solution. After stirring overnight the solution was poured into a saturated (sat.) aqueous solution of sodium chloride (2.5 L). The resulting precipitate was filtered and dried. For purification the precipitate was stirred in hot DMF for 2 h under reflux conditions, filtered and washed with acetone. After drying 20.45 g of the product were yielded (35.85 mmol, 82 %).

Step 2: *N,N',N''*-Tris(4-aminophenyl)-1,3,5-benzene tricarboxamide (**1**)

The 4-nitrophenyl compound (5.00 g, 8.76 mmol) was placed in a flask equipped with a nitrogen inlet and *N,N*-dimethyl acetamide (DMAc; 200 mL). Palladium on charcoal (10 %, 0.80 g) and 2.73 mL of hydrazine hydrate (2.81 g, 8.76 mmol) were added under nitrogen atmosphere under constant stirring. The mixture was refluxed at 130 °C overnight and subsequently filtered over Alox. After precipitation in water, filtration and drying under reduced pressure 3.33 g of compound **1** were yielded as yellow powder (6.93 mmol, 79 %).

Overall yield of **1**: 65 %.

¹H NMR (300 MHz, [D₆]DMSO, 25°C): δ = 10.14 (s, 3 H, NH), 8.57 (s, 3 H, H-1), 7.42 (d, ³J (H,H) = 8.7 Hz, 6 H, H-5, H-9), 6.57 (d, ³J (H,H) = 8.7 Hz, 6 H, H-6, H-8), 4.99 ppm (s, 6 H, NH₂).

¹³C NMR (100 MHz, [D₆]DMSO, 25°C): δ = 164.3 (C-3), 145.9 (C-7), 136.2 (C-2), 129.4 (C-1), 128.4 (C-4), 122.6 (C-5, C-9), 114.2 ppm (C-6, C-8).

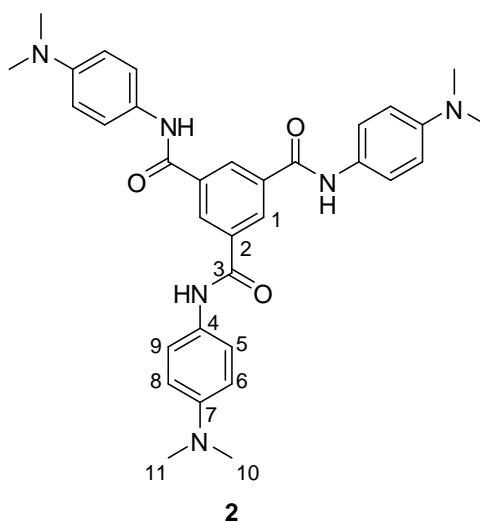
To remove traces of DMAc, compound **1** was rinsed with methylene chloride in a soxhlet apparatus prior to MS, elemental, and thermal analysis.

MS (70 eV): m/z (%): 480 (97) [M^+], 373 (14), 319 (27), 265 (12), 210 (17), 107 (100), 44 (12).

Elemental analysis calculated (calcd) (%) for $C_{27}H_{24}N_6O_3 \times 3 H_2O$: C 60.66, H 5.66, N 15.72; found: C 61.45, H 5.01, N 15.53.

Thermal analysis: loss of water (7.3 %) at 85°C; decomposition at 314°C. The loss of water corresponds to a molar ratio of 1 : 2 (**1** : H_2O).

9.3.2 *N,N',N''*-Tris[4-(*N,N*-dimethyl)-aminophenyl]-1,3,5-benzene tricarboxamide **2**



To a solution of *N,N*-dimethyl-1,4-phenyldiamine (5.06 g, 37.15 mmol) in acetone (150 mL), a solution of 1,3,5-benzenetricarbonyl trichloride (3.31 g, 12.38 mmol) in acetone (50 mL) was slowly added at r. t. under constant stirring. After stirring for 1 h at room temperature (r. t.), *n*-hexane (350 mL) was added. The resulting grey precipitate was filtered and washed with *n*-hexane and acetone. After drying under reduced pressure the hydrochloride salt of **2** was dissolved in water (300 mL) and compound **2** was precipitated by adding 1 M NaOH solution until a pH of 8 was reached. Filtration of the precipitate gave 5.99 g of compound **2** as a green solid (10.60 mmol, 86 %).

1H NMR (300 MHz, $[D_6]$ DMSO, 25°C): δ = 10.30 (s, 3 H, NH), 8.63 (s, 3 H, H-1), 7.63 (d, 3J (H,H) = 8.7 Hz, 6 H, H-5, H-9), 6.76 (d, 3J (H,H) = 8.7 Hz, 6 H, H-6, H-8), 2.89 ppm (s, 18 H, H-10, H-11).

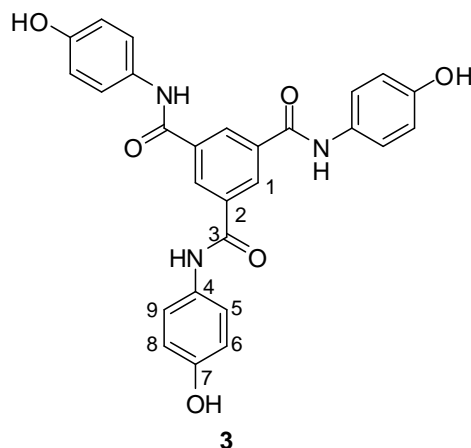
^{13}C NMR (100 MHz, $[\text{D}_6]\text{DMSO}$, 25°C): δ = 164.3 (C-3), 147.9 (C-7), 136.1 (C-2), 129.6 (C-1), 129.1 (C-4), 122.2 (C-5, C-9), 112.9 (C-6, C-8), 40.9 ppm (C-10, C-11).

MS (70 eV): m/z (%): 564 (7) $[\text{M}^+]$, 488 (5), 459 (37), 401 (14), 297 (3), 263 (3), 176 (16), 163 (20), 135 (100), 108 (5), 44 (12).

Elemental analysis calcd (%) for $\text{C}_{33}\text{H}_{36}\text{N}_6\text{O}_3$: C 70.19, H 6.43, N 14.88; found: C 69.32, H 6.43, N 14.37.

Thermal analysis: no loss of water; decomposition at 302°C.

9.3.3 *N,N',N''*-Tris(4-hydroxyphenyl)-1,3,5-benzene tricarboxamide **3**



To a mixture of 3.27 g of 4-aminophenol (30.00 mmol), 2.7 mL of pyridine (2.61 g, 33.00 mmol) and 100 mL of *N*-methyl-2-pyrrolidone (NMP), a solution of 2.65 g of 1,3,5-benzenetricarbonyl trichloride (10.00 mmol) in 20 mL of NMP was slowly added at r. t. under constant stirring. After stirring the white suspension for 1 h at r. t., it was poured into 400 mL of ice water under vigorous stirring. After stirring for another hour, the white precipitate was filtered and washed with 400 mL of desalted water. Drying at the rotary evaporator at 60 °C for 3 h and under high vacuum (4×10^{-3} mbar) overnight yielded 3.30 g of compound **3** as a brown powder (6.80 mmol, 68 %).

^1H NMR (300 MHz, $[\text{D}_6]\text{DMSO}$, 25°C): δ = 10.33 (s, 3 H, NH), 9.30 (s, 3 H, OH), 8.61 (s, 3 H, H-1), 7.58 (d, 3J (H,H) = 8.8 Hz, 2 H, H-5, H-9), 6.77 ppm (d, 3J (H,H) = 8.8 Hz, 2 H, H-6, H-8).

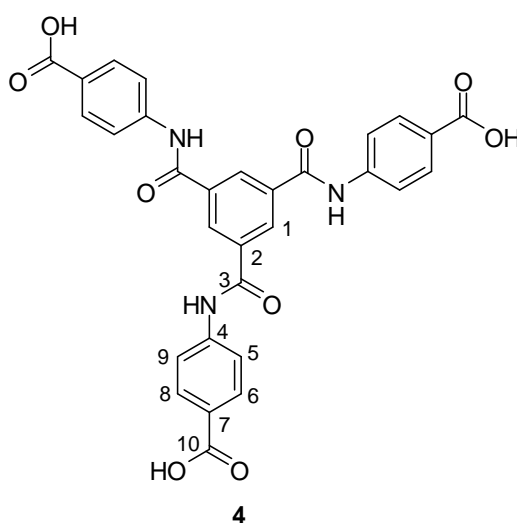
^{13}C NMR (100 MHz, $[\text{D}_6]\text{DMSO}$, 25°C): δ = 164.5 (C-3), 154.4 (C-7), 136.1 (C-2), 131.0 (C-4), 129.7 (C-1), 122.7 (C-5, C-9), 115.5 ppm (C-6, C-8).

MS (70 eV): m/z (%): 385 (8), 336 (8), 259 (27), 181 (15), 149 (100), 71 (40), 57 (79).

Elemental analysis calcd (%) for $C_{27}H_{21}N_3O_6 \times 0.5 H_2O$: C 65.87, H 4.47, N 8.54; found: C 65.58, H 4.43, N 8.51.

Thermal analysis: loss of water (0.9 %) at 63°C; decomposition at 387°C. The loss of water corresponds to a molar ratio of 1 : 0.25 (**3** : H_2O).

9.3.4 *N,N',N''*-Tris(4-carboxyphenyl)-1,3,5-benzene tricarboxamide **4**



To a mixture of 4.94 g of 4-aminobenzoic acid (36.00 mmol), 5.0 mL of triethylamine (3.64 g, 36.00 mmol), and 100 mL of acetone, a solution of 3.19 g of 1,3,5-benzenetricarbonyl trichloride (12.00 mmol) in 20 mL of acetone was slowly added at r. t. under constant stirring. After stirring the white suspension for 1 h at r. t., it was poured into 100 mL of ice water under vigorous stirring. After stirring for another hour, the white precipitate was filtered and washed with 400 mL of desalted water, 100 mL of acetone, and 100 mL of methanol. Drying using a rotary evaporator at 60 °C for 3 h and subsequently under high vacuum (4×10^{-3} mbar) overnight yielded 6.04 g (10.64 mmol, 89 %) of a slightly hygroscopic, white powder. Recrystallization from DMSO/ H_2O (2:1) resulted in 5.03 g of compound **4** (8.86 mmol, 74 %). Note: Upon cooling the DMSO/water mixture in the recrystallization process a white suspension with an enhanced viscosity is obtained. Therefore, a centrifugation step is recommended before the filtration, washing and drying procedure.

1H NMR (300 MHz, $[D_6]DMSO$, 25°C): δ = 12.82 (br_s, 3 H, COOH), 10.87 (s, 3 H, NH), 8.75 (s, 3 H, H-1), 7.98 ppm (m, 12 H, H-5, H-6, H-8, H-9).

^{13}C NMR (100 MHz, $[\text{D}_6]\text{DMSO}$, 25°C): δ = 167.4 (C-10), 165.2 (C-3), 143.4 (C-4), 135.7 (C-2), 130.8 (C-6, C-8, C-1), 126.4 (C-7), 120.1 ppm (C-5, C-9).

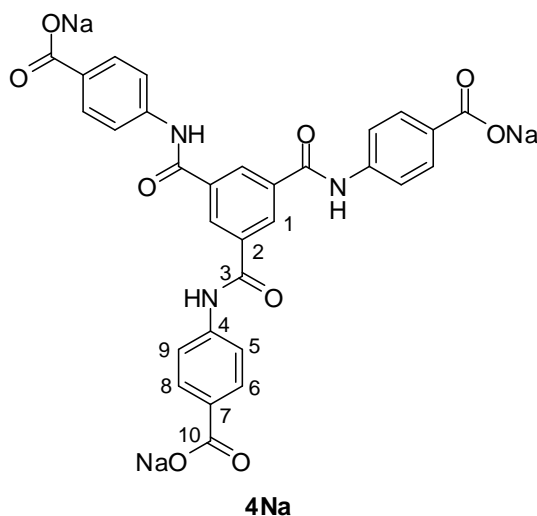
MS (70 eV): m/z (%): 403 (1), 329 (22), 193 (100), 165 (19), 120 (18), 65 (16).

To remove traces of water, compound **4** was dried at 90 °C under high vacuum (4×10^{-3} mbar) prior to the elemental and thermal analysis.

Elemental analysis calcd (%) for $\text{C}_{30}\text{H}_{21}\text{N}_3\text{O}_9 \times 1.5 \text{H}_2\text{O}$: C 60.61, H 4.07, N 7.07; found: C 60.75, H 4.34, N 6.96.

Thermal analysis: loss of water (1.9 %) at 80°C; decomposition at 309°C. The loss of water corresponds to a molar ratio of 1 : 0.6 (**4** : H_2O).

9.3.5 Sodium salt of *N,N',N''*-tris(4-carboxyphenyl)-1,3,5-benzene tricarboxamide **4Na**



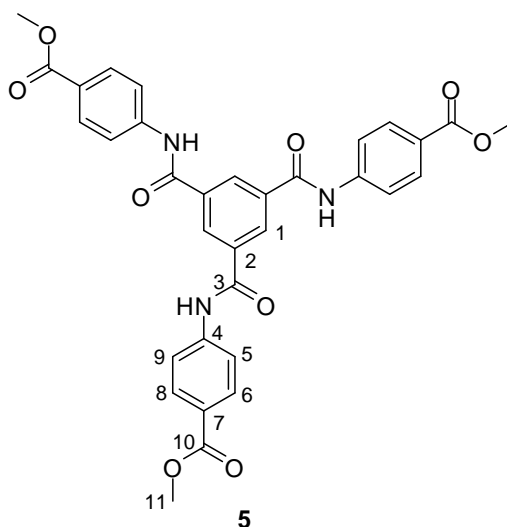
To a suspension of 6.14 g (10.82 mmol) of compound **4** in 50 mL of desalted water, a solution of 1.30 g NaOH in desalted water (20 mL) was added at r. t. under constant stirring. After complete dissolution of **4**, the respective sodium salt was precipitated by addition of 400 mL of *iso*-propanol. The white precipitate was filtered and washed with *iso*-propanol (100 mL). Drying under high vacuum (5×10^{-3} mbar) yielded 5.50 g of compound **4Na** (8.68 mmol, 80 %).

^1H NMR (300 MHz, D_2O , 25°C): δ = 8.59 (s, 3 H, H-1), 7.93 (pd, 3J (H,H) = 8.7 Hz, 6 H, H-6, H-8), 7.68 ppm (pd, 3J (H,H) = 8.7 Hz, 6 H, H-5, H-9).

^{13}C NMR (100 MHz, D_2O , 25°C): δ = 174.9 (C-10), 167.2 (C-3), 139.4 (C-4), 135.2 (C-2), 133.2 (C-7), 129.9 (C-1, C-6, C-8), 121.3 ppm (C-5, C-9).

Thermal analysis: loss of water (15.4 %) at 109°C; decomposition at 330°C. The loss of water corresponds to a molar ratio of 1 : 6.4 (**4Na** : H_2O).

9.3.6 *N,N',N''*-Tris(4-carboxyphenyl)-1,3,5-benzene tricarboxamide tri-methyl ester **5**



To a mixture of 5.44 g of 4-aminobenzoate (36.00 mmol), 5.0 mL of triethylamine (3.64 g, 36.00 mmol), and 100 mL of acetone, a solution of 3.19 g of 1,3,5-benzenetricarbonyl trichloride (12.00 mmol) in 20 mL of acetone was slowly added at r. t. under constant stirring. After stirring the white suspension for 2 h at r. t., it was poured into 400 mL of ice water under vigorous stirring. After stirring for another hour, the white precipitate was filtered and washed with 400 mL of desalted water, acetone, and again water, until all triethylamine was removed. Drying under high vacuum (4×10^{-3} mbar) overnight yielded a product that was still contaminated with residues of water and acetone. Therefore, the product was dissolved in DMSO and precipitated in ice water. Drying under high vacuum (4×10^{-3} mbar) overnight yielded 6.67 g of compound **5** as white powder (10.94 mmol, 91 %).

^1H -NMR (300 MHz, DMSO- d_6): δ (ppm) = 10.93 (3 H, s, N-H), 8.76 (3 H, s, H-1), 8.00 (12 H, m, H-5, H-6, H-8, H-9), 3.85 (9 H, s, H-11).

^{13}C -NMR (100 MHz, DMSO- d_6): δ (ppm) = 166.3 (C-10), 165.3 (C-3), 143.8 (C-4), 135.6 (C-2), 130.8 (C-7), 130.7 (C-6, C-8), 125.2 (C-1), 120.2 (C-5, C-9), 52.4 (C-11).

MS (70 eV): m/z (%): 609 (33) [M^+], 578 (14), 490 (22), 459 (100), 340 (54), 282 (37), 207 (21), 121 (20), 75 (23), 44 (18).

Elemental analysis calcd (%) for $C_{33}H_{27}N_3O_9 \cdot x \cdot 2 H_2O$: C 61.39, H 4.84, N 6.51; found: C 62.22, H 4.69, N 6.54.

Thermal analysis: loss of water (2.8 %) at *ca.* 80 °C; melting at 327.6 °C; decomposition at 362.8 °C. The loss of water corresponds to a molar ratio of 1 : 1 (**5** : H_2O).

9.4 Advanced methods and preparation techniques

Determination of the water uptake (moisture analyzer)

To quantify the water uptake of the compounds **4** and **4Na**, a moisture analyzer MA 145 (Sartorius) was used. *Approx.* 5 g of the respective solid were weighed in and heated to 140 °C *via* infra-red radiation until the weight loss of the samples was less than 1 mg per minute (min). The overall weight loss is automatically calculated by the software and given in % and mg. The average weight loss in % of three measurements is displayed in this study. If not stated otherwise, the samples were cooled down to r. t. and stored in the indicated atmosphere for 1 h between measurements.

Fourier transform infrared (FT-IR) spectroscopy

All samples were powdered prior to the FT-IR measurements. All FT-IR spectra were recorded with a Perkin-Elmer Spectrum 100 FT-IR spectrometer in ATR (attenuated total reflection) mode.

- *compounds 1 - 5, and 4Na as obtained from synthesis*

Bulk materials of compounds **1**–**5**, and **4Na** were measured as obtained from synthesis. Compound **4** was additionally analyzed after crystallization from a DMSO-water mixture. Due to the high water uptake of **4**, the sample was tempered at 90 °C under high vacuum (4×10^{-3} mbar) overnight prior to the analysis.

- *of compounds 2 - 4 after the pH-sensitivity tests*

Compounds **2** and **3** as obtained after the pH-sensitivity tests (chapter 9.4.2) were filtered, washed with desalted water and dried under high vacuum (4×10^{-3} mbar). Hydrogel samples of compound **4** were prepared from solutions of **4Na** with a concentration of 10 g L^{-1} by addition of 4 equivalents (eq.) of glucono-delta-lactone (GdL). After gelation overnight the hydrogel

samples were put on paper pulp and dried under high vacuum (4×10^{-3} mbar). For details regarding the preparation of hydrogels using GdL see chapter 9.4.3.

Molecular modeling

Molecular dimensions were calculated using Chem3D Ultra 10.0 (MM2 energy minimization).

9.4.1 Morphological studies and X-ray diffraction investigations

Scanning electron microscopic (SEM) study

All samples were mounted on a standard sample holder by a conductive adhesion pad and sputtered with platinum prior to SEM imaging.

- *compounds 1 - 5, and 4Na as obtained from synthesis*

The dried samples of compounds **1 - 5**, and **4Na** as obtained from synthesis, as well as compound **4** after crystallization from a DMSO-water mixture were mounted on a standard sample holder by a conductive adhesion pad. Samples of compound **3** after synthesis were investigated with a Zeiss LEO Ultra Plus (FE-SEM with Schottky-field-emission cathode; SE2 detector) using an accelerating voltage of 3 kV. All other samples were examined with a Zeiss LEO 1530 (FE-SEM with Schottky-field-emission cathode; in-lens detector) using an accelerating voltage of 3 kV.

- *of compounds 2 and 3 after the pH-sensitivity tests*

Compounds **2** and **3** as obtained after the pH-sensitivity tests (chapter 9.4.2) were filtered, washed with desalted water and dried under high vacuum (4×10^{-3} mbar). Small fragments of hydrogels of **4** prepared with aqueous hydrochloric acid solution as described for the pH-sensitivity tests (chapter 9.4.2) were washed three times with desalted water for at least 3 hours and dried on a piece of paper pulp under ambient conditions. All samples were examined with a Zeiss LEO 1530 (FE-SEM with Schottky-field-emission cathode; in-lens detector) using an accelerating voltage of 3 kV.

- *of xerogels of 4*

Hydrogels of **4** were prepared using **4Na** solutions with a concentration of 10 g L^{-1} . Gelation was either induced by diffusion of hydrochloric acid vapor or by the addition of 4 eq. of glucono-delta-lactone (GdL) as described in chapter 9.4.3. Small fragments of the resulting gels were washed three times with desalted water for at least 3 h. The samples were put on a piece of paper pulp and then dried under high vacuum (4×10^{-3} mbar) overnight. The xerogels were examined with a Zeiss LEO 1530 (FE-SEM with Schottky-field-emission cathode; in-lens detector) using an accelerating voltage of 3 kV.

- *of a film of 4 prepared from a DMSO solution*

A drop of a solution of **4** (40 g L^{-1} of **4**) in DMSO was put on top of an aluminum plate (diameter approx. 10 mm). The sample was dried in an oven at $100 \text{ }^\circ\text{C}$ for at least 1 h. SEM images were taken using a Zeiss LEO 1530 (FE-SEM with Schottky-field emission cathode, in-lens detector) using at an accelerating voltage of 3 kV.

X-ray diffraction (XRD) measurements

XRD analysis was performed on a Huber Guinier-Diffraktometer 6000, equipped with a Huber Quarz-Monochromator 611, a Cu-anode ($\text{CuK}_{\alpha 1}$ -beam, $\lambda = 154.051 \text{ pm}$, X-ray generator from Seifert Company), a Huber SMC 9000 stepping motor controller and a self-developed gate system, primary beam stopper and sample oven. If not stated otherwise, the measurements were carried out at r. t. in sealed Mark tubes with an outer diameter of 1 mm and a wall thickness of 0.01 mm.

- *compounds 1 - 5, and 4Na as obtained from synthesis*

Bulk materials of compounds **1 - 5**, and **4Na** were measured as obtained from synthesis. Compound **4** was additionally analyzed after crystallization from a DMSO-water mixture.

- *of compounds 2 and 3 after the pH-sensitivity tests*

Samples of compounds **2** and **3** after the pH-sensitivity tests were analogously prepared to the samples used for the SEM study.

- *of xerogels of 4*

Xerogels of **4** for XRD measurements were prepared analogously to the xerogels used for the SEM studies.

- *of wet hydrogels of 4*

Wet hydrogels of **4** for XRD measurements were prepared using a **4Na** solution with a concentration of 50 g L^{-1} . Gelation was induced by the addition of 4 eq. of GdL as described in chapter 9.4.3. Immediately after the addition of the GdL the solution was filled into a Mark tube with an outer diameter of 2.0 mm and a wall thickness of 0.01 mm. The tube was sealed and left to stand overnight at r. t. in a highly humid atmosphere. The measurement itself was performed at r. t. under standard humid atmosphere.

- *of a film of 4 prepared from a DMSO solution*

A drop casted film of **4** was prepared analogously to the one used for the SEM studies and powdered prior to the XRD measurement.

9.4.2 Investigations regarding the pH-sensitive aggregation and gel formation

Solubility and pH-sensitivity tests

To test the solubility of compounds **1** – **5**, approx. 10 mg were weight into a vial and around 1 mL of the respective solvent was added to achieve a fixed concentration of 10 g L⁻¹. The used acidic and alkaline solutions with different pH values were prepared by a dilution series of the respective 1 M stock solution.

To test the pH-sensitivity of **2**, a solution of **2** in hydrochloric acid solution with a concentration of 10 g L⁻¹ and a pH value of 1 was prepared. Compound **3** and **4** were dissolved in diluted NaOH solution with a pH value of 14 to achieve a concentration of 10 g L⁻¹, respectively. After addition of a few drops of 1 M NaOH to the solution of **2** and a few drops of 1 M HCl to solutions of **3** and **4**, respectively, the vial was sealed and shortly, but vigorously stirred.

pH-Titration experiments and time-dependent optical transmittance measurements

Titration experiments and pH-dependent optical transmittance measurements were performed using a titrator (Titrande 809, Metrohm), equipped with a titration unit (Dosino 800, Metrohm) and a Metrohm stirrer unit 801. Optical transmittance of the solution was detected by a turbidity probe ($\lambda_0 = 523$ nm, Spectrosense 6.1109.100, Metrohm) and was normalized in relation to pure water, which consequently has a relative (rel.) transmittance of 1. The pH value and temperature of the solution was determined by a glass membrane pH-electrode (Aquatrode Plus, pH: 0-13/0-60°C, Nr. 6.0257.000., Pt1000/ B/ 2/ 3 M KCl, Metrohm). The software Tiamo 1.2 was used to control titration parameters.

- *titration with an aqueous alkaline or acidic titer solution*

Solutions of compounds **2**, **3** and **4** were prepared with a volume of 80 mL and a compound concentration of 1 g L⁻¹ in desalted water, respectively. To adjust the pH value to 2.25 (**2**), 11.76 (**3**), and 10.70 (**4**) the respective amount of HCl or NaOH was added. While for compound **2** a titer solution of 0.1 M NaOH (Titrisol, Merck) was used, compounds **3** and **4** were titrated with 0.1 M HCl solution (Normadose, VWR). The injection rate of the titer solution was set to 0.02 mL min⁻¹.

- *time-dependent change of pH by the hydrolysis of glucono-delta-lactone (GdL)*

For the time-dependent optical transmittance measurements upon change of pH due to the hydrolysis of GdL, solutions of **4Na** with a concentration of 1 g L⁻¹ were prepared in desalted water (80 mL). The amounts of added GdL were 4 eq. (90.0 mg), 5 eq. (112.2 mg), and 6 eq. (134.7 mg), respectively. Details about the calculation of the GdL amounts can be found in chapter 9.4.3. After the addition of GdL to the solution of **4Na**, the pH value and the optical transmittance of the solution were recorded as a function of time over 8 h. For comparison

reasons a solution with 22.5 mg GdL in 80 mL desalted water without the gelator sodium salt **4Na** was measured under the same conditions. This amount corresponds to the excess of 1 eq. of GdL with regard to a solution of 80 mL of **4Na** with a concentration of 1 g L^{-1} .

Dynamic light scattering (DLS) and DLS-titration experiments

DLS experiments were performed on an ALV DLS/SLS-SP 5022F compact goniometer with ALV 5000/E cross-correlator and a He-Ne laser ($\lambda_0 = 632.8 \text{ nm}$). The solutions were filtered with a $0.45 \mu\text{m}$ nylon syringe filter prior to the measurement. To perform pH-dependent measurements the DLS device was combined with a titrator (Titrande 809, Metrohm). The scattering intensity data correspond to an average of three measurements, conducted at a detection angle of 90° for 1 min each.

- *titration with an aqueous alkaline or acidic titer solution*

For the titration experiments a solution of compound **4** in diluted NaOH solution was prepared with a concentration of 1 g L^{-1} , a pH value of 12.16, and a volume of 16 mL. As titer solution a 0.1 M aqueous HCl solution (Normadose, Prolabo) was added in steps of 0.02 mL with a subsequent stirring phase of 3 min and an equilibrium phase of 2 min before a DLS measurement consisting of three runs was performed.

- *time-dependent change of pH by the hydrolysis of GdL*

A solution of **4Na** in desalted water with a concentration of 1 g L^{-1} and a volume of 16 mL was measured with three DLS runs to show that no pre-aggregates of **4Na** are present in the solution. Two minutes after the addition of 4 eq. of GdL (18.0 mg) to this solution a single DLS run with a duration of 1 min was performed.

Cryogenic-transmission electron microscopy (cryo-TEM) studies

A solution of compound **4** was prepared with a concentration of 1 g L^{-1} in desalted water with 0.1 mL of a 5 M NaOH solution to adjust the pH value to 10.3. The solution was filtered with a $0.45 \mu\text{m}$ nylon syringe filter. With the pH-titration set up (Titrande 809 with the titration unit Dosino 800 and the stirrer unit 801, all from Metrohm) and the titration program as described above a 0.1 M HCl solution was added with an injection rate of 0.02 mL min^{-1} . At a pH value of 7.5 and 5.9 the titration was stopped and samples were taken for cryo-TEM studies.

A $2 \mu\text{l}$ droplet of each sample was put on a hydrophilized lacey carbon filmed copper grid (200 mesh, Science Services), where most of the liquid was removed with blotting paper leaving a thin film stretched over the carbon net holes. The specimens were instantly shock frozen by rapid immersion into liquid ethane and cooled to approximately 90 K by liquid nitrogen in a temperature-controlled freezing unit (Zeiss Cryobox, Zeiss NTS GmbH). After

freezing the specimens, the remaining ethane was removed using blotting paper. The temperature was monitored and kept constant in the chamber during all the sample preparation steps. The specimen was inserted into a cryotransfer holder (CT3500, Gatan) and transferred to a Zeiss EM922 EFTEM (Zeiss NTS GmbH). Examinations were carried out at temperatures around 90 K. The TEM was operated at an acceleration voltage of 200 kV. Zero-loss filtered images ($\Delta E = 0$ eV) were taken under reduced dose conditions (ca. 100–1000 e nm⁻²). All images were registered digitally by a bottom mounted CCD camera system (Ultrascan 1000, Gatan), that was combined and processed with a digital imaging processing system (Digital Micrograph 3.10 for GMS 1.8, Gatan).

TEM studies

For the TEM studies at r. t. hydrophilized lacey carbon filmed copper grids (200 mesh, Science Services) were dipped in a **4Na** solution (2 mL) with a concentration of 10 g L⁻¹, 2 min after the addition of 4 eq. of GdL (22.5 mg). Most liquid was removed with blotting paper, before the grid was dipped into desalted water to remove the remaining GdL and to stop the decrease of the pH value. The liquid was again removed by blotting paper and the sample was shortly dried at r. t. before images were taken at a Zeiss CEM902 (Zeiss NTS GmbH) at an acceleration voltage of 80 kV.

9.4.3 Gel preparation methods

*Gel preparation using solutions of **4Na** and aqueous acids*

Seven solutions of **4Na** in desalted water, each with a concentration of 10 g L⁻¹ and a volume of 2 mL were prepared in a screw cap vial (maximum volume: 4 mL, diameter: 15 mm). To the solutions five drops of a 1 M HCl solution, a 1 M H₂SO₄ solution, a 1 M CH₃COOH solution, a 1 M H₃PO₄ solution, a 1 M HNO₃ solution, a saturated (sat.) NaHSO₄ solution (1080 g L⁻¹), and a sat. NaH₂PO₄ solution (850 g L⁻¹) were added, respectively. After the addition of the aqueous acids the vials were immediately sealed and the mixtures were shortly but vigorously shaken. Gel state was defined if no gravitational flow occurred at inversion of the vial. For better visualization of inhomogeneities in the gels, the samples were irradiated with UV-light at 366 nm to induce blue luminescence.

*Gel preparation using solutions of **4Na** and acidic vapor or gas*

Solutions of **4Na** were prepared with a concentration of 10 g L⁻¹ in 2 mL of desalted water in a screw cap vial (maximum volume: 4 mL, diameter: 15 mm). 12 mL of concentrated

hydrochloric (32 %) or acetic acid (99 %) were filled in a Petri dish with a diameter of 6 cm. The Petri dish and the open vial with the gelator solution were put under a glass cover (inner diameter: 10 cm) for *approx.* 3 h until complete gelation was achieved.

Gels could also be prepared in an acidic atmosphere with HCl gas from a 200 bar compressed gas cylinder (HCl Brauchgas; Fa. Linde; degree of purity: 2.8). A high quality steel needle valve without pressure reading was used to dose the HCl gas flow. The open vial with gelator solution was put in a 50 ml-Schlenk flask, which was flushed with HCl gas. To neutralize the excess of HCl gas a washing bottle set up (1 M NaOH solution and water) was used.

*Gel preparation using solutions of **4Na** and glucono-delta-lactone (GdL)*

In this study the amount of GdL was calculated in respect to the molar amount of gelator **4Na** using the following equation:

$$m(\text{GdL}) = x \cdot c(\mathbf{4Na}) \cdot V \cdot \frac{M(\text{GdL})}{M(\mathbf{4Na})} \quad (9.1)$$

with $m(\text{GdL})$ representing the mass of GdL in [g], x the factor of molar excess of GdL compared to **4Na** in [eq.], $c(\mathbf{4Na})$ the concentration of the gelator sodium salt **4Na** in solution in [g L^{-1}], V the volume of the gelator solution, and $M(\text{GdL})$ and $M(\mathbf{4Na})$ the molar masses of GdL and compound **4Na**, respectively.

Therefore, the mass of added GdL varies depending on the concentration of **4Na**, the volume of gelator solution and the factor x . In this study four, five or six times the molar amount of GdL ($x = 4$ eq., $x = 5$ eq. or $x = 6$ eq.) compared to the molar amount of gelator **4Na** present in the solution were used.

To solutions of **4Na** with a concentration of 10 g L^{-1} and a volume of 2 mL 22.5 mg (4 eq.), 28.1 mg (5 eq.) and 33.7 mg (6 eq.) were added, respectively. After the addition of the GdL to the respective gelator solutions, the screw cap vials (maximum volume: 4 mL, diameter: 15 mm) were agitated until all GdL was dissolved and subsequently left to stand at r. t. for at least 8 h.

After the gelation the residual GdL and its hydrolysis products, such as gluconic acid, can be removed by a repeatedly applied washing procedure with desalted water. To prove the efficiency of this washing procedure, several hydrogel samples were prepared, washed, dried in high vacuum (4×10^{-3} mbar), and dissolved in DMSO- d_6 . The absence of the characteristic signals of gluconic acid and / or GdL in the $^1\text{H-NMR}$ spectrum proves the effectiveness of the washing procedure and that no GdL is incorporated or adsorbed on the fiber network of the gel.

9.4.4 Characterization of gel properties

Determination of the critical gelation concentration (cgc) by the “inverse tube test” and the “falling steel ball method”

For the determination of the cgc samples with a volume of 2 mL and seven different **4Na** concentrations (0.5 g L^{-1} , 1.0 g L^{-1} , 2.0 g L^{-1} , 4.0 g L^{-1} , 6.0 g L^{-1} , 8.0 g L^{-1} , and 10.0 g L^{-1}) were prepared in a 4 ml-screw cap vial with a diameter of 15 mm. For each concentration two samples were gelled by diffusion of HCl vapor and by addition of 4 eq., 5 eq., and 6 eq. of glucono-delta-lactone (GdL), respectively.

One sample of each gelator concentration and gelation method was used for the inverse tube test. Thereby, the gel stability is determined, if no gravitational flow occurs upon inversion of the test tube.

The other samples were used for the falling steel ball experiments. A small stainless steel sphere with a diameter of 2 mm and an average mass of 32.6 mg was gently put on the gel sample. Gels were defined as stable, if the steel ball did not sink in the gel within a week at r. t..

For the temperature-dependent measurements gel samples with a volume of 1 mL and 4 eq. of GdL were prepared with either a **4Na** concentration of 2 g L^{-1} or 10 g L^{-1} . The samples were heated in an oil bath with a heating rate of $1 \text{ }^\circ\text{C min}^{-1}$ using a high precision hotplate PZ 44 ET with a temperature control unit PR 5 SR-N (Harry Gestigkeit GmbH). As reference the temperature was measured in a vial with 1 mL of desalted water with a NiCr-Ni sensor.

Indentation experiments

Indentation experiments were performed on a universal testing machine INSTRON 5565. In the load cell with a maximum capacity of $F_{\text{max}} = 10 \text{ N}$ a cylindrical stainless steel reference block with a cross section dimension of 7 mm was attached. The gel sample with a volume of 35 mL was prepared in a 40 mL-glass vial with a diameter of 30 mm. The vial was inserted in the testing machine and the reference block was manually drawn near the surface of the gel. Subsequently an automatic measurement with a feed rate of 2 mm min^{-1} was started to gain the indentation stress-indentation depth-diagram.

Gels were prepared with 4 eq. of GdL and a **4Na** concentration of 2.0 g L^{-1} , 4.0 g L^{-1} , 6.0 g L^{-1} , 8.0 g L^{-1} and 10.0 g L^{-1} , respectively. Further, gels prepared with a **4Na** concentration of 2.0 g L^{-1} and 5 eq. and 6 eq. of GdL, respectively, were investigated. Additionally, solutions of **4Na** with a concentration of 10.0 g L^{-1} were gelled with HCl vapor.

The buoyancy of the reference block in a pure GdL solution (393.7 mg of GdL in 35 mL desalted water) is 3.5 mN at an indentation depth of 10.0 mm. This is negligible, as the indentation

stress for the performed measurements are in the range of several hundreds of mN at an indentation depth of 10.0 mm.

Gel stability against various solvents

For the stability tests against various solvents small gel samples with a gelator concentration of 10.0 g L^{-1} and 4 eq. GdL were prepared in small wells with a volume of 0.3 mL (Ambrose Mesa Mold with 12 round wells, Ted Pella, Inc.). To remove hydrolysis products of GdL, gels were washed three times with 3 mL of desalted water for 24 h. After this washing procedure gels were put in 3 mL of the respective solvent, which was renewed after 24 h. This procedure was repeated three times to ensure the complete exchange of the gelation medium. The condition of the gel samples in the different solvents was noted after the addition of the solvent (10 min), after complete exchange of the gelation medium (3 days) and after 14 days.

For tests with solvents that are immiscible with water, such as n-hexane, ethyl acetate, dichloromethane, and chloroform, gels were at first transferred into organogels by exchanging the water with ethanol (3 mL of solvent renewed after 24 h for at least three times).

9.4.5 Spectroscopic investigations

UV-Vis spectroscopy

- *of compounds **4** and **4Na** in solution*

The UV-Vis spectra in solution were recorded using a U-3000 Spectrophotometer (Fa. Hitachi) and 10 mm quartz glass cuvettes (Hellma QS-100). For compound **4** dilution series with concentrations of $10^{-3} \text{ mol L}^{-1}$, $10^{-4} \text{ mol L}^{-1}$, $5 \cdot 10^{-5} \text{ mol L}^{-1}$, $10^{-5} \text{ mol L}^{-1}$, $10^{-6} \text{ mol L}^{-1}$, $10^{-7} \text{ mol L}^{-1}$, and $10^{-8} \text{ mol L}^{-1}$ were prepared in DMSO and DMF, respectively. For compound **4Na** desalted water was used as a solvent and concentrations of $10^{-3} \text{ mol L}^{-1}$, $10^{-4} \text{ mol L}^{-1}$, $10^{-5} \text{ mol L}^{-1}$, and $10^{-6} \text{ mol L}^{-1}$ were measured.

- *of a film of **4** prepared from a DMSO solution*

A film of **4** was prepared by drop casting 50 μL of a DMSO solution with a concentration of 20 g L^{-1} onto a quartz glass substrate followed by evaporation of the solvent at $80 \text{ }^\circ\text{C}$ for 1 h. Ten absorbance spectra of the film were measured using a U-3000 Spectrophotometer (Fa. Hitachi) and the average spectrum of these ten spectra was calculated.

- *of compound **4Na/4** during the gelation with glucono-delta-lactone (GdL)*

To obtain absorbance spectra during the gelation process 3 mL of a **4Na** solution with a concentration of $10^{-5} \text{ mol L}^{-1}$ were prepared and filled in a 10 mm quartz glass cuvette (Hellma QS-100). After addition of 40 eq. of GdL (0.21 mg) the cuvette was closed, shortly but

vigorously shaken and UV-Vis measurements were performed using a U-3000 Spectrophotometer (Fa. Hitachi). Each absorbance spectra was measured using a scan speed of 600 nm min^{-1} , so that one spectrum could be obtained in 83 seconds.

Photoluminescence (PL) measurements

- *of compounds **4** and **4Na** in solution*

The PL spectra in solution were recorded using a Spectrofluorometer RF-5301 (Fa. Shimadzu) at an excitation wavelength of $\lambda_{\text{exc}} = 300 \text{ nm}$. Solutions of compound **4** in DMSO and DMF were prepared with a concentration of 10 g L^{-1} , respectively and measured in 10 mm quartz glass cuvettes (Hellma QS-111). Compound **4Na** was dissolved at a concentration of 10 g L^{-1} in desalted water and analogously measured.

- *of a film of **4** prepared from a DMSO solution*

A film of **4** was prepared by drop casting $50 \mu\text{L}$ of a DMSO solution with a concentration of 20 g L^{-1} onto a quartz glass substrate followed by evaporation of the solvent at $80 \text{ }^\circ\text{C}$ for 1 h. Ten PL spectra of the film were measured using a Spectrofluorometer RF-5301 (Fa. Shimadzu) at an excitation wavelength of $\lambda_{\text{exc}} = 330 \text{ nm}$. The average spectrum of these ten spectra was calculated and normalized to 1.

- *of compound **4** in hydrogel state after gelation with GdL*

The hydrogel sample of **4** for PL investigations was prepared using 3 mL of a **4Na** solution in desalted water at a concentration of 10 g L^{-1} and 4 eq. of GdL (33.7 mg). After mixing the **4Na** solution with GdL the solution was shortly but vigorously shaken and then immediately filled in a quartz glass cuvette (Hellma 111-QS). The sample was left to stand at r. t. for 24 h before ten PL spectra were recorded on a Spectrofluorometer RF-5301 (Fa. Shimadzu) at an excitation wavelength of $\lambda_{\text{exc}} = 330 \text{ nm}$. The average spectrum of these ten spectra was calculated and normalized to 1.

- *of compound **4Na/4** during the gelation with GdL*

To obtain time-dependent PL spectra during the gelation with GdL, a hydrogel sample of **4** was prepared as described above with 10 g L^{-1} of **4Na** in desalted water and 4 eq. of GdL. After the addition of the GdL, the solution was shortly but vigorously shaken, and immediately filled in a quartz glass cuvette (Hellma 111-QS). PL spectra were recorded after distinct time intervals using a Spectrofluorometer RF-5301 (Fa. Shimadzu) at an excitation wavelength of $\lambda_{\text{exc}} = 300 \text{ nm}$. The spectra were recorded using a *medium* scan speed, which correlates to a recording time for one spectrum of about 100 seconds. Upon increasing the scan speed the signal to noise ratio decreased, so that no reasonable spectra could be obtained.

Analogously a gel sample was prepared in a 4 ml-screw cap vial with a diameter of 15 mm. Optical images were taken under UV-irradiation at 366 nm at distinct times, corresponding to the times at which PL spectra were recorded.

9.4.6 Theoretical calculations

Computational details of the density functional theory (DFT) and time-dependent (TD) DFT calculations

The programs Gaussian 03³⁸⁵ and Turbomole³⁸⁶ were used to carry out the DFT and TDDFT calculations for the monomer, dimer, trimer, and tetramer of **4**, where the three-parameter semi-empirical hybrid functional B3LYP,^{387,388} together with the basis set 6-31G** were used for all atoms. No constraints in the geometry optimizations were applied. The reliability of the optimized geometries was checked by calculation of vibrational frequencies. The (ground state) optimized geometries obtained from the DFT calculations were used to compute the energies of the excited states (singlets and triplets) using TDDFT. The xyz coordinates of the optimized structures can be found in the literature.¹⁰²

9.4.7 Biocompatibility tests

*Antiproliferative effects and cytotoxicity of compounds **4** and **4Na***

Antiproliferative effects and cytotoxicity of the compounds **4** and **4Na** were evaluated at the Hans-Knöll Institute Jena, Germany, according to methods described elsewhere.³⁸⁹ Cells were incubated with dilutions of the test substances for 72 h at 37 °C. The results are summarized in Table 9.1 and can be interpreted using the following legend:

GI₅₀: concentration for 50 % inhibition of cell growth; CC₅₀: concentration for 50 % cell death

- > 50 µg mL⁻¹ : not or marginally cytotoxic / antiproliferative
- 10 - 50 µg mL⁻¹ : moderately cytotoxic / antiproliferative
- 1-10 µg mL⁻¹ : highly cytotoxic / antiproliferative
- < 1 µg mL⁻¹ : extremely cytotoxic / antiproliferative

Table 9.1: Antiproliferative effects and cytotoxicity of compounds **4** and **4Na**. HUVEC: human umbilical vein endothelial cells. K-562: human immortalized myelogenous leukaemia cells. HeLa: human cervix carcinoma cells. GI₅₀: concentration for 50 % inhibition of cell growth. CC₅₀: concentration for 50 % cell death.

| compound | antiproliferative effect | | cytotoxicity |
|------------|--|--|--|
| | HUVEC | K 562 | HeLa |
| | GI ₅₀ [$\mu\text{g mL}^{-1}$] | GI ₅₀ [mg mL^{-1}] | CC ₅₀ [$\mu\text{g mL}^{-1}$] |
| 4 | > 50 | > 50 | > 50 |
| 4Na | > 50 | > 50 | > 50 |

Antimicrobial activity of compounds 4 and 4Na

The antimicrobial activity of compounds **4** and **4Na** was determined at the Hans-Knöll Institute Jena, Germany, by agar diffusion assays. 34 mL of nutrient agar were liquefied and inoculated with a suspension of the corresponding microorganisms so that a final concentration of 10^7 cells per 34 mL of nutrient agar was reached. The inoculated nutrient medium was put immediately into the test plates resulting in an even layer with a thickness of about 3 mm. 12 holes per test plate were punched out using an appropriate device. 50 μL of a solution of the test substances in DMSO or distilled water (A. dest.) with a concentration of 1000 mg mL^{-1} of test substance were put in each hole, respectively. For comparison purposes, pure solvents (DMSO and A. dest.) were also tested. The test plates were cultivated for 18 h at 37 °C. Evaluation of the antimicrobial activity was done by detection of the zones of growth inhibition by the naked eye (diameter in mm) according to Table 9.2.

Compounds **4** and **4Na** were tested for their influence on the growth of the following microorganisms:

Bacillus subtilis

Staphylococcus aureus

Escherichia coli

Pseudomonas aeruginosa

Penicillium notatum

Table 9.2: Characterization of the antimicrobial activity using the diameter of the inhibition zone.

| diameter of the inhibition zone [mm] | description |
|---|--------------------|
| 0 | no activity |
| 15 - 21 | moderate activity |
| 21 - 25 | good activity |
| > 25 | very good activity |

The results of the agar diffusion assays are presented in Table 9.3.

Table 9.3: Antimicrobial activity of compounds **4** and **4Na** determined by agar diffusion assays. Values: zone of growth inhibition (diameter in mm). p: few colonies in the zone of growth inhibition. P: many colonies in the zone of growth inhibition. A: indication for growth inhibition. (F: promotion of growth.)

| compound | solvent | c [$\mu\text{g mL}^{-1}$] | <i>Bacillus</i> <i>subtilis</i> | <i>Staphylococcus</i> <i>aureus</i> | <i>Escherichia</i> <i>coli</i> | <i>Pseudomonas</i> <i>aeruginosa</i> | <i>Penicillium</i> <i>notatum</i> |
|------------|----------|--------------------------------|------------------------------------|--|-----------------------------------|---|--------------------------------------|
| | | | ATCC 6633 B1 | SG511 B3 | SG458 B4 | K799/61 B9 | JP36 P1 |
| 4 | DMSO | 1000 | 0 | 0 | 12A | 0 | 0 |
| 4Na | A. dest. | 1000 | 0 | 0 | 0 | 0 | 0 |
| | A. dest. | | 0 | 0 | 0 | 0 | 0 |
| | DMSO | | 0 | 0 | 14P | 16P | 14p |

DMSO: dimethyl sulphoxide; A. dest. : distilled water

9.4.8 Investigations regarding the adsorption properties of gels of **4**

BET measurements

Krypton physisorption was conducted at 77 K on a Quantachrome Autosorb 1 instrument by Lena Geiling at the Department of Inorganic Chemistry I (Prof. J. Breu) of the University of Bayreuth. Prior to the measurements, compound **4** after recrystallization and compound **4Na** as obtained from synthesis were degassed at 423 K for 24 h. Gel samples of **4** were prepared analog to the samples examined by SEM imaging and either degassed at 423 K or 523 K for 24 h.

Calibration curve of rhodamine B in desalted water

- *preparation of the rhodamine B solutions*

For the calibration curve rhodamine B solutions with 12 different concentrations were used (Table 9.4). Therefore, a solution with a concentration of 907.4 mg L^{-1} was prepared by weighing in 90.74 mg of rhodamine B in 100 mL of desalted water. This solution was diluted by a factor of five with desalted water to get a stock solution for the dilution series with a concentration of 0.18148 g L^{-1} of rhodamine B (*1st stock solution generation, 1.0 eq.*).

This *1st* generation stock solution was used to prepare solutions for the calibration curve with a volume of 5 mL and a rhodamine B concentration of 0.03630 g L^{-1} (0.20 eq.) and 0.01815 g L^{-1} (0.10 eq.), respectively.

Furthermore, this stock solution was diluted to achieve 20 mL of a rhodamine B solution with a concentration of 0.01815 g L^{-1} (0.10 eq., 2^{nd} stock solution generation). From this 2^{nd} stock solution solutions with a volume of 5 mL and the following concentrations were prepared as shown in Table 9.4: 0.01452 g L^{-1} (0.08 eq.), 0.01089 g L^{-1} (0.06 eq.), 0.00726 g L^{-1} (0.04 eq.), 0.00336 g L^{-1} (0.02 eq.), and 0.00181 g L^{-1} (0.01 eq.).

A 3^{rd} generation stock solution with a volume of 20 mL and a rhodamine B concentration of $0.00181 \text{ mg L}^{-1}$ (0.01 eq.) was prepared from the 2^{nd} stock solution. The 3^{rd} generation stock solution was diluted to prepare the solutions with a concentration of 0.00145 g L^{-1} (0.008 eq.), 0.00109 g L^{-1} (0.006 eq.), 0.00073 g L^{-1} (0.004 eq.), 0.00036 g L^{-1} (0.002 eq.), and 0.00018 g L^{-1} (0.001 eq.).

Table 9.4: Dilution series of the rhodamine B solutions that were used for the generation of the calibration curve.

| stock solution generation | c [g L^{-1}] | molar ratio dye/gelator [eq.] ^a | mass ratio dye/gelator [mg g^{-1}] ^a | preparation | | | | O.D. at 553 nm ^b |
|---------------------------|------------------------------|--|--|------------------------|---------------------|--------------------------|---------------|-----------------------------|
| | | | | V(stock solution) [mL] | used stock solution | V(H ₂ O) [mL] | V(total) [mL] | |
| 1 st | 0.18148 | 1.0 | 756.2 | 1.0 | - | 4.0 | 5.0 | - |
| | 0.03630 | 0.2 | 151.2 | 1.0 | 1 st | 4.0 | 5.0 | 7.771 |
| | 0.01815 | 0.1 | 75.6 | 0.5 | 1 st | 4.5 | 5.0 | 3.587 |
| 2 nd | 0.01815 | 0.1 | 75.6 | 2.0 | 1 st | 18.0 | 20.0 | - |
| | 0.01452 | 0.08 | 60.5 | 4.0 | 2 nd | 1.0 | 5.0 | 3.327 |
| | 0.01089 | 0.06 | 45.4 | 3.0 | 2 nd | 2.0 | 5.0 | 2.505 |
| | 0.00726 | 0.04 | 30.2 | 2.0 | 2 nd | 3.0 | 5.0 | 1.711 |
| | 0.00363 | 0.02 | 15.1 | 1.0 | 2 nd | 4.0 | 5.0 | 0.958 |
| | 0.00181 | 0.01 | 7.6 | 0.5 | 2 nd | 4.5 | 5.0 | 0.426 |
| 3 rd | 0.00181 | 0.01 | 7.6 | 2.0 | 2 nd | 18.0 | 20.0 | - |
| | 0.00145 | 0.008 | 6.0 | 4.0 | 3 rd | 1.0 | 5.0 | 0.382 |
| | 0.00109 | 0.006 | 4.5 | 3.0 | 3 rd | 2.0 | 5.0 | 0.288 |
| | 0.00073 | 0.004 | 3.0 | 2.0 | 3 rd | 3.0 | 5.0 | 0.215 |
| | 0.00036 | 0.002 | 1.5 | 1.0 | 3 rd | 4.0 | 5.0 | 0.132 |
| | 0.00018 | 0.001 | 0.8 | 0.5 | 3 rd | 4.5 | 5.0 | 0.054 |

^a assuming a volume of the dye solution of 5 mL and a gelator (**4Na**) concentration of 10 g L^{-1} at a gel volume of 0.12 mL, which are the usual testing conditions for the concentration-dependent adsorption studies; ^b average of the optical density (O.D.) at 553 nm of 4 measurements.

- *generation of the calibration curve*

UV-Vis spectra of the solutions were recorded from 300 nm to 700 nm on a spectrophotometer Hitachi U-3000. For the baseline measurements and as reference in the double beam spectrophotometer desalted water was used. Each of the dye solutions was measured four times in a 1 mm quartz glass cuvette (Hellma QS-100). The optical density of all

recorded spectra was manually set to zero at a wavelength of 625 nm. The absorption maxima at 553 nm were determined and the average and standard deviation of the four obtained data points for each concentration were plotted versus the concentration (Figure 5.3, chapter 5.2.1.1). The regression curve was calculated with the “linear fit”-function of the software OriginPro 8 (v8.0724, Microsoft). For the calculation the intercept was set to zero.

Preparation of the PDMS molds

The molds for the preparation of the hydrogels used in the adsorption and release studies are made of polydimethylsiloxane (PDMS). Therefore, the silicon elastomer “Sylgard 184” (88 g) and the silicon elastomer curing agent “Sylgard A84” (8 g; both from Dow Corning®, used as received) were mixed in a ratio of approximately 10 to 1. The mixture was poured into a custom-made Teflon® mold with inner dimensions of ca. 6.5 cm x 6.5 cm x 1.0 cm and 25 cylindrical elevations of 0.5 cm in height and diameter. The PDMS form was left to harden at r. t. for three days and was then removed from the Teflon® mold. The resulting PDMS mold had consequently 25 wells with a depth and diameter of 0.5 cm, respectively.

Preparation of defined hydrogel samples for the adsorption experiments

If not stated otherwise, the hydrogel samples for the adsorption experiments were prepared by mixing 40 mg of the gelator sodium salt **4Na** with 4 mL of desalted water (chapter 9.4.3). After addition of 45.0 mg of GdL (4 eq. in respect to the molar amount of **4Na**), the solution was shaken until complete dissolution of the GdL and immediately transferred into the wells of the PDMS mold with an Eppendorf pipette. Each well was filled with 0.12 mL of the gelator/GdL-solution. To ensure complete gelation the samples were left to stand at r. t. overnight. A highly humid atmosphere was established to prevent dehydration of the samples. Each gel sample was then transferred with a small spatula to a glass vial with 5 mL of desalted water to remove the sodium gluconate that is a byproduct of the gelation process. After 24 h the water was renewed and again left to stand at r. t. for 24 h. This washing process was performed three times, before the gel samples were used for further experiments.

Tests evaluating the influence of mechanical agitation on the adsorption kinetics

For the tests investigating the influence of agitation on the adsorption properties, gel samples with a volume of 0.10 mL and an initial **4Na** concentration of 10 g L^{-1} were prepared analogously to the procedure described above. As the gels contained 1.0 mg of **4Na** (1.58 μmol), respectively, 5 mL of a rhodamine B solution with a dye content of 0.05 eq. in respect to the molar amount of **4Na** were prepared containing 0.038 mg of rhodamine B,

which corresponds to a concentration of 0.0076 g L^{-1} and a mass ratio of 38 mg g^{-1} dye per gelator.

A stock solution was prepared with 11.3 mg of rhodamine B in 30 mL desalted water ($c = 0.38 \text{ g L}^{-1}$). This stock solution was diluted by a factor of ten to achieve a diluted stock solution with a concentration of 0.038 mg mL^{-1} . 1 mL of this diluted stock solution was mixed with 4 mL of desalted water to obtain a rhodamine B solution with the desired concentration of 0.0076 g L^{-1} (0.05 eq. , 38 mg g^{-1}). Four solutions with this concentration and a volume of 5 mL were prepared analogously from the diluted stock solution. To each solution a washed hydrogel sample with a gelator **4Na** content of 1.0 mg ($V = 0.1 \text{ mL}$) was added. Two samples with the same rhodamine B concentration were agitated on a Vibrax VXR basic from IKA® at *ca.* 200 rpm and two were left to stand without any disturbances. Both experiments were performed at r. t.. After 24 h , 48 h , 72 h , 96 h and 168 h UV-Vis absorbance measurements were performed analogously to the UV-Vis measurements described for the calibration curve. After the optical densities of these spectra were set to zero at a wavelength of 625 nm , the absorbance maxima were determined at 553 nm . The average value and the standard deviation of the two measurements with and without agitation were calculated. The adsorption capacities in dependence of time q_t were calculated as described in chapter 5.2.1.

Time-dependent adsorption studies with different initial dye concentrations

For the adsorption studies hydrogels of **4** were prepared as described above with a volume of 0.12 mL , a gelator sodium salt (**4Na**) concentration of 10 g L^{-1} , and 4 eq. of GdL in respect to the molar amount of the gelator. The hydrogel samples were washed as described above to remove the sodium gluconate. The rhodamine B solutions with concentrations of 0.005 eq. (0.00091 g L^{-1}), 0.01 eq. (0.00181 g L^{-1}), 0.02 eq. (0.00363 g L^{-1}), 0.05 eq. (0.00907 g L^{-1}), 0.10 eq. (0.01815 g L^{-1}) and 0.20 eq. (0.03630 g L^{-1}) were prepared analogously to the solutions for the calibration curve.

The washed hydrogels were each put in 5 mL of the rhodamine B solution with the respective concentration and left to stand undisturbed at r. t.. After 1 h , 3 h , 6 h , 24 h , 48 h , 72 h , and 240 h UV-Vis absorbance measurements were performed analogously to the UV-Vis measurements described for the calibration curve. The absorbance maxima were determined at 553 nm after the optical densities of these spectra were set to zero at a wavelength of 625 nm . Each experiment was performed three times to get an average value and a standard deviation of the optical density.

The adsorption capacity in dependence of time q_t and the decolorization efficiency d_e were calculated as described in chapter 5.2.1.

Thermal stability test of adsorbed dye-gel systems

Hydrogels of **4** were prepared as described above with a volume of 0.12 mL, a gelator sodium salt (**4Na**) concentration of 10 g L^{-1} , and 4 eq. of GdL. After the washing procedure the gel samples were put in 5 mL of a rhodamine B solution with a concentration of 0.00907 g L^{-1} (0.05 eq.) for ten days analogously to the performed time-dependent adsorption studies. Subsequently, the gel samples were put in 5 mL of desalted water at r.t. and $40 \text{ }^\circ\text{C}$, respectively. After 1 d, 2 d, 3 d, 4 d, and 10 d UV-Vis absorbance measurements were performed analogously to the UV-Vis measurements described for the calibration curve to determine the cumulative release of rhodamine B in dependence of time. Each experiment was performed in triplicate.

9.4.9 Hydrogel formation in presence of rhodamine B and release in water

Preparation of defined hydrogel samples in presence of rhodamine B

Rhodamine B solutions with 9 different concentrations were prepared for the formation of hydrogels in presence of distinct amounts of the dye. A stock solution with a concentration of 7.56207 g L^{-1} of rhodamine B was prepared by weighing in 302.4828 mg of rhodamine B into 40 mL of desalted water. This equals 1.0 eq. of rhodamine B in one gel sample with regard to the molar amount of gelator **4** in a gel sample with a volume of 0.12 mL and a concentration of 10 g L^{-1} of **4Na**. The other solutions were prepared from this stock solution by a dilution series as shown in Table 9.5.

Table 9.5: Preparation of rhodamine B solutions for the hydrogel formation in presence of the dye.

| stock solution generation | c [g L^{-1}] | molar ratio dye/gelator [eq.] ^a | mass ratio dye/gelator [mg g^{-1}] ^a | V(stock solution) [mL] | preparation used stock solution | V(H_2O) [mL] | V(total) [mL] |
|---------------------------|------------------------------|--|--|------------------------|---------------------------------|--------------------------------|---------------|
| 1 st | 7.56207 | 1.00 | 756.2 | - | - | - | 40.0 |
| | 6.04965 | 0.80 | 605.0 | 4.0 | 1 st | 1.0 | 5.0 |
| | 4.53724 | 0.60 | 453.7 | 3.0 | 1 st | 2.0 | 5.0 |
| | 3.78103 | 0.50 | 378.1 | 2.5 | 1 st | 2.5 | 5.0 |
| | 3.02483 | 0.40 | 302.5 | 2.0 | 1 st | 3.0 | 5.0 |
| | 2.26862 | 0.30 | 226.9 | 1.5 | 1 st | 3.5 | 5.0 |
| | 1.51241 | 0.20 | 151.2 | 1.0 | 1 st | 4.0 | 5.0 |
| | 0.75621 | 0.10 | 75.6 | 0.5 | 1 st | 4.5 | 5.0 |
| | 0.37810 | 0.05 | 37.8 | 0.25 | 1 st | 4.75 | 5.0 |

^a assuming a gelator (**4Na**) concentration of 10 g L^{-1} at a gel volume of 0.12 mL, which are the usual testing conditions for the concentration-dependent release studies.

To the different rhodamine B solutions gelator sodium salt **4Na** ($c = 10 \text{ g L}^{-1}$) and GdL (4 eq. in respect to the molar amount of **4Na**) were added. Gels with a volume of 0.12 mL were prepared in the wells of the PDMS mold by gelation overnight in a highly humid atmosphere.

Time-dependent release of rhodamine B in water

After gelation overnight the gels prepared in the presence of different amounts of rhodamine B were each put in 5 mL of desalted water and left to stand at r. t. undisturbed. As gels with rhodamine B contents higher than 0.50 eq. could not be removed from the wells without gel destruction, the concentration-dependent release study was only performed with rhodamine B concentrations of 0.05 eq., 0.10 eq., 0.20 eq., 0.30 eq., 0.40 eq., and 0.50 eq.. After 1.5 h, 3 h, 6 h, 24 h, 48 h, 72 h, and 240 h absorbance spectra of the accepting solutions were recorded in a 1 mm quartz glass cuvette (Hellma QS-100) analogously to the spectra recorded for the calibration curve in water. Each experiment was performed in triplicate. The data were processed as described above to get the average value and standard deviation of the concentration present in the solution after a specific time. From this concentration the cumulative release M_{rel} , the amount of still encapsulated and adsorbed amount M_{encaps} , and the loading efficiency I_e can be calculated as described in chapter 5.3.1.

9.4.10 Release studies in biologically relevant media

Preparation of the biologically relevant media

- *phosphate buffered saline (PBS)*

Dulbecco's PBS (without Ca & Mg) with a pH value of 7.4 was purchased from PAA Laboratories (Pasching, Austria) and used as received.

- *simulated body fluid (SBF)*

The SBF was prepared by subsequently adding the ingredients displayed in Table 9.6 to approximately 750 mL of Milli-Q water in a 1 L-volumetric flask. Especially the tris(hydroxymethyl)amino methane was added very slowly to avoid precipitation. The pH value was adjusted to 7.65 at 25 °C using 1 M HCl titer solution to obtain a pH value of 7.4 at 37 °C. Subsequently the volumetric flask was filled to 1 L with Milli-Q water.

Table 9.6: Chemicals used for the preparation of SBF in the order of addition.

| order | chemical | amount [g] (for solids) |
|-------|--|----------------------------|
| 1 | NaCl | 7.996 |
| 2 | NaHCO ₃ | 0.350 |
| 3 | KCl | 0.224 |
| 4 | K ₂ HPO ₄ ·3H ₂ O | 0.228 |
| 5 | MgCl ₂ ·6H ₂ O | 0.305 |
| 6 | 1M HCl (aq.) | 35ml |
| 7 | CaCl ₂ ·2H ₂ O | 0.368 |
| 8 | Na ₂ SO ₄ | 0.071 |
| 9 | tris(hydroxymethyl)amino methane NH ₂ C(CH ₂ OH) ₃ | 6.057 |

- *simulated gastric fluid (SGF)*

The fasted state SGF was prepared analogous to the composition published in the literature.^{297,310,390} First, a buffer solution with 999.3 mg sodium chloride (analytic. grade) in 400 mL of Milli-Q water was prepared. The pH was adjusted to 1.6 at a temperature of 37 °C by addition of approximately 9 mL of 1 M HCl titer solution. To 250 mL of this buffer solution 21.5 mg of sodium taurocholate hydrate (NaTC ≥ 97 %) were added. A lecithin solution (L- α -Phosphatidylcholine from egg yolk, type XVI-E, ≥ 99 %, lyophilized powder) in DCM (dichloromethane, analytic. grade) was prepared with a concentration of 100 g L⁻¹. 92.6 μ L of this solution were added to the buffer solution with the NaTC under slight stirring. The DCM was subsequently removed under mild conditions at the rotary evaporator. The pH value was again set to 1.6 at 37 °C with 1 M HCl. Subsequently, 500.0 mg of pepsin from porcine gastric mucosa (*Ph. Eur.*) and the residual buffer solution were added. The pH value was again adjusted at 37 °C and finally the volumetric flask was filled with Milli-Q water to 500 mL.

- *simulated intestinal fluid (SIF)*

The fasted state SIF was prepared analog to the composition published in the literature.^{297,310,390} First, a buffer solution in 400 mL of Milli-Q water was prepared with 2.005 g of sodium chloride (analytic. grade), 1.1096 g of maleic acid (> 99 %), and 696.0 mg of sodium hydroxide (analytic. grade). The pH value was set to 6.5 at 37 °C by addition of 1 M NaOH titer solution. To 250 mL of this buffer solution 806.5 mg of sodium taurocholate hydrate (NaTC, ≥ 97 %) were added. A lecithin solution (L- α -Phosphatidylcholine from egg yolk, type XVI-E, ≥ 99 %, lyophilized powder) in DCM (analytic. grade) was prepared with a concentration of 100 g L⁻¹. 0.76 mL of this solution was added to the buffer solution with the NaTC under slight stirring. The DCM was subsequently removed under mild conditions at the rotary evaporator.

The pH value was set to 6.5 at 37 °C with 1 M NaOH. The residual buffer solution was added, the pH value was again adjusted at 37 °C, and finally the volumetric flask was filled with Milli-Q water to 500 mL.

Stability of pure hydrogels of 4 in biologically relevant media

To test the stability of the pure hydrogels in the biologically relevant media PBS, SBF, SGF, and SIF, hydrogels with of **4** with a volume of 0.12 mL and a gelator concentration of 10 g L⁻¹ of **4Na** were prepared with 4 eq. of GdL and washed analogous to the hydrogel samples used for the adsorption studies. The resulting gels were put in 5 mL of the respective accepting media and the quantitative dissolution behavior of the gels was monitored by a series of optical images, that were taken after distinct time intervals.

In PBS the stability of hydrogels of **4** was investigated at r. t., while in SBF the study was performed at r. t. and 37 °C. In SGF and SIF the stability of the gels was monitored at 37 °C.

Stability of hydrogels of 4 prepared in the presence of rhodamine B in biologically relevant media

Hydrogels of **4** with a volume of 0.12 mL and a gelator concentration of 10 g L⁻¹ of **4Na** were prepared with 4 eq. of GdL in presence of 0.05 eq. (37.8 mg g⁻¹) of rhodamine B as described above (chapter 9.4.9) and put in 5 mL of the respective accepting media. The stability of the gels and the release of rhodamine B were monitored by optical images and UV-Vis spectroscopy after distinct time intervals at r. t. for studies in PBS and at 37 °C for studies in SBF, SGF and SIF. The UV-Vis spectra were recorded in a 1 mm quartz glass cuvette (Hellma QS-100) analogously to the spectra recorded for the calibration curve in water. For the studies at elevated temperature the biologically relevant media were preheated to 37 °C and the samples were stored at 37 °C in a cooled incubator (KB53 from Binder) during the whole experiment. Samples were only taken out for recording the optical images and the UV-Vis spectra. Due to the experimental effort of conducting UV-Vis measurements, such as filling 0.3 mL of each solution in a 1 mL cuvette, the measurement itself and the returning of the measured solution back into the respective sample, at each time interval the samples were exposed to r. t. for approx. 15 minutes.

Each experiment was performed in triplicate and spectroscopic data were processed as described above for the release studies in water (chapter 9.4.9). As none of the simulated fluids showed significant absorbance in the relevant range of 300 nm to 700 nm, desalted water was used for the baseline measurement as described above.

Calibration curve of rhodamine B in PBS and preparation of reference samples

A calibration curve of rhodamine B in PBS was developed with six different rhodamine B concentrations: 0.03630 g L^{-1} , 0.01815 g L^{-1} , 0.00907 g L^{-1} , 0.00363 g L^{-1} , 0.00181 g L^{-1} , 0.00091 g L^{-1} . The solutions were prepared by a dilution series from a stock solution in PBS analogously to the solutions prepared for the calibration curve in water. The absorbance spectra of the solutions were recorded in triplicate and processed as described above. The position of the relative maximum could be found at 553 nm in each spectrum, *i. e.* it was independent of the concentration of rhodamine B. Therefore, a calibration curve could be developed, which is shown in Figure 9.1. The regression curve was calculated with the “linear fit”-function of the software OriginPro 8 (v8.0724, Microsoft). For the calculation the intercept was set to zero.

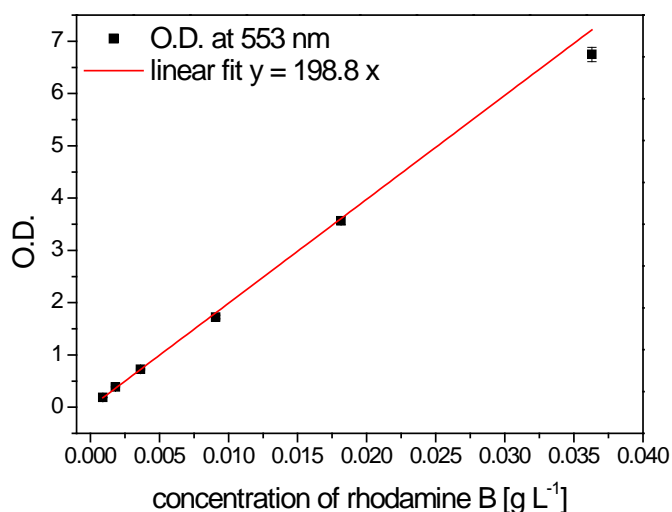


Figure 9.1: Calibration graph with 6 different rhodamine B concentrations in PBS; each data point is the average of three measurements.

To test the hypothesis that all rhodamine B is released after 24 h in PBS, two types of reference samples were prepared. As reference sample with solely rhodamine B in PBS, the three solutions with a rhodamine B concentration of 0.00907 g L^{-1} were used that were originally prepared for the generation of the calibration curve in PBS. Furthermore, three reference samples with this rhodamine B concentration, as well as 1.2 mg of **4Na**, 1.35 mg of GdL, and 0.12 mL of water were prepared by the following procedure. The amount of GdL was weighed in into 5 mL of PBS. The mixture was left to stand at *r. t.* overnight, so that the GdL molecules were hydrolyzed. Subsequently, 1.2 mg of the gelator sodium salt **4Na** was added, as well as 0.12 mL of the rhodamine B solution with a concentration of 0.37810 g L^{-1} .

Preparation of reference samples in SBF

The reference sample with only rhodamine B in SBF was prepared by a dilution series, analogous to that prepared in PBS, to yield 5 mL of SBF with a rhodamine B concentration of 0.00907 g L^{-1} . For the other reference sample to 5 mL of such a rhodamine B solution in SBF with a concentration of 0.00907 g L^{-1} , 1.2 mg of **4Na** were added. The UV-Vis spectra were recorded and processed analogously to the spectra recorded for the calibration curve in water.

Calibration curve of rhodamine B in SGF

A calibration curve of rhodamine B in SGF was developed with six different rhodamine B concentrations: 0.03630 g L^{-1} , 0.01815 g L^{-1} , 0.00907 g L^{-1} , 0.00363 g L^{-1} , 0.00181 g L^{-1} , 0.00091 g L^{-1} . The solutions were prepared by three independently prepared dilution series from a stock solution in SGF analogously to the solutions prepared for the calibration curve in PBS. The absorbance spectra of the solutions were measured and processed analogously to the spectra recorded for the calibration curve in water. The spectra showed a respective maximum at 556 nm each, independent of the concentration of rhodamine B.

Calibration curves of rhodamine B in SIF

A calibration curve of rhodamine B in SIF was developed analogous to the one developed in PBS with six different rhodamine B concentrations: 0.03630 g L^{-1} , 0.01815 g L^{-1} , 0.00907 g L^{-1} , 0.00363 g L^{-1} , 0.00181 g L^{-1} , 0.00091 g L^{-1} . Additionally a calibration curve with the same rhodamine B concentrations and additional 1.2 mg of **4Na** in 5 mL of the respective solution was prepared to simulate the conditions at the end of the release study with the respective maximum optical density at 559 nm.

9.4.11 Hydrogel film formation *via* electrogelation*Proof-of-principle experiment of the electrogelation*

For the proof of principle experiment a standard thin layer chromatography (TLC) chamber filled with a **4Na** solution (1 g L^{-1}) was used. A stainless steel slide acted as cathode, while the anode consisted of an indium tin oxide (ITO)-covered glass substrates. Both electrodes were connected to a 9-volt battery for about 10 min.

Preparation of hydrogel films by electrogelation

The preparation of hydrogel films using the electrolysis of water was carried out using a custom-made three-electrode set up connected to a scanning potentiostat (model 362,

Princeton Applied Research Corp.), which was set to potential controlled mode. While a graphite wire was used as counter electrode, a silver wire acted as pseudo-reference electrode. The working electrodes were 25 x 25 mm indium tin oxide (ITO)-covered glass substrates. As electrochemical cell a rectangular chamber for thin layer chromatography (TLC) was employed and filled with 30 mL of gelator solution, respectively. Five different electrogelation parameters were systematically varied to test their influence on the gel film formation. As standard condition for these tests the distance between the electrodes was set to 3 cm, a potential of 1.5 V was applied, a gelator sodium salt (**4Na**) concentration of 1 g L⁻¹, a background electrolyte (NaCl) concentration of 10 mM, and a gelation time of 10 min was employed. The substrates were dipped into desalted water immediately after the electrogelation to wash away the dissolved NaCl. While optical images were taken in the wet state after the washing process, further analysis of the hydrogel films, such as the determination of the film thickness as well as SEM and spectroscopic investigations, was performed after drying the samples at ambient temperatures.

Determination of the average thickness of dried hydrogel films prepared by electrogelation

The thickness of the gel films was measured using a Dektak 3030 ST from Veeco Instruments. If not stated otherwise, the average thickness of a film was calculated from nine measurements per film.

*SEM study of dried hydrogel films of **4** prepared by electrogelation*

All samples were sputtered with platinum prior to SEM imaging.

The washed and dried hydrogel films of **4** were mounted on a standard sample holder by a conductive adhesion pad and examined with a Zeiss LEO 1530 (FE-SEM with Schottky-field-emission cathode; in-lens detector) using an accelerating voltage of 3 kV.

*UV-Vis spectroscopy on dried hydrogel films of **4** prepared by electrogelation*

The UV-Vis spectra of the washed and dried hydrogel films prepared *via* electrogelation were recorded using a U-3000 Spectrophotometer (Fa. Hitachi).

*PL measurements on dried hydrogel films of **4** prepared by electrogelation*

The PL spectra of the washed and dried hydrogel films prepared *via* electrogelation were recorded using a Spectrofluorometer RF-5301 (Fa. Shimadzu) at an excitation wavelength of $\lambda_{\text{exc}} = 320$ nm.

10 References

- 1 A. Nussinovitch; Hydrocolloid Applications, Springer US; Imprint; Springer, Boston, MA, **1997**.
- 2 K. Y. Lee, D. J. Mooney; Hydrogels for Tissue Engineering, in *Chemical Reviews*, **2001**, vol. 101, 7, pp. 1869–1880.
- 3 Y. Gao, Y. Kuang, Z.-F. Guo, Z. Guo, I. J. Krauss, B. Xu; Enzyme-Instructed Molecular Self-assembly Confers Nanofibers and a Supramolecular Hydrogel of Taxol Derivative, in *J. Am. Chem. Soc.*, **2009**, vol. 131, 38, pp. 13576–13577.
- 4 R. G. Weiss; The Past, Present, and Future of Molecular Gels. What Is the Status of the Field, and Where Is It Going?, in *J. Am. Chem. Soc.*, **2014**, vol. 136, 21, pp. 7519–7530.
- 5 J. D. Lloyd, in *Colloid Chemistry I*, **1926**, vol. 1, pp. 767–782.
- 6 K. Almdal, J. Dyre, S. Hvidt, O. Kramer; Towards a phenomenological definition of the term 'gel', in *Polymer Gels and Networks*, **1993**, vol. 1, 1, pp. 5–17.
- 7 P. H. Hermans, in *Colloid Science II*, **1949**, pp. 483–494.
- 8 P. J. Flory; Introductory Lecture, in *Faraday Discussions of the Chemical Society*, **1974**, vol. 57, 57, pp. 7–18.
- 9 M. de Loos, B. L. Feringa, J. H. van Esch; Design and Application of Self-Assembled Low Molecular Weight Hydrogels, in *European Journal of Organic Chemistry*, **2005**, 17, pp. 3615–3631.
- 10 L. A. Estroff, A. D. Hamilton; Water Gelation by Small Organic Molecules, in *Chemical Reviews*, **2004**, vol. 104, 3, pp. 1201–1716.
- 11 P. K. Vemula, G. John; Crops: A Green Approach toward Self-Assembled Soft Materials, in *Accounts of Chemical Research*, **2008**, vol. 41, 6, pp. 769–782.
- 12 A. M. Bieser; Oberflächenmodifizierung durch Hydrogele und durch Beschichtung mit antimikrobiellen Cellulosederivaten, Dissertation, Albert-Ludwigs-Universität Freiberg im Breisgau, **2007**.
- 13 A. Yaghmur, O. Glatter; Characterization and potential applications of nanostructured aqueous dispersions, in *Advances in Colloid and Interface Science*, **13//**, 147-148, pp. 333–342.
- 14 G. D. Rees, B. H. Robinson; Microemulsions and organogels: Properties and novel applications, in *Advanced Materials*, **1993**, vol. 5, 9, pp. 608–619.
- 15 *Xerogel - Definition* in *Compendium of chemical terminology*, ed. A. D. McNaught and A. Wilkinson, Blackwell Science, Oxford, England; Malden, MA, USA, 2nd ed., **1997**.
- 16 C. K. Kuo, P. X. Ma; Ionically crosslinked alginate hydrogels as scaffolds for tissue engineering: Part 1. Structure, gelation rate and mechanical properties, in *Biomaterials*, **2001**, vol. 22, 6, pp. 511–521.
- 17 R. Orbach, L. Adler-Abramovich, S. Zigerson, I. Mironi-Harpaz, D. Seliktar, E. Gazit; Self-Assembled Fmoc-Peptides as a Platform for the Formation of Nanostructures and Hydrogels, in *Biomacromolecules*, **2009**, vol. 10, 9, pp. 2646–2651.
- 18 N. G. Rim, J. H. Lee, S. in Jeong, B. K. Lee, C. H. Kim, H. Shin; Modulation of Osteogenic Differentiation of Human Mesenchymal Stem Cells by Poly[(L-lactide)-co-(ϵ -caprolactone)]/Gelatin Nanofibers, in *Macromol. Biosci.*, **2009**, vol. 9, 8, pp. 795–804.

- 19 N. Han, J. K. Johnson, P. A. Bradley, K. S. Parikh, J. J. Lannutti, J. O. Winter; Cell Attachment to Hydrogel-Electrospun Fiber Mat Composite Materials, in *JFB*, **2012**, vol. 3, 4, pp. 497–513.
- 20 H. J. Lee, W.-G. Koh; Hydrogel Micropattern-Incorporated Fibrous Scaffolds Capable of Sequential Growth Factor Delivery for Enhanced Osteogenesis of hMSCs, in *ACS Appl. Mater. Interfaces*, **2014**, vol. 6, 12, pp. 9338–9348.
- 21 M. M. C. Bastings, S. Koudstaal, R. E. Kieltyka, Y. Nakano, A. C. H. Pape, D. A. M. Feyen, F. J. van Slochteren, P. A. Doevendans, J. P. G. Sluijter, E. W. Meijer, S. A. J. Chamuleau, P. Y. W. Dankers; A Fast pH-Switchable and Self-Healing Supramolecular Hydrogel Carrier for Guided, Local Catheter Injection in the Infarcted Myocardium, in *Advanced Healthcare Materials*, **2014**, vol. 3, 1, pp. 70–78.
- 22 G. Sadowski and W. Richtering, eds.; *Intelligent Hydrogels*, Springer International Publishing, **2013**.
- 23 H. Ghandehari, P. Kopečková, J. Kopecek; In vitro degradation of pH-sensitive hydrogels containing aromatic azo bonds, in *Biomaterials*, **1997**, vol. 18, 12, pp. 861–872.
- 24 H. Kaşgöz; New sorbent hydrogels for removal of acidic dyes and metal ions from aqueous solutions, in *Polym. Bull.*, **2006**, vol. 56, 6, pp. 517–528.
- 25 H. Kaşgöz, A. Durmus; Dye removal by a novel hydrogel-clay nanocomposite with enhanced swelling properties, in *Polym. Adv. Technol.*, **2008**, vol. 19, 7, pp. 838–845.
- 26 Š. Selimović, J. Oh, H. Bae, M. Dokmeci, A. Khademhosseini; Microscale Strategies for Generating Cell-Encapsulating Hydrogels, in *Polymers*, **2012**, vol. 4, 4, pp. 1554–1579.
- 27 J. P. Gong; Why are double network hydrogels so tough?, in *Soft Matter*, **2010**, vol. 6, 12, p. 2583.
- 28 B. Kim, K. La Flamme, N. A. Peppas; Dynamic swelling behavior of pH-sensitive anionic hydrogels used for protein delivery, in *J. Appl. Polym. Sci.*, **2003**, vol. 89, 6, pp. 1606–1613.
- 29 L. Pan, G. Yu, D. Zhai, H. R. Lee, W. Zhao, N. Liu, H. Wang, B. C.-K. Tee, Y. Shi, Y. Cui, Z. Bao; Hierarchical nanostructured conducting polymer hydrogel with high electrochemical activity, in *Proceedings of the National Academy of Sciences*, **2012**, vol. 109, 24, pp. 9287–9292.
- 30 D. Žugić, P. Spasojević, Z. Petrović, J. Djonlagić; Semi-interpenetrating networks based on poly(N-isopropyl acrylamide) and poly(N-vinylpyrrolidone), in *J. Appl. Polym. Sci.*, **2009**, vol. 113, 3, pp. 1593–1603.
- 31 D. Schmaljohann; Thermo- and pH-responsive polymers in drug delivery, in *Advanced Drug Delivery Reviews*, **2006**, vol. 58, 15, pp. 1655–1670.
- 32 D. J. Cornwell, B. O. Okesola, D. K. Smith; Hybrid polymer and low molecular weight gels - dynamic two-component soft materials with both responsive and robust nanoscale networks, in *Soft Matter*, **2013**, vol. 9, 36, pp. 8730–8736.
- 33 R. V. Ulijn, N. Bibi, V. Jayawarna, P. D. Thornton, S. J. Todd, R. J. Mart, A. M. Smith, J. E. Gough; Bioresponsive hydrogels, in *Materials Today*, **2007**, vol. 10, 4, pp. 40–48.
- 34 Q. Wang, J. L. Mynar, M. Yoshida, E. Lee, M. Lee, K. Okuro, K. Kinbara, T. Aida; High-water-content mouldable hydrogels by mixing clay and a dendritic molecular binder, in *Nature*, **2010**, vol. 463, 7279, pp. 339–343.
- 35 K. Jindřich, Y. Jiyuan; Hydrogels as smart biomaterials, in *Polymer International*, **2007**, vol. 56, 9, pp. 1078–1098.

- 36 R. Huang, W. Qi, L. Feng, R. Su, Z. He; Self-assembling peptide–polysaccharide hybrid hydrogel as a potential carrier for drug delivery, in *Soft Matter*, **2011**, vol. 7, 13, p. 6222.
- 37 Y. Long, H. Song, B. He, Y. Lai, R. Liu, C. Long, Z. Gu; Supramolecular Self-assembly of Monoend-functionalized Methoxy Poly(ethylene glycol) and alpha-Cyclodextrin: from Micelles to Hydrogel, in *Journal of Biomaterials Applications*, **2012**, vol. 27, 3, pp. 333–344.
- 38 Le Zhang, E. M. Furst, K. L. Kiick; Manipulation of hydrogel assembly and growth factor delivery via the use of peptide–polysaccharide interactions, in *Journal of Controlled Release*, **2006**, vol. 114, 2, pp. 130–142.
- 39 N. M. Sangeetha, U. Maitra; Supramolecular gels: Functions and uses, in *Chemical Society Reviews*, **2005**, vol. 34, 10, pp. 821–836.
- 40 Y. J. Seo, S. Bhuniya, B. H. Kim; Reversible sol-gel signaling system with epMB for the study of enzyme- and pH-triggered oligonucleotide release from a biotin hydrogel, in *Chem. Commun*, **2007**, pp. 1804–1806.
- 41 M. Bassil, J. AL Moussawel, M. Ibrahim, G. Azzi, M. El Tahchi; Electrospinning of highly aligned and covalently cross-linked hydrogel microfibers, in *J. Appl. Polym. Sci.*, **2014**, vol. 131, 22, p. 41092.
- 42 L. Timbart, M. Y. Tse, S. C. Pang, O. Babasola, B. G. Amsden; Low Viscosity Poly(trimethylene carbonate) for Localized Drug Delivery: Rheological Properties and in vivo Degradation, in *Macromol. Biosci.*, **2009**, vol. 9, 8, pp. 786–794.
- 43 S. R. Raghavan; Distinct Character of Surfactant Gels: A Smooth Progression from Micelles to Fibrillar Networks †, in *Langmuir*, **2009**, vol. 25, 15, pp. 8382–8385.
- 44 R. G. Weiss, P. Terech; *Molecular Gels*, Springer, Dordrecht, **2006**.
- 45 S. Mukhopadhyay, U. Maitra, Ira, G. Krishnamoorthy, J. Schmidt, Y. Talmon; Structure and Dynamics of a Molecular Hydrogel Derived from a Tripodal Chalamide, in *Journal of the American Chemical Society*, **2004**, vol. 126, 48, pp. 15905–15914.
- 46 A. Heeres, C. van der Pol, M. Stuart, A. Friggeri, B. L. Feringa, J. van Esch; Orthogonal Self-Assembly of Low Molecular Weight Hydrogelators and Surfactants, in *Journal of the American Chemical Society*, **2003**, vol. 125, 47, pp. 14252–14253.
- 47 P. Terech, R. G. Weiss; Low Molecular Mass Gelators of Organic Liquids and the Properties of Their Gels, in *Chemical Reviews*, **1997**, vol. 97, 8, pp. 3133–3160.
- 48 D. J. Abdallah, R. G. Weiss; Organogels and Low Molecular Mass Organic Gelators, in *Advanced Materials*, **2000**, vol. 12, 17, pp. 1237–1247.
- 49 Maaïke de Loos, Jan H. van Esch, Richard M. Kellogg, Ben L. Feringa; C3-Symmetric, Amino Acid Based Organogelators and Thickeners: A Systematic Study of Structure - Property Relations, in *Tetrahedron*, **2007**, vol. 38, 39, pp. 7285–7301.
- 50 P. Dastidar; Supramolecular gelling agents: can they be designed?, in *Chem. Soc. Rev.*, **2008**, vol. 37, 12, pp. 2699–2715.
- 51 Z. Yang, B. Xu; Supramolecular hydrogels based on biofunctional nanofibers of self-assembled small molecules, in *Journal of Materials Chemistry*, **2007**, vol. 17, 23, pp. 2385–2393.
- 52 Jan H. van Esch, Ben L. Feringa; New Functional Materials Based on Self-Assembling Organogels: From Serendipity towards Design, in *Angewandte Chemie International Edition*, **2000**, vol. 39, 13, pp. 2263–2266.

- 53 A.-M. Tang, W.-J. Wang, B. Mei, W.-L. Hu, M. Wu, G.-L. Liang; DEVD-Based Hydrogelator Minimizes Cellular Apoptosis Induction, in *Sci. Rep.*, **2013**, vol. 3, p. 1848.
- 54 Z. Sun, Z. Li, Y. He, R. Shen, L. Deng, M. Yang, Y. Liang, Y. Zhang; Ferrocenoyl Phenylalanine: A New Strategy Toward Supramolecular Hydrogels with Multistimuli Responsive Properties, in *J. Am. Chem. Soc.*, **2013**, vol. 135, 36, pp. 13379–13386.
- 55 M. L. Bushey, T.-Q. Nguyen, W. Zhang, D. Horoszewski, C. Nuckolls; Using Hydrogen Bonds to Direct the Assembly of Crowded Aromatics, in *Angewandte Chemie International Edition*, **2004**, vol. 43, 41, pp. 5446–5453.
- 56 A. R. Hirst, B. Escuder, J. F. Miravet, D. K. Smith; High-Tech Applications of Self-Assembling Supramolecular Nanostructured Gel-Phase Materials: From Regenerative Medicine to Electronic Devices, in *Angewandte Chemie International Edition*, **2008**, vol. 47, 42, pp. 8002–8018.
- 57 J.-M. Lehn; Supramolecular chemistry: from molecular information towards self-organization and complex matter, in *Reports on Progress in Physics*, **2004**, vol. 67, 3, p. 249.
- 58 J.-M. Lehn; *Supramolecular Chemistry - Scope and Perspectives*, Molecules - Supermolecules - Molecular Devices, Nobel Lecture, Stockholm, **1987**.
- 59 K. Petkau-Milroy, L. Brunsveld; Self-Assembling Multivalency – Supramolecular Polymers Assembled from Monovalent Mannose-Labelled Discotic Molecules, in *Eur. J. Org. Chem.*, **2013**, vol. 2013, 17, pp. 3470–3476.
- 60 L. Albertazzi, F. J. Martinez-Veracochea, C. M. A. Leenders, I. K. Voets, D. Frenkel, E. W. Meijer; Spatiotemporal control and superselectivity in supramolecular polymers using multivalency, in *Proceedings of the National Academy of Sciences*, **2013**, vol. 110, 30, pp. 12203–12208.
- 61 H. Liu, Z. Lv, K. Ding, X. Liu, L. Yuan, H. Chen, X. Li; Incorporation of tyrosine phosphate into tetraphenylethylene affords an amphiphilic molecule for alkaline phosphatase detection, hydrogelation and calcium mineralization, in *J. Mater. Chem. B*, **2013**, vol. 1, 41, pp. 5550–5556.
- 62 L. Baldini, F. Sansone, A. Casnati, R. Ungaro; *Protein and nucleic acid targeting in Applications of supramolecular chemistry*, ed. H.-J. Schneider, CRC Press, Boca Raton, **2012**, pp. 363–390.
- 63 T. F. A. de Greef, M. M. J. Smulders, M. Wolfs, A. P. H. J. Schenning, R. P. Sijbesma, E. W. Meijer; Supramolecular Polymerization, in *Chemical Reviews*, **2009**, vol. 109, 11, pp. 5687–5754.
- 64 G. Yu, X. Yan, C. Han, F. Huang; Characterization of supramolecular gels, in *Chem. Soc. Rev.*, **2013**, vol. 42, pp. 6697–6722.
- 65 B. Ding, Y. Li, M. Qin, Y. Ding, Y. Cao, W. Wang; Two approaches for the engineering of homogeneous small-molecule hydrogels, in *Soft Matter*, **2013**, vol. 9, 18, pp. 4672–4680.
- 66 A. Bernet, M. Behr, R. Albuquerque, M. Schmidt, J. Senker, H.-W. Schmidt; *Supramolecular Chromaticity and Thermoresponsive Hydrogels: A Self-Assembly Study on Maleamic Acid-Based Amphiphiles* in *Intelligent Hydrogels*, ed. G. Sadowski and W. Richtering, Springer International Publishing, **2013**, vol. 140, pp. 1-13.
- 67 R. N. Mitra, D. Das, S. Roy, P. K. Das; Structure and Properties of Low Molecular Weight Amphiphilic Peptide Hydrogelators, in *The Journal of Physical Chemistry B*, **2007**, vol. 111, 51, pp. 14107–14113.

- 68 B. J. Cafferty, I. Gállego, M. C. Chen, K. I. Farley, R. Eritja, N. V. Hud; Efficient Self-Assembly in Water of Long Noncovalent Polymers by Nucleobase Analogues, in *J. Am. Chem. Soc.*, **2013**, vol. 135, 7, pp. 2447–2450.
- 69 P. Kumar Vemula, U. Aslam, V. Ajay Mallia, G. John; In Situ Synthesis of Gold Nanoparticles Using Molecular Gels and Liquid Crystals from Vitamin-C Amphiphiles, in *Chem. Mater.*, **2007**, vol. 19, 2, pp. 138–140.
- 70 T. Kar, S. Debnath, D. Das, A. Shome, P. Das; Organogelation and Hydrogelation of Low-Molecular-Weight Amphiphilic Dipeptides: pH Responsiveness in Phase-Selective Gelation and Dye Removal, in *Langmuir*, **2009**, vol. 25, 15, pp. 8639–8648.
- 71 M. Suzuki, M. Yumoto, H. Shirai, K. Hanabusa; Supramolecular Gels Formed by Amphiphilic Low-Molecular-Weight Gelators of $\alpha, \text{N}\epsilon$ -Diacyl-L-Lysine Derivatives, in *Chem. Eur. J.*, **2008**, vol. 14, 7, pp. 2133–2144.
- 72 P. Duan, M. Liu; Design and Self-Assembly of L-Glutamate-Based Aromatic Dendrons as Ambidextrous Gelators of Water and Organic Solvents, in *Langmuir*, **2009**, vol. 25, 15, pp. 8706–8713.
- 73 J. Raeburn, G. Pont, L. Chen, Y. Cesbron, R. Lévy, D. J. Adams; Fmoc-diphenylalanine hydrogels: understanding the variability in reported mechanical properties, in *Soft Matter*, **2012**, 8, pp. 1168–1174.
- 74 J. C. Tiller; Increasing the Local Concentration of Drugs by Hydrogel Formation, in *Angew. Chem. Int. Ed.*, **2003**, vol. 42, 27, pp. 3072–3075.
- 75 G. Wang, S. Cheuk, H. Yang, N. Goyal, P. V. N. Reddy, B. Hopkinson; Synthesis and Characterization of Monosaccharide-Derived Carbamates as Low-Molecular-Weight Gelators, in *Langmuir*, **2009**, vol. 25, 15, pp. 8696–8705.
- 76 A. Bernet, M. Behr, H.-W. Schmidt; Supramolecular hydrogels based on antimycobacterial amphiphiles, in *Soft Matter*, **2012**, vol. 8, pp. 4873–4876.
- 77 A. Bernet, M. Behr, H.-W. Schmidt; Supramolecular nanotube-based fiber mats by self-assembly of a tailored amphiphilic low molecular weight hydrogelator, in *Soft Matter*, **2011**, vol. 7, 3, pp. 1058–1065.
- 78 N. E. Shi, H. Dong, G. Yin, Z. Xu, S. H. Li; A Smart Supramolecular Hydrogel Exhibiting pH-Modulated Viscoelastic Properties, in *Advanced Functional Materials*, **2007**, vol. 17, 11, pp. 1837–1843.
- 79 P. K. Vemula, G. A. Cruikshank, J. M. Karp, G. John; Self-assembled prodrugs: An enzymatically triggered drug-delivery platform, in *Biomaterials*, **2009**, vol. 30, 3, pp. 383–393.
- 80 M. Tena-Solsona, S. Alonso-de Castro, J. F. Miravet, B. Escuder; Co-assembly of tetrapeptides into complex pH-responsive molecular hydrogel networks, in *J. Mater. Chem. B*, **2014**, vol. 2, 37, pp. 6192–6197.
- 81 A. Saha, S. Manna, A. K. Nandi; Hierarchical tuning of 1-D macro morphology by changing the composition of a binary hydrogel and its influence on the photoluminescence property, in *Chem. Commun.*, **2008**, 32, pp. 3732–3734.
- 82 H. Wang, Z. Yang, D. J. Adams; Controlling peptidebased hydrogelation, in *Materials Today*, **2012**, vol. 15, 11, pp. 500–507.
- 83 S. Ray, A. K. Das, A. Banerjee; pH-Responsive, Bolaamphiphile-Based Smart Metallo-Hydrogels as Potential Dye-Adsorbing Agents, Water Purifier, and Vitamin B 12 Carrier, in *Chem. Mater.*, **2007**, vol. 19, 7, pp. 1633–1639.

- 84 Kjeld J. C. van Bommel, Cornelia van der Pol, Inouk Muizebelt, Arianna Friggeri, André Heeres, Auke Meetsma, Ben L. Feringa, Jan van Esch; Responsive Cyclohexane-Based Low-Molecular-Weight Hydrogelators with Modular Architecture, in *Angewandte Chemie International Edition*, **2004**, vol. 43, 13, pp. 1663–1667.
- 85 C.-a. Tao, J. Wang, S. Qin, Y. Lv, Y. Long, H. Zhu, Z. Jiang; Fabrication of pH-sensitive graphene oxide-drug supramolecular hydrogels as controlled release systems, in *J. Mater. Chem*, **2012**, vol. 22, 47, pp. 24856–24861.
- 86 Aurelie Brizard, Marc Stuart, Kjeld van Bommel, Arianna Friggeri, Menno de Jong, Jan van Esch; Preparation of Nanostructures by Orthogonal Self-Assembly of Hydrogelators and Surfactants¹³, in *Angewandte Chemie International Edition*, **2008**, vol. 47, 11, pp. 2063–2066.
- 87 B. Adhikari, G. Palui, A. Banerjee; Self-assembling tripeptide based hydrogels and their use in removal of dyes from waste-water, in *Soft Matter*, **2009**, vol. 5, 18, pp. 3452–3460.
- 88 S. Sutton, N. L. Campbell, A. I. Cooper, M. Kirkland, W. J. Frith, D. J. Adams; Controlled Release from Modified Amino Acid Hydrogels Governed by Molecular Size or Network Dynamics, in *Langmuir*, **2009**, vol. 25, 17, pp. 10285–10291.
- 89 S. R. Haines, R. G. Harrison; Novel resorcinarene-based pH-triggered gelator, in *Chem. Commun*, **2002**, 23, pp. 2846–2847.
- 90 F. Fages; Durch Metallkoordination zu molekularen Gelen!, in *Angewandte Chemie*, **2006**, vol. 118, 11, pp. 1710–1712.
- 91 S. Matsumoto, S. Yamaguchi, S. Ueno, H. Komatsu, M. Ikeda, K. Ishizuka, Y. Iko, K. V. Tabata, H. Aoki, S. Ito, H. Noji, I. Hamachi; Photo Gel–Sol/Sol–Gel Transition and Its Patterning of a Supramolecular Hydrogel as Stimuli-Responsive Biomaterials, in *Chem. Eur. J*, **2008**, vol. 14, 13, pp. 3977–3986.
- 92 M. Ayabe, T. Kishida, N. Fujita, K. Sada, S. Shinkai; Binary organogelators which show light and temperature responsiveness, in *Organic & Biomolecular Chemistry*, **2003**, vol. 1, 15, pp. 2744–2747.
- 93 J. Raeburn, T. O. McDonald, D. J. Adams; Dipeptide hydrogelation triggered via ultraviolet light, in *Chem. Commun.*, **2012**, vol. 48, 75, pp. 9355–9357.
- 94 K. Murata, M. Aoki, T. Nishi, A. Ikeda, S. Shinkai; New cholesterol-based gelators with light- and metal-responsive functions, in *Journal of the Chemical Society, Chemical Communications*, **1991**, 24, pp. 1715–1718.
- 95 K. J. C. van Bommel, M. C. A. Stuart, B. L. Feringa, J. van Esch; Two-stage enzyme mediated drug release from LMWG hydrogels, in *Org. Biomol. Chem*, **2005**, vol. 3, 16, pp. 2917–2920.
- 96 F. O. Akong, A. Pasc, M. Emo, C. Gérardin-Charbonnier; A supramolecular hydrogel based on an original pseudopeptidic catanionic surfactant, in *New J. Chem.*, **2013**, vol. 37, 3, p. 559.
- 97 A. Dasgupta, J. H. Mondal, D. Das; Peptide hydrogels, in *RSC Adv.*, **2013**, vol. 3, 24, p. 9117.
- 98 D. J. Adams, M. F. Butler, W. J. Frith, M. Kirkland, L. Mullen, P. Sanderson; A new method for maintaining homogeneity during liquid-hydrogel transitions using low molecular weight hydrogelators, in *Soft Matter*, **2009**, vol. 5, 9, pp. 1856–1862.

- 99 L. Chen, K. Morris, A. Laybourn, D. Elias, M. R. Hicks, A. Rodger, L. Serpell, D. J. Adams; Self-Assembly Mechanism for a Naphthalene-Dipeptide Leading to Hydrogelation, in *Langmuir*, **2010**, vol. 26, 7, pp. 5232–5242.
- 100 H. Huang, S. Lü, X. Zhang, Z. Shao; Glucono- δ -lactone controlled assembly of graphene oxide hydrogels with selectively reversible gel–sol transition, in *Soft Matter*, **2012**, 8, pp. 4609–4615.
- 101 L. Chen, K. Morris, A. Laybourn, D. Elias, M. R. Hicks, A. Rodger, L. Serpell, D. J. Adams; Self-Assembly Mechanism for a Naphthalene-Dipeptide Leading to Hydrogelation, in *Langmuir*, **2010**, vol. 26, 26 (7), pp. 5232–5242.
- 102 A. Bernet, R. Q. Albuquerque, M. Behr, S. T. Hoffmann, H.-W. Schmidt; Formation of a supramolecular chromophore: a spectroscopic and theoretical study, in *Soft Matter*, **2012**, vol. 8, 1, pp. 66–69.
- 103 Y. Pocker, E. Green; Hydrolysis of D-glucono-delta-lactone. I. General acid-base catalysis, solvent deuterium isotope effects, and transition state characterization, in *Journal of the American Chemical Society*, **1973**, vol. 95, 1, pp. 113–119.
- 104 G. C. Maity; Supramolecular Hydrogels, in *Journal of Physical Sciences*, **2008**, vol. 12, pp. 173–186.
- 105 Brenziger K.; Zur Kenntniss des Cystins und des Cysteins, in *Zeitschrift für Physiologische Chemie*, **1892**, vol. 16, 6, pp. 552–588.
- 106 J. H. Fuhrhop, S. Svenson, C. Boettcher, E. Roessler, H. M. Vieth; Long-lived micellar N-alkylaldonamide fiber gels. Solid-state NMR and electron microscopic studies, in *J. Am. Chem. Soc.*, **1990**, vol. 112, 11, pp. 4307–4312.
- 107 J. H. Fuhrhop, P. Schnieder, J. Rosenberg, E. Boekema; The chiral bilayer effect stabilizes micellar fibers, in *J. Am. Chem. Soc.*, **1987**, vol. 109, 11, pp. 3387–3390.
- 108 M. Kogiso, T. Hanada, K. Yase, T. Shimizu; Intralayer hydrogen-bond-directed self-assembly of nano-fibers from dicarboxylic valylvaline bolaamphiphiles, in *Chem. Commun*, **1998**, pp. 1791–1792.
- 109 L. Frkanec, M. Jokić, J. Makarević, K. Wolsperger, M. Žinić; Bis(PheOH) Maleic Acid Amide–Fumaric Acid Amide Photoisomerization Induces Microsphere-to-Gel Fiber Morphological Transition: The Photoinduced Gelation System, in *J. Am. Chem. Soc.*, **2002**, vol. 124, 33, pp. 9716–9717.
- 110 F. M. Menger, H. Zhang, K. L. Caran, V. A. Seredyuk, R. P. Apkarian; Gemini-Induced Columnar Jointing in Vitreous Ice. Cryo-HRSEM as a Tool for Discovering New Colloidal Morphologies, in *J. Am. Chem. Soc.*, **2002**, vol. 124, 7, pp. 1140–1141.
- 111 F. M. Menger, V. A. Seredyuk, R. P. Apkarian, E. R. Wright; Colloidal Assemblies of Branched Geminis Studied by Cryo-etch-HRSEM, in *J. Am. Chem. Soc.*, **2002**, vol. 124, 42, pp. 12408–12409.
- 112 M. Ikeda, R. Ochi, A. Wada, I. Hamachi; Supramolecular hydrogel capsule showing prostate specific antigen-responsive function for sensing and targeting prostate cancer cells, in *Chem. Sci.*, **2010**, vol. 1, 4, pp. 491–498.
- 113 G. Godeau, P. Barthélémy; Glycosyl-Nucleoside Lipids as Low-Molecular-Weight Gelators, in *Langmuir*, **2009**, vol. 25, 15, pp. 8447–8450.
- 114 Y. Ono, K. Nakashima, M. Sano, Y. Kanekiyo, K. Inoue, S. Shinkai, J. Hojo; Organic gels are useful as a template for the preparation of hollow fiber silica, in *Chem. Commun.*, **1998**, 14, pp. 1477–1478.

- 115 A. Friggeri, B. L. Feringa, J. van Esch; Entrapment and release of quinoline derivatives using a hydrogel of a low molecular weight gelator, in *Journal of Controlled Release*, **2004**, vol. 97, 2, pp. 241–248.
- 116 S. Cao, X. Fu, N. Wang, H. Wang, Y. Yang; Release behavior of salicylic acid in supramolecular hydrogels formed by L-phenylalanine derivatives as hydrogelator, in *International Journal of Pharmaceutics*, **2008**, vol. 357, 1-2, pp. 95–99.
- 117 J. J. Panda, A. Mishra, A. Basu, V. S. Chauhan; Stimuli Responsive Self-Assembled Hydrogel of a Low Molecular Weight Free Dipeptide with Potential for Tunable Drug Delivery, in *Biomacromolecules*, **2008**, vol. 9, 8, pp. 2244–2250.
- 118 J. Boekhoven, M. Koot, T. A. Wezendonk, R. Eelkema, J. H. van Esch; A Self-Assembled Delivery Platform with Post-production Tunable Release Rate, in *J. Am. Chem. Soc.*, **2012**, vol. 134, 31, pp. 12908–12911.
- 119 S. Bhattacharya, S. Sengupta, S. Bala, A. Goswami, S. Ganguly, R. Mondal; Pyrazole-Based Metallogels Showing an Unprecedented Colorimetric Ammonia Gas Sensing through Gel-to-Gel Transformation with a Rare Event of Time-Dependent Morphology Transformation, in *Crystal Growth & Design*, **2014**, vol. 14, 5, pp. 2366–2374.
- 120 S. Sengupta, A. Goswami, R. Mondal; Silver-promoted gelation studies of an unorthodox chelating tripodal pyridine-pyrazole-based ligand: templated growth of catalytic silver nanoparticles, gas and dye adsorption, in *New J. Chem.*, **2014**, vol. 38, 6, pp. 2470–2479.
- 121 M.-O. M. Piepenbrock, G. O. Lloyd, N. Clarke, J. W. Steed; Metal- and Anion-Binding Supramolecular Gels, in *Chemical Reviews*, **2010**, vol. 110, 4, pp. 1960–2004.
- 122 M. K. Okajima, S. Miyazato, T. Kaneko; Cyanobacterial Megamolecule Sacran Efficiently Forms LC Gels with Very Heavy Metal Ions, in *Langmuir*, **2009**, vol. 25, 15, pp. 8526–8531.
- 123 S. Song, L. Feng, A. Song, J. Hao; Room-Temperature Super Hydrogel as Dye Adsorption Agent, in *J. Phys. Chem. B*, **2012**, vol. 116, 42, pp. 12850–12856.
- 124 S. Huang, L. Yang, M. Liu, S. L. Phua, W. A. Yee, W. Liu, R. Zhou, X. Lu; Complexes of Polydopamine-Modified Clay and Ferric Ions as the Framework for Pollutant-Absorbing Supramolecular Hydrogels, in *Langmuir*, **2013**, vol. 29, 4, pp. 1238–1244.
- 125 A. Saha, B. Roy, A. Garai, A. K. Nandi; Two-Component Thermoreversible Hydrogels of Melamine and Gallic Acid, in *Langmuir*, **2009**, vol. 25, 15, pp. 8457–8461.
- 126 R. Haller; Ueber Farbstoffgellerten, in *Kolloid-Zeitschrift*, **1918**, vol. 22, 2, pp. 49–53.
- 127 Y.-L. Zhao, J. F. Stoddart; Azobenzene-Based Light-Responsive Hydrogel System, in *Langmuir*, **2009**, vol. 25, 15, pp. 8442–8446.
- 128 S. Lee, S. Oh, J. Lee, Y. Malpani, Y.-S. Jung, B. Kang, J. Y. Lee, K. Ozasa, T. Isoshima, S. Y. Lee, M. Hara, D. Hashizume, J.-M. Kim; Stimulus-Responsive Azobenzene Supramolecules: Fibers, Gels, and Hollow Spheres, in *Langmuir*, **2013**, vol. 29, 19, pp. 5869–5877.
- 129 R. N. Das, Y. P. Kumar, S. Pagoti, A. J. Patil, J. Dash; Diffusion and Birefringence of Bioactive Dyes in a Supramolecular Guanosine Hydrogel, in *Chemistry – A European Journal*, **2012**, vol. 18, 19, pp. 6008–6014.
- 130 L. Estroff, A. Hamilton; Effective Gelation of Water Using a Series of Bis-urea Dicarboxylic Acids, in *Angewandte Chemie International Edition*, **2000**, vol. 39, 19, pp. 3447–3450.
- 131 C. M. A. Leenders, T. Mes, M. B. Baker, M. M. E. Koenigs, P. Besenius, A. R. A. Palmans, E. W. Meijer; From supramolecular polymers to hydrogel materials, in *Mater. Horiz.*, **2014**, 1, pp. 116–120.

- 132 P. J. M. Stals, J. F. Haveman, R. Martin-Rapun, C. F. C. Fitie, A. R. A. Palmans, E. W. Meijer; The influence of oligo(ethylene glycol) side chains on the self-assembly of benzene-1,3,5-tricarboxamides in the solid state and in solution, in *Journal of Materials Chemistry*, **2009**, vol. 19, 1, pp. 124–130.
- 133 Theodor Curtius; Hydrazide und Azide organischer Säuren, in *J. Prakt. Chem.*, **1915**, vol. 91, 134, pp. 39–102.
- 134 S. Cantekin, T. F. A. de Greef, A. R. A. Palmans; Benzene-1,3,5-tricarboxamide: a versatile ordering moiety for supramolecular chemistry, in *Chem. Soc. Rev.*, **2012**, vol. 41, pp. 6125–6137.
- 135 M. P. Lightfoot, F. S. Mair, R. G. Pritchard, J. E. Warren; New supramolecular packing motifs: π -stacked rods encased in triply-helical hydrogen bonded amide strands, in *Chem. Commun.*, **1999**, pp. 1945–1946.
- 136 A. Palmans, E. Meijer; Amplification of Chirality in Dynamic Supramolecular Aggregates, in *Angewandte Chemie International Edition*, **2007**, vol. 46, 47, pp. 8948–8968.
- 137 V. Nagarajan, V. R. Pedireddi; Gelation and Structural Transformation Study of Some 1,3,5-Benzenetricarboxamide Derivatives, in *Crystal Growth & Design*, **2014**, vol. 14, 4, pp. 1895–1901.
- 138 A. Timme, R. Kress, R. Q. Albuquerque, H.-W. Schmidt; Phase Behavior and Mesophase Structures of 1,3,5-Benzene- and 1,3,5-Cyclohexanetricarboxamides: Towards an Understanding of the Losing Order at the Transition into the Isotropic Phase, in *Chem. Eur. J.*, **2012**, vol. 18, 27, pp. 8329–8339.
- 139 R. Q. Albuquerque, A. Timme, R. Kress, J. Senker, H.-W. Schmidt; Theoretical Investigation of Macrodipoles in Supramolecular Columnar Stackings, in *Chem. Eur. J.*, **2012**, vol. 19, 5, pp. 1647–1657.
- 140 R. Takasawa, K. Murota, I. Yoshikawa, K. Araki; Steric-Factor-Directed Alternating Supramolecular Copolymer Composed of Hydrogen-Bonded Cyclohexanetricarboxamide Units, in *Macromol. Rapid Commun.*, **2003**, vol. 24, 4, pp. 335–339.
- 141 Arianna Friggeri, Cornelia van der Pol, Kjeld J. C. van Bommel, André Heeres, Marc C. A. Stuart, Ben L. Feringa, Jan van Esch; Cyclohexane-Based Low Molecular Weight Hydrogelators: A Chirality Investigation, in *Chemistry - A European Journal*, **2005**, vol. 11, 18, pp. 5353–5361.
- 142 L. Sardone, V. Palermo, E. Devaux, D. Credgington, M. de Loos, G. Marletta, F. Cacialli, J. van Esch, P. Samorì; Electric-Field-Assisted Alignment of Supramolecular Fibers, in *Advanced Materials*, **2006**, vol. 18, 10, pp. 1276–1280.
- 143 F. Abraham, R. Kress, P. Smith, H.-W. Schmidt; A New Class of Ultra-Efficient Supramolecular Nucleating Agents for Isotactic Polypropylene, in *Macromol. Chem. Phys.*, **2013**, vol. 214, 1, pp. 17–24.
- 144 M. Blomenhofer, S. Ganzleben, D. Hanft, H.-W. Schmidt, M. Kristiansen, P. Smith, K. Stoll, D. Mader, K. Hoffmann; "Designer" Nucleating Agents for Polypropylene, in *Macromolecules*, **2005**, vol. 38, 9, pp. 3688–3695.
- 145 M. Wegner; Solid-State NMR on Columnar Supramolecular Structures, Dissertation, Johannes Gutenberg-Universität Mainz, **2010**.
- 146 X. Hou, M. Schober, Q. Chu; A Chiral Nanosheet Connected by Amide Hydrogen Bonds, in *Crystal Growth & Design*, **2012**, vol. 12, 11, pp. 5159–5163.

- 147 M. Wegner, D. Dudenko, D. Sebastiani, A. R. A. Palmans, T. F. A. de Greef, R. Graf, H. W. Spiess; The impact of the amide connectivity on the assembly and dynamics of benzene-1,3,5-tricarboxamides in the solid state, in *Chem. Sci*, **2011**, vol. 2, 10, p. 2040.
- 148 A. Demenev, S. H. Eichhorn, T. Taerum, D. F. Perepichka, S. Patwardhan, F. C. Grozema, L. D. A. Siebbeles, R. Klenkler; Quasi Temperature Independent Electron Mobility in Hexagonal Columnar Mesophases of an H-Bonded Benzotrithiophene Derivative, in *Chem. Mater.*, **2010**, vol. 22, 4, pp. 1420–1428.
- 149 K. K. Bejagam, G. Fiorin, M. L. Klein, S. Balasubramanian; Supramolecular Polymerization of Benzene-1,3,5-tricarboxamide: A Molecular Dynamics Simulation Study, in *J. Phys. Chem. B*, **2014**, vol. 118, 19, pp. 5218–5228.
- 150 C. F. C. Fitié, W. S. C. Roelofs, P. C. M. M. Magusin, M. Wübbenhorst, M. Kemerink, R. P. Sijbesma; Polar Switching in Trialkylbenzene-1,3,5-tricarboxamides, in *J. Phys. Chem. B*, **2012**, vol. 116, 3, pp. 3928–3937.
- 151 C. Kulkarni, S. K. Reddy, S. J. George, S. Balasubramanian; Cooperativity in the stacking of benzene-1,3,5-tricarboxamide: The role of dispersion, in *Chemical Physics Letters*, **2011**, vol. 515, 4-6, pp. 226–230.
- 152 J. J. van Gorp, J. A. J. M. Vekemans, E. W. Meijer; C₃-Symmetrical Supramolecular Architectures: Fibers and Organic Gels from Discotic Trisamides and Trisureas, in *Journal of the American Chemical Society*, **2002**, vol. 124, 49, pp. 14759–14769.
- 153 T. Mes, S. Cantekin, D. W. R. Balkenende, M. M. M. Frissen, M. A. J. Gillissen, B. F. M. de Waal, I. K. Voets, E. W. Meijer, A. R. A. Palmans; Thioamides: Versatile Bonds To Induce Directional and Cooperative Hydrogen Bonding in Supramolecular Polymers, in *Chem. Eur. J.*, **2013**, vol. 19, 26, pp. 8642–8649.
- 154 B. E. Durif-Verambon, R. Salle and B. Sillion; Neue Triolverbindung, Verfahren zu deren Herstellung sowie deren Anwendung, Institut Francais du Petrole des Carburants et Lubrifiants, 2149709, **1970**.
- 155 S. Russo, A. Boulares, R. A. Da; Hyperbranched aramids by direct polyamidation of two reactant systems. Synthesis and properties, in *Macromol. Symp*, **1999**, vol. 143, *World Polymer Congress, 37th International Symposium on Macromolecules, 1998*, pp. 309–321.
- 156 M. E. Cosulich, S. Russo, S. Pasquale, A. Mariani; Performance evaluation of hyperbranched aramids as potential supports for protein immobilization, in *Polymer*, **2000**, vol. 41, 13, pp. 4951–4956.
- 157 S. M. Aharoni, N. S. Murthy, K. Zero, S. F. Edwards; The fractal nature of 1-step highly-branched rigid rodlike macromolecules and their gelled-network progenies, in *Macromolecules*, **1990**, vol. 23, 9, pp. 2533–2549.
- 158 S. M. Aharoni; Networks and gels of stiff zigzag polyamides, in *Macromolecules*, **1992**, vol. 25, 5, pp. 1510–1515.
- 159 S. M. Aharoni, G. R. Hatfield, K. P. O'Brien; Bending of polyamide rigid rodlike segments, in *Macromolecules*, **1990**, vol. 23, 5, pp. 1330–1342.
- 160 S. M. Aharoni, S. F. Edwards; Gels of rigid polyamide networks, in *Macromolecules*, **1989**, vol. 22, 8, pp. 3361–3374.
- 161 S. M. Aharoni; Gels of rigid polyamide networks, in *Polym. Prepr. (Am. Chem. Soc., Div. Polym. Chem.)*, **1989**, vol. 30, 1, pp. 125–6.
- 162 M. E. McDonnell, K. Zero, S. M. Aharoni; Light scattering studies of the structure of rigid polyamide gels, in *Polym. Mater. Sci. Eng*, **1992**, vol. 66, pp. 154–5.

- 163 S. Russo, A. Boulares, A. Mariani; Synthesis of hyperbranched aromatic polyamides by direct polycondensation, in *Macromol. Symp*, **1998**, vol. 128, *International Symposium on New Approaches in Polymer Synthesis and Macromolecular Formation, 1997*, pp. 13–20.
- 164 Z. Qian, J. R. LaRochelle, B. Jiang, W. Lian, R. L. Hard, N. G. Selner, R. Luechapanichkul, A. M. Barrios, D. Pei; Early Endosomal Escape of a Cyclic Cell-Penetrating Peptide Allows Effective Cytosolic Cargo Delivery, in *Biochemistry*, **2014**, vol. 53, 24, pp. 4034–4046.
- 165 W. Lian, B. Jiang, Z. Qian, D. Pei; Cell-Permeable Bicyclic Peptide Inhibitors against Intracellular Proteins, in *Journal of the American Chemical Society*, **2014**, vol. 136, 28, pp. 9830–9833.
- 166 G. Cafeo, G. Gattuso, F. H. Kohnke, G. Papanikolaou, A. Profumo, C. Rosano; Host–Guest Chemistry of Aromatic-Amide-Linked Bis- and Tris-Calix[4]pyrroles with Bis-Carboxylates and Citrate Anion, in *Chem. Eur. J.*, **2014**, vol. 20, 6, pp. 1658–1668.
- 167 M. L. Talaga, N. Fan, A. L. Fueri, R. K. Brown, Y. M. Chabre, P. Bandyopadhyay, R. Roy, T. K. Dam; Significant Other Half of a Glycoconjugate: Contributions of Scaffolds to Lectin–Glycoconjugate Interactions, in *Biochemistry*, **2014**, vol. 53, 27, pp. 4445–4454.
- 168 A. Darehkordi, S. Ghazi; Synthesis of a New Class of Tris- and Bis(1,3,4-thiadiazol-2-amine) Methyl and Ethyl Tris- and Bis-2-(2-(2-benzoyl hydrazinyl)-4-oxothiazolidine) Acetate Derivatives, in *Journal of Chemistry*, **2013**, vol. 2013, 7, pp. 1–8.
- 169 M. Cavazzini, S. Quici, S. Orlandi, C. Sissa, F. Terenziani, A. Painelli; Intimately bound coumarin and bis(alkylaminostyryl)benzene fragments: synthesis and energy transfer, in *Tetrahedron*, **2013**, vol. 69, 13, pp. 2827–2833.
- 170 K. Naito; Quantitative Relations between Glass Transition Temperatures and Thermodynamic Parameters for Various Materials: Molecular Design for Nonpolymeric Organic Dye Glasses with Thermal Stability, in *Chem. Mater*, **1994**, vol. 6, 12, pp. 2343–2350.
- 171 J. D. Howgego, C. P. Butts, M. P. Crump, A. P. Davis; An accessible bicyclic architecture for synthetic lectins, in *Chem. Commun.*, **2013**, vol. 49, 30, p. 3110.
- 172 W. Lian, P. Upadhyaya, C. A. Rhodes, Y. Liu, D. Pei; Screening Bicyclic Peptide Libraries for Protein–Protein Interaction Inhibitors: Discovery of a Tumor Necrosis Factor- α Antagonist, in *J. Am. Chem. Soc.*, **2013**, vol. 135, 32, pp. 11990–11995.
- 173 Q. Li, T.-T. Yan, S. Niu, Y.-T. Zhao, X.-B. Meng, Z.-H. Zhao, Z.-J. Li; Synthesis of a series of multivalent homo-, and heteroglycosides and their anti-adhesion activities, in *Carbohydrate Research*, **2013**, vol. 379, 0, pp. 78–94.
- 174 R. B. Conrow and S. Bernstein; Phenyltris(carbonylimino) multianionic triphenyl acids and salts, American Cyanamid Co., USA, *US Pat.*, US 4123455, **1978**.
- 175 L. Rajput, K. Biradha; Three crystalline forms of 1,3,5-benzene-tri(3-pyridinyl)carboxamide from the same solvent system, in *Journal of Molecular Structure*, **2008**, vol. 876, 1-3, pp. 339–343.
- 176 N. Lomadze, H.-J. Schneider; Reversal of polyamine selectivity for DNA and RNA by steric hindrance, in *Tetrahedron Letters*, **2002**, vol. 43, 24, pp. 4403–4405.
- 177 F. Han, H. Zhang, J. Zhao, Y. Zhao, X. Yuan; In situ encapsulation of hydrogel in ultrafine fibers by suspension electrospinning, in *Polym Eng Sci*, **2012**, vol. 52, 12, pp. 2695–2704.
- 178 D. Hu, R. Kluger; Efficient generation of dendritic arrays of cross-linked hemoglobin: symmetry and redundancy, in *Org. Biomol. Chem*, **2008**, vol. 6, 1, pp. 151–156.

- 179 X. Lou, M. Fransen, P. J. M. Stals, T. Mes, R. Bovee, J. J. L. Dongen, E. W. Meijer; Unusual Analyte-Matrix Adduct Ions and Mechanism of Their Formation in MALDI TOF MS of Benzene-1,3,5-Tricarboxamide and Urea Compounds, in *J. Am. Soc. Mass Spectrom.*, **2013**, vol. 24, 9, pp. 1405-1412.
- 180 L. Robinson, P. V. V. S. V. Manchem, N. Cairns and S. R. Chow; Benzene tricarboxylic acid derivatives as insulin receptor activators, Robinson, Louise; Manchem, Prasad V. V. S. V.; Cairns, Nicolas; Schow, Steven R., *US Pat.*, WO 02/20464 A2, **2001**.
- 181 T. V. Esipova, X. Ye, J. E. Collins, S. Sakadzic, E. T. Mandeville, C. B. Murray, S. A. Vinogradov; Dendritic upconverting nanoparticles enable in vivo multiphoton microscopy with low-power continuous wave sources, in *Proceedings of the National Academy of Sciences*, **2012**, vol. 109, 51, pp. 20826–20831.
- 182 H. Lee, T. H. Noh, O.-S. Jung; Halogen effects on photoluminescence and catalytic properties: a series of spatially arranged trimetallic zinc(ii) complexes, in *Dalton Trans.*, **2014**, vol. 43, 10, p. 3842.
- 183 K. L. Peterson, M. J. Margherio, P. Doan, K. T. Wilke, V. C. Pierre; Basis for Sensitive and Selective Time-Delayed Luminescence Detection of Hydroxyl Radical by Lanthanide Complexes, in *Inorg. Chem.*, **2013**, vol. 52, 16, pp. 9390–9398.
- 184 V. N. Dokorou, A. K. Powell, G. E. Kostakis; Two pseudopolymorphs derived from alkaline earth metals and the pseudopeptidic ligand trimesoyl-tris-glycine, in *Polyhedron*, **2013**, vol. 52, pp. 538–544.
- 185 M. Jørgensen, F. C. Krebs; A new prearranged tripodant ligand N,N',N''-trimethyl-N,N',N''-tris(3-pyridyl)-1,3,5-benzene tricarboxamide is easily obtained via the N-methyl amide effect, in *Tetrahedron Letters*, **2001**, vol. 42, 28, pp. 4717–4720.
- 186 R. K. Bera, D. Sharma, S. K. Sahoo, B. K. Kanungo; Potentiometric Study of a Benzene-based Tripodal Triamine as Chelator for Zn(II) Ion, in *Acta Chimica Slovenica (Acta Chim. Slov.)*, **2011**, vol. 58, 3, pp. 590–595.
- 187 N. C. A. Baker, N. C. Fletcher, P. N. Horton, M. B. Hursthouse; Ruthenium cryptates with an unusual selectivity for nitrate, in *Dalton Trans*, **2012**, vol. 41, 23, pp. 7005–7012.
- 188 M. Vasylyev, R. Popovitz-Biro, L. J. W. Shimon, R. Neumann; Inorganic–organic hybrid materials based on keggin type polyoxometalates and organic polyammonium cations, in *Journal of Molecular Structure*, **2003**, vol. 656, 1–3, pp. 27–35.
- 189 J. Zhang, H. Yu, C. Zhang, C. He, C. Duan; Cerium-based M4L4 tetrahedrons containing hydrogen bond groups as functional molecular flasks for selective reaction prompting, in *New J. Chem.*, **2014**, vol. 38, 7, pp. 3137–3145.
- 190 X. Jiang, Z. Li, Y. Zhai, G. Yan, H. Xia, Z. Li; Porous coordination polymers based on azamacrocyclic complex: syntheses, solvent-induced reversible crystal-to-crystal transformation and gas sorption properties, in *CrystEngComm*, **2014**, vol. 16, 5, pp. 805–813.
- 191 L. Rajput, R. Banerjee; Mechanochemical Synthesis of Amide Functionalized Porous Organic Polymers, in *Crystal Growth & Design*, **2014**, vol. 14, 6, pp. 2729–2732.
- 192 X.-Z. Luo, X.-J. Jia, J.-H. Deng, J.-L. Zhong, H.-J. Liu, K.-J. Wang, D.-C. Zhong; A Microporous Hydrogen-Bonded Organic Framework: Exceptional Stability and Highly Selective Adsorption of Gas and Liquid, in *J. Am. Chem. Soc.*, **2013**, vol. 135, 32, pp. 11684–11687.
- 193 L. Rajput, V. V. Chernyshev, K. Biradha; Assembling triple helical amide-to-amide hydrogen bonded columns of tris(4-halophenyl)benzene-1,3,5-tricarboxamides into

- porous materials via halogen···halogen interactions, in *Chem. Commun*, **2010**, vol. 46, 35, p. 6530.
- 194 A. R.A.Palmans, J. A. J. M. Vekemans, E. W. Meijer, H. Kooijman, A. L. Spek; Hydrogen-bonded porous solid derived from trimesic amide, in *Chem. Commun.*, **1997**, 22, pp. 2247–2248.
- 195 B. Gong, C. Zheng, Y. Yan; Structure of N,N',N''-tris(carboxymethyl)-1,3,5-benzenetricarboxamide trihydrate, in *Journal of Chemical Crystallography*, **1999**, vol. 29, 6, pp. 649–652.
- 196 L. D. Rajput, G. Mukherjee, K. Biradha; Influence of solvents in assembling Tris(4-halophenyl)benzene-1,3,5-tricarboxamides: Interplay of N-H···O and Halogen···Halogen Interactions, in *Crystal Growth & Design*, **2012**, vol. 12, 11, pp. 5773–5782.
- 197 Y. Zou, Y. Li, C. Yu, F. Yin, M. S. Lah; A supramolecular self-assembled flexible open framework based on the coordination of honeycomb layers possessing octahedral and tetrahedral Coll geometries, in *RSC Adv.*, **2013**, vol. 3, 43, p. 19889.
- 198 J. Duan, M. Higuchi, M. L. Foo, S. Horike, K. P. Rao, S. Kitagawa; A Family of Rare Earth Porous Coordination Polymers with Different Flexibility for CO₂/C₂H₄ and CO₂/C₂H₆ Separation, in *Inorg. Chem.*, **2013**, vol. 52, 14, pp. 8244–8249.
- 199 L. Rajput, D. Kim, M. S. Lah; Conformational control of ligands to create a finite metal–organic cluster and an extended metal–organic framework, in *CrystEngComm*, **2012**, vol. 15, 2, p. 259.
- 200 X. Song, Y. Zou, X. Liu, M. Oh, M. S. Lah; A two-fold interpenetrated (3,6)-connected metal-organic framework with rutile topology showing a large solvent cavity, in *New J. Chem*, **2010**, vol. 34, 11, pp. 2396–2399.
- 201 Y.-Q. Chen, S.-J. Liu, Y.-W. Li, G.-R. Li, K.-H. He, Z. Chang, X.-H. Bu; Mn(II) metal-organic frameworks based on Mn₃ clusters: from 2D layer to 3D framework by the "pillaring" approach, in *CrystEngComm*, **2013**, vol. 15, 8, pp. 1613–1617.
- 202 B. Liu, D.-S. Li, L. Hou, G.-P. Yang, Y.-Y. Wang, Q.-Z. Shi; An unprecedented acylamide-functionalized 2D [rightward arrow] 3D microporous metal-organic polycatenation framework exhibiting highly selective CO₂ capture, in *Dalton Trans*, **2013**, vol. 42, 27, pp. 9822–9825.
- 203 R. Ma, C. Chen, B. Sun, X. Zhao, N. Zhang; A new 3D metal–organic framework with (4, 8)-connected AIB₂ topology constructed from coordinated evolution of a C₃ symmetry ligand, in *Inorganic Chemistry Communications*, **2011**, vol. 14, 9, pp. 1532–1536.
- 204 H.-Y. Bai, S.-M. Wang, W.-Q. Fan, C.-B. Liu, G.-B. Che; Metal(II) coordination polymers based on a flexible N,N',N''-tris(3-pyridyl)-1,3,5-benzenetricarboxamide ligand and organic polycarboxylate ligands: Syntheses, structures, and luminescence, in *Polyhedron*, **2013**, vol. 50, 1, pp. 193–199.
- 205 K. Tang, R. Yun, Z. Lu, L. Du, M. Zhang, Q. Wang, H. Liu; High CO₂/N₂ Selectivity and H₂ Adsorption of a Novel Porous Yttrium Metal–Organic Framework Based on N,N',N'' - Tris(isophthalyl)-1,3,5-benzenetricarboxamide, in *Crystal Growth & Design*, **2013**, vol. 13, 4, pp. 1382–1385.
- 206 H.-x. Huang, F. Luo, G.-m. Sun, Y.-m. Song, X.-z. Tian, Y. Zhu, Z.-j. Yuan, X.-f. Feng, M.-b. Luo; The first 2D →3D polycatenation array built on (3,4)-connected bilayer nets, in *CrystEngComm*, **2012**, vol. 14, 23, pp. 7861–7864.

- 207 T. Pham, K. A. Forrest, P. Nugent, Y. Belmabkhout, R. Luebke, M. Eddaoudi, M. J. Zaworotko, B. Space; Understanding Hydrogen Sorption in a Metal–Organic Framework with Open-Metal Sites and Amide Functional Groups, in *J. Phys. Chem. C*, **2013**, vol. 117, 18, pp. 9340–9354.
- 208 H. Lee, T. H. Noh, O.-S. Jung; Construction of kagome-type networks via tridentate ligand: structural properties as alcohol reservoir, in *CrystEngComm*, **2013**, vol. 15, 10, pp. 1832–1835.
- 209 S.-M. Wang, L. Qian, H.-Y. Bai, W.-Q. Fan, C.-B. Liu, G.-B. Che; Synthesis, structures, and photoluminescence properties of three metal(II) coordination polymers derived from a flexible tripodal ligand and 2,6-pyridinedicarboxylic acid, in *Transition Met Chem*, **2013**, vol. 38, 2, pp. 157–163.
- 210 Y. Zhang, Q. Wang, Y.-J. Xiao, J. Han, X.-L. Zhao; Structure diversity of a series of new coordination polymers based on a C₃-symmetric tridentate ligand with rosette architecture, in *Polyhedron*, **2012**, vol. 33, 1, pp. 127–136.
- 211 E. Kim, H. Lee, T. H. Noh, O.-S. Jung; Suprachannels via a Molecular Array of 2D Networks: Solvent Effects, Anion Exchange, and Physicochemical Properties of Silver(I) Complexes Bearing N,N',N''-Tris(2-pyridinylethyl)-1,3,5-benzenetricarboxamide, in *Crystal Growth & Design*, **2014**, vol. 14, 4, pp. 1888–1894.
- 212 A. Timme; Flüssigkristalline supramolekulare Systeme, Dissertation, Universität Bayreuth, **2012**.
- 213 F. Camerel, C. F. J. Faul; Combination of ionic self-assembly and hydrogen bonding as a tool for the synthesis of liquid-crystalline materials and organogelators from a simple building block, in *Chemical Communications*, **2003**, 15, pp. 1958–1959.
- 214 Patrick J. M. Stals, Maarten M. J. Smulders, Rafael Martín-Rapún, Anja R. A. Palmans, E. W. Meijer; Asymmetrically Substituted Benzene-1,3,5-tricarboxamides: Self-Assembly and Odd-Even Effects in the Solid State and in Dilute Solution, in *Chemistry - A European Journal*, **2009**, vol. 15, 9, pp. 2071–2080.
- 215 C. F. C. Fitié, I. Tomatsu, D. Byelov, W. H. de Jeu, R. P. Sijbesma; Nanostructured Materials through Orthogonal Self-Assembly in a Columnar Liquid Crystal, in *Chemistry of Materials*, **2008**, vol. 20, 6, pp. 2394–2404.
- 216 Shinto Varghese, Nambalan S. Saleesh Kumar, Anjali Krishna, Doddamane S. Shankar Rao, Subbarao Krishna Prasad, Suresh Das; Formation of Highly Luminescent Supramolecular Architectures Possessing Columnar Order from Octupolar Oxadiazole Derivatives: Hierarchical Self-Assembly from Nanospheres to Fibrous Gels, in *Advanced Functional Materials*, **2009**, vol. 19, 13, pp. 2064–2073.
- 217 I. Paraschiv, M. Giesbers, B. van Lagen, F. C. Grozema, R. D. Abellon, L. D. A. Siebbeles, A. T. M. Marcelis, H. Zuilhof, E. J. R. Sudhölter; H-Bond-Stabilized Triphenylene-Based Columnar Discotic Liquid Crystals, in *Chemistry of Materials*, **2006**, vol. 18, 4, pp. 968–974.
- 218 A. R. A. Palmans, J. A. J. M. Vekemans, H. Fischer, R. A. Hikmet, E. W. Meijer; Extended-Core Discotic Liquid Crystals Based on the Intramolecular H-Bonding in N-Acylated 2,2'-Bipyridine-3,3'-diamine Moieties, in *Chem. Eur. J*, **1997**, vol. 3, 2, pp. 300–307.
- 219 M. H. C. J. van Houtem, F. Benaskar, C. F. C. Fitié, R. Martin-Rapun, J. A. J. M. Vekemans, E. W. Meijer; Helical self-assembly and co-assembly of fluorinated, preorganized discotics, in *Org. Biomol. Chem*, **2012**, vol. 10, 30, pp. 5898–5908.
- 220 D. Kluge, J. C. Singer, B. R. Neugirg, J. W. Neubauer, H.-W. Schmidt, A. Fery; Top-down meets bottom-up: A comparison of the mechanical properties of melt electrospun and

- self-assembled 1,3,5-benzenetrisamide fibers, in *Polymer*, **2012**, vol. 53, 25, pp. 5754–5759.
- 221 M. G. McKee, J. M. Layman, M. P. Cashion, T. E. Long; Phospholipid Nonwoven Electrospun Membranes, in *Science*, **2006**, vol. 311, 5759, pp. 353–355.
- 222 F. Abraham, S. Ganzleben, D. Hanft, P. Smith, H.-W. Schmidt; Synthesis and Structure–Efficiency Relations of 1,3,5-Benzenetrisamides as Nucleating Agents and Clarifiers for Isotactic Poly(propylene), in *Macromol. Chem. Phys.*, **2010**, vol. 211, 2, pp. 171–181.
- 223 F. Abraham, H.-W. Schmidt; 1,3,5-Benzenetrisamide based nucleating agents for poly(vinylidene fluoride), in *Polymer*, **2010**, vol. 51, 4, pp. 913–921.
- 224 M. Kristiansen, P. Smith, H. Chanzy, C. Baerlocher, V. Gramlich, L. McCusker, T. Weber, P. Pattison, M. Blomenhofer, H.-W. Schmidt; Structural Aspects of 1,3,5-Benzenetrisamides—A New Family of Nucleating Agents, in *Crystal Growth & Design*, **2009**, vol. 9, 6, pp. 2556–2558.
- 225 N. Mohmeyer, N. Behrendt, X. Zhang, P. Smith, V. Altstädt, G. M. Sessler, H.-W. Schmidt; Additives to improve the electret properties of isotactic polypropylene, in *Polymer*, **2007**, vol. 48, 6, pp. 1612–1619.
- 226 M. Kersch, L. Pischke, H.-W. Schmidt, V. Altstädt; Influence of trisamide-based additives on the morphological and mechanical properties of isotactic polypropylene, in *Polymer*, **2014**, vol. 55, 15, pp. 3227–3233.
- 227 Y. Nakano, A. J. Markvoort, S. Cantekin, I. A. W. Filot, H. M. M. t. Eikelder, E. W. Meijer, A. R. A. Palmans; Conformational analysis of chiral supramolecular aggregates; modeling the subtle difference between hydrogen and deuterium, in *J. Am. Chem. Soc.*, **2013**, vol. 135, 44, pp. 16497–16506.
- 228 M. Raynal, F. Portier, P. W. N. M. van Leeuwen, L. Bouteiller; Tunable Asymmetric Catalysis through Ligand Stacking in Chiral Rigid Rods, in *J. Am. Chem. Soc.*, **2013**, vol. 135, 47, pp. 17687–17690.
- 229 S. Cantekin, Y. Nakano, J. C. Everts, P. van der Schoot, E. W. Meijer, A. R. A. Palmans; A stereoselectively deuterated supramolecular motif to probe the role of solvent during self-assembly processes, in *Chem. Commun*, **2012**, vol. 48, 32, p. 3803.
- 230 M. M. J. Smulders, M. M. L. Nieuwenhuizen, M. Grossman, I. A. W. Filot, C. C. Lee, T. F. A. de Greef, A. P. H. J. Schenning, A. R. A. Palmans, E. W. Meijer; Cooperative Two-Component Self-Assembly of Mono- and Ditopic Monomers, in *Macromolecules*, **2011**, vol. 44, 16, pp. 6581–6587.
- 231 M. A. J. Veld, D. Haveman, A. R. A. Palmans, E. W. Meijer*; Sterically demanding benzene-1,3,5-tricarboxamides: tuning the mechanisms of supramolecular polymerization and chiral amplification, in *Soft Matter*, **2011**, vol. 7, 2, p. 524.
- 232 D. Kluge, J. C. Singer, J. W. Neubauer, F. Abraham, H.-W. Schmidt, A. Fery; Influence of the Molecular Structure and Morphology of Self-Assembled 1,3,5-Benzenetrisamide Nanofibers on their Mechanical Properties, in *Small*, **2012**, vol. 8, 16, pp. 2563–2570.
- 233 A. Iwan, H. Janeczek, B. Kaczmarczyk, J. Jurusik, Z. Mazurak, D. Sek, P. Rannou, J.-P. Bonnet, A. Pron; Supramolecular associations of poly(ketani)s with sulfonic acid derivatives of benzenetricarboxamide via Brönsted acid–base interactions: Preparation, spectroscopic morphological and thermal investigations, in *Synthetic Metals*, **2009**, vol. 159, 3–4, pp. 282–291.
- 234 P. J. M. Stals, P. A. Korevaar, M. A. J. Gillissen, T. F. A. de Greef, C. F. C. Fitié, R. P. Sijbesma, A. R. A. Palmans, E. W. Meijer; Symmetry Breaking in the Self-Assembly of

- Partially Fluorinated Benzene-1,3,5-tricarboxamides, in *Angew. Chem.*, **2012**, vol. 124, 45, pp. 11459–11463.
- 235 Y. Huang, Y. Cong, J. Li, D. Wang, J. Zhang, L. Xu, W. Li, L. Li, G. Pan, C. Yang; Anisotropic ionic conductivities in lyotropic supramolecular liquid crystals, in *Chem. Commun.*, **2009**, vol. 0, 48, pp. 7560–7562.
- 236 Y. Huang, D. Wang, L. Xu, Y. Cong, J. Li, L. Li; Multiscale fibers via supramolecular self-assembly of a fully rigid, discotic aromatic aramid molecule, in *European Polymer Journal*, **2013**, vol. 49, 6, pp. 1682–1687.
- 237 D. Wang, Y. Huang, J. Li, L. Xu, M. Chen, J. Tao, L. Li; Lyotropic Supramolecular Helical Columnar Phases Formed by C₃-Symmetric and Unsymmetric Rigid Molecules, in *Chem. Eur. J.*, **2013**, vol. 19, 2, pp. 685–690.
- 238 Y. Dai, X. Zhao, X. Su, G. Li, A. Zhang; Supramolecular Assembly of C₃ Peptidic Molecules into Helical Polymers, in *Macromol. Rapid Commun.*, **2014**, vol. 35, 15, pp. 1326–1331.
- 239 K. Hanabusa, C. Koto, M. Kimura, H. Shirai, A. Kakehi; Remarkable Viscoelasticity of Organic Solvents Containing Trialkyl-1,3,5-benzenetricarboxamides and their Supramolecular Structure, in *Chemistry Letters*, **1997**, vol. 5, 2a, pp. 429–430.
- 240 F. Aparicio, F. García, L. Sánchez; Supramolecular Polymerization of C₃-symmetric organogelators: cooperativity, solvent, and gelation relationship, in *Chem. Eur. J.*, **2013**, 19, pp. 3239–3248.
- 241 H. Cao, P. Duan, X. Zhu, J. Jiang, M. Liu; Self-Assembled Organic Nanotubes through Instant Gelation and Universal Capacity for Guest Molecule Encapsulation, in *Chemistry – A European Journal*, **2012**, vol. 18, 18, pp. 5546–5550.
- 242 P. Jana, A. Paikar, S. Bera, S. K. Maity, D. Haldar; Porous Organic Material from Discotic Tricarboxamide: Side Chain–Core interactions, in *Org. Lett.*, **2014**, vol. 16, 1, pp. 38–41.
- 243 J. H. Jung, J. Ahn, S. Park, J. H. Lee, S. H. Jung, S.-J. Moon; Fluorescent hydrogels formed by CH–[small pi] and [small pi]–[small pi] interactions as the main driving forces: an approach toward understanding the relationship between fluorescence and structure, in *Chem. Commun*, **2012**, 49, pp. 2109–2111.
- 244 M. A. J. Gillissen, T. Terashima, E. W. Meijer, A. R. A. Palmans, I. K. Voets; Sticky Supramolecular Grafts Stretch Single Polymer Chains, in *Macromolecules*, **2013**, vol. 46, 10, pp. 4120–4125.
- 245 E. Huerta, P. J. M. Stals, E. W. Meijer, A. R. A. Palmans; Consequences of Folding a Water-Soluble Polymer Around an Organocatalyst, in *Angew. Chem. Int. Ed.*, **2013**, vol. 52, 10, pp. 2906–2910.
- 246 Y. Zhao, T. Imura, L. J. Leman, L. K. Curtiss, B. E. Maryanoff, M. R. Ghadiri; Mimicry of High-Density Lipoprotein: Functional Peptide–Lipid Nanoparticles Based on Multivalent Peptide Constructs, in *J. Am. Chem. Soc.*, **2013**, vol. 135, 36, pp. 13414–13424.
- 247 M. Artar, T. Terashima, M. Sawamoto, E. W. Meijer, A. R. A. Palmans; Understanding the catalytic activity of single-chain polymeric nanoparticles in water, in *J. Polym. Sci. Part A: Polym. Chem.*, **2014**, vol. 52, 1, pp. 12–20.
- 248 T. Terashima, T. Mes, T. F. A. de Greef, M. A. J. Gillissen, P. Besenius, A. R. A. Palmans, E. W. Meijer; Single-Chain Folding of Polymers for Catalytic Systems in Water, in *J. Am. Chem. Soc.*, **2011**, vol. 133, 13, pp. 4742–4745.
- 249 N. Hosono, M. A. J. Gillissen, Y. Li, S. S. Sheiko, A. R. A. Palmans, E. W. Meijer; Orthogonal Self-Assembly in Folding Block Copolymers, in *J. Am. Chem. Soc.*, **2013**, vol. 135, 1, pp. 501–510.

- 250 N. Hosono, A. R. A. Palmans, E. W. Meijer; "Soldier-Sergeant-Soldier" triblock copolymers: revealing the folded structure of single-chain polymeric nanoparticles, in *Chem. Commun.*, **2014**, vol. 50, 59, pp. 7990–7993.
- 251 E. Huerta, B. van Genabeek, P. J. M. Stals, E. W. Meijer, A. R. A. Palmans; A Modular Approach to Introduce Function into Single-Chain Polymeric Nanoparticles, in *Macromol. Rapid Commun.*, **2014**, vol. 35, 15, pp. 1320–1325.
- 252 M. A. J. Gillissen, M. M. E. Koenigs, A. J. H. Spiering, J. A. J. M. Vekemans, A. R. A. Palmans, I. K. Voets, E. W. Meijer; Triple helix formation in amphiphilic discotics: Demystifying solvent effects in supramolecular self-assembly, in *J. Am. Chem. Soc.*, **2014**, vol. 136, 1, pp. 336–343.
- 253 C. M. A. Leenders, L. Albertazzi, T. Mes, M. M. E. Koenigs, A. R. A. Palmans, E. W. Meijer; Supramolecular polymerization in water harnessing both hydrophobic effects and hydrogen bond formation, in *Chem. Commun.*, **2013**, vol. 49, 19, p. 1963.
- 254 P. Besenius, K. P. van den Hout, H. M. H. G. Albers, T. F. A. de Greef, L. L. C. Olijve, T. M. Hermans, B. F. M. de Waal, P. H. H. Bomans, N. A. J. M. Sommerdijk, G. Portale, A. R. A. Palmans, M. H. P. van Genderen, J. A. J. M. Vekemans, E. W. Meijer; Controlled Supramolecular Oligomerization of C₃-Symmetrical Molecules in Water: The Impact of Hydrophobic Shielding, in *Chem. Eur. J.*, **2011**, vol. 17, 18, pp. 5193–5203.
- 255 I. de Feijter, P. Besenius, L. Albertazzi, E. W. Meijer, A. R. A. Palmans, I. K. Voets; Mechanistic control over morphology: self-assembly of a discotic amphiphile in water, in *Soft Matter*, **2013**, vol. 9, 42, pp. 10025–10030.
- 256 P. Besenius, G. Portale, P. H. H. Bomans, H. M. Janssen, A. R. A. Palmans, E. W. Meijer; Controlling the growth and shape of chiral supramolecular polymers in water, in *Proceedings of the National Academy of Sciences*, **2010**, vol. 107, 42, pp. 17888–17893.
- 257 C. Schaefer, I. K. Voets, A. R. A. Palmans, E. W. Meijer, P. van der Schoot, P. Besenius; Controlling the Cooperativity in the Supramolecular Polymerization of Ionic Discotic Amphiphiles via Electrostatic Screening, in *ACS Macro Lett*, **2012**, vol. 1, 7, pp. 830–833.
- 258 M. von Gröning, I. de Feijter, M. C. A. Stuart, I. K. Voets, P. Besenius; Tuning the aqueous self-assembly of multistimuli-responsive polyanionic peptide nanorods, in *J. Mater. Chem. B*, **2013**, vol. 1, 15, p. 2008.
- 259 J. Li, N. Huang, D. Wang, L. Xu, Y. Huang, M. Chen, J. Tao, G. Pan, Z. Wu, L. Li; Highly ordered, ultra long nanofibrils via the hierarchical self-assembly of ionic aromatic oligoamides, in *Soft Matter*, **2013**, 9, pp. 4642–4647.
- 260 H. Frisch, J. P. Unsleber, D. Lüdeker, M. Peterlechner, G. Brunklaus, M. Waller, P. Besenius; pH-Switchable Ampholytic Supramolecular Copolymers, in *Angew. Chem. Int. Ed.*, **2013**, vol. 52, 38, pp. 10097–10101.
- 261 L. Albertazzi, D. van der Zwaag, C. M. A. Leenders, R. Fitzner, R. W. van der Hofstad, E. W. Meijer; Probing Exchange Pathways in One-Dimensional Aggregates with Super-Resolution Microscopy, in *Science*, **2014**, vol. 344, 6183, pp. 491–495.
- 262 S. Lee, J.-S. Lee, C. H. Lee, Y.-S. Jung, J.-M. Kim; Nonpolymeric Thermosensitive Benzenetricarboxamides, in *Langmuir*, **2011**, vol. 27, 5, pp. 1560–1564.
- 263 L. Brunsveld, B. G. G. Lohmeijer, J. A. J. M. Vekemans, E. W. Meijer; Chirality amplification in dynamic helical columns in water, in *Chem. Commun.*, **2000**, 23, pp. 2305–2306.
- 264 E. Weber; Tenside mit neuer Strukturcharakteristik, in *Angewandte Chemie*, **1983**, vol. 95, 8, pp. 632–632.

- 265 D. K. Kumar, D. A. Jose, P. Dastidar, A. Das; Nonpolymeric Hydrogelators Derived from Trimesic Amides, in *Chemistry of Materials*, **2004**, vol. 16, 12, pp. 2332–2335.
- 266 N. Shi, G. Yin, M. Han, Z. Xu; Anions bonded on the supramolecular hydrogel surface as the growth center of biominerals, in *Colloids and Surfaces B: Biointerfaces*, **2008**, vol. 66, 1, pp. 84–89.
- 267 R. C. T. Howe, A. P. Smalley, A. P. M. Guttenplan, M. W. R. Doggett, M. D. Eddleston, J. C. Tan, G. O. Lloyd; A family of simple benzene 1,3,5-tricarboxamide (BTA) aromatic carboxylic acid hydrogels, in *Chem. Commun.*, **2013**, 49, pp. 4268–4270.
- 268 R. Grönker, V. Bon, P. Müller, U. Stoeck, S. Krause, U. Mueller, I. Senkovska, S. Kaskel; A new metal–organic framework with ultra-high surface area, in *Chem. Commun.*, **2014**, vol. 50, 26, p. 3450.
- 269 C. Zaharia, D. Suteu; *Textile Organic Dyes – Characteristics, Polluting Effects and Separation/Elimination Procedures from Industrial Effluents – A Critical Overview in Organic Pollutants Ten Years After the Stockholm Convention - Environmental and Analytical Update*, ed. T. Puzyn, InTech, **2012**.
- 270 H. A. Aziz, M. N. Adlan, C. S. Hui, M. S. M. Zahari, B. H. Hameed; Removal of Ni. Cd. Pb, Zn and colour from aqueous solution using potential low cost adsorbent, in *Indian Journal of Engineering and Materials Sciences*, **2005**, vol. 12, 3, pp. 248–258.
- 271 V. K. GUPTA, D. MOHAN, S. SHARMA, M. SHARMA; Removal of Basic Dyes (Rhodamine B and Methylene Blue) from Aqueous Solutions Using Bagasse Fly Ash, in *Separation Science and Technology*, **2000**, vol. 35, 13, pp. 2097–2113.
- 272 sigma-aldrich; Rhodamine B, Material Safety Data Sheet, available at: <http://www.sigmaaldrich.com/MSDS/MSDS/DisplayMSDSPage.do?country=DE&language=de&productNumber=R6626&brand=SIGMA&PageToGoToURL=http%3A%2F%2Fwww.sigmaaldrich.com%2Fcatalog%2Fsearch%3Finterface%3DAll%26term%3DRhodamine%2BB%26N%3D0%26mode%3Dmatch%2520partialmax%26focus%3Dproduct%26lang%3Dde%26region%3DDE>, accessed 20 October 2014.
- 273 I. L. Arbeloa, K. K. Rohatgi-Mukherjee; Solvent effect on photophysics of the molecular forms of rhodamine B. Solvation models and spectroscopic parameters, in *Chemical Physics Letters*, **1986**, vol. 128, 5–6, pp. 474–479.
- 274 N. Boens, W. Qin, N. Basarić, J. Hofkens, M. Ameloot, J. Pouget, J.-P. Lefèvre, B. Valeur, E. Gratton, M. vandeVen, N. D. Silva, Y. Engelborghs, K. Willaert, A. Sillen, G. Rumbles, D. Phillips, A. J. W. G. Visser, A. van Hoek, J. R. Lakowicz, H. Malak, I. Gryczynski, A. G. Szabo, D. T. Krajcarski, N. Tamai, A. Miura; Fluorescence Lifetime Standards for Time and Frequency Domain Fluorescence Spectroscopy, in *Anal. Chem.*, **2007**, vol. 79, 5, pp. 2137–2149.
- 275 P. Bairi, B. Roy, A. K. Nandi; pH and anion sensitive silver(i) coordinated melamine hydrogel with dye absorbing properties: metastability at low melamine concentration, in *J. Mater. Chem*, **2011**, vol. 21, 32, pp. 11747–11749.
- 276 C. Namasivayam, N. Kanchana, R. T. Yamuna; Waste banana pith as adsorbent for the removal of rhodamine-B from aqueous solutions, in *Waste Management*, **1993**, vol. 13, 1, pp. 89–95.
- 277 I. Moreno-Villoslada, M. Jofré, V. Miranda, R. González, T. Sotelo, S. Hess, B. L. Rivas; pH Dependence of the Interaction between Rhodamine B and the Water-Soluble Poly(sodium 4-styrenesulfonate), in *The Journal of Physical Chemistry B*, **2006**, vol. 110, 24, pp. 11809–11812.

- 278 K. V. Kumar; Linear and non-linear regression analysis for the sorption kinetics of methylene blue onto activated carbon, in *Journal of Hazardous Materials*, **2006**, vol. 137, 3, pp. 1538–1544.
- 279 V. Gómez, M. S. Larrechi, M. P. Callao; Kinetic and adsorption study of acid dye removal using activated carbon, in *Chemosphere*, **2007**, vol. 69, 7, pp. 1151–1158.
- 280 J. Karam, J. A. Nicell; Potential Applications of Enzymes in Waste Treatment, in *J. Chem. Technol. Biotechnol.*, **1997**, vol. 69, 2, pp. 141–153.
- 281 A. Sayari, S. Hamoudi, Y. Yang; Applications of Pore-Expanded Mesoporous Silica. 1. Removal of Heavy Metal Cations and Organic Pollutants from Wastewater, in *Chem. Mater.*, **2005**, vol. 17, 1, pp. 212–216.
- 282 M. Arkas, D. Tsiourvas, C. M. Paleos; Organosilicon Dendritic Networks in Porous Ceramics for Water Purification, in *Chem. Mater.*, **2005**, vol. 17, 13, pp. 3439–3444.
- 283 I. Ali; New Generation Adsorbents for Water Treatment, in *Chem. Rev.*, **2012**, vol. 112, 10, pp. 5073–5091.
- 284 Y. S. Ho, G. McKay; Kinetic Models for the Sorption of Dye from Aqueous Solution by Wood, in *Process Safety and Environmental Protection*, **1998**, vol. 76, 2, pp. 183–191.
- 285 Y. S. Ho, G. McKay; Sorption of dye from aqueous solution by peat, in *Chemical Engineering Journal*, **1998**, vol. 70, 2, pp. 115–124.
- 286 W. M. Antunes, A. S. Luna, C. A. Henriques, A. C. A. Da Costa; An evaluation of copper biosorption by a brown seaweed under optimized conditions, in *Electron. J. Biotechnol.*, **2003**, vol. 6, 3.
- 287 E. J. Cho, I. Y. Jeong, S. J. Lee, W. S. Han, J. K. Kang, J. H. Jung; Terpyridine-based smart organic–inorganic hybrid gel as potential dye-adsorbing agent for water purification, in *Tetrahedron Letters*, **2008**, vol. 49, 6, pp. 1076–1079.
- 288 F. Rodriguez-Llansola, B. Escuder, J. F. Miravet, D. Hermida-Merino, I. W. Hamley, C. J. Cardin, W. Hayes; Selective and highly efficient dye scavenging by a pH-responsive molecular hydrogelator, in *Chem. Commun*, **2010**, vol. 46, 42, pp. 7960–7962.
- 289 X. Dou, P. Li, D. Zhang, C.-L. Feng; C₂-symmetric benzene-based hydrogels with unique layered structures for controllable organic dye adsorption, in *Soft Matter*, **2012**, vol. 8, 11, p. 3231.
- 290 B. O. Okesola, D. K. Smith; Versatile supramolecular pH-tolerant hydrogels which demonstrate pH-dependent selective adsorption of dyes from aqueous solution, in *Chem. Commun.*, **2013**, vol. 49, 95, pp. 11164–11166.
- 291 H. Wang, W. Xu, S. Song, L. Feng, A. Song, J. Hao; Hydrogels Facilitated by Monovalent Cations and Their Use as Efficient Dye Adsorbents, in *J. Phys. Chem. B*, **2014**, vol. 118, 17, pp. 4693–4701.
- 292 G. M. Peters, L. P. Skala, T. N. Plank, B. J. Hyman, G. N. Manjunatha Reddy, A. Marsh, S. P. Brown, J. T. Davis; A G₄-K + Hydrogel Stabilized by an Anion, in *J. Am. Chem. Soc.*, **2014**, vol. 136, 36, pp. 12596–12599.
- 293 D. Asma, S. Kahraman, S. Cing, O. Yesilada; Adsorptive removal of textile dyes from aqueous solutions by dead fungal biomass, in *J. Basic Microbiol.*, **2006**, vol. 46, 1, pp. 3–9.
- 294 C. I. Pearce, J. R. Lloyd, J. T. Guthrie; The removal of colour from textile wastewater using whole bacterial cells: a review, in *Dyes and Pigments*, **2003**, vol. 58, 3, pp. 179–196.

- 295 A. Hillery, A. Lloyd, J. Swarbrick; Drug Delivery and Targeting: For Pharmacists and Pharmaceutical Scientists, Taylor & Francis, **2002**.
- 296 A. Mohr, R. Haag; *Supramolecular Drug-Delivery Systems in Applications of supramolecular chemistry*, ed. H.-J. Schneider, CRC Press, Boca Raton, **2012**, pp. 341–362.
- 297 M. R. C. Marques, R. Loebenberg, M. Almukainzi; Simulated Biological Fluids with Possible Application in Dissolution Testing, in *Dissolution Technologies*, **2011**, vol. 18, 3, pp. 15–28.
- 298 J. B. Dressman, G. L. Amidon, C. Reppas, V. P. Shah; Dissolution Testing as a Prognostic Tool for Oral Drug Absorption: Immediate Release Dosage Forms, in *Pharm Res*, **1998**, vol. 15, 1, pp. 11-22.
- 299 Y. Wang, L. Tang, J. Yu; Investigation on the assembled structure–property correlation of supramolecular hydrogel formed from low-molecular-weight gelator, in *Journal of Colloid and Interface Science*, **2008**, vol. 319, 1, pp. 357–364.
- 300 G. Liang, Z. Yang, R. Zhang, L. Li, Y. Fan, Y. Kuang, Y. Gao, T. Wang, W. W. Lu, B. Xu; Supramolecular Hydrogel of a d -Amino Acid Dipeptide for Controlled Drug Release in Vivo †, in *Langmuir*, **2009**, vol. 25, 15, pp. 8419–8422.
- 301 F. Zhao, M. L. Ma, B. Xu; Molecular hydrogels of therapeutic agents, in *Chem. Soc. Rev.*, **2009**, vol. 38, 4, pp. 883–891.
- 302 S. Bhuniya, Y. J. Seo, B. H. Kim; (S)-(+)-Ibuprofen-based hydrogelators: an approach toward anti-inflammatory drug delivery, in *Tetrahedron Letters*, **2006**, vol. 47, 40, pp. 7153–7156.
- 303 Z. Yang, K. Xu, L. Wang, H. Gu, H. Wei, M. Zhang, B. Xu; Self-assembly of small molecules affords multifunctional supramolecular hydrogels for topically treating simulated uranium wounds, in *Chem. Commun.*, **2005**, 35, p. 4414.
- 304 B. Xing, P. L. Ho, C.-W. Yu, K.-H. Chow, H. Gu, B. Xu; Self-assembled multivalent vancomycin on cell surfaces against vancomycin-resistant enterococci (VRE), in *Chem. Commun.*, **2003**, 17, pp. 2224–2225.
- 305 S. Marchesan, Y. Qu, L. J. Waddington, C. D. Easton, V. Glattauer, T. J. Lithgow, K. M. McLean, J. S. Forsythe, P. G. Hartley; Self-assembly of ciprofloxacin and a tripeptide into an antimicrobial nanostructured hydrogel, in *Biomaterials*, **2013**, vol. 34, 14, pp. 3678–3687.
- 306 J. Naskar, G. Palui, A. Banerjee; Tetrapeptide-Based Hydrogels: for Encapsulation and Slow Release of an Anticancer Drug at Physiological pH, in *The Journal of Physical Chemistry B*, **2009**, vol. 113, 35, pp. 11787–11792.
- 307 D. D. Diaz, E. Morin, E. M. Schon, G. Budin, A. Wagner, J.-S. Remy; Tailoring drug release profile of low-molecular-weight hydrogels by supramolecular co-assembly and thiol-ene orthogonal coupling, in *J. Mater. Chem.*, **2011**, vol. 21, 3, pp. 641–644.
- 308 Z. Yang, G. Liang, B. Xu; Enzymatic Hydrogelation of Small Molecules, in *Accounts of Chemical Research*, **2008**, vol. 41, 2, pp. 315–326.
- 309 Yuan Gao, Zhimou Yang, Yi Kuang, Man-Lung Ma, Jiayang Li, Fan Zhao, Bing Xu; Enzyme-instructed self-assembly of peptide derivatives to form nanofibers and hydrogels, in *Peptide Science*, **2010**, vol. 94, 1, pp. 19–31.
- 310 E. Jantratid, N. Janssen, C. Reppas, J. Dressman; Dissolution Media Simulating Conditions in the Proximal Human Gastrointestinal Tract: An Update, in *Pharm Res*, **2008**, vol. 25, 7, pp. 1663-1676.

- 311 C. J. H. Porter, N. L. Trevaskis, W. N. Charman; Lipids and lipid-based formulations: optimizing the oral delivery of lipophilic drugs, in *Nat Rev Drug Discov*, **2007**, vol. 6, 3, pp. 231–248.
- 312 M. Yamanaka, K. Sada, M. Miyata, K. Hanabusa, K. Nakano; Construction of superhydrophobic surfaces by fibrous aggregation of perfluoroalkyl chain-containing organogelators, in *Chem. Commun.*, **2006**, 21, pp. 2248–2250.
- 313 C. H. Hamann, A. Hamnett, W. Vielstich; *Electrochemistry*, Wiley-VCH, Weinheim, 2nd ed., **2007**.
- 314 O. Guillaume-Gentil, D. Abbruzzese, E. Thomasson, J. Vörös, T. Zambelli; Chemically Tunable Electrochemical Dissolution of Noncontinuous Polyelectrolyte Assemblies: An In Situ Study Using ecAFM, in *ACS Applied Materials & Interfaces*, **2010**, vol. 2, 12, pp. 3525–3531.
- 315 A. P. Ngankam, P. R. van Tassel; Continuous polyelectrolyte adsorption under an applied electric potential, in *Proceedings of the National Academy of Sciences*, **2007**, vol. 104, 4, pp. 1140–1145.
- 316 O. Guillaume-Gentil, N. Graf, F. Boulmedais, P. Schaaf, J. Voros, T. Zambelli; Global and local view on the electrochemically induced degradation of polyelectrolyte multilayers: from dissolution to delamination, in *Soft Matter*, **2010**, vol. 6, 17, pp. 4246–4254.
- 317 F. Boulmedais, C. S. Tang, B. Keller, J. Vörös; Controlled Electrodeposition of Polyelectrolyte Multilayers: A Platform Technology Towards the Surface-Initiated Delivery of Drugs, in *Adv. Funct. Mater.*, **2006**, vol. 16, 1, pp. 63–70.
- 318 L. Dieguez, N. Darwish, N. Graf, J. Voros, T. Zambelli; Electrochemical tuning of the stability of PLL/DNA multilayers, in *Soft Matter*, **2009**, vol. 5, 12, pp. 2415–2421.
- 319 R. Fernandes, L.-Q. Wu, T. Chen, H. Yi, G. W. Rubloff, R. Ghodssi, W. E. Bentley, G. F. Payne; Electrochemically Induced Deposition of a Polysaccharide Hydrogel onto a Patterned Surface, in *Langmuir*, **2003**, vol. 19, 10, pp. 4058–4062.
- 320 F. Lottspeich; *Bioanalytik*, Spektrum, Heidelberg, 3rd ed., **2012**.
- 321 S. Yamamichi, Y. Jinno, N. Haraya, T. Oyoshi, H. Tomitori, K. Kashiwagi, M. Yamanaka; Separation of proteins using supramolecular gel electrophoresis, in *Chem. Commun*, **2011**, 47, pp. 10344–10346.
- 322 S. Cosnier, A. Karyakin; *Electropolymerization: Concepts, Materials and Applications*, Wiley, **2011**.
- 323 M.-k. Leung, Y.-S. Lin, C.-C. Lee, C.-C. Chang, Y.-X. Wang, C.-P. Kuo, N. Singh, K.-R. Lin, C.-W. Hu, C.-Y. Tseng, K.-C. Ho; Benzenetricarboxamide-cored triphenylamine dendrimer: nanoparticle film formation by an electrochemical method, in *RSC Adv.*, **2013**, vol. 3, 44, p. 22219.
- 324 M. Gabi, T. Sannomiya, A. Larmagnac, M. Puttaswamy, J. Voros; Influence of applied currents on the viability of cells close to microelectrodes, in *Integr. Biol*, **2009**, vol. 1, 1, pp. 108–115.
- 325 T. Sawai, H. Shinohara, Y. Ikariyama, M. Aizawa; Electrical modulation of the solution pH near polyaniline and its composite electrodes, in *Journal of Electroanalytical Chemistry*, **1990**, vol. 283, 1-2, pp. 221–230.
- 326 R. Shacham, D. Mandler, D. Avnir; Electrochemically Induced Sol–Gel Deposition of Zirconia Thin Films, in *Chem. Eur. J*, **2004**, vol. 10, 8, pp. 1936–1943.

- 327 S. Rentsch, H. Siegenthaler, G. Papastavrou; Diffuse Layer Properties of Thiol-Modified Gold Electrodes Probed by Direct Force Measurements, in *Langmuir*, **2007**, vol. 23, 17, pp. 9083–9091.
- 328 N. N. Bernhard, T. J.-C. Lo, G. G. Leisk and D. L. Kaplan; Active silk muco-adhesives, silk electrogelation process, and devices, *USA Pat.*, WO2010/036992 A2, **2009**.
- 329 Gary G. Leisk, Tim J. Lo, Tuna Yucel, Qiang Lu, David L. Kaplan; Electrogelation for Protein Adhesives, in *Advanced Materials*, **2010**, vol. 22, 6, pp. 711–715.
- 330 E. K. Johnson, D. J. Adams, P. J. Cameron; Directed Self-Assembly of Dipeptides to Form Ultrathin Hydrogel Membranes, in *Journal of the American Chemical Society*, **2010**, vol. 132, 14, pp. 5130–5136.
- 331 M. Raue, A. Bernet, M. Küppers, S. Stapf, H.-W. Schmidt, B. Blümich, T. Mang; *Sodium NMR Relaxation: A Versatile Non-invasive Tool for the Monitoring of Phase Transitions and the Estimation of Effective Pore Sizes of Supramolecular Hydrogels* in *Intelligent Hydrogels*, ed. G. Sadowski and W. Richtering, Springer International Publishing, **2013**, vol. 140, pp. 45–51.
- 332 Y. Ishida, M. Jikei, M.-a. Kakimoto; Rapid Synthesis of Aromatic Polyamide Dendrimers by an Orthogonal and a Double-Stage Convergent Approach, in *Macromolecules*, **2000**, vol. 33, 9, pp. 3202–3211.
- 333 P. Wang and G. Yang; Polyester composition containing hyperbranched polyamide, CN1990545A, **2007**.
- 334 I. Washio, Y. Shibasaki, M. Ueda; Facile Synthesis of Polyamide Dendrimers from Unprotected AB₂, in *Macromolecules*, **2005**, vol. 38, 6, pp. 2237–2246.
- 335 S. Shabbir, S. Zulfiqar, Z. Ahmad, M. Ilyas Sarwar; Synthesis and properties of hyperbranched polyamide-esters derived from 1,3,5-tris(4'-hydroxyphenylcarbamoyl)benzene, in *Tetrahedron*, **2010**, vol. 66, 6, pp. 1389–1398.
- 336 S. Shabbir, S. Zulfiqar, M. I. Sarwar; Amine-terminated aromatic and semi-aromatic hyperbranched polyamides: synthesis and characterization, in *J Polym Res*, **2011**, vol. 18, 6, pp. 1919–1929.
- 337 Y. Jiao, J. Zhang, L. Zhang, Z. Lin, C. He, C. Duan; Metal-organic polyhedra containing 36 and 24 folds of amide groups for selective luminescent recognition of natural disaccharides, in *Chem. Commun.*, **2012**, vol. 48, 48, pp. 6022–6024.
- 338 M. Behr; Synthese und Charakterisierung von Trimesinsäuretrisamid-basierten Hydrogelatoren, Diplomarbeit, Universität Bayreuth, **2009**.
- 339 M. Hesse, H. Meier, B. Zeeh; *Spektroskopische Methoden in der organischen Chemie*, Thieme, Stuttgart, 5th ed., **1995**.
- 340 M. Smith; *Organic synthesis*, Academic Press, an imprint of Elsevier, [Boston], **2011**.
- 341 C. Tang, A. M. Smith, R. F. Collins, R. V. Ulijn, A. Saiani; Fmoc-Diphenylalanine Self-Assembly Mechanism Induces Apparent pKa Shifts, in *Langmuir*, **2009**, vol. 25, 16, pp. 9447–9453.
- 342 R. Gomes, C. A. T. Laia, F. Pina; On the Mechanism of Photochromism of 4'-N,N-Dimethylamino-7-hydroxyflavylium in Pluronic F127, in *The Journal of Physical Chemistry B*, **2009**, vol. 113, 32, pp. 11134–11146.
- 343 J. Boekhoven, J. M. Poolman, C. Maity, F. Li, L. van der Mee, C. B. Minkenberg, E. Mendes, van EschJan H., R. Eelkema; Catalytic control over supramolecular gel formation, in *Nat Chem*, **2013**, vol. 5, 5, pp. 433–437.

- 344 P. W. Atkins, J. de Paula; Physical chemistry, W.H. Freeman, New York, 9th ed., **2010**.
- 345 J. B. Birks; Photophysics of aromatic molecules, Wiley-Interscience, London, New York, **1970**.
- 346 R. H. Friend, R. W. Gymer, A. B. Holmes, J. H. Burroughes, R. N. Marks, C. Taliani, D. D. C. Bradley, D. A. D. Santos, J. L. Bredas, M. Logdlund, W. R. Salaneck; Electroluminescence in conjugated polymers, in *Nature*, **1999**, vol. 397, 6715, pp. 121–128.
- 347 J. Luo, Z. Xie, J. W. Y. Lam, L. Cheng, H. Chen, C. Qiu, H. S. Kwok, X. Zhan, Y. Liu, D. Zhu, B. Z. Tang; Aggregation-induced emission of 1-methyl-1,2,3,4,5-pentaphenylsilole, in *Chem. Commun*, **2001**, 18, pp. 1740–1741.
- 348 Y. Hong, J. W. Y. Lam, B. Z. Tang; Aggregation-induced emission, in *Chem. Soc. Rev*, **2011**, 40, p. 5361.
- 349 J. Mei, Y. Hong, J. W. Y. Lam, A. Qin, Y. Tang, B. Z. Tang; Aggregation-Induced Emission: The Whole Is More Brilliant than the Parts, in *Adv. Mater.*, **2014**, vol. 26, 31, pp. 5429–5479.
- 350 R. Deans, J. Kim, M. R. Machacek, T. M. Swager; A Poly(p-phenyleneethynylene) with a Highly Emissive Aggregated Phase, in *Journal of the American Chemical Society*, **2000**, vol. 122, 35, pp. 8565–8566.
- 351 M. K. Nayak, B.-H. Kim, J. E. Kwon, S. Park, J. Seo, J. W. Chung, S. Y. Park; Gelation-Induced Enhanced Fluorescence Emission from Organogels of Salicylanilide-Containing Compounds Exhibiting Excited-State Intramolecular Proton Transfer: Synthesis and Self-Assembly, in *Chem. Eur. J.*, **2010**, vol. 16, 25, pp. 7437–7447.
- 352 B.-K. An, S.-K. Kwon, S.-D. Jung, S. Y. Park; Enhanced Emission and Its Switching in Fluorescent Organic Nanoparticles, in *Journal of the American Chemical Society*, **2002**, vol. 124, 48, pp. 14410–14415.
- 353 J. Chen, C. C. W. Law, J. W. Y. Lam, Y. Dong, S. M. F. Lo, I. D. Williams, D. Zhu, B. Z. Tang; Synthesis, Light Emission, Nanoaggregation, and Restricted Intramolecular Rotation of 1,1-Substituted 2,3,4,5-Tetraphenylsiloles, in *Chemistry of Materials*, **2003**, vol. 15, 7, pp. 1535–1546.
- 354 Z. Zhao, J. W. Y. Lam, B. Z. Tang; Self-assembly of organic luminophores with gelation-enhanced emission characteristics, in *Soft Matter*, **2013**, 9, pp. 4564–4579.
- 355 S. Y. Ryu, S. Kim, J. Seo, Y.-W. Kim, O.-H. Kwon, D.-J. Jang, S. Y. Park; Strong fluorescence emission induced by supramolecular assembly and gelation: luminescent organogel from nonemissive oxadiazole-based benzene-1,3,5-tricarboxamide gelator, in *Chemical Communications*, **2004**, 1, pp. 70–71.
- 356 Y. Chen, Y. Lv, Y. Han, B. Zhu, F. Zhang, Z. Bo, C.-Y. Liu; Dendritic Effect on Supramolecular Self-Assembly: Organogels with Strong Fluorescence Emission Induced by Aggregation, in *Langmuir*, **2009**, vol. 25, 15, pp. 8548–8555.
- 357 A. Rochefort, É. Bayard, S. Hadj-Messaoud; Competitive Hydrogen Bonding in π -Stacked Oligomers, in *Adv. Mater.*, **2007**, vol. 19, 15, pp. 1992–1995.
- 358 S. Banerjee, N. N. Adarsh, P. Dastidar; A crystal engineering rationale in designing a CdII coordination polymer based metallo gel derived from a C3 symmetric tris-amide-tris-carboxylate ligand, in *Soft Matter*, **2012**, vol. 8, 29, p. 7623.
- 359 D. Markovitsi, S. Marguet, J. Bondkowski, S. Kumar; Triplet Excitation Transfer in Triphenylene Columnar Phases, in *J. Phys. Chem. B*, **2001**, vol. 105, 7, pp. 1299–1306.

- 360 M. Montalti, L. S. Dolci, L. Prodi, N. Zaccheroni, M. C. A. Stuart, K. J. C. van Bommel, A. Friggeri; Energy Transfer from a Fluorescent Hydrogel to a Hosted Fluorophore, in *Langmuir*, **2006**, vol. 22, 5, pp. 2299–2303.
- 361 M. R. Molla, S. Ghosh; Hydrogen-Bonding-Mediated Vesicular Assembly of Functionalized Naphthalene–Diimide-Based Bolaamphiphile and Guest-Induced Gelation in Water, in *Chem. Eur. J.*, **2012**, vol. 18, 32, pp. 9860–9869.
- 362 J.-H. Kim, E. Lee, Y.-H. Jeong, W.-D. Jang; Unique Photoluminescence of Diacetylene Containing Dendrimer Self-Assemblies: Application in Positive and Negative Luminescence Patterning, in *Chem. Mater*, **2012**, vol. 24, 12, pp. 2356–2363.
- 363 M. Bierenstiel, M. Schlaf; δ -Galactonolactone: Synthesis, Isolation, and Comparative Structure and Stability Analysis of an Elusive Sugar Derivative, in *Eur. J. Org. Chem*, **2004**, vol. 2004, 7, pp. 1474–1481.
- 364 F. D. Lewis, T. M. Long, C. L. Stern, W. Liu; Structures and Excited States of Extended and Folded Mono-, Di-, and Tri-N-Arylbenzamides, in *The Journal of Physical Chemistry A*, **2003**, vol. 107, 18, pp. 3254–3262.
- 365 Y. Huang, D.-H. Kim; Light-controlled synthesis of gold nanoparticles using a rigid, photoresponsive surfactant, in *Nanoscale*, **2012**, 4, pp. 6312–6317.
- 366 J. Heldt, D. Gormin, M. Kasha; Intramolecular charge-transfer transition in benzanilides and its dielectric medium modulation, in *J. Am. Chem. Soc*, **1988**, vol. 110, 24, pp. 8255–8256.
- 367 I. Azumaya, H. Kagechika, Y. Fujiwara, M. Itoh, K. Yamaguchi, K. Shudo; Twisted intramolecular charge-transfer fluorescence of aromatic amides: conformation of the amide bonds in excited states, in *J. Am. Chem. Soc*, **1991**, vol. 113, 8, pp. 2833–2838.
- 368 O. Yesilada, D. Asma, S. Cing; Decolorization of textile dyes by fungal pellets, in *Process Biochemistry*, **2003**, vol. 38, 6, pp. 933–938.
- 369 N. Al Nakeeb; Adsorptions- und Desorptionsverhalten eines supramolekularen pH-sensitiven Hydrogels, Bachelor thesis, Universität Bayreuth, **2012**.
- 370 B. E. Reed, M. R. Matsumoto; Modeling Cadmium Adsorption by Activated Carbon Using the Langmuir and Freundlich Isotherm Expressions, in *Separation Science and Technology*, **1993**, vol. 28, 13-14, pp. 2179–2195.
- 371 H. Qiu, L. Lv, B.-c. Pan, Q.-j. Zhang, W.-m. Zhang, Q.-x. Zhang; Critical review in adsorption kinetic models, in *J. Zhejiang Univ. Sci. A*, **2009**, vol. 10, 5, pp. 716–724.
- 372 Y. S. Ho, G. McKay; A Comparison of Chemisorption Kinetic Models Applied to Pollutant Removal on Various Sorbents, in *Process Safety and Environmental Protection*, **1998**, vol. 76, 4, pp. 332–340.
- 373 S. Y. Lagergren; Zur Theorie der sogenannten Adsorption gelöster Stoffe, in *Kungliga Svenska Vetenskapsakademiens. Handlingar*, **1898**, vol. 24, 4, pp. 1–39.
- 374 W. Rudzinski, W. Plazinski; On the applicability of the pseudo-second order equation to represent the kinetics of adsorption at solid/solution interfaces: a theoretical analysis based on the statistical rate theory, in *Adsorption*, **2009**, vol. 15, 2, pp. 181–192.
- 375 X. Huang, C. S. Brazel; On the importance and mechanisms of burst release in matrix-controlled drug delivery systems, in *Journal of Controlled Release*, **2001**, vol. 73, 2–3, pp. 121–136.
- 376 T. Higuchi; Rate of release of medicaments from ointment bases containing drugs in suspension, in *J. Pharm. Sci.*, **1961**, vol. 50, 10, pp. 874–875.

- 377 A. Fick; Ueber Diffusion, in *Ann. Phys.*, **1855**, vol. 170, 1, pp. 59–86.
- 378 J. Siepmann, N. A. Peppas; Higuchi equation: Derivation, applications, use and misuse, in *Mathematical modeling of drug delivery systems: Fifty years after Takeru Higuchi's models*, **2011**, vol. 418, 1, pp. 6–12.
- 379 N. M. Franson, N. A. Peppas; Influence of copolymer composition on non-fickian water transport through glassy copolymers, in *J. Appl. Polym. Sci.*, **1983**, vol. 28, 4, pp. 1299–1310.
- 380 www.medicago.se; Product sheet of Phosphate Buffered Saline (PBS), pH 7.4 and 7.2, available at: http://www.medicago.se/sites/default/files/pdf/productsheets/PBS_Buffer_v._01.pdf, accessed 25 November 2013.
- 381 A. Oyane, H.-M. Kim, T. Furuya, T. Kokubo, T. Miyazaki, T. Nakamura; Preparation and assessment of revised simulated body fluids, in *J. Biomed. Mater. Res.*, **2003**, vol. 65, 2, pp. 188–195.
- 382 K. M. Abou El-Nour, A. Eftaiha, A. Al-Warthan, R. A. Ammar; Synthesis and applications of silver nanoparticles, in *Arabian Journal of Chemistry*, **2010**, vol. 3, 3, pp. 135–140.
- 383 S. Roy, A. Banerjee; Amino acid based smart hydrogel: formation, characterization and fluorescence properties of silver nanoclusters within the hydrogel matrix, in *Soft Matter*, **2011**, vol. 7, 11, p. 5300.
- 384 H. Basit, A. Pal, S. Sen, S. Bhattacharya; Two-Component Hydrogels Comprising Fatty Acids and Amines: Structure, Properties, and Application as a Template for the Synthesis of Metal Nanoparticles, in *Chem. Eur. J.*, **2008**, vol. 14, 21, pp. 6534–6545.
- 385 M. J. Frisch, G. W. Trucks, H. B. Schlegel, G. E. Scuseria, M. A. Robb, J. R. Cheeseman, J. A. Jr. Montgomery, T. Vreven, K. N. Kudin, J. C. Burant, J. M. Millam, S. S. Iyengar, J. Tomasi, V. Barone, B. Mennucci, M. Cossi, G. Scalmani, N. Rega, G. A. Petersson, H. Nakatsuji, M. Hada, M. Ehara, K. Toyota, R. Fukuda, J. Hasegawa, M. Ishida, T. Nakajima, Y. Honda, O. Kitao, H. Nakai, M. Klene, X. Li, J. E. Knox, H. P. Hratchian, J. B. Cross, V. Bakken, C. Adamo, J. Jaramillo, R. Gomperts, R. E. Stratmann, O. Yazyev, A. J. Austin, R. Cammi, C. Pomelli, J. W. Ochterski, P. Y. Ayala, K. Morokuma, G. A. Voth, P. Salvador, J. J. Dannenberg, V. G. Zakrzewski, S. Dapprich, A. D. Daniels, M. C. Strain, O. Farkas, D. K. Malick, A. D. Rabuck, K. Raghavachari, J. B. Foresman, J. V. Ortiz, Q. Cui, A. G. Baboul, S. Clifford, J. Cioslowski, B. B. Stefanov, G. Liu, A. Liashenko, P. Piskorz, I. Komaromi, R. L. Martin, D. J. Fox, T. Keith, M. A. Al-Laham, C. Y. Peng, A. Nanayakkara, M. Challacombe, P. M. W. Gill, B. Johnson, W. Chen, M. W. Wong, C. Gonzalez, J. A. Pople; Gaussian03, Revision C. 02., Gaussian, Inc., Wallingford, CT, **2004**.
- 386 R. Ahlrichs, M. Bär, M. Häser, H. Horn, C. Kölmel; Electronic structure calculations on workstation computers: The program system turbomole, in *Chemical Physics Letters*, **1989**, vol. 162, 3, pp. 165–169.
- 387 A. D. Becke; Density-functional thermochemistry. III. The role of exact exchange, in *The Journal of Chemical Physics*, **1993**, vol. 98, 7, pp. 5648–5652.
- 388 C. Lee, W. Yang, R. G. Parr; Development of the Colle-Salvetti correlation-energy formula into a functional of the electron density, in *Phys. Rev. B*, **1988**, vol. 37, 2, pp. 785–789.
- 389 F. Krauth, H.-M. Dahse, H.-H. Rüttinger, P. Froberg; Synthesis and characterization of novel 1,2,4-triazine derivatives with antiproliferative activity, in *Bioorganic & Medicinal Chemistry*, **2010**, vol. 18, 5, pp. 1816–1821.

- 390 E. Jantratid, J. Dressman; Biorelevant Dissolution Media Simulating the Proximal Human Gastrointestinal Tract: An Update, in *Dissolution Technologies*, **2009**, vol. 16, 3, pp. 21–25.

List of Publications

Andreas Bernet, Rodrigo Q. Albuquerque, Marina Behr, Sebastian T. Hoffmann, Hans-Werner Schmidt

Formation of a supramolecular chromophore: a spectroscopic and theoretical study

Soft Matter, **2012**, vol. 8, 1, pp. 66–69.

DOI: 10.1039/c1sm06789c

Publications not included in this thesis:

Andreas Bernet, Marina Behr, Hans-Werner Schmidt

Supramolecular nanotube-based fiber mats by self-assembly of a tailored amphiphilic low molecular weight hydrogelator

Soft Matter, **2011**, vol. 7, 3, pp. 1058–1065.

DOI: 10.1039/c0sm00456a

Andreas Bernet, Marina Behr, Hans-Werner Schmidt

Supramolecular hydrogels based on antimycobacterial amphiphiles

Soft Matter, **2012**, vol. 8, pp. 4873–4876.

DOI: 10.1039/c2sm07456g

Andreas Bernet, Marina Behr, Rodrigo Q. Albuquerque, Marco Schmidt, Jürgen Senker, Hans-Werner Schmidt

Supramolecular Chromaticity and Thermoresponsive Hydrogels: A Self-Assembly Study on Maleamic Acid-Based Amphiphiles

in *Intelligent Hydrogels*, Gabriele Sadowski and W. Richtering (eds.),

Progress in Colloid and Polymer Science, Springer International Publishing, **2013**, vol. 140, pp. 1-13.

DOI: 10.1007/978-3-319-01683-2_1

Danksagung

An dieser Stelle möchte ich allen, die direkt oder indirekt zum Gelingen dieser Arbeit beigetragen haben, meinen herzlichsten Dank aussprechen.

Allen voran möchte ich meinem Doktorvater Prof. Dr. Hans-Werner Schmidt für das äußerst spannende und vielschichtige Thema, interessante wissenschaftliche Diskussionen und die Freiheit wissenschaftliche Fragestellungen nach eigenem Ermessen zu verfolgen danken. Zudem danke ich für die Bereitstellung eines gut ausgestatteten Laborplatzes sowie die Möglichkeit interdisziplinär im Rahmen des Bayreuther Instituts für Makromolekülforschung (BIMF) und des Bayreuther Zentrums für Kolloid- und Grenzflächenforschung (BZKG) zu forschen.

Die Dissertation wurde von der Deutschen Forschungsgemeinschaft im Rahmen des Teilprojekts „Entwicklung responsiver Hydrogele durch Self-Assembly von niedermolekularen Hydrogelatoren“ im Schwerpunktprogramm SPP 1559 „Intelligente Hydrogele“ finanziell unterstützt.

Bei Dr. Andreas Bernet bedanke ich mich herzlich für die vielseitige Unterstützung bei Forschungsfragen, die zahlreichen aufschlussreichen Diskussionen, die vielen hilfreichen Tipps und Tricks im Laboralltag, sowie die kreativen Ideen zur Problemlösung. Deine aufmunternden Worte, sowie deine Begeisterung für unerwartete Ergebnisse und neue wissenschaftliche Fragestellungen haben mich immer wieder motiviert und inspiriert.

Ferner möchte ich mich bei meinen Kooperationspartnern für die gute Zusammenarbeit bedanken, die mir durch viele Diskussionen und Gespräche Einblicke in ihre Forschungsgebiete ermöglichten. Vielen Dank an Prof. Dr. Rodrigo Q. Albuquerque für die Durchführung und Interpretation der theoretischen Berechnungen. Prof. Dr. Anna Köhler, Dr. Sebastian T. Hoffmann und Dr. Sergey Bagnich gilt mein Dank für zahlreiche spektroskopische Messungen und hilfreiche Diskussionen bei der Untersuchung der aggregations- und gelations-induzierten Photolumineszenz. Für die unkomplizierte und erfolgreiche Zusammenarbeit bei der *in-situ* Untersuchung von elektrogelierten Gelfilmen mittels AFM möchte ich mich besonders bei Prof. Dr. Georg Papastavrou, Dr. Volodymyr Kuznetsov, Maren Lehmann und Nicolas Helfricht bedanken. Prof. Dr. Stephan Förster und Sebastian With möchte ich für die Untersuchung des Gelbildungsverhaltens unter Mikrofluidikbedingungen danken.

Dank gilt auch meinen Praktikanten Tobias Güttler, Alessia Weiß, Daniel Hohenberger, Daniela Hendricks und Manuel Suchy für ihre Arbeit bei der Synthese und Charakterisierung

von BTA Derivaten. Besonders möchte ich Noah Al Nakeeb danken, der in seiner Bachelorarbeit das Freisetzungsverhalten von Rhodamin B aus Gelen untersucht hat.

Dem gesamten Team aus der Elektronenmikroskopie der Universität Bayreuth möchte ich für die Unterstützung bei der Probenpräparation und den verschiedenen Messungen danken. Hier gilt mein Dank vor allem Martina Heider und Dr. Beate Förster für die Anfertigung zahlreicher REM-Aufnahmen, Dr. Markus Drechsler für die cryo-TEM Experimente und Carmen Kunert für Aufnahme von TEM-Bildern bei Raumtemperatur. Außerdem möchte ich mich bei den Mitarbeitern des Lehrstuhls Makromolekulare Chemie II, Dr. Stefan Reinecke und Dr. Eva Betthausen, für ihre Einweisungen am Titrand-Messgerät und an der DLS bedanken.

Einen ganz besonderen Dank möchte ich an meine Arbeitskollegen am Lehrstuhl Makromolekulare Chemie I aussprechen. Die stete Hilfsbereitschaft, die vielen fachlichen Diskussionen sowie der kollegiale und freundschaftliche Umgang haben dazu geführt, dass ich mich stets am Lehrstuhl wohl gefühlt habe. Besonders möchte ich meinen Laborkollegen Andreas, Ruth, Holger und Paul für den vielen Spaß danken, den wir gemeinsam hatten. Ob der „schlechte Wortwitz-Freitag“, der Zitat-Kalender oder gesungene Kinderlieder: Dank euch werde ich mich immer gerne an meine Promotionszeit und das „Spaß-Labor“ erinnern.

Großer Dank gilt auch unseren akademischen Räten, Post-Docs, Technikern und Technikerinnen, sowie unseren beiden Sekretärinnen am Lehrstuhl Makromolekulare Chemie I. Vielen Dank an: Dr. Reiner Giesa, Dr. Christian Neuber, Dr. Klaus Kreger, Sandra Ganzleben, Irene Bauer, Doris Hanft, Rika Schneider, Helga Wietasch, Martina Fried, Alexander Kern, Christina Wunderlich, Petra Weiß und ganz besonders Jutta Failner. Eure organisatorischen Arbeiten erleichtern uns Doktoranden den Arbeitsalltag und mit eurer steten Bereitschaft nicht nur euer fachliches Wissen, sondern auch eure Lebenserfahrung an uns weiterzugeben, tragt ihr maßgeblich zu einem angenehmen Arbeitsklima an unserem Lehrstuhl bei.

Vielen Dank an meine Freunde, die es mit viel Kreativität, Interesse und Geduld immer wieder geschafft haben mich zu motivieren, die mir aber auch gezeigt haben, dass es wichtigere Dinge gibt als einen Dokortitel. Vielen lieben Dank!

Ein herzliches Dankeschön geht auch an meine Familie dafür, dass sie mich während meines Studiums und meiner Doktorarbeit immer unterstützt und an mich geglaubt hat. Danke, dass ihr mir immer wieder Mut und Kraft gegeben habt meine Ziele zu verfolgen.

Johannes, für deine Großzügigkeit, deine Geduld und dein Verständnis möchte ich dir von ganzem Herzen danken. Danke für deine Ehrlichkeit und Zuversicht!

Ohne Euch, wäre diese Arbeit so nicht möglich gewesen!

Vielen Dank!

(Eidesstattliche) Versicherungen und Erklärungen

Promotionsordnung (PromO) der Bayreuther Graduiertenschule für Mathematik und Naturwissenschaften (BayNAT) vom 20. März 2014.

Hiermit erkläre ich mich damit einverstanden, dass die elektronische Fassung meiner Dissertation unter Wahrung meiner Urheberrechte und des Datenschutzes einer gesonderten Überprüfung hinsichtlich der eigenständigen Anfertigung der Dissertation unterzogen werden kann.

(§ 8 S. 2 Nr. 6 PromO)

Hiermit erkläre ich eidesstattlich, dass ich die Dissertation selbständig verfasst und keine anderen als die von mir angegebenen Quellen und Hilfsmittel benutzt habe.

(§ 8 S. 2 Nr. 8 PromO)

Ich habe die Dissertation nicht bereits zur Erlangung eines akademischen Grades anderweitig eingereicht und habe auch nicht bereits diese oder eine gleichartige Doktorprüfung endgültig nicht bestanden.

(§ 8 S. 2 Nr. 9 PromO)

Hiermit erkläre ich, dass ich keine Hilfe von gewerblichen Promotionsberatern bzw. -vermittlern in Anspruch genommen habe und auch künftig nicht nehmen werde.

(§ 8 S. 2 Nr. 10 PromO)

Bayreuth, November 2014

Marina Behr

